Proceedings of

MMM

Third International Conference

Multiscale Materials Modeling

September 18-22, 2006, Freiburg, Germany

Symposium 6
Multiscale modeling of irradiation and aging of materials

Peter Gumbsch
Editor and Conference Chair

Organized by Fraunhofer-Institute for Mechanics of Materials.
Hosted by University of Freiburg.

IWM
Fraunhofer Institut
Werkstoffmechanik

ALBERT-LUDWIGS-
UNIVERSITÄT FREIBURG

Imprint

Papers published in this volume constitute the proceedings of the Third International Conference on Multiscale Materials Modeling. Papers were selected by the program committee for oral or poster presentation. They are published as submitted, in the interest of timely dissemination.

Contact
Fraunhofer Institute for Mechanics of Materials IWM
Woehlerstraße 11
79108 Freiburg
Germany
Phone + 49 761 5142 0
Fax + 49 761 5142 110

The complete proceedings of the conference are available at

Fraunhofer Information-Centre for Regional Planning and Building Construction IRB
P.O. Box 80 04 69, D-70504 Stuttgart
Nobelstrasse 12, D-70569 Stuttgart
Fon +49 (0) 7 11/9 70-25 00
Fax +49 (0) 7 11/9 70-25 07
E-Mail irb@irb.fraunhofer.de
URL www.irb.fraunhofer.de
ISBN-10: 3-8167-7206-4
ISBN-13: 978-3-8167-7206-4

Foreword

Computational modeling of materials behavior by multiscale materials modeling (MMM) approaches is becoming a reliable tool to underpin scientific investigations and to complement traditional theoretical and experimental approaches of component assessment. At transitional (microstructural) scales continuum approaches begin to break down and atomistic methods reach inherent limitations in time and length scale. Transitional theoretical frameworks and modeling techniques are developed to bridge the gap between the different length scales.

Industrial success in high technology fields relies on the possibility to specifically engineer materials and products with improved performance. The success factor is the ability to make these material related developments timely at relatively low-costs. This demands not only the rapid development of new or improved processing techniques but also better understanding and control of material chemistry, processing, structure, performance, durability, and their relationships. This scenario usually involves multiple length and time scales and multiple processing and performance stages, which are usually only accessible via multi-scale / multi-stage modeling or simulation.

In high-payoff, high-risk technologies such as the design of large structures in the aerospace and nuclear industries, the effects of aging and environment on failure mechanisms cannot be left to conservative approaches. Increasing efforts are now focused on advancing MMM approaches to develop new material systems components and devices. Appropriate validation experiments are crucial to verify that the models predict the correct behavior at each length scale. Thus, one of the advantages of these MMM approaches is that, at each scale, physically meaningful parameters are predicted and used in models for subsequent scales, avoiding the use of empiricism and fitting parameters.

Recent interest in nanotechnology is challenging the scientific community to design nanometer to micrometer size devices for applications in new generations of computers, electronics, photonics or drug delivery systems. These new application areas of multiscale materials modeling require novel and sophisticated science-based approaches for design and performance evaluation. Theory and modeling are playing an increasing role to reduce development costs and manufacturing times. With the sustained progress in computational power and MMM methodologies, new materials and new functionalities are increasingly more likely discovered by MMM approaches than by traditional trial and error approach. This is part of a paradigm shift in modeling, away from reproducing known properties of known materials towards simulating the behavior of hypothetical composites as a forerunner to finding real materials with these novel properties.

The MMM 2006 conference provides an international forum for the scientific advances of multiscale modeling methodologies and their applications.

I would like to thank the members of the international advisory committee, the local program committee and particularly the organizing team, the symposium organizers and the session chairs and the University of Freiburg for their engagement and support. Without their hard work and their devotion of time and ressources, the Third International Conference Multiscale Materials Modeling would not have been possible.

Finally, I would like to thank our conference sponsors for their financial support: The German Research Foundation DFG, Accelrys Inc., Plansee S.E. and the Ministry of Science, Research and Art, Baden-Württemberg.

Peter Gumbsch
Conference Chair

Conference Committee

International Advisory Committee

Prof. Bacon, David	University of Liverpool, UK
Dr. Baskes, Michael	Los Alamos National Laboratory, USA
Prof. Busso, Esteban	Imperial College, London, UK
Prof. Cale, Timothy S.	Rensselaer Polytechnic Institute, Troy, USA
Dr. Diaz de la Rubia, Tomas	Lawrence Livermore National Lab., USA
Prof. Ghoniem, Nasr	University of California, Los Angeles, USA
Prof. Guo, Xiao	Queens College, London, UK
Prof. Iwata, Shuichi	University of Tokyo, Japan
Prof. Kratochvil, Jan	Technical University, Prague, Czech Republic
Prof. Kremer, Kurt	Max Planck Institute, Mainz, Germany
Dr. Kubin, Ladislas	ONERA-LEM, Chatillon, France
Dr. LeSar, Richard	Los Alamos National Laboratory, USA
Prof. Meguid, Shaker	University of Toronto, Canada
Prof. Needleman, Alan	Brown University, Providence, USA
Prof. Odette, Robert	University of California, Santa Barbara, USA
Prof. Ortiz, Michael	California Institute of Technology, USA
Prof. Pettifor, David	Oxford University, UK
Prof. Phillips, Robert	California Institute of Technology, USA
Prof. Raabe, Dierk	Max Planck Institute, Düsseldorf, Germany
Prof. Shibutani, Yoji	Osaka University, Japan
Dr. Soneda, Naoki	Komae Research Laboratory, Tokyo, Japan
Prof. Suresh, Subra	Massachusetts Institute of Technology, USA
Prof. Tomita, Yoshihiro	Kobe University, Japan
Prof. Van der Giessen, Erik	University of Groningen, Netherlands
Prof. Walgraef, Daniel	Free University of Brussels, Belgium
Dr. Wolf, Dieter	Argonne National Laboratory, USA
Prof. Yip, Sidney	Massachusetts Institute of Technology, USA
Dr. Zinkle, Steve	Oak Ridge National Laboratory, USA

Organizing Committee

M. J. Alava	Helsinki University of Technology, Finland
D. Dimiduk	The Ohio State University, USA
M. Dao	Massachusetts Institute of Technology, USA
M. Doi	University of Tokyo, Japan
C. Elsässer	Fraunhofer IWM, Germany
E. v. d Giessen	University of Gronigen, Netherlands
N. Gov	The Weizmann Institute of Science, Israel
H. J. Herrmann	University of Stuttgart, Germany
R. James	University of Minnesota, USA
K. Kremer	Max Planck Institute for Polymer Research, Germany
J. Korvink	IMTEK, University of Freiburg, Germany
J. Li	The Ohio State University, USA
S. Müller	Max Planck Institute for Mathematics in the Sciences, Germany
A. Paxton	Queen’s University, Belfast, UK
M. Payne	University of Cambridge, UK
D. Raabe	Max Planck Institute fuer Eisenforschung, Germany
N. Soneda	Central Research Institute of Electric Power Industry, Japan
M. Zaiser	University of Edinburgh , UK
S. Zapperi	University of Rome, Italy
F. Willaime	Commissariat a l’Energie Atomique (CEA), France
B. Wirth	University of California, Berkely, USA

Contents

Symposium 6

Symposium 6

Multiscale modeling of irradiation and aging of materials

Effect of undersized Fe atoms on dynamic behavior of interstitial configuration near an edge dislocation in V using molecular dynamics simulation

Y. Abe and H. Matsui

Institute for Materials Research, Tohoku University, 2-1-1 Katahira, Aoba-ku, Sendai, Japan, 980-0812, e-mail; y_abe@imr.tohoku.ac.jp

ABSTRACT

It is well-known that the dislocation bias should be responsible for the large swelling. In V-Fe alloys, the extremely large swelling has been observed, which indicates that undersized Fe must play a significant role for the modification of 1-dimensional (1D) motion. In the present study, we performed the MD simulations with a newly constructed empirical potential based on the Finnis-Sinclair (FS) type embedded atom method (EAM) to investigate the effect of undersized Fe on the dynamic process of the 1D motion of interstitial atoms under the strain field of several sizes of interstitial loops and an edge dislocation. The results show that the undersized Fe atoms tend to form a mix-dumbbell configuration rather than the crowdion configuration as often observed in the case of SIAs and the occupation probabilities for the V-Fe mixed-dumbbell below an edge dislocation core becomes larger than that of a SIA, suggesting that the migration to the dislocation core may become possible in V-Fe alloy.

1. Introduction

It has been recognized that various kinds of bias factors are significantly important for the formation of the clusters. The interaction between SIAs and edge dislocations is stronger than that between vacancies and edge dislocations, resulting in the unbalance between the vacancy flow and the interstitial flow into the sinks, and this makes the formation of each cluster possible. This is so-called dislocation bias which causes void swelling, dislocation loops, and dislocation networks.

It has been reported that extremely large void swelling could occur in V-5Fe alloys after neutron irradiation [1]. This finding is anomalous in bcc metals, especially in vanadium which shows good resistance to swelling, and it has been suggested that this is closely related to undersized solute Fe atoms. To solve this problem, it is important that the detailed configuration of interstitial atoms near the edge dislocation should be investigated at the atomistic level. However, the experimental techniques are rather difficult to definitely measure and analyze the dynamical behavior of interstitial atoms near the edge dislocations. Most promising methods overcoming this difficulty are atomistic simulations using some types of interatomic potentials.

Until today, one-dimensional motion of a SIA under the core of an edge dislocation has been simulated, and this one-dimensional motion may prevent SIAs from absorbing into dislocation core [2], although dislocation bias is well-known mechanism that SIAs are preferably absorbed into dislocation core rather than vacancies due to high mobility of SIAs. Moreover, the efffect of undersized Fe atoms on the static and dynamic properties of interstitial configurations near an edge dislocation in V-Fe alloys has not been investigated so far.

In the present study, we performed the MD simulations with a newly constructed empirical potential based on the Finnis-Sinclair (FS) type embedded atom method (EAM) to investigate the effect of undersized Fe on the dynamic process of the 1D motion of interstitial atoms under the strain field of several sizes of interstitial loops and an edge dislocation.

2. Numerical Procedure

The Finnis-Sinclair (FS) potential [3], which provides a similar framework to the EAM potential, was chosen to construct a V-Fe cross potential. The interatomic potentials for pure elements were taken from Han et al. [4] and Ackland et al. [5] for V and Fe, respectively. To construct a V-Fe cross potential, the scheme proposed by Konishi et al. [6] was adopted. According to this approach, the two adjustable parameters α and β were fit to experimental values for the alloy, such as the mixing enthalpy and the lattice constants. The obtained values of parameters α and β are 1.04 and 0.65, respectively.

For the cases of SIA clusters, simulations were performed in a cubic system of size 54000+n(a $30a_0\times30a_0\times30a_0$ computational cell, where the equilibrium cubic lattice parameter a_0=3.03A) where n=19,37,61. The periodic boundary condition was applied for all cases. These clusters were generated by an annealing process, which involved increasing temperature in 1ps steps of 10K between 0 and 1000K. To obtain the zero temperature structure, the system was quenched to 0K. All final configurations consisted of perfect dislocation loops with Burgers vector **b**=1/2<111>. On the other hand, the initial configuration including the edge dislocation was determined by displacing the all atoms in consistent with the elastic theory. Then, the system was fully relaxed to the equilibrium configuration. The fixed boundary conditions were applied to <111> and <110> directions, while the periodic boundary condition was applied to <112> direction in order to effectively provide an infinite extension of the structure.

The interstitial atom was introduced in the form of <111>-crowdion or <110>-dumbbell at various distances below the slip plane of SIA clusters and an edge dislocation. After complete relaxation of the whole lattice, the total energy of the lattice was calculated for each distance between a dislocation line and an interstitial atom. According to Heald [7], the effective interaction range L, where the interaction energy becomes equal to kT must be determined to estimate the bias factor.

3. Results and discussion

For the example of the behavior of the interaction between several sizes of dislocation loops and an interstitial atom, variation of the formation energy difference between a <111>-crowdion and a <110>-dumbbell around a dislocation loop consisted of 19 interstitial atoms in V was calculated and are shown in Fig. 1(a) for a SIA and (b) for an interstitial Fe atom. Here, the axis of a <111>-crowdion is parallel to the Burgers vector of a dislocation loop, and the capture range within which the formation energy difference is larger than 0.067eV (value of kT, T=500◦C) is also plotted. The <110>-dumbbell having its axis ~35◦ shifted compared to the <111>-crowdion was assumed to be a suddle point for an interstitial diffusion path into the edge of a dislocation loop. A little difference is seen between these two results, suggesting that whether the types of the interstitial atom is SIA or small sized Fe, the interstitial migration to the edge of relatively small dislocation loop may not be affected.

On the other hand, in the case of the diffusion process in a perfect lattice, a remarkably high rotation frequencies can be observed and their activation energies are extremely low in V-Fe alloys as shown in Fig. 2, suggesting that the migration to extended region through three dimensional motions can take place easily in V-Fe alloys compared to those in pure V. This high frequency rotation can be considered that the V-Fe mixed dumbbell is the most stable configuration as obtained from MS calculations and the strain field around the V-Fe mixed dumbbell are much smaller than those of V-V dumbbell, thus the rotation can be considerably easier in the cases of V-Fe alloys than those of pure V. Thus, it may be considered that the formation energy difference for an interstitial Fe atom between a <111>-crowdion and a <110>-dumbbell around a dislocation loop, i.e. the capture range, becomes larger than that of a SIA with increasing the sizes of a dislocation loop.

The occupation probabilities for V-V and V-Fe dumbbells below an edge dislocation core were analyzed and shown in Fig. 3. For the Fe interstitial, the relative probability for intermediate configurations between <111>-crowdion and <110>-dumbbell became significantly higher compared with that of V. The molecular static (MS) simulations have also shown that the binding energy of <110>-dumbbell is greatly higher than that of <111>-crowdion for V-Fe configuration. It is considered that the effect of the undersized Fe is to strongly bind the neighboring V atom, causing easily rotation around their center of gravity. Thus, the effective activation energy against the potential barrier between <111>-crowdion and <110>-dumbbell may be reduced. This suggests that the migration to the dislocation core is possible, causing the large dislocation bias in V-Fe alloy.

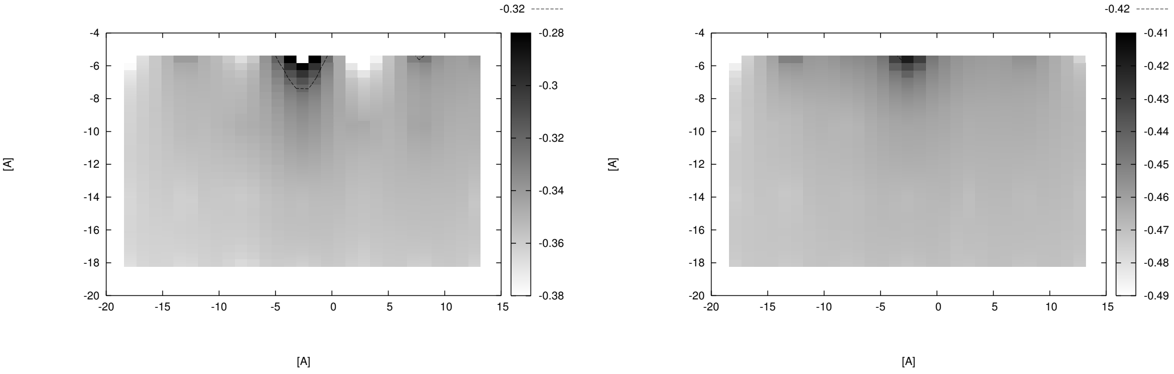

(a) SIA (b) Interstitial Fe atom

Figure 1. Calculated formation energy difference between a <111>-crowdion and a <110>-dumbbell for (a) SIA and (b) interstitial Fe atom near a dislocation loop consisted of 19 interstitial atoms in V. Capture range within which the formation energy difference is larger than 0.067eV (value of kT, T=500◦C) is also drown.

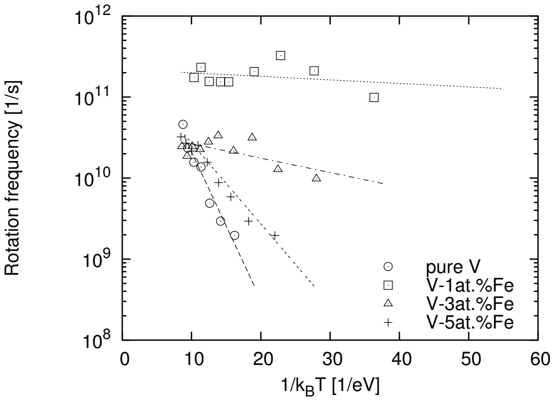

Figure 2. Rotation frequency of the interstitial atom for various concentration of Fe atoms in V. This result was obtained by analyzing the diffusion process in perfect lattice systems.

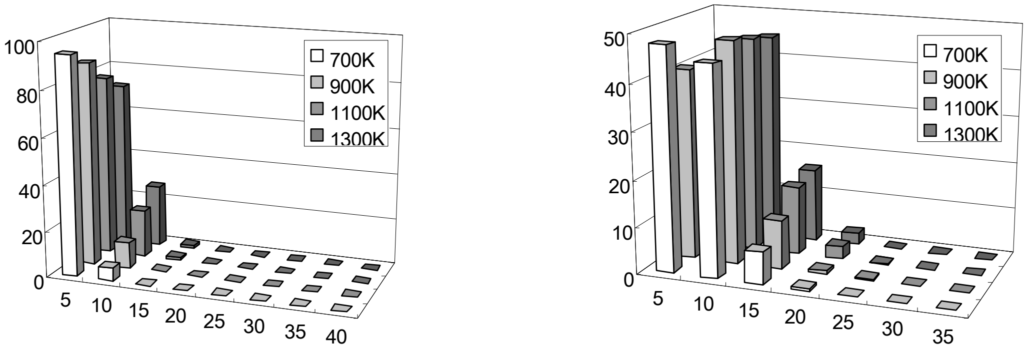

(a) V-V dumbbell (b) V-Fe dumbbell

Figure 3. Relative probability for V-V and V-Fe dumbbells occupying different configurations between a <111>-crowdion and a <110>-dumbbell between 700 and 1300K at 5 atomic distances below the slip plane of an edge dislocation in V.

References

[1] H. Matsui, D. S. Gelles, and Y. Kohno, Proc. 15th Int. Symp. on the Effects of Radiation on Materials, ASTM STP 1125 (1991)

[2] H. Kamiyama, H. Rafii-Tabar, Y. Kawazoe, and H. Matsui, J. Nucl. Mater. 212-215 (1991) 231.

[3] M. W. Finnis, J. E. Sinclair, Philos. Mag. A 50 (1984) 45-55.

[4] S. Han, L. A. Ackland, R. Car, D. J. Srolovitz, J. Appl. Phys. 93 (2003) 3328-3335.

[5] G. J. Ackland, D. J. Bacon, A. F. Calder, T. Harry, Philos. Mag. A. 75 (1997) 713-732.

[6] T. Konishi, K. Ohsawa, H. Abe, E. Kuramoto, Comput. Mater. Sci. 14 (1999) 108-113.

[7] P. T. Heald, Philos. Mag. 31 (1975) 551.

On the correlation between microstructure and hardening evolution under irradiation of low Cu RPV steel in comparison with model alloys

Abderrahim Al Mazouzi[1], *M. Jardin*[1], *M. Lambrecht*[1], *L. Malerba*[1]

[1]*SCK-CEN, Reactor Materials Research Departement, LHMA/ Boeretang 200, 2400 Mol, Belgium*

Fe-Cu binary alloys are often used to mimic the post-irradiation behaviour of RPV steels. Within the EU-Perfect project, following the REVE initiative, SCK-CEN has performed an irradiation campaign of model alloys of growing complexity, ranging from pure Fe to a low copper RPV steel, to different doses at 300°C. These alloys have been then characterized in terms of tensile properties and hardness and very recently they have been analysed by means of positron annihilation techniques. The use of two complementary measurements methods, namely lifetime and coincidence Doppler broadening, allowed the identification of the type of the defects that are considered to play a major role in the hardening of RPV-steels, also in terms of local chemical environment. In this presentation, we will be discussing the correlation between the spectra obtained by PAS techniques and the hardening of 6 alloys after irradiation up to 0.2 dpa in a high flux reactor. It is found that only model alloys containing Ni and Mn exhibit the same behaviour as RPV steels, with delayed saturation of radiation-induced hardening, and that the explanation of this behaviour can be found in the different association of vacancies and vacancy clusters to solute atoms.

Surface Roughening Mechanisms for Tungsten Exposed to Laser, Ion, and X-ray Pulses

Michael Andersen[1], *Nasr M. Ghoniem*[1]

[1]*University of California-Los Angeles, 48-121 Engineering IV, Westwood Plaza, 90034 Los Angeles, United States of America*

Tungsten is a candidate material for a variety of applications in Magnetic and Inertial Fusion Energy (IFE) fusion systems. For example, it is proposed as a divertor plate material in a duplex structure attached to a copper heat sink for high heat flux applications in ITER. Also, it is proposed as an armor material for the High Average Power Laser (HAPL) IFE dry wall chamber design because of its high temperature capabilities. However, experimental data show that the surface of tungsten exposed to laser, ion, and X-ray irradiation undergoes substantial roughening with a variety of patterns and features. Control of surface conditions is essential to the design of these systems, since it can lead to crack formation, adverse effects on heat absorption because of emissivity changes, and eventual failure.

We first review recent experimental data on the effects of laser, ion and x-ray energetic pulses on the evolution of surface morphology and roughness of single and polycrystalline tungsten to identify the variety of patterns and length scales and their dependence on the type and magnitude of irradiation pulses. Then we present a model for the evolution of surface roughness as a result of the balance between destabilizing elastic strain energy caused by thermomechanical strains and near surface accumulation of defects on the one hand, and stabilizing surface and near surface atomic diffusion on the other. Results of the model determine the conditions for surface roughness evolution and the effects of radiation fluence and pulse intensity on surface morphology.

Fission spectra for cladding formed by zirconium alloys: application to Monte Carlo simulations

C. Arévalo[1], M. J. Caturla[2] and J. M. Perlado[1]

[1] Instituto de Fusión Nuclear, Universidad Politécnica de Madrid, c/ José Gutiérrez Abascal, 2. 28006 Madrid, Spain
[2] Universidad de Alicante, Dep. Física Aplicada, Alicante, Spain

ABSTRACT

Several multiscale modelling simulations steps have been used in order to understand the microscopical fission reactor cladding behaviour. We have focused on zirconium alloys claddings (Zircaloy-4 and Zr-2.5%Nb). The first step simulated has been the neutron spectra. Spectra for current pressure water reactors (PWR) and high burn-up advanced reactors have been obtained. Neutron spectra in several burnt steps have been presented. Taking these results as input data we have reproduced the Primary Knock-on Atom (PKA) spectra. From those data a systematic analysis of primary damage has been obtained using a binary collisions code for high energy recoils, in order to get distribution of cascades and subcascades for these recoil energies. With these data the evolution of the microstructure during irradiation under environment conditions of 600K, dose rate 10-6 dpa/s could be calculated.

1. Introduction

The first barrier (cladding) of the radioactive material from fission reactions in current light water reactor is built up of Zirconium alloys. Advanced Zr alloys are proposed to be used for high burnup applications as well as for cladding and reactor internal components in future Generation III and IV reactors. Consequently, understanding the effect of irradiation on the mechanical properties of these alloys is crucial for safe operation of reactors. This work focuses on the description of microscopic effects of irradiation using computer simulations in a multi-scale approach.

Two different Zirconium alloys have been considered as cladding: Zircaloy-4 and Zr-2.5%Nb. Typical isotopic compositions of these two alloys are presented in Tab.1 [1,2].

Table 1. Typical isotopic compositions for Zircaloy-4 and Zr-2.5%Nb.

Alloy	Weight (%)						
	Sn	Fe	Cr	O	Cu	Nb	Zr
Zircaloy-4	1.5	0.21	0.1	0.13	0	0	98.06
Zr-2.5%Nb	0.001	0.005	0.05	0.13	0.002	2.55	97.26

The first step in the study of the microscopical effects is the knowledge of the neutron spectra, that is, neutron flux versus energy that different zirconium alloys as cladding suffers under different conditions of burnup. These calculations have been made using the code called Monteburns. Taking these results as input data, primary knock-on atom (PKA) spectra have been reproduced through neutron damage code called SPECTER.

2. Neutron spectra for claddings in fission reactors

Monteburns [3] was designed to link the Monte Carlo N-Particle Transport Code MCNP and the radioactive decay and burnup code ORIGEN2 into an automated tool. MCNP generates a statistical history for a neutron based random samples from probability distributions. These distributions are used in calculations to determine the type of interaction the particle undergoes at each moment of its life, the resulting energy of the particle if it scatters, if it is absorbed, the number of particles that "leak" from the system because of geometry constraints, and the number of neutrons produced if the neutron causes a fission or (n,xn) reaction. The fluxes of neutrons determined in this way can then be used to tally a wide variety of information (reaction rates, heating rates, doses, etc.) for the system.

Spectra for current light water reactors (uranium enriched to 3.5%) and advanced high burnup light water reactor (uranium enriched to 9.75%) have been calculated; concretely a standard Westinghouse pressure water reactors (PWR) pin cell benchmark has been used in this work.

In Fig.1 neutron spectra is shown (neutron flux by energy versus energy) for a current pressure water reactor and cladding was built of Zircaloy-4 and Zr-2.5%Nb. These results have been represented for the first burnt step and for the final burnt step corresponding to a burnt of 40GWD/tU. We have observed that flux is practically the same for both alloys and increases when the burnt increases. Neutron energies go from 10^{-11} MeV to 10 MeV.

In Fig.2 neutron spectra is presented for an advanced light water reactor and a cladding built of Zircaloy-4 and Zr-2.5%Nb. Results have been represented for the first burnt step and for the final high burnt step that corresponds to 100GWD/tU. It is observed that flux is higher for the case of Zircaloy-4 and increases with the burnt. In comparison with Figure 1 the spectrum is lightly lower in the case of advanced reactors than current ones.

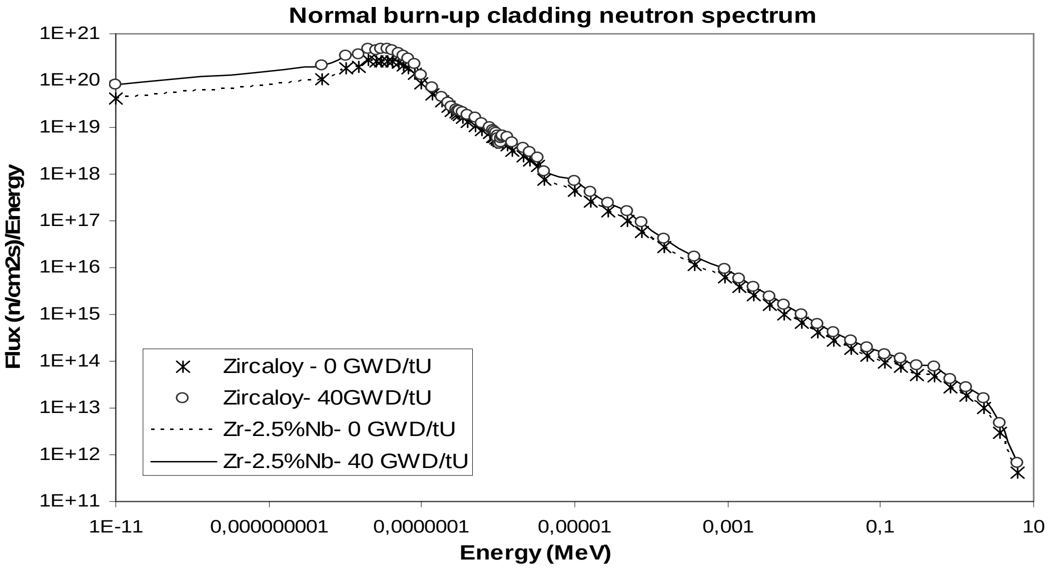

Figure 1. Neutron spectrum the cladding in a pressure water reactor receives using two different materials for cladding: Zircaloy-4 and Zr-2.5%Nb.

3. PKA spectra

SPECTER (Calculation of Energy Distribution of Nuclear Reaction Products) [4] calculates the energy spectra of particle emerging from reactions of the types (y,n), (y,p), (y,alpha), (y,2n), (y,np), (y,pn) and (y,2p) where the incident particle y may be either n, p ó alpha. In addition, the code calculates the cross section for each of these reactions. Moreover, it calculates recoil spectra, gas production, and total damage energy.

Spectra calculations made in the section before have been used as input in the SPECTER code in order to obtain the primary damage in these materials.

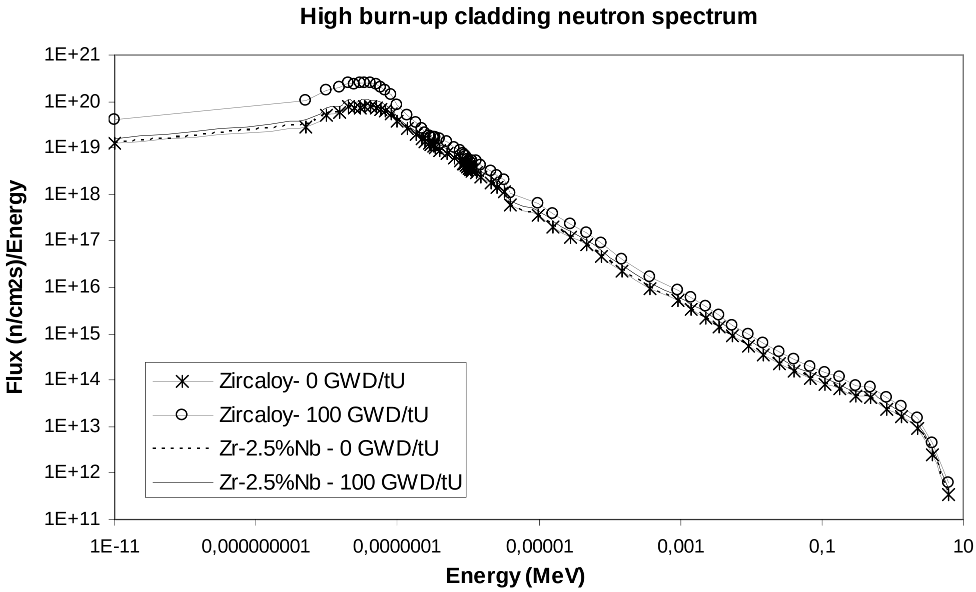

Figure 2. Neutron spectrum the cladding in a high burn-up light water reactor receives using two different materials for cladding: Zircaloy-4 and Zr-2.5%Nb.

Fig.3 shows primary knock-on atom spectra (PKA fraction by energy versus the energy of the atom) for a current PWR in the same conditions than Figure 1. The same results in the four cases can be observed. PKA spectrum does not be affected neither the kind of cladding material nor burnup rate. Maximum PKA energy for Zircaloy-4 is 260keV and for Zr-2.5%Nb 280keV.

Fig.4 represents primary knock-on atom spectra for an advanced LWR in the same conditions than Figure 2. PKA spectra in these cases are higher for Zr-2.5%Nb case than for Zircaloy-4 one but there is a light difference.

4. Conclusions

Neutron spectra for current and high burnup light water reactors have been carried out using Monteburns code. Results show neutron flux increases when steps of burnup increase. Using these data as input, PKA spectra have been made for the same conditions using SPECTER code. Results are independent the cladding and the burnup step. This similarity between values is in good agreement with previous neutron and PKA spectra results in several materials [5].

These data are very useful to understand the microscopic evolution of Zirconium alloys that is being studied using Molecular Dynamics and kinetic Monte Carlo simulations.

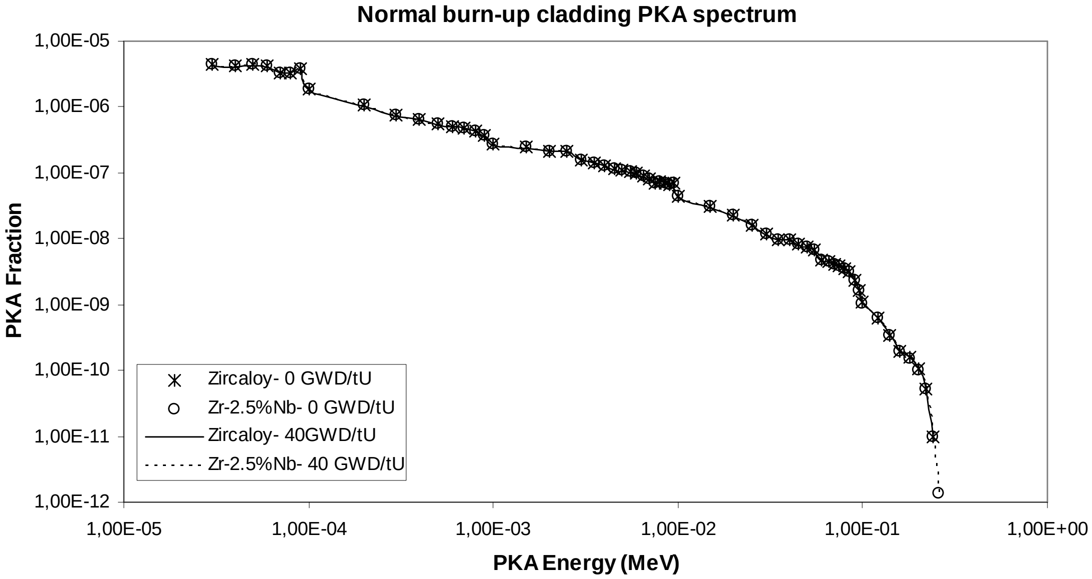

Figure 3. PKA spectrum from the cladding in a high burn-up light water reactor using two different materials for cladding: Zircaloy-4 and Zr-2.5%Nb.

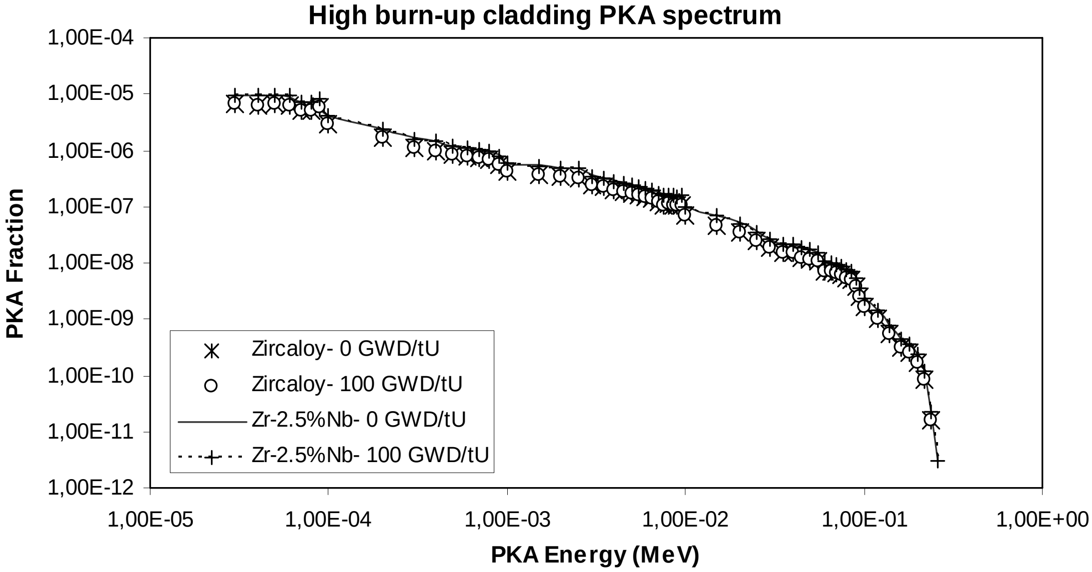

Figure 4. PKA spectrum from the cladding in a high burn-up light water reactor using two different materials for cladding: Zircaloy-4 and Zr-2.5%Nb.

5. References

[1] Martin Steinbruck, Jour. of Nucl. Mater. 334 (2004) 58-64

[2] A. Yilmazbayhan et al., Jour. of Nucl. Mater. 324 (2004) 6-22

[3] H.R. Trellue and D.I. Poston, \User's Manual, Version 2.0 for Monteburns, Version 5B",Los Alamos National Laboratory, preprint LA-UR-99-4999 (1999); H.R. Trellue, private communication (April 2000).

[4] R. Show and M.C. George, “A Computer Code for Calculating the Energy Distribution of Nuclear Reaction Products” SMSD-SSL-1100 (February 1970).
SPECTER-ANL. Neutron damage calculations for material irradiations, PSR-0263. ANL/FPP/TM-197 (1985).

[5] R.E. Stoller and L.R. Greenwood, Effects of Radiation on Materials: 20th International Symposium, ASTM STP 1405 (2000).

On the Direct Relationship between Macroscopic Phenomena of Plastic Flow Localization and Solids Microcharacteristics

Lev B. Zuev, **Svetlana A. Barannikova and Vladimir I. Danilov**

Institute of Strength Physics and Materials Science, SB RAS,
634021, Tomsk, Russia. E-mail: lbz@ispms.tsc.ru

ABSTRACT

The macrolocalization behavior of plastic deformation in metals and alloys is addressed in the framework of a new approach, which enables one to relate the characteristics of autowave processes involved in flow localization on a macro- and a micro-scale level.

1. Introduction

It is known that plastic flow tends to localize from yield point to ductile failure [1, 2]. Interpretation of experimental data on flow macrolocalization is a complicated task that still remains to be solved. To date the phenomenology of the localization effect has been elucidated and the space-time regularities, which are characteristic for localization development, have been established. Localization might be regarded as a typical example of self-organization if the term "self-organization" is used in the meaning proposed by Haken, i.e. acquisition by a system of a spatial, a temporal or a functional structure in the absence of any specific action from without [3]. Plastic flow localization has all the characteristic features of autowave processes [1]. Thus at the stage of linear work hardening, the localization of plastic flow occurs in the form of phase autowaves having length $5 \le \lambda \le 15$ mm and propagation velocity $10^{-5} \le V_{aw} \le 10^{-4}$ m/s (Figure 1). A special technique of double-exposure speckle photography intended for visualization of localized plasticity patterns has been developed [1]. This enabled one to obtain a vast array of data on the above quantities for a range of materials.

2. Relationship between micro- and macro-scale characteristics

The autowave nature of plastic flow localization in a deforming medium is addressed in the framework of a fundamentally new approach proposed in [4]. In order to describe the autowaves of localized deformation discussed in detail elsewhere [1, 2], the de Broglie equation $\lambda = h/mV$ is used (here h is the Planck constant). It has turned out that the mass values calculated with the help of this equation correlate with the atomic masses of the respective metals [4]. In our work [5] we used the same method in a consistent manner employing the de Broglie equation written in the form $m_{ef} = h/\lambda V_{aw}$; this allowed us to derive effective masses $m_{ef} \approx 1.5$ a.m.u. for Cu, Al, Zr, V, Fe and Ni. A numerical analysis yielded

$$m_{ef} \approx \rho \cdot r_{ion}^3 , \tag{1}$$

where ρ is the density of metal and r_{ion} is its ionic radius. In fact, the estimations above is an attempt to introduce a certain quasi-particle corresponding with localized plasticity autowaves and having the effective mass $\sim m_{ef}$ and propagating velocity V_{aw}. Clearly, Eq. 1 is equivalent to the relation

$$\lambda V_{aw} = h / \rho \cdot r_{ion}^3 = const\,. \qquad (2)$$

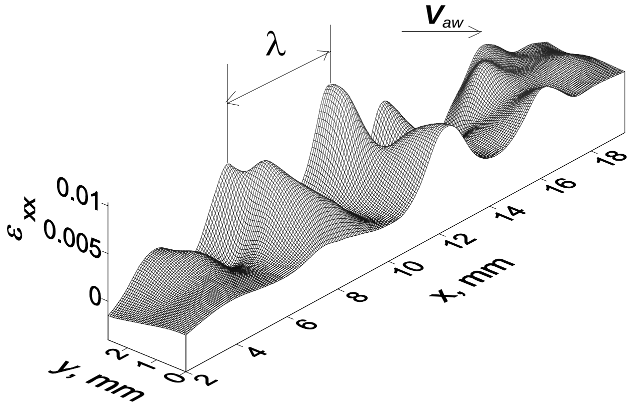

Figure 1. The set of active localization zones ε_{xx} moving in a concerted manner along the extension axis in the Cu specimen; ε_{xx} is a local elongation

Numerical data processing reveals that condition (2) corresponds, with a reasonable degree of accuracy – at least by the order of magnitude, to the equality

$$2\lambda \cdot V_{aw} \approx d \cdot V_{\perp}\,, \qquad (3)$$

where d is the spacing between close-packed planes of the respective metal lattice and $V_{\perp}$ is the propagation velocity of transverse ultrasound waves in the same metal (see Table 1). The average ratio $\langle 2\lambda \cdot V_{aw} / d \cdot V_{\perp} \rangle$ = 1.06 ≈ 1 was obtained for the metals listed in Table 1. Eq. 3 establishes a quantitative relationship between the characteristics of elastic wave processes (d and $V_{\perp}$) and those of localized plastic flow autowaves (λ and V_{aw}).

Table 1. On the matching of $\lambda \cdot V_{aw}$ and $d \cdot V_{\perp}$ values

Metal	$\lambda \cdot V_{aw} \times 10^7$	$d \times 10^{10}$	$V_{\perp} \times 10^{-3}$	$d \cdot V_{\perp} \times 10^7$	$2\lambda \cdot V_{aw} / d \cdot V_{\perp}$
	m^2/s	m	m/s	m^2/s	
Cu	3.6	2.08	2.30	4.78	1.5
Al	7.92	2.33	3.23	7.52	2.1
Zr	1.92	2.46	2.25	5.53	0.7
V	2.8	2.14	2.83	6.06	0.92
Fe	2.55	2.07	3.32	6.87	0.74
Ni	2.1	2.03	3.22	6.54	0.64
Sn	2.34	2.91	1.79	5.20	0.9

Let us rewrite Eq. 1 in the form

$$\lambda \cdot V_{aw} \cdot m_{ef} = \lambda \cdot V_{aw} \cdot \rho \cdot r_i^3 = h\,, \qquad (4)$$

which can be used for calculating the Planck constant values h. The wavelength and propagation rate of autowaves were measured experimentally; ρ and r_{ion} values were borrowed from handbooks. Evidently, the calculated values generalized in Table 2 are close to the Planck constant true value h = 6.626·10^{-34} J·s. The average value obtained for seven metals investigated $\langle h \rangle$=(6.34±0.48)·10^{-34} J·s and the ratio $\langle h \rangle / h$ =0.96±0.07. A good agreement is observed for V, Fe, Ni, Sn, and Zr and a slightly worse one for Al and Cu.

3. Discussion of results

The above suggests that resorting to quantum concept of plastic flow evolution in solids is justified. A similar approach might seem unexpected to physicists dealing with plasticity problems who maintain a long-sustained belief that the spatial scales of micro- and macro-effects are incommensurable. On the microscopic (dislocation) scale level, however, the idea of quantization would not appear to be out of place since in view of lattice discreteness, a minimal probable shear by the Burgers vector having microscale $b \approx d \approx 10^{-10}$ m may be regarded as "a shear deformation quantum". At the same time, it follows from (3) that micro- and macro-scale phenomena occurring during deformation are interrelated, which speaks in favor of applying the quantization concept to the macro-scale level.

Table 2. The Planck constant values calculated from Eq. 4

Metal	$r_{ion} \times 10^{10}$	$\lambda \times 10^{3}$	$V_{aw} \times 10^{5}$	$h \times 10^{34}$
	m	m	m/s	J·s
Cu	0.96	4.0	2.6	8.14
Al	0.51	8.0	18	5.0
Zr	0.79	5.5	3.5	6.13
V	0.59	4.0	7.0	6.52
Fe	0.64	6.5	5.2	6.32
Ni	0.69	3.5	6.0	6.17
Sn	0.71	4.2	5.5	6.14

Evidently, the fact that the handbook values of the Planck constant agree with the ones calculated from data derived in rather "coarse" macroexperiments may be attributed to the manifestation of so-called "universality concept" [6]. In accordance with this concept, a system's measurable characteristics are independent of the distribution of most of its microscopic properties. In other words, qualitative and quantitative substructural characteristics of the deforming medium may be responsible only to an insignificant extent for the flow stress, the coefficient of work hardening and other mechanical characteristics.

Application of the concept of "wave-particle dualism" to the description of processes involved in localization of deformation appears to be sufficiently suitable. The above results considered as a whole imply that in a plastically deforming multi-scale system for which the following ratio holds true $L_{macro}/L_{micro} \approx \lambda/r_{ion} \geq 10^{8}$ the macro-scale phenomena ($L_{macro} \approx \lambda$) can be directly related to the micro-scale ones ($L_{micro} \approx r_{ion}$). In our previous investigations [2] the wave characteristics of plastic flow were measured for a pre-deformed metal whose dislocation substructures differed in their spatial parameters.

On the base of above findings a new two-component model of plastic flow is proposed, which relates information subsystem and dynamic the same in the deforming medium. Kadomtsev [7] was the first to use this concept to explain self-organization phenomena emerging in complex systems. It is believed herein that plastic flow information subsystem can be related to the acoustic emission pulses (phonons) that are generated in the course of elementary acts of plasticity (for example, dislocation shears or twinning). Such pulses propagate through the medium, triggering thereby the thermal activated processes of dislocation motion in the dynamic subsystem of the deforming body. In this model the lattice values d and $V_{\perp} \approx 2\Theta_D k_B d/h$ [6] characterize the phonon (elastic) subsystem and the autowave parameters λ and V_{aw} are related to the dynamic subsystem of the medium, i.e. solids plasticity in the commonly used meaning. Here Θ_D is the Debye temperature, k_B is the Boltzmann constant. In this case it is believed that Eq. 3 reflects the condition of self-consistent occurrence of the processes at the micro- and macro-scale levels in the deforming medium. Thus, Eq. 3 directly and quantitatively relates the events developing in the acoustic and dislocation subsystems in the course of material plastic flow.

All the motions occurring in the deforming system should probably be determined by hybridized spectrum of elementary excitation to unify the dispersion curve for phonons and quasi-particles of localized plastic flow. Similar unified curve is shown schematically in Figure 2, which includes the straight line $\omega \approx V_S \cdot k$ for phonons and the quadratic parabola $\omega = \omega_0 + \alpha(k - k_0)^2$ [8] for localized plastic flow autowaves. The co-ordinates $\hat{\omega}$ and $\hat{\lambda}$ of the intersection point of these plots have the following meaning: $\hat{\omega}$ is close to the Debye frequency, i.e. $\hat{\omega} \approx \omega_D \approx 10^{13}$ Hz, whereas $\hat{k}$ corresponds to the minimal wavelength of the same order of magnitude as the spacing between close-packed planes in crystals, i.e. $\hat{\lambda} \approx \lambda_{\min} = 2\pi/k_{\max} \approx d$. Such coincidence is indirect evidence for the validity of plastic flow description as phonon gas interaction with localized plastic flow quasi-particles.

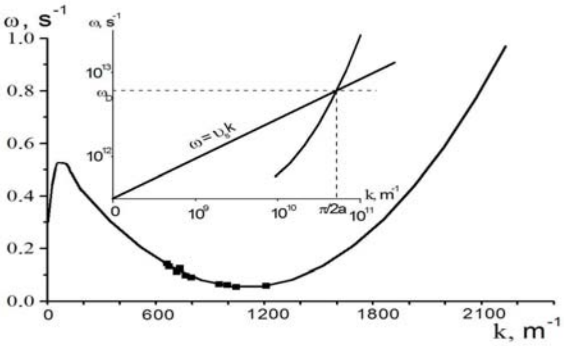

Figure 2. The hybridized elementary excitation spectrum

Conclusions

1. On the base of the above considerations a direct relationship has been established between the micro- and macro-scale characteristics of the deforming medium. In so doing, microscopic process parameters may be responsible for the generation of localized plastic flow autowaves having typically macroscopic length.
2. An inevitable step might be necessary to develop the above two-component model by invoking the idea that the plastic flow can be described as exchange phonon interaction between quasi-particles, corresponding to localized plastic flow autowaves.

Acknowledgements

This work was partly supported by the grants given to S.A. Barannikova by BRHE (No.TO-016-02), Russian Science Support Foundation and SB RAS (No.29) for young scientists.

References

1. L. B. Zuev and V. I. Danilov, Phil. Mag. A **79**, 43 (1999).
2. L. B. Zuev, Ann. Phys. **10**, 965 (2001).
3. H. Haken, *Information and Self-Organization. A Macroscopic Approach to Complex Systems* (Springer Verlag, Berlin, 1988).
4. J. P. Billingsley, Int. J. Solids Structures **38,** 4221 (2001).
5. L. B. Zuev, Int. J. Solids Structures **42**, 943 (2005).
6. Y. Imry, *Introduction to Mesoscopic Physics* (University Press, Oxford, 2002).
7. B. B. Kadomtsev, *Dynamics and Information* (UFN Publ., Moscow, 1997, in Russian).
8. S. A. Barannikova, Tech. Phys. Lett. **30**, 338 (2004).

Generalized Phase Field Modeling for Microstructural Evolutions in Irradiated Materials

A. Badillo, Y. Liu, P. Krasnochtchekov, R. S. Averback, P. Bellon

Department of Materials Science and Engineering, University of Illinois at Urbana-Champaign, 1304 W. Green St., Urbana, IL, 61801, USA; bellon@uiuc.edu

ABSTRACT

The potentials and the challenges of simulating the evolution of alloys under irradiation by phase field models are discussed. A simple energetic model is combined with a coarse graining approach to derive expressions for the required thermodynamics and kinetic quantities. Selected applications focus on the role of length scales and on the validity of using linearized equations in far-from-equilibrium situations.

1. Introduction

The evolution of microstructures in alloys under irradiation involves a wide range of time and length scales, from picoseconds and Angstroms for displacement cascades to decades and millimeters for segregation and precipitation reactions. While atomistic simulation methods have provided unique and valuable information, the range of relevant scales is so large that it is impossible to model the complete evolution of an alloy under irradiation by solely relying on these methods. Continuum methods such as phase field models, on the other hand, make it possible to reach long time scales and simulate large system sizes while accounting for diffusive and displacive processes, stress effects, and recently dislocations, but at the loss of some atomistic detail. Our goal is to develop and validate a robust phase field model that can be used for quantitative predictions of the evolution of the microstructure in irradiated alloys.

In this present work we consider the case of a binary alloy system with positive heat of mixing that is subjected to continuous irradiation. It is assumed that the nuclear collisions produced by irradiation lead to a ballistic, i.e., random, mixing of the two chemical species. This assumption is supported by experimental results for alloy systems with moderate heats of mixing, $\leq$ 10 kJ at the equiatomic composition, such as Ag-Cu and Co-Cu [1]. We use this simplified model to address here the following questions. First, all existing phase field models rely on the linear response theory to derive the rate of evolution of the fields describing the microstructure. While this linearization is valid near equilibrium, it remains to be proven that it can also be applied to far-from-equilibrium evolutions, in particular when the overall evolution of the microstructure results from competing dynamics, each of them dictated by different driving forces. Second, current phase field models rely on continuum field variables defined at an arbitrary scale, and they thus lack an intrinsic length scale; exceptions are the recent works by Mohri [2] and by Finel *et al.* [3]. This limitation has important consequences for irradiated alloys, since for the model to be realistic it must include the specificity of the various recoil spectra produced by irradiating particles. The hard recoil spectrum produced by heavy ions or neutrons, for instance, should translate into larger fluctuations of the field variables, and this can only be implemented if the absolute size of the cells used to define the field variables are known. Third, most phase field models do not explicitly consider point defects. This approximation is already questionable for evolutions during thermal annealing since it implies that vacancies are homogeneously distributed. It is clearly not suitable for the modeling of alloys under irradiation. Point defects, either isolated or clustered, must therefore be added to the list of variables describing the microstructure.

2. Phase field models for alloys subjected to ballistic mixing

In the first part of this article, we review briefly the limitations of current phase field models, which rely on phenomenological equations. We then propose to derive the phase field equation by coarse graining a simple atomistic model, where point defects are ignored. We then extend the model to take into account point defects and present some selected results.

2.1 Limitations of conventional phase field modeling

Phase field equations are usually derived from a phenomenological approach (see [4] for a recent review). In the case of a binary alloy described by its composition field, $C(\boldsymbol{r},t)$, the corresponding kinetic equation is the so-called Cahn-Hilliard diffusion equation and reads

$$\frac{\partial C(\mathbf{r},t)}{\partial t} = -\nabla\left(-M\nabla\frac{\delta F}{\delta C(\mathbf{r},t)}\right) \tag{1}$$

where $F\{C(\boldsymbol{r},t)\}$ is the free energy functional of the alloy system and M the atomic mobility. This equation is linear in the sense that the rate of evolution of C is directly proportional to the driving force for diffusion, the gradient of chemical potential, $\nabla(\delta F/\delta C)$. Following Cahn [5], $F\{C(\boldsymbol{r},t)\}$ is written as a volume integral containing two terms, a homogeneous free energy density, f, and an inhomogeneous term due to the existence of composition gradients:

$$F\{C(r,t)\} = \int_V \left(f + \kappa|\nabla C|^2\right)dV \tag{2}$$

where κ is the gradient energy coefficient. Inside the miscibility gap, the homogeneous free energy density is often described by a double-well potential, with an energy barrier between the two locally stable states referred to as Δf. There are situations where it is not sufficient to rely on the deterministic Eqn. (1), for instance, nucleation. Cook [6] proposed a phenomenological approach to add fluctuations by taking advantage of fluctuation-dissipation relationship, thus transforming Eqn. (1) into a Langevin-type equation

$$\frac{\partial C(\mathbf{r},t)}{\partial t} = -\nabla\left(-M\nabla\frac{\delta F}{\delta C(\mathbf{r},t)}\right) + \xi(\mathbf{r},t) \tag{3}$$

with the noise term satisfying the following equation

$$\left\langle \xi(\mathbf{r},t),\xi(\mathbf{r}',t')\right\rangle = -2k_B T M\nabla^2\delta(\mathbf{r}-\mathbf{r}')\delta(t-t') \tag{4}$$

This approach is however problematic, as it is observed that a straightforward application of Eqn. (4) leads to large and unphysical fluctuations [7]. A practical solution often implemented is rescaling the amplitude of the noise by some small factor. Such a practice, however, raises concerns about the validity of the results that are produced.

Phase field models fall into the category of diffuse-interface models. The model parameters Δf and κ play a determinant role regarding interfaces since it can be shown that the excess interfacial free energy scales as $\sigma \propto \sqrt{\Delta f \cdot \kappa}$, whereas the equilibrium interfacial width follows $\xi \propto \sqrt{\kappa / \Delta f}$. Eqns. (1) or (3) are solved by mapping the space onto a grid, and using an explicit or implicit solver to integrate the equations forward in time. In order to obtain a stable numerical integration, it is necessary for any interface to be spread over about five grid points. Experimental results and Monte Carlo simulations indicate that the equilibrium width of interfaces in phase separating systems under practical conditions may be as small as ≈1 nm. In order to reproduce this width, one would need to use grid spacing smaller than ≈0.2 nm. Such fine grid spacings, however, require cells that contain about one atom, a number that is incompatible with the volume required to define the continuous field variable $C(\boldsymbol{r},t)$ from a space and time coarse graining of atomistic information. One possible solution is to rely on a phase field crystal model [8], where the coarse graining is restricted to the time domain, but this approach results in unacceptable limits on the time scale and length scales that can be modeled. In conventional phase field models, one is thus left with the expedient of using interfacial widths that are larger than the physical ones. Typical values of cell sizes are 1 to a few nm, which are appropriate for interfacial widths exceeding 10 nm. An important verification is then to test the sensitivity of the results to the particular choice of interfacial width. In the case of solidification, such tests and the comparison with analytical solutions for sharp interfaces has led to the development of quantitative models [9]. In the case of solid-state transformations, however, such tests are not performed systematically.

An additional complication in the case of alloys under irradiation is that displacement cascades introduce various new length scales that are in the range of a few Angstroms to several nanometers. The chemical mixing forced by displacement cascades, for example, can be modeled by an exponential decay with a decay length, R which ranges from 1 Å to ≈ 4 Å [10], while disordered zones produced by cascades extend from sub-nanometric to ≈ 10 nm [11]. Finally, energetic displacement cascades produces point-defect clusters that are comprised of 2 to several tens of individual point defects. While the smaller clusters can migrate, the larger ones are essentially immobile, and they are likely to play an important role in the evolution of the microstructure during prolonged irradiation. If one were to ignore these three length scales introduced by displacement cascades, one would not be able to model the effect of recoil spectra on microstructural evolutions under irradiation. One empirical approach used by Enomoto *et al.* [12] for the study of the relocation distance R is to use artificially large values of R, extending over several grid points. As already noted, however, one needs then to demonstrate that the results can be extrapolated to realistic R-values by some rescaling.

2.2 Phase field model derived by a coarse graining approach

Many of the limitations of conventional phase field models are rooted in the phenomenological derivations of Eqns. (1,2). Langer [13] showed however that these phenomenological equations can be derived starting from a microscopic description and performing a coarse graining in time and space to define the field variables. It is assumed that within each cell the characteristic time required to reach local equilibrium is much faster than the time involved in the transfer of atomic occupancies from cells to cells. Langer did not use any particular model to describe the energetics of the alloy, and thus his derivation does not provide any insight on the homogeneous and inhomogeneous terms of the free energy functional implicit in Eqn. (2). We propose here to derive the kinetic equation for the composition field by combining a coarse graining approach, as in Langer's work, with a bond model for the energetics and the kinetics. Martin [14] showed that such a bond model can be used to derive analytically kinetic equations that are fully consistent with an energetic model, as well as to shed light on the definition of the mobility coefficient once the kinetic equation is linearized with respect to the driving force for diffusion.

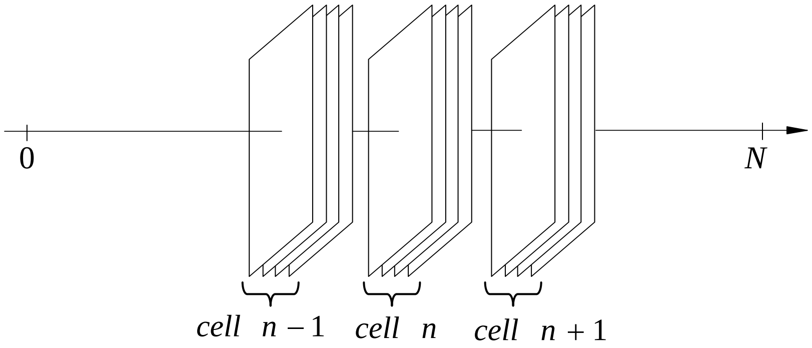

Figure 1. Schematic drawing of coarse graining in a one dimensional model.

Following Martin [14], we assume that the cohesion of the solid can be described by additive pairwise interaction energies between nearest neighbor A and B atoms, ε_{ij}, with i,j=A,B. In this section, for simplicity, we will ignore the point defects and assume that the kinetics is mediated by direct exchanges between atoms, either through thermally activated jumps at frequencies determined by rate theory, or by ballistic exchanges at frequency dictated by the irradiation flux and particle. Also for simplicity, we will derive the kinetic equations in one dimension, but the generalization to two- and three-dimensions is straightforward. The system is comprised of a stack of N planes of finite extension, each plane containing Ω atomic sites (see Fig. 1). The number of B atoms contained in plane p is designated by B_p. As a result of the coarse graining procedure, the planes are grouped into cells, each containing m planes. The B concentration in any given cell "n" is obtained by summing the number of B atoms located in all the planes belonging to a given cell, divided by mΩ:

$$C(n,t)=\sum_{p\in n}\frac{B_p}{m\Omega} \tag{5}$$

The excess internal energy of a composition profile **B** is calculated by a simple bond counting procedure, and the configurational entropy is estimated in the usual way, leading to

$$F(\mathbf{B})=m\Omega\left[Z\omega\sum_{n=1}^{N/m}C_n\overline{C_n}+\frac{\Omega_b}{m\Omega}z\omega\sum_{n=1}^{N/m}(C_{n+1}-C_n)^2+k_BT\sum_{n=1}^{N/m}(C_nLnC_n+\overline{C_n}Ln\overline{C_n})\right] \tag{6}$$

where $C_n=C(n,t)$, $\overline{C_n}=1-C_n$, Z is the total coordination number, e.g., Z=12 for an fcc lattice, z is the coordination number for bonds connecting atoms from adjacent cells, ω is the ordering energy defined as $\omega=\varepsilon_{AB}-(\varepsilon_{AA}+\varepsilon_{BB})/2$, and Ω_b is the number of atom sites in one cell that can form bonds with atoms belonging to adjacent cells. Periodic boundary conditions have been assumed in the derivation. In the case m=1, it is natural to choose $\Omega_b=\Omega$, and one recovers the free energy derived by Martin. This is expected since in Martin's model the continuous variables are defined by averaging the number of atoms within each single plane. This latter definition, however, makes it problematic to generalize the model in three dimensions. In contrast, with the present coarse graining approach, Eqn. (6) can be easily extended to two and three dimensions. The first remarkable result is that, if one transforms the sums in Eqn. (6) into integrals, the inhomogeneous term has exactly the dependence expected from the phenomenological Eqn. (2). The second remarkable property of the free energy is that, while the homogeneous internal energy term and the entropy are extensive quantities, i.e., proportional to $m\Omega$, the inhomogeneous contribution to the internal energy–the second term in the RHS of Eqn. (6), scales with Ω_b, the number of interfacial sites. The free energy expression given by Eqn. (6) for a discrete profile can be transformed to a continuous profile by using $(C_{n+1}-C_n)^2=(md)^2|\nabla C|^2$, where d is the interplanar spacing distance. By identification with Eqn. (2), the gradient energy coefficient κ is found to scale as

$$\kappa \propto m\frac{\Omega_b}{\Omega}d^2\omega \tag{7}$$

In particular, if one makes the choice that $\Omega_b=\Omega$, κ is a function of the coarse graining size, in contrast to the widely used phenomenological expression Eqn. (2). We note, however, that Finel [3] is proposing a new derivation of the phase field equation, also starting from a coarse graining of microscopic quantities, and he finds as well that κ depends on the size of the cells used for coarse graining.

The chemical potential corresponding to the free energy F is given by

$$\mu_n=\frac{1}{m\Omega}\frac{\partial F}{\partial C_n}=-2\omega\left(ZC_n+\frac{\Omega_b}{m\Omega}z\Delta C_n\right)+k_BT\ln\left(\frac{C_n}{\overline{\overline{C_n}}}\right) \tag{8}$$

In the partial derivative in Eqn. (8), one has to keep constant all concentrations in the other planes, as well as $\overline{C_n}$ to obtain the correct expression for the chemical potential.

Again, following Martin's procedure, we now derive the kinetic equation governing the evolution of the coarse grained variables C_n. The rate of change of B concentration in cell n is written as a divergence of net fluxes:

$$\frac{\partial C_n}{\partial t}=\frac{1}{m\Omega}\left(J_{n-1\to n}-J_{n\to n+1}\right) \tag{9}$$

with the net fluxes given by

$$\begin{aligned}J_{n-1\to n}&=\Omega_b\left[C_{n-1}(1-C_n)z\Gamma_{n-1\to n}-C_n(1-C_{n-1})z\Gamma_{n\to n-1}\right]\\ J_{n\to n+1}&=\Omega_b\left[C_n(1-C_{n+1})z\Gamma_{n\to n+1}-C_{n+1}(1-C_n)z\Gamma_{n+1\to n}\right]\end{aligned} \tag{10}$$

and the jump frequencies are a sum of thermally activated and ballistic exchanges

$$\Gamma_{n\to n+1}=\nu\exp\left(-\beta E_{n\to n+1}\right)+\Gamma_b \tag{11}$$

where Γ_b is the ballistic exchange frequency; here we assume that the ballistic mixing is restricted to adjacent cells. The activation energy for an A-B exchange between two adjacent cells is the energy required to break the bonds formed by these two atoms, minus the energy gained by placing the two atoms into a saddle point configuration, E_S. For simplicity, this term is here assumed to be a constant. This leads to

$$E_{n\to n+1} = E_s + Z\left[C_n\varepsilon_{BB} + (1-C_n)\varepsilon_{AB} + (1-C_{n+1})\varepsilon_{AA} + C_{n+1}\varepsilon_{AB}\right] + \frac{\Omega_b}{m\Omega} z\left[\Delta C_n(\varepsilon_{BB}-\varepsilon_{AB}) + \Delta C_{n+1}(\varepsilon_{AB}-\varepsilon_{AA})\right] \tag{12}$$

As in Martin's work, it can be shown that the net thermal fluxes are related to chemical potential gradients by applying Polkowicz's identity to the forward and backward components *p* and *q* of the net flux:

$$J^{th}_{n\to n+1} = p - q = \sqrt{pq}\left(\sqrt{p/q} - \sqrt{q/p}\right) \tag{13}$$

By identification with the chemical potential derived above, Eqn. (8), one finds that

$$J^{th}_{n\to n+1} = \Omega_b z\left(C_n\overline{C_n}C_{n+1}\overline{C_{n+1}}\right)^{1/2}\exp\left(-\frac{E_0}{k_BT}\right)\sinh\left(\frac{\mu_{n+1}-\mu_n}{k_BT}\right) \tag{14}$$

where, with the simplifying assumption $\varepsilon_{AA} = \varepsilon_{BB}$, E_0 is a constant involving the pairwise interactions. When the chemical potential gradient is small, one can linearize Eqn. (14) and recover kinetic equations that can be identified term by term to Eqns. (1-2). As emphasized by Martin, this procedure makes it possible to derive the expression of the mobility *M* as a function of the model parameters, instead of relying on a phenomenological expression.

In the presence of ballistic exchanges, a similar approach yields an expression for the effective chemical potential gradient that drives the overall net fluxes in the alloy

$$\frac{\mu^{eff}_{n+1} - \mu^{eff}_n}{k_BT} = Ln\frac{\Gamma_{n+1\to n} + \Gamma_b}{\Gamma_{n\to n+1} + \Gamma_b} + Ln\frac{C_{n+1}\overline{C_n}}{\overline{C_{n+1}}C_n} \tag{15}$$

This expression is analogous to one derived by Vaks and Kamyshenko [15] starting from a microscopic model and using a mean field approximation. We also note that the effective mobility is modified by the presence of ballistic exchanges.

2.3 Application to selected cases

The first issue raised in the introduction was that conventional phase field models lack intrinsic definition of absolute length scale. As seen from Eqns. (6-8), the coarse graining procedure yields explicit scale dependence, for the gradient energy term and for the atomic mobility. Similar results have been obtained by Finel [3]. Work is in progress to compare microstructures generated by this quantitative phase field model with atomistic Monte Carlo simulations.

The second issue raised is the validity of linearizing each kinetic contribution with respect to its own driving force, whereas the overall evolution of the microstructure is driven by a different, effective driving force. In order to carry out specific tests, we chose ω=67.8 meV, yielding a critical temperature T_C=1573 K, $\varepsilon_{AA} = \varepsilon_{BB}$, and we used the reduced ballistic jump frequency $\gamma_b = \Gamma_b/[\upsilon\exp(-E_s/k_BT)]$. In Fig. 2a, we present steady state composition profiles obtained by integrating numerically Eqns. (9-12) in one dimension using an implicit method with variable time step. The compositions of the two coexisting phases are then used to build steady-state phase diagrams, as exemplified in Fig. 2b. In Fig. 2, we compare results obtained with (i) the full kinetic model, (ii) a kinetic model where the thermal diffusion has been linearized, and (iii) using the effective temperature criterion introduced by Martin [16]. It is clearly seen that the linearized model, as well as the effective temperature model, provide excellent approximations of the correct steady-state phase diagram.

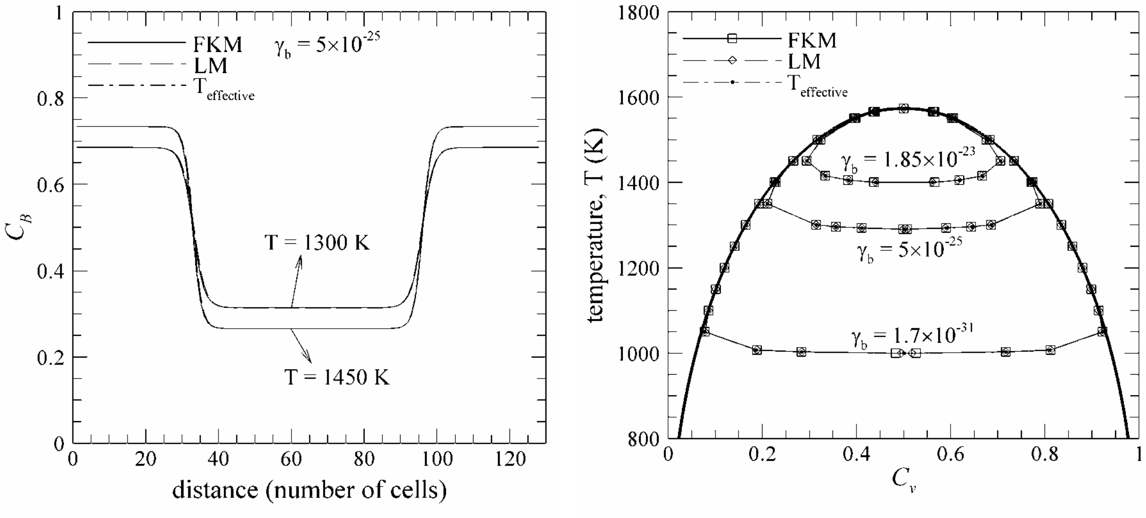

Figure 2. Steady state composition profiles (a, left) and steady-state phase diagrams (b, right) obtained at various temperatures and reduced ballistic frequency γ_b (see text for definition) using (i) the full kinetic model (FKM), (ii) the linearized model (LM), and (iii) the effective temperature criterion.

The procedure described in this section can be easily extended to three dimensions; it is also possible to include vacancies, interstitials, and defect clusters. For instance, Fig. 3 illustrates the decomposition of an alloy by the thermally activated migration of vacancies in a two-dimensional model at 1300 K. The details of these extensions will be presented elsewhere.

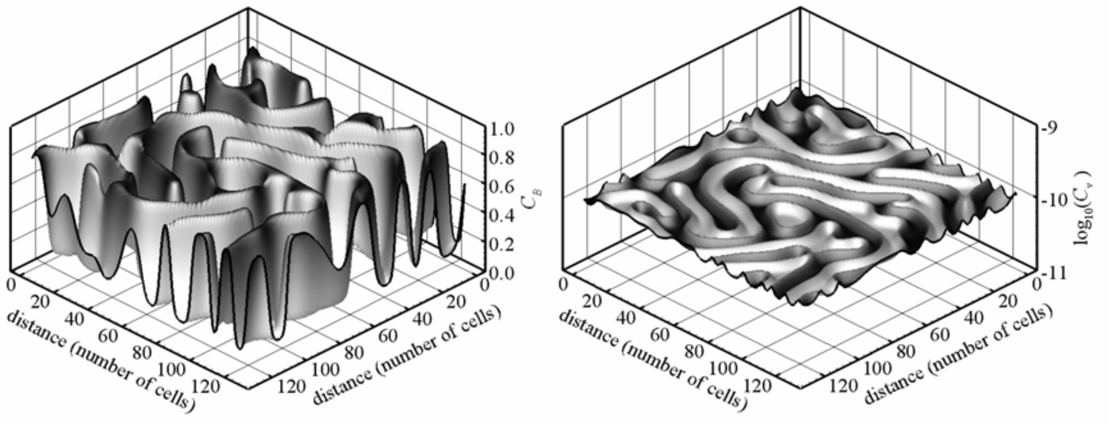

Figure 3. Composition field C_B (left) and vacancy concentration field (right) during thermal decomposition at 1300 K of a $A_{50}B_{50}$ alloy (same alloy parameters as in Fig. 2).

3. Conclusions

By combining a coarse graining of atomistic information and a pairwise interaction energetic model, we derive expressions for the free energy functional of an inhomogeneous alloy, and for the kinetic evolution of its composition field in the presence of short-range ballistic mixing. We show that this procedure yields gradient energy coefficient and atomic mobility that depends on the size of the volume used for coarse graining, thus introducing explicitly an absolute length scale in the model. In the presence of ballistic mixing, it is shown that the linearized kinetic equations provide a satisfactory approximation of the full evolution equations. The linearization also yields an analytical expression for the effective chemical potential gradient of the alloy under irradiation. The present derivation of phase field equations can be generalized to include point defects.

Acknowledgements

This material is based upon work supported by the U.S. Department of Energy, Division of Materials Sciences under Award No. DEFG02-05ER46217, through the Frederick Seitz Materials Research Laboratory at the University of Illinois at Urbana-Champaign

References

[1] P. Krasnochtchekov, R. S. Averback, P. Bellon, “Phase separation and dynamic patterning in $Cu_{1-x}Co_x$ films under ion irradiation”, Phys. Rev. B **72**, 174102 (2005).
[2] T. Mohri, in *Alloy Physics*, Edited by W. Pfeiler (Wiley-VCH, Weinheim), in press.
[3] A. Finel (private communication).
[4] L.-Q. Chen, “Phase-field models for microstructure evolution”, Annu. Rev. Mater. Res. **32**, 113 (2002).
[5] J. W. Chan and J. E. Hilliard, “Free energy of a nonuniform system. I. Interfacial free energy”, J. Chem Phys. **28**, 258 (1958).
[6] H. E. Cook, “Brownian motion in spinodal decomposition”, Acta Metall. **18**, 297 (1970).
[7] V. Yu. Dobretsov, I. R. Pankratov, and V. G. Vaks, “Stochastic description of phase separation near the spinodal curve in alloys”, JETP Lett. **80**, 602 (2005).
[8] K.-A. Wu, A. Karma, J. J. Hoyt, and M. Asta, “Ginzburg-Landau theory of crystalline anisotropy for bcc-liquid interfaces”, Phys. Rev. B **73**, 094101 (2006).
[9] B. Echebarria, R. Folch, A. Karma, and M. Plapp, “Quantitative phase-field model of alloy under solidification”, Phys. Rev. E **70**, 061604 (2004).
[10] R. A. Enrique, K. Nordlund, R. S. Averback, and P. Bellon, “Simulations of dynamical stabilization of Ag–Cu nanocomposites by ion-beam processing”, J. Appl. Phys. **93**, 2917 (2003).
[11] M. L. Jenkins and C. A. English, “Characterization of displacement cascade damage in ordered alloys using transmission electron-microscopy”, J. Nucl. Mater. **108-109**, 46 (1982).
[12] Y. Enomoto and M. Sawa, “Compositional patterning in irradiated immiscible alloys”, Surf. Sci. **514**, 68 (2002).
[13] J. S. Langer, “Theory of spinodal decomposition in alloys”, Ann. Phys. **65**, 53 (1971).
[14] G. Martin, “Atomic mobility in Cahn’s diffusion model”, Phys. Rev. B **41**, 2279 (1990).
[15] V. G. Vaks and V. V. Kamyshenko, “On the theory of open systems-Statistical thermodynamics and decomposition type phase-transitions for the model of an alloy uder irradiation”, Phys. Lett. **177**, 269 (1993).
[16] G. Martin, “Phase stability under irradiation: Ballistic effects”, Phys. Rev. B **30**, 1424 (1984).

Phase field modeling of the evolution of composition in a binary alloy under irradiation.

Pascal Bellon [1] , *Robert S. Averback* [1], *Arnoldo Badillo* [1], *Pavel Krasnochtchekov* [1], *Yang Liu* [1]

[1] *University of Illinois at Urbana-Champaign, 104. S. Goodwin Av., 61801 Urbana, United States of America*

We have developed a phase field model (PFM) to describe the coupled evolution of composition and point defects in a binary alloy subjected to sustained irradiation. Kinetics equations in conventional PFM are derived in the framework of the linear response theory. In irradiated materials, however, new processes such as the mixing forced by atomic collisions drive these systems into nonequilibrium configurations, and eventually into nonequilibrium steady states. Therefore, the evolution of the alloy is no longer controlled by the minimization of some thermodynamic potential. As a result, the validity of using a superposition of linearized kinetic terms to describe the overall kinetic evolution becomes questionable. Starting from a microscopic description of thermal and ballistic atomic jumps, we derive a fully non-linear kinetic equation for the evolution of the composition field. We also obtain linearized versions of this model, either by performing a global linearization, i.e., with respect to the total driving force that operates under irradiation, or by a piecewise linearization, i.e., where each kinetic term is linearized as if it were operating in the absence of the other processes. We performed a systematic numerical comparison of these three models by monitoring the kinetics of evolution and the steady state shape of interfaces in a model two-phase alloy with pairwise interactions. These results are also compared with lattice kinetic Monte Carlo simulations. Finally, KMC simulations are employed to evaluate the role of the coupling between interstitials and local composition on phase separation under irradiation.

Monte Carlo Simulation of Helium Thermal Desorption from Bcc Iron

V.A. Borodin[1], P.V. Vladimirov[2], A. Möslang[2]

[1]RRC Kurchatov Institute, 123182 Moscow, Russia, e-mail: borodin@dni.polyn.kiae.su;
[2]Forschungszentrum Karlsruhe GmbH, Institut für Materialforschung I, P.O. Box 36 40, 76021 Karlsruhe, Germany, e-mail: Pavel.Vladimirov@imf.fzk.de, Anton.Moeslang@imf.fzk.de

ABSTRACT

Computer simulation of thermal desorption of helium pre-implanted into bcc iron has been performed using kinetic lattice Monte Carlo with *ab initio* defect interaction parameters. Quick formation of vacancy-helium clusters occurs at relatively low temperatures and limits helium release from the sample up to temperature of at least 700°C.

1. Introduction

Ferritic-martensitic steels accumulate in radiation environment of fusion facilities noticeable amounts of helium. At hundreds appm of implanted helium and elevated temperatures pronounced helium clustering is possible, which bears potential risk of mechanical property degradation of irradiated steels. Thus investigations of helium clustering in ferritic steels are important for prediction of He effects on the steel radiation stability.

Recent first-principles calculations of formation, binding and migration energies for vacancies, He atoms and their clusters in bcc iron have demonstrated the presence of efficient binding between He atoms and vacancies, which extends to the second nearest neighbor (NN) separations [1,2]. Such interaction creates favorable conditions for the long-range diffusion of He-V clusters via the so-called “ring” mechanism. The accelerated diffusion of small He-vacancy clusters has indeed been demonstrated in a numeric experiment [3] and it is interesting to check, whether experimental evidences in its favor can be found. One such possibility can be provided by experiments on the kinetics of He thermal desorption from He-implanted iron.

The typical scheme of experiment includes the room temperature implantation of He into iron samples up to quite high doses (so that the peak concentrations of He atoms can vary from hundreds of ppm to tens of percent), followed by annealing at the permanently increasing temperature from the ambient one to values above 1000°C. The rate of He desorption during the annealing is measured and the peaks at the desorption curve indicate the activation energies of different He release processes occurring in the annealed sample. Thus, in an experiment on thermal annealing of 8 keV He implanted iron [4] a number of peaks are observed, some of which are tentatively interpreted by the authors and some are not. Thus the lowest energy peak (at 200-250°C) is interpreted as the desorption of subsurface He, the peaks at ~500 and 750°C are attributed to the decomposition of He-rich clusters He_nV (with $n > 1$) and He_nV_m ($n > m > 1$), respectively, a broad peak at 800-900°C is assumed to be due to either the detrapping of He atoms from substitutional positions or to $\alpha \rightarrow \gamma$ transformation in iron, while the peak at ~1100°C has got no interpretation at all.

This tentative attribution is not very convincing. For example, the decomposition of He-rich vacancies is doubtful. The reason is not that such clusters are impossible (according to some numerical calculations, a vacancy can easily adopt two He atoms and maybe more), but the fact that each incident ion creates a lot of Frenkel pairs (~40 for the conditions of the above mentioned experiment of Sugano et al. [4], as evidenced by calculations with the code TRIM) and thus an "ovepressurized" He-V complex can easily capture sufficient amount of vacancies and decrease the chances of He emission back into the bulk. The dissociation of substitutional He into a vacancy and interstitial He requires, according to recent calculations [2], more than 2 eV and as such is also not a very efficient process even at quite high temperatures.

Some alternative mechanisms have been proposed in the literature and include in particular He transport to the sample surface along short-cuts (e.g. dislocation cores [5]) or the diffusion of small He-vacancy clusters [6]. The release peaks at high temperatures can be also associated with distinct surface damage features (such as blisters) [7]. One of these explanations is in line with our resent demonstration of accelerated diffusion of small He-V clusters. Unfortunately, it is not a trivial task to associate this mechanism with that or other desorption peak. In order to do it, one might mimic a real experimental situation with lattice kinetic Monte-Carlo (LKMC) simulations of He thermal desorption with the use of the first principles energies of He and vacancy interaction in iron, without "external" fitting parameters, and to look how closely the simulation predictions fit the experimental observations. In this paper we report some of the first results of such numerical simulations with realistic He and vacancy parameters.

2. Simulation details and results

Our approach to simulation of He-vacancy cluster nucleation and growth in irradiated alpha-iron, which is considered as a model material with the behavior closely resembling that of real ferritic steels, is a typical example of multiscale approach, which combines the results of quantum mechanical (*ab-initio*) calculations of He-V cluster energies with the atomistic kinetic Monte-Carlo and provides the detailed description of He diffusion and clustering that can be further dealt with at longer timescales by rougher techniques (object KMC or standard rate theory).

Simulations in this work have been performed using our Monte-Carlo code CASINO-LKMC. The code implements "continuous time" algorithm, where each Monte-Carlo step represents one successful jump and the real time per each jump is tracked. The input parameters (He and vacancy binding energies) were taken from *ab initi*o calculations [1,2], which provide the most reliable up to date estimates of defect energies. The simulation cell of 256x64x64 lattice parameters, as shown in Fig.1, is elongated in x direction (sample depth). Open boundary condition along x-direction are used, so that a vacancy or He atom reaching these cell boundaries are immediately removed. In y and z directions the boundary conditions are periodic. The initial depth distribution of He atoms, as shown in the left part of Fig.1, nearly exactly reproduced the profile predicted by TRIM calculations. Vacancy distribution follows the TRIM shape, but the peak ratio V/He was reduced to 4:1, in order to take into account the fact that typically only ~10% of atomic displacements survive the intra-cascade annealing [8]. The computational cost of simulations, which required hundreds of millions of MC steps within one run, is quite high and only several already terminated annealing runs are discussed.

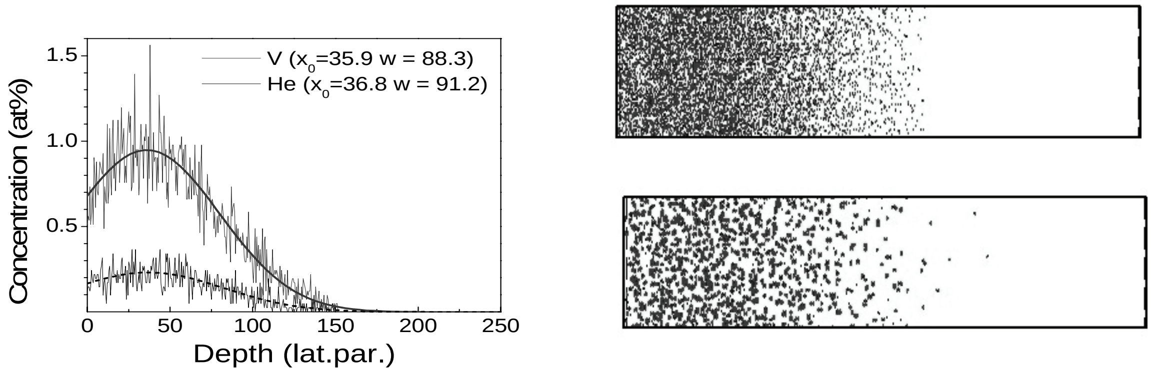

Figure 1. Left: Depth distribution of implanted He atoms (lower) and vacancies (upper curve), as predicted by TRIM for 8 keV He implantation up to $5x10^{14}$ He/cm^2 into iron. Right: Distribution of He atoms and vacancies in LKMC simulation cell: at the beginning of simulation (above) and after KMC annealing at 200°C for 0.2 s.

First of all, the annealing at 200°C was performed for as long as 0.2 s. By this time no vacancy monomers were left in the bulk, even though at the start of the simulation nearly all the vacancies were monomers. Very small amount of vacancies left the cell through the free surface, but the absolute majority formed clusters that contained relatively low content of He, see Fig. 2a. It is interesting to note that not only vacancy monomers, but pure vacancy clusters and He-V complexes with the sizes up to 4 disappeared (cluster size means here the number of lattice sites in the cluster, either empty of filled with He atoms). This results from the fact that such clusters are highly mobile [3] and coalesce with bigger ones.

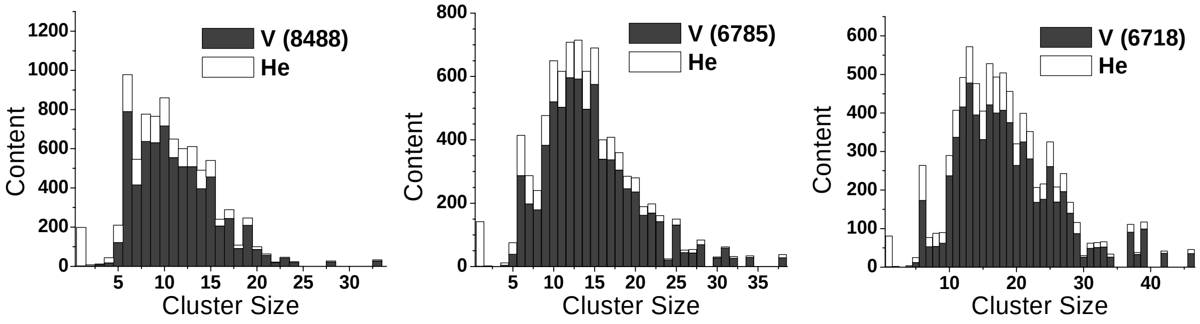

(a) **(b)** **(c)**

Figure 2. The content of point defects in clusters of different sizes after annealing at 200°C (a), 400°C (b) and 700°C (c). The relative parts of vacancies and He atoms within clusters of each particular size are shown in dark gray and white. The numbers in the legends indicate the total numbers of vacancies left in the simulation cell.

Only small amount of helium close to the free surface were lost. However, in real experiments the free surface is much larger than that of our simulation cell. Consequently helium leakage might be qualitatively consistent with the above mentioned interpretation of the experimentally observed weak He desorption peak at this temperature.

The final distribution of He-vacancy clusters obtained in the run at 200°C was used as a starting configuration for two runs at higher temperatures, namely at 400°C and 700°C. The final distributions of He clusters in the simulation cell are shown in Fig. 3. At both temperatures the active thermal emission of vacancies from clusters is observed, which results in the cluster ripening and the loss of vacancies at the free surface. As can be seen in the legends in Fig.2, the total loss of vacancies in both runs was comparable, which is due to the comparable numbers of MC steps at both temperatures. However, the ripening at 700°C is more pronounced, cf. Figs. 2b and 2c.

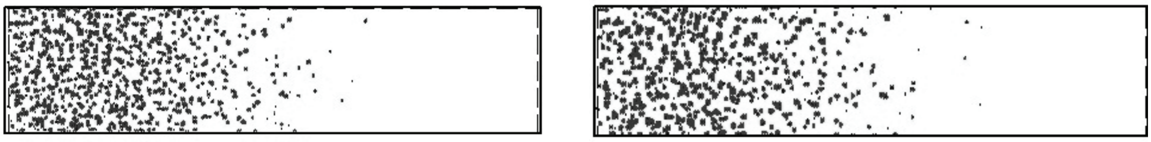

(a) **(b)**

Figure 3. The distribution of He-vacancy clusters in LKMC simulation cell after KMC annealing at 400°C for 1.7 ms (a) and at 700°C for 40 μs (b).

In contrast to the vacancy loss, the loss of He atoms was noticeably different. While practically no He emission was observed at 400°C, ~ 0.1% of helium atoms was lost during the run at 700°C. As can be judged from Figs.2b and c, the desorbed He involves mostly the atoms dissolved in the matrix in the form of substitutional monomers and the transport mechanism seems to be related to the formation of He-V pairs and their migration to the free sample surface.

3. Conclusions

He-V clustering during the linear annealing of helium ion implanted iron samples is dominated by the formation of small helium clusters at the very beginning of the temperature ramp and the ripening of the cluster ensemble at temperatures below at least 700°C. Very little part of implanted helium was lost at the surface during the KMC times reached. Yet, there is a clear trend of increasing He desorption when the temperature of 700°C is reached.

Acknowledgements

This research has been supported in part by the Russian Foundation of Basic Research through research grants #05-02-16994 and #06-08-81031. Part of the work was performed during a guest stay (V.A.B.) at Forschungszentrum Karlsruhe.

References

[1] C. Domain and C. S. Becquart, Ab initio calculations of defects in Fe and dilute Fe-Cu alloys, Phys. Rev. B, 65, 024103, 2001.
[2] C.-C. Fu and F. Willaime, Ab initio study of helium in α-Fe: Dissolution, migration, and clustering with vacancies, Phys. Rev. B, 72, 064117, 2005.
[3] V.A. Borodin, P.V. Vladimirov and A. Möslang, Lattice kinetic Monte-Carlo modelling of helium-vacancy cluster formation in bcc iron, Proc. 12th. Int. Conf. on Fusion Reactor Materials, to be published in J. Nucl. Mater.
[4] R. Sugano, K. Morishita and A. Kimura, Helium accumulation behavior in iron based model alloys, Fus. Sci. Technol. 44, 446, 2003.
[5] V.A. Borodin, V.M. Manichev and A.I. Ryazanov, The influence of dissociation of small helium-vacancy clusters on the growth of helium bubbles, the accumulation of helium at the grain boundaries and the kinetics of helium desorption from irradiated materials, J. Nucl. Mater., 154, 263, 1988.
[6] R. Vassen, H. Trinkaus and P. Jung, Helium desorption from Fe and V by atomic diffusion and bubble migration, Phys. Rev. B, 44, 4206, 1991.
[7] T. Yamauchi, S. Yamanaka and M. Miyake, Thermal release behavior of helium implanted into nickel, J. Nucl. Mater., 179-181, 308, 1991.
[8] R.E. Stoller, The role of cascade energy and temperature in primary defect formation in iron, J. Nucl. Mater., 276, 22, 2000.

The impact of point defects, small clusters and dislocations on the thermal conductivity and dimensional stability of 3C-SiC

Tjacka Bus [1], *Brian D. Wirth* [1], *Yutai Katoh* [1], *Lance L. Snead* [1]

[1] *University of California, Berkeley, 4151 Etcheverry Hall, 94720 Berkeley, United States of America*

Silicon carbide intrinsically displays excellent thermal conductivity, good dimensional stability and high strength at temperatures ranging from below room temperature to well above 1200º C, making it a candidate structural material for advanced fission and fusion reactors. Defects introduced during the manufacturing process and due to radiation exposure while in service, can significantly degrade the properties. In particular, the thermal conductivity degradation and swelling of neutron irradiated SiC are key issues which may limit its application in nuclear reactors. Recent neutron irradiation experiments suggest that the same type of defects is responsible for both swelling and loss of thermal conductivity, although the responsible defects and their evolution are not well understood. Following a brief review of atomistic simulations of point defect properties and displacement cascade evolution in 3C-SiC, we present results of molecular dynamics simulations to calculate the thermal conductivity and relaxation volume of perfect and defected 3C-SiC. The defects investigated include point defect clusters, dislocation dipoles and interstitial dislocation loops. The thermal conductivity was calculated using the Green-Kubo approach, as outlined by Li and co workers [Li et al., J. Nuc. Mat., 255 (1998) p139]. The results will be discussed in light of developing models of defect and property evolution of SiC under fusion relevant conditions.

Modeling radiation damage in FeCr alloys.

Alfredo Caro[1], *M. Caro*[1], *S. G. Srivilliputhur*[2], *D. A. Crowson*[3], *E. M. Lopasso*[4]

[1]*Lawrence Livermore National Laboratory, 7000 East Avenue, CA 94550 Livermore, United States of America*
[2]*Los Alamos National Laboratory, 87545 Los Alamos, United States of America*
[3]*Virginia Polytechnic Institute and State University, 24061 Blaksburg, United States of America*
[4]*Centro Atomico Bariloche, 8400 Bariloche, Argentina*

FeCr alloys are the base of steels used for nuclear applications. Modeling its behavior under irradiation is a challenge due to its complex nature originated in its magnetic structure. Recent ab initio results show how magnetic frustration effects account for the change in sign of the formation energy of the alloy, which in turn is at the basis of the change from ordering to segregation tendency observed at low Cr composition, in the range used in nuclear applications.

In this presentation I review our work on this system, in particular, the alloy potential, the properties of solutes, the properties of intrinsic point defects, the implications of the ab initio energetics on its phase diagram, nucleation and growth of α′ precipitates, and its behavior under irradiation:

- We developed a general formalism to construct empirical potentials for the alloy that mimic the formation energy obtained ab initio, in particular its change in sign and non- symmetric character. The alloy potential correctly predicts the inversion of order found experimentally, the ab initio results for Cr-Cr interaction vs distance, and predicts the properties of the vacancy and interstitials as a function of composition [A. C. et al. PRL 95, 075702 (2005)].

- With a computational thermodynamic package that we developed to find free energies of empirical potentials [A. C. et al. JNM 349, 317 (2006)], we predict the new location of the miscibility gap in the ferromagnetic phase of the alloy and find that ab initio results have strong influence on the solubility limit at the temperature of interest for nuclear applications [A. C. et al. APL in press].

- With our recently developed massive parallel Monte Carlo code in the transmutation ensemble with displacements, we study the nucleation and growth processes involved in the α′ precipitation. We analyze homogeneous and heterogeneous precipitation and discuss its implications for embritlement.

- With the implementation of the new potential in Lammps, we are analyzing the early stagers of radiation damage in the alloy at various compositions, in particular the nature of the defects surviving the thermal phase of the collision cascades.

This work was performed under the auspices of the U.S. Department of Energy by the University of California, Lawrence Livermore National Laboratory under Contract No. W-7405-Eng-48.

Spatial correlation effects in irradiated materials: rate theory vs. kinetic Monte Carlo simulations

C. J. Ortiz, **M. J. Caturla**

Dept. de Física Aplicada, Universidad de Alicante, Alicante E-03690, Spain

ABSTRACT

We have developed a rate theory (RT) model to study the evolution of defects produced during irradiation in metals such as Fe. These types of models are based on a mean field approach and can treat very efficiently the evolution of damage in time. However, this approximation implies a loss of spatial correlation between defects. Kinetic Monte Carlo (kMC) models, on the other hand, include the position of every defect produced and therefore correlations are taken into account. This gain in accuracy results in longer computational effort, in particular for high irradiation dose or long annealing times. Coupling between these two simulation methods is therefore desirable, but in order to do this coupling it is necessary to know their limitations and when to apply each model. We compare kMC and RT calculations for different irradiation conditions. We consider a case where only Frenkel pairs are produced, such as under electron irradiation. The evolution of defects under isochronal annealing is obtained and the two models are compared. We are currently studying the case when clusters of defects are directly produced during the irradiation, such as in the case of heavy ion implantation. Parameters of the model are obtained from *ab initio* calculations and molecular dynamics simulations and results are compared with available experimental data.

1. Introduction

Rate theory (RT) models can treat very efficiently the diffusion of defects in solids. However, this mean field approach includes a series of approximations, such as the lack of spatial correlations. When defects are produced by irradiation, such as electron or ion irradiation, or in the case of fusion and fission reactors by neutron irradiation, there is a certain spatial correlation between the defects created. Therefore, the approximations in the model must be analyzed under these conditions. Calculations by J. Dalla Torre *et. al* [1] have indeed shown the importance of these correlations in modeling electron irradiation of Fe by comparing kinetic Monte Carlo (kMC) calculations, where these correlations are included, and cluster dynamics.

We present kMC and RT calculations of electron irradiated Fe during isochronal annealing. The effect of lack of correlation on the position of the annealing stages is checked within the same model, that is, using only kMC calculations. The results of kMC are also compared to the RT calculations.

2. Rate theory and kinetic Monte Carlo models

A RT model has been developed that includes the following interactions between defects:

1 Self-interstitials can interact with each other to create self-interstitial clusters
$I_n + I \rightarrow I_{n+1}$ where n is the number of interstitials in a cluster
2 The same reaction can occur among vacancies creating vacancy clusters:
$V_n + V \rightarrow V_{n+1}$ where n is the number of vacancies in a cluster
3 Bulk recombination between self-interstitials and clusters:
$V + I \rightarrow 0$
4 Recombination between vacancies and interstitial clusters are also included:
$I_n + V \rightarrow I_{n-1}$

The kinetic Monte Carlo has been explained elsewhere [2]. The input parameters for both the kMC and the RT model are those described in reference [3].

Electron irradiation of Fe: resistivity curve with kMC and RT

Calculations of defect evolution during isochronal annealing of electron irradiated Fe have been performed using both kMC and RT, similarly to references [1, 3]. The initial defect concentration in the kMC simulations is introduced through a distribution of Frenkel pairs while a homogeneous concentration of vacancies and self-interstitials is used in the RT model. A dose of 2×10^{-6} dpa is considered in both cases. The concentration of vacancies and self-interstitials is followed during annealing starting with a temperature of 77.2 K and increasing the temperature by 3% every 300s, similarly to experiments in reference [4]. The derivative of the total number of defects with temperature is obtained to identify the different annealing stages. The changes in the position and height of these peaks depending on the simulation method or initial conditions are analyzed.

In order to study the expected shifts in the position of these peaks due to the absence of spatial correlations we have made used of kMC simulations alone. In this way there are no issues regarding the parameters used in the two models or the approximations, and therefore the differences obtained are only due to the existence or absence of this correlation. To perform this study two different initial conditions are considered. On one hand Frenkel pairs are generated with an average distance between vacancies and self-interstitials of 1.5nm, that is, close to the I-V recombination distance obtained experimentally [4]. On a second simulation the average distance between Frenkel pairs was set to 5.7nm, in order to eliminate correlated recombination. Fig. 1(a) shows the total number of defects as a function of temperature for the two kMC simulations, while Fig. 1(b) shows the derivative of these curves with temperature. The different recovery stages can be observed from this second figure, where ID2 corresponds to correlated recombination, IE to uncorrelated recombination, II to di-interstitial cluster migration and III to vacancy migration, following the nomenclature of reference [3]. From Fig. 1(a) it can be observed that the total number of defects when there is no-close recombination between I-V is higher than when this correlation is taken into account, as expected. Consequently, the peak corresponding to stage ID2 is not present when the initial distance between

I-V is very large, and the subsequent peaks are more intense. This observation is in agreement with the calculations in reference [1] where kMC and RT are compared. However, unlike in that work, the position of the peaks does not change significantly between these two cases.

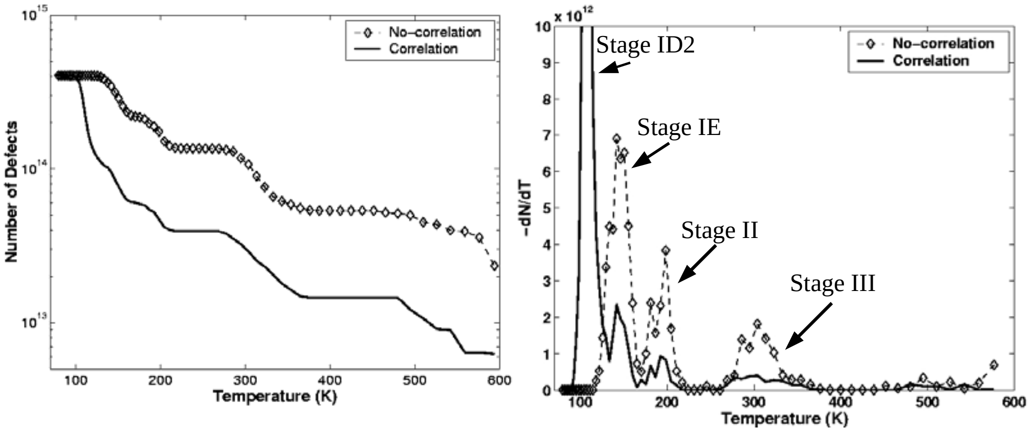

(a) *(b)*

Figure 1: (a) Number of defects as a function of temperature for isochronal anneal and (b) derivative of the number of defects with temperature. KMC with and without correlation between V and I.

The RT model has also been compared to kMC calculations using the same input parameters for defect mobility and binding energies. However, the RT model developed at this point did not include the mobility of clusters, only the mobility of single defects. Therefore, in order to compare the two models kMC calculations have been performed also considering all clusters immobile. Figure 2 shows the derivative of the total number of defects with temperature obtained from RT (solid line) and from kMC calculations (triangles). The kMC calculations result in three peaks. The first peak is related to the correlation between close Frenkel-pairs (stage ID2), the second peak is due to the mobility of the self-interstitial or uncorrelated recombination (stage IE) and the third peak is related to the mobility of the vacancy (stage III). As mentioned above, since the mobility of di-interstitials or other clusters of defects is not included stage II does not occur in these calculations. The RT calculation only shows two peaks: one for stage IE and one for stage III. That is, as expected, stage ID2 related to spatial correlations between vacancies and interstitials can not be reproduced by a RT model, as already pointed out in reference [1]. Since this recombination does not occur, the total number of defects in the RT model is much higher than those predicted by the kMC, as can be observed by the much higher peaks obtained from the RT calculations. Notice also that there is a slight shift in the position of the peaks for stage IE and III between RT and kMC, with lower temperature values for kMC. This shift, however, is much smaller than those reported earlier in similar comparisons [1].

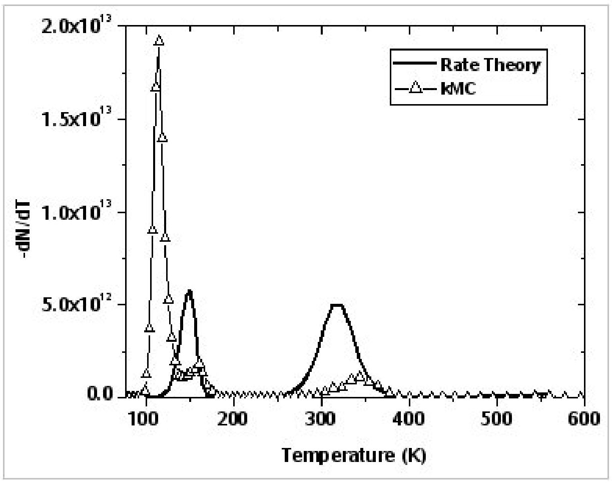

Figure 2: Annealing stages obtained from RT (solid lines) and kMC calculations (triangles).

Clusters of all sizes considered immobile.

4. Conclusions

Comparison using the same model, kMC, with and without spatial correlation between Frenkel-pairs shows the same position for the annealing stages of electron irradiated Fe and a different height of these peaks due to the difference in defect concentration. Comparison between kMC and RT shows the lack of spacial correlation in the later, and a slight shift of the peaks. This shift could be related to differences between the parameters used in the two models, in particular, pre-factors or capture radius. The differences however, are very small. Calculations including clusters of defects, such as those produced under ion irradiation, are being performed.

Acknowledgments

Thanks to C. C. Fu and F. Willaime for useful discussions. This work has been supported by the EC though the integrated project PERFECT and the EURATOM fellowship TOOLSPIE. One of the authors (MJC) thanks the Spanish MEC for support under the Ramón y Cajal program.

References

[1] J. Dalla Torre, C. C. Fu, F. Willaime, A. Barbu, J.-L. Bocquet, “Resistivity recovery simulations of electron-irradiated iron:kinetic Monte Carlo versus Cluster Dynamics”, J. of Nuclear Materials, in press.
[2] M. J. Caturla, N. Soneda, E. Alonso, B. D. Wirth, T. Diaz de la Rubia, J. M. Perlado, “Comparative study of radiation damage accumulation inCu and Fe”, J. of Nucl. Mater. **276** (2000) 13
[3] C. C. Fu, J. Dalla Torre, F. Willaime, J. L. Bocquet, A. Barbu, “ Multiscale modelling of defect kinetics in irradiated iron”, Nature Materials 4 (2005) 68
[4] S. Takaki, J. Fuss, J. Kugler, U. Dedek, H. Schultz, “The resistivity recovery of high purity and carbon doped iron following low temperature electron irradiation”, Radiat. Eff. **79** (1983) 87

Influence of Carbon impurities on He migration and clustering in α-Fe

M. J. Caturla[1], **C. C. Fu**[2], **C. J. Ortiz**[1], **F. Willaime**[2]

[1] **Dept. Física Aplicada, Universidad de Alicante, Alicante E-03690, Spain**
[2]**Service de Recherches de Métallurgie Physique, CEA/Saclay, 91191 Gif-sur-Yvette Cedex, France**

ABSTRACT

It is well known that impurities affect the migration of intrinsic defects in metals. In particular, Carbon is a common impurity in Fe that can significantly affect the mobility of vacancies. On the other hand, under fusion irradiation conditions high levels of He will be produced. Helium can interact with vacancies produced during irradiation and nucleate He-vacancy clusters that can affect the mechanical properties of the material. Therefore, in order to develop a predictive model of damage evolution in Fe it is necessary to understand the interaction between intrinsic defects (vacancies and self-interstitials), C and He. We have used kinetic Monte Carlo (kMC) together with a rate theory (RT) model to study He desorption from irradiated Fe during isothermal annealing. The results have been compared to experimental measurements. From these calculations conclusions are drawn about the effect of impurities on defect diffusion. Density functional theory calculations were performed to investigate the migration mechanisms and activation energies of He as well as C in Fe. The binding energies of small He-vacancy clusters and how they are affected by the presence of carbon were also studied. This information is now being included in the kMC and RT models.

1. Introduction

Understanding the effect of He in metals is crucial for the development of materials resistant to irradiation under fusion and fission conditions. Although the basic He migration mechanisms are well known since many years [1], due to the complexity of the problem there are still many unknowns regarding He migration in the presence of defects [2]. Based on *ab initio* calculations [3], which provide accurate values for the binding energies of He-vacancy clusters, we have developed a kinetic model to follow the evolution of defects produced during irradiation of Fe in the presence of He. This model allows us to compare directly with experimental observations, providing information about the different migration mechanisms, as well as the initial stages of nucleation of He-vacancy clusters, pre-cursors of bubbles and voids.

The migration of self-interstitial clusters in metals is one of the controversial points in modeling damage accumulation. In Fe in particular it is known from *ab initio* calculations [4] that small interstitial clusters are mobile, while the mobility of larger clusters has been studied with empirical potentials by several authors [5, 6]. This information has then been used to study damage evolution using rate theory or kinetic Monte Carlo models. However, Domain et al. [7] have shown that in order to reproduce neutron irradiation experiments using kMC it is necessary to introduce the presence of traps for these mobile self-interstitial clusters.

In this paper we present rate theory calculations of He desorption from implanted Fe under isothermal annealing. The assumptions of the model will be discussed. In particular, the effect of self-interstitial cluster mobility on these calculations will be studied using an object kinetic Monte Carlo model (OKMC). We discuss the results in terms of the possible effects of traps such as Carbon and conclude describing the current calculations that include He-C-Fe interactions obtained from *ab initio* simulations.

2. Thermal desorption of He from Fe: rate theory calculations

A rate theory model has been developed that includes the interaction between vacancies, self-interstitials and He. Therefore it includes the formation of He-vacancy complexes. In this model only single vacancies and single self-interstitials as well as He at interstitial positions (He_i) are mobile, while all other defects are immobile. He at substitutional places (He_s) can move into an interstitial position, and therefore migrate, through either the dissociative mechanism o by interaction with a self-interstitial atom. Migration energies for I and He_i as well as formation energies of I_n, V_n and He_nV_p clusters (where *n* and *p* are the number of defects in the cluster) are taken from *ab initio* [3, 4]. For the case of single V, effective formation and migration energies of 1.6 and 1.1 eV were used, respectively.

Using the model described above we have simulated the desorption experiments carried out by Vassen *et al.* [8]. Briefly, in these experiments the authors investigated thermal desorption of helium from homogeneously implanted iron during isothermal annealing for various temperatures, foil thicknesses and initial He concentrations. To determine the initial concentration of point defects generated by the irradiation process, we performed TRIM simulations which indicate that on average 200 I-V pairs are generated per implanted He. Considering the defects present after irradiation, *i.e.*, $He_{i,}$ I and V, we first simulated the evolution of the system at room temperature (300 K) until steady state is reached. These simulations show that after steady state is reached at room temperature, most of the $He_{i,}$ atoms have recombined with vacancies and are at substitutional sites. As expected, simulations confirm that most vacancies persist as isolated defects at room temperature, due to their relatively high migration energy. Finally, our model predicts that at room temperature, most self-interstitial atoms that are created during implantation diffuse and agglomerate into small I_n clusters. This result is expected since I are mobile at low temperature and clusters can not dissociate at 300 K. In summary, at 300 K, the main defects are He_s , V and I_n.

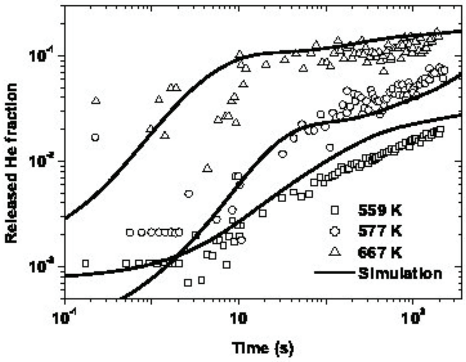

Figure 1: Released He fraction from implanted Fe during isothermal annealing. Results of experiments by Vassen [8] (points) together with RT calculations (lines).

After the 300 K calculation, He desorption during isothermal anneal was simulated for the experimental conditions described in ref.[8]. In Fig. 1 we present the simulated released fraction of implanted He for isothermal annealing at temperatures of 559, 577 and 667 K. The experimental data obtained by Vassen [8] are also reported for comparison. As we can see, our model is in good agreement with the experimental observations and describes all the different phases of He desorption. Three different regimes can be observed, an initial plateau (not observed for the highest temperature), followed by a rapid He release and a slower desorption rate at later times.

As explained above after the room temperature anneal, all He is located at substitutional sites. The migration of He must be either through the dissociative mechanism, where a He at a substitutional site moves into an interstitial site leaving a vacancy behind, or through the replacement mechanism, where a He at a substitutional site is replaced by a self-interstitial produced by the irradiation and the He again ends up at an interstitial position. In order to check the influence of this last mechanism we have performed calculations where it is suppressed. We simulated the He desorption at 559 and 667 K, without including self-interstitials. As initial conditions we considered that only He_i and V are present, as assumed in ref. [8]. As shown in Fig. 2, with this assumption we observe large differences, pointing to the significant contribution of the replacement mechanism to He migration in Fe under these conditions.

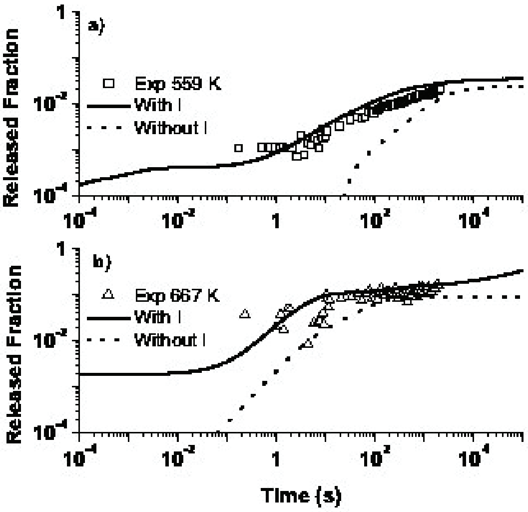

Figure 2: Released He fraction from implanted Fe. Influence of the replacement mechanism. Solid lines include this mechanism while dashed lines do not. Points are the experimental data by Vassen [8] for comparison.

3. Effect of self-interstitial cluster migration: Object kinetic Monte Carlo calculations

Several are the assumptions included in the RT model above. In particular, all self-interstitial and vacancy clusters are considered immobile, while, as explained in the introduction, both *ab initio* and calculations with empirical potentials have shown the mobility of these clusters. We have used OKMC calculations to check the effect of this mobility on the fraction of He released during isothermal annealing. Fig. 3 shows the fraction of He released as a function of time obtained for a 2.6μm thickness sample annealed at 667K for an initial He concentration of 0.109 at. ppm. The curves shown are the result of three different assumptions for self-interstitial cluster migration: (a) only single self-interstitial is mobile, (b) single self-interstitial (I), self-interstitial cluster of size two (I_2) and of size three (I_3) are mobile and (c) self-interstitial clusters of all sizes are mobile. For this last case the mobilities used are the *ab initio* values of [5] for sizes 1, 2 and 3, and the values obtained by Soneda [6] for clusters larger than 3. It is clear from this figure that the mobility of self-interstitial clusters plays a very significant role on He desorption. Helium is released at very short times when all self-interstitial clusters are considered immobile. Including mobile self-interstitial clusters delays the release of He by orders of magnitude.

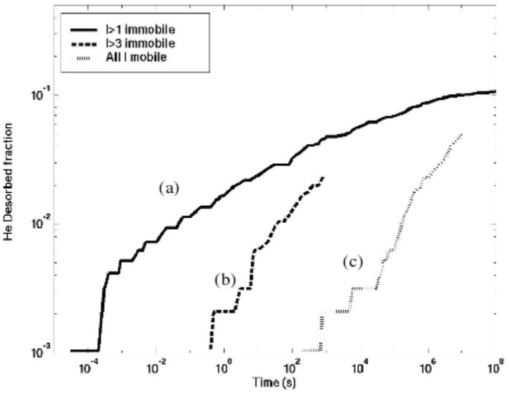

Figure 3: Released He fraction from OkMC. Influence of I_n migration.

4. Conclusions and current work

The simulations presented here show that the fraction of He released from implanted Fe at different temperatures can be modeled using a rate theory approach. However, several assumptions must be included. On one hand, the mobility of self-interstitial clusters affect the fraction of released He and results are in better agreement with experiments when these clusters are considered immobile. This is in agreement with other kMC calculations, where also large self-interstitial clusters are considered immobile or trapped to impurities [4,7]. On the other hand the values for vacancy migration energy and vacancy formation energy have been modified with respect to the *ab initio* values. The higher migration energy for vacancies can be explained by the presence of C which traps vacancies. We are currently studying the effect of Carbon on the stability of He-V clusters using data from *ab initio* calculations of He-V-C complexes.

Acknowledgments

M.J. Caturla thanks the Spanish MEC for support under the Ramón y Cajal program. C. J. Ortiz acknowledges the EC for support through the Euratom Fellowship FI60-012648.

References

[1] L.K. Mansur, E.H. Lee, P.J. Maziasz, A.P. Rowcliffe, J. Nucl. Mater. **141-143**, 633 (1986)
[2] H. Trinkaus, B. N. Singh, J. Nucl. Mater. **323**, 229 (2003)
[3] C. C. Fu and F. Willaime, Phys. Rev. B **72**, 064117 (2005)
[4] C. C. Fu, J. Dalla Torre, F. Willaime, J. L. Bocquet, A. Barbu, " Multiscale modelling of defect kinetics in irradiated iron", Nature Materials **4** (2005) 68
[5] B. D. Wirth, G. R. Odette, D. Maroudas, G. E. Lucas, J. Nucl. Mater. **276** (2000) 33
[6] N. Soneda & T. Diaz de la Rubia, Phil. Mag. **A 81** (2001) 331
[7] C. Domain, C. S. Becquart, L. Malerba, J. of Nucl. Mater. **335** (2004) 121 – 145
[8] R. Vassen, H. Trinkaus, P. Jung, Phys. Rev. B **44**, 4206 (1991)

3-D atomic-scale experimental and modelling studies of copper precipitation in low alloy steels

Alfred Cerezo[1], *S. Hirosawa*[1], *A. Morley*[1], *G. Sha*[1], *G. D. W. Smith*[1]

[1]*University of Oxford, Parks Road, OX1 3PH, Oxford, United Kingdom*

The 3-dimensional atom probe (3DAP) is a powerful tool for investigating the early stages of diffusional phase transformations. Kinetic Monte Carlo (KMC) simulations are increasingly being used to study diffusional phase transformations of alloys, by modelling realistic atomic-scale diffusion processes over appropriate timescales. By combining 3DAP analysis with KMC simulations, it is possible to compare directly atomic-scale observations with atomistic modelling. The model allows time and temperature regimes to be explored that are inaccessible to experiment, and also has the potential for helping in the design of new materials and heat treatments.

The present work is a combined 3DAP and KMC study of copper embrittlement in reactor pressure vessels (RPV) steels during thermal ageing. A number of commercial alloy compositions, representative of RPV weld and plate material, have been thermally aged for up to 5 years at temperatures in the range 608K to 678K. Alloy microstructures have been characterised on the nanometre scale with 3DAP, and the results compared with KMC simulations of the precipitation process. For these complex alloys, it has been necessary to simplify the interatomic potentials used, and the model is based on nearest neighbour pairwise interactions. Nonetheless, the KMC simulation accurately reproduces the development of precipitate size and density, and the temperature dependence of segregation to the precipitate-matrix interface. Based on the potentials in the model, it is possible to predict the elements that are likely to segregate to the precipitate/matrix interface and so enhance the nucleation rate. The model also provides new insights into pre-precipitation clustering of Mn and Ni, and the cluster assisted nucleation of the Cu precipitates. It seems likely that synergistic effects such as these are of widespread importance in precipitation processes in multicomponent systems, but until recently there has been very little experimental or theoretical basis for understanding such phenomena.

Crack nucleation from dislocation-grain boundary interaction in tungsten

Yuanfeng Cheng[1], *Matous Mrovec*[2], *Peter Gumbsch*[1,2]

[1]*Institut für Zuverlässigkeit von Bauteilen und Systemen, Universität Karlsruhe (TH), Kaiserstrasse 12, 76131 Karlsruhe, Germany*

[2]*Fraunhofer-Institut für Werkstoffmechanik IWM, Woehlerstrasse 11, 79108 Freiburg, Germany*

Without preexisting flaws, crack nucleation is the starting point of mechanical failure in brittle metals. Twin intersections and dislocation-grain boundary interaction are believed to be the decisive processes. Using the Finnis-Sinclair interatomic potential for tungsten we have studied crack nucleations at selected grain boundaries and from the interaction of dislocations with grain boundaries. When a dislocation is absorbed by a grain boundary, stress concentration develops at the absorbing site and crack nucleation is significantly facilitated under an applied stress. To establish an atomistically motivated criterion, crack nucleation is investigated under both uniaxial and biaxial loading conditions.

Dislocation interaction with the local stress field of a ∑9 tilt grain boundary in body centred cubic tungsten

Yuanfeng Cheng[1], **Matous Mrovec**[1,2], **Peter Gumbsch**[1,2]

[1]IZBS, Universität Karlsruhe (TH), 76131 Karlsruhe, Germany; email: yfen@izbs.uni-karlsruhe.de; [2]Fraunhofer-Institut für Werkstoffmechanik, 79108 Freiburg, Germany

ABSTRACT

We report the results of a molecular dynamics study of the interaction between edge dislocations and a ∑9{221}⟨110⟩ tilt grain boundary in body centred cubic (bcc) tungsten using the Finnis-Sinclair interatomic potential. Our simulations have revealed that the outcome of the dislocation/grain boundary interaction depends sensitively on the precise position of dislocation impact into the grain boundary. As the dislocation approaches the grain boundary, its stress field interacts with the local stress field of the grain boundary which can lead to a rearrangement of atoms within the grain boundary and result in dislocation absorption. At other locations in the boundary such rearrangements do not occur and the dislocation is transmitted. A detailed analysis of grain boundary structure and local stresses during dislocation absorption and transmission is presented.

1. Introduction

Grain boundaries play an important role in controlling mechanical strength of polycrystalline metals since they can act as dislocation barriers, as sinks or as sources of dislocations[1-2]. Dislocation/grain boundary interaction is usually regarded as a combination of elastic interactions due to image forces from elastic anisotropy between the participating grains and atomistic effects. The latter are mainly due to changes in the Burgers vector of the dislocation as it attempts to pass through the grain boundary but may also be generically atomistic in origin[2].

2. Simulation Setup

An a/2⟨111⟩ edge dislocation is introduced into one grain of a tungsten bicrystal containing a ∑9{221}⟨110⟩ tilt grain boundary. The orientation of the left grain is x_1 [2-21], y_1 [-114], z [-1-10], the orientation of the right grain is x_2 [2-2-1], y_2 [1-14], z [-1-10]. Periodic boundary conditions of minimal length are applied in the z-direction. Simple shear is applied to the bicrystal by rigidly displacing the upper- and lowermost layers of the simulation cell in x-direction. The shear strain is applied in steps of 0.05%. The structure is relaxed at every step using a recently developed relaxation scheme[3]. The Finnis-Sinclair potential for tungsten[4] is applied to describe the atomic interactions. Local atomic stress is calculated following the description in [5].

3. Results and Discussion

The structure of the grain boundary and the hydrostatic stress field are shown in Fig. 1. A region of high stresses is clearly visible in the immediate vicinity of the grain boundary extending only a few atomic layers to either side.

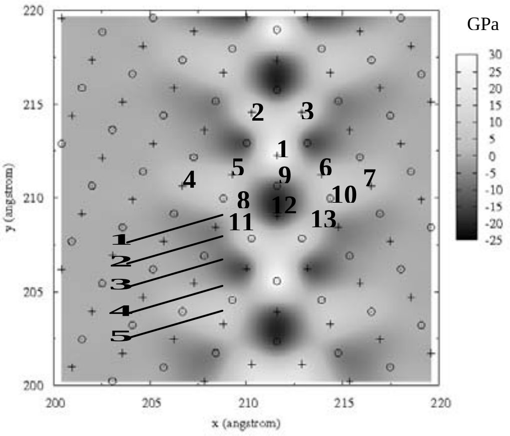

Figure 1. Hydrostatic stress field of the grain boundary. Bright shading indicates compression, black indicates tension. Atoms are shown as circles or crosses for different height in viewing direction. Also indicated are 5 different (-112) glide planes ending within one structural unit repeat distance.

An edge dislocation approaching the grain boundary on glide plane 1 arrives at allocation in the boundary where the stress field of the boundary has the same sign as the stress field of the dislocation itself. Consequently, the dislocation is repelled by the boundary and stopped about 6 Å before reaching the boundary as in Fig. 2(a1). The transmission is a stick-slip process (Fig. 3) and accompanied by migration of the lower part of the grain boundary (Fig. 2(a2)).

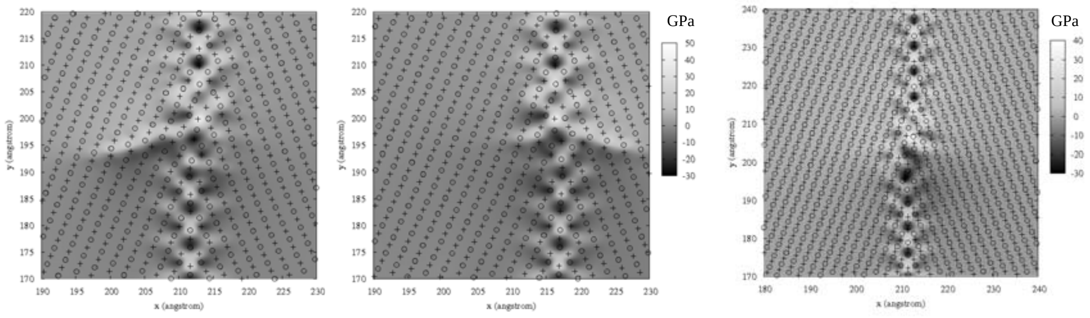

(a1) (a2) (b)

Figure 2. An edge dislocation: (a1) stoppage before reaching the grain boundary and (a2) transmission through the boundary; (b) absorption into the boundary approaching on glide plane 2. Hydrostatic stresses are indicated by the shading as in Fig. 1.

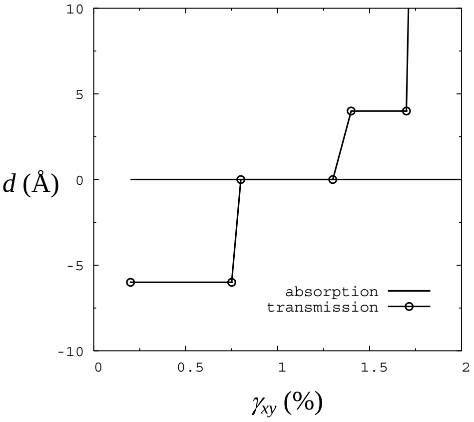

Figure 3. Location of the dislocation *d* with respect to the grain boundary plane as a function of the applied simple shear strain γ_{xy}.

In contrast, a dislocation approaching the grain boundary on any other plane leads to local rearrangements in the boundary plane. It appears as if the compressive part of the dislocation core neutralizes some of the local tensile stresses in the grain boundary and vice versa. This eventually leads to significant rearrangements in the boundary plane and to the immediate absorption of the dislocation (Fig. 2 (b)). The dislocation was not able to leave the boundary again in the range of applied stresses investigated here. A superimposed tensile stress normal to the grain boundary can lead to crack nucleation.

Dislocation transmission through a grain boundary appears in general to be somewhat more complicated than previously assumed. Even in the seemingly ideal case studied here, where glide planes meet on a common line in the plane of the boundary and where the residual Burgers vector of the grain boundary dislocation after transmission is small, is the transmission of the dislocation a rare event. Dislocation absorption and spreading of the dislocation core along the boundary – introducing some climb dissociation in the plane of the boundary – appears to be more frequent. Consequently, purely kinematic, stress based transmission criteria appear to be applicable only to very special cases like coherent twin boundaries[6]. In a more general setting, the transmission should probably rather be viewed as a thermally activated re-nucleation event as proposed in [7]. Whether it is sufficient to just focus on the residual Burgers vector as a measure of the activation energy (as in [7]) is, however, again questionable. Grain boundary migration in conjunction with the transmission appears to be a frequently observed phenomenon (see [6,8]).

4. Conclusion

Dislocation/grain boundary interaction in tungsten studied by atomistic simulations shows that the dislocation may be absorbed, stopped in front of the boundary or transmitted, depending on the interaction of the stress field of the dislocation core and the local stress field of the grain boundary. Furthermore, grain boundary migration is found to accompany the transmission process.

Acknowledgements

Financial support from the European Commission through the Marie-Curie Research Training Network SizeDepEn (MRTN-CT-2003-504634) is gratefully acknowledged.

References

[1] Z. Shen, R.H. Wagoner, and W.A.T. Clark, Acta Metall. **36**, 3231 (1988).
[2] B.J. Pestman et al., Phil. Mag. A **64**, 951 (1991).
[3] E. Bitzek, P. Koskinen, F. Gaehler, M. Moseler, and P. Gumbsch, unpublished
[4] G.J. Ackland, R. Thetford, Phil. Mag. A **56**, 15 (1987).
[5] M. Hashimoto, Y. Ishida, R. Yamamoto, and M. Doyama, Acta Metall. **32**, 1 (1984).
[6] Z.H. Jin et al., Scripta Mater. **54**, 1163 (2006).
[7] A. Ma, F. Roters, and D. Raabe, Acta Mater. **54**, 2181 (2006).
[8] D.E. Spearot, K.I. Jacob, D.L. McDowell, Acta Mater. **53**, 3579 (2005).

The Vacancy-Edge Dislocation Interaction in FCC Metals

Emmanuel Clouet

SRMP - CEA/Saclay, 91191 Gif-sur-Yvette, France.

ABSTRACT

The interaction between vacancies and edge dislocations is studied in face centered cubic metals (Al, Au, Cu, Ni) at different length scales. Using empirical potentials and static relaxation, atomic simulations gives us a precise description of this interaction when the separation distance between both defects is small, whereas elasticity theory can be used for larger distances. In addition, the interaction of a vacancy with an edge dislocation that contains a jog or a super-jog is discussed.

1. Introduction

Understanding the interaction between dislocations and vacancies is a key point in material science. In metal plasticity, this interaction controls dislocation climb and thus the plastic strain of a metal at high temperature when the glide of dislocations is blocked by obstacles like precipitates or the dislocation forest. This interaction also plays an important role in phase transformations. Indeed, as dislocations act as sinks and sources for vacancies, they control the way vacancies adjust their concentration in non-isothermal kinetics and thus the diffusion. Moreover, the vacancy super-saturation along dislocations leads to an enhancement of diffusion in their vicinity: dislocations behave thus as short-circuits, a phenomenon known as pipe diffusion.

2. Perfect edge dislocation

2.1 Atomic calculations

We first perform atomistic static relaxations to study the interaction between a vacancy and a perfect dislocation [1]. The simulation cell is fully periodic and contains two edge dislocations with opposite Burgers vectors. Its dimensions typically corresponds to the stacking of 160 [110], 120 [112] and 60 [111] planes. These calculations are done using EAM potentials corresponding to different fcc metals (Al, Au, Cu and Ni) [2-5]. The vacancy-dislocation interaction energy is calculated with a conjugate gradient algorithm for all possible positions of the vacancy in the simulation box. As expected, compressive regions attract the vacancy whereas tensile zones are repulsive, these two regions being separated by the dislocation glide plane. For potentials presenting a low stacking fault energy (Au, Cu and Ni), an attractive and a repulsive basin can be associated with each one of the partial dislocations as they are well dissociated.

For all potentials, the most attractive position is located in the core of the partial dislocations, on the edge of the supplementary half-plane above the glide plane in the compressive region (Fig. 1). Looking at the variation of the interaction energy in the plane just above the glide plane in the compressive region, one can see that the binding in the stacking fault is smaller than the one in the core of the partial dislocations. Therefore, vacancies cannot easily migrate from one partial dislocation to the other as they have to cross the stacking fault. In such a case, one expects that diffusion is faster along the partial dislocations than in-between. Above the glide plane, in the tensile zone, most of the vacancy positions are repulsive and only a few ones are slightly attractive.

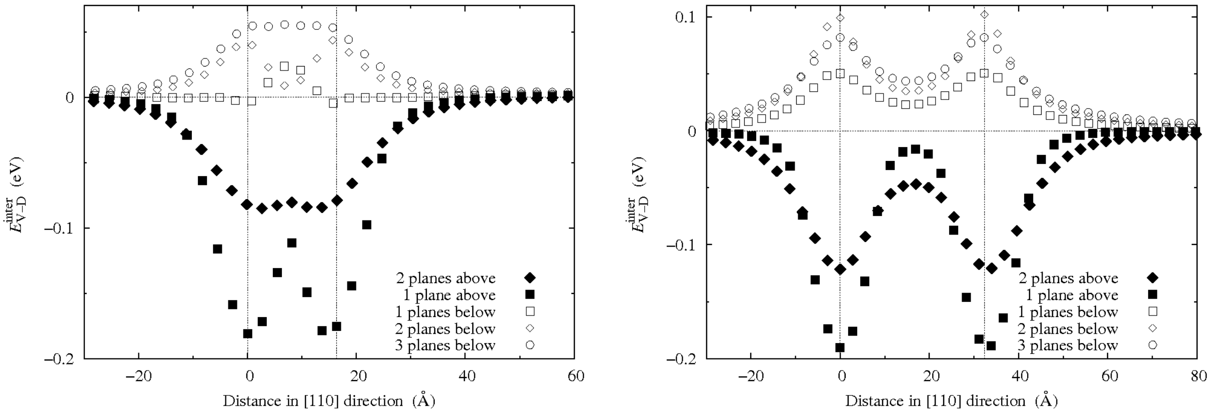

(a) Al (b) Au

Figure 1. Vacancy-dislocation interaction energy $E^{\rm inter}_{\rm V-D}$ as a function of distance from the center of one of the two partial dislocations. Scans are performed in the [110] direction for different $(\bar{1}11)$ planes lying above (in the compressive) or below the glide plane (in the tensile zone).

2.2 Elasticity theory

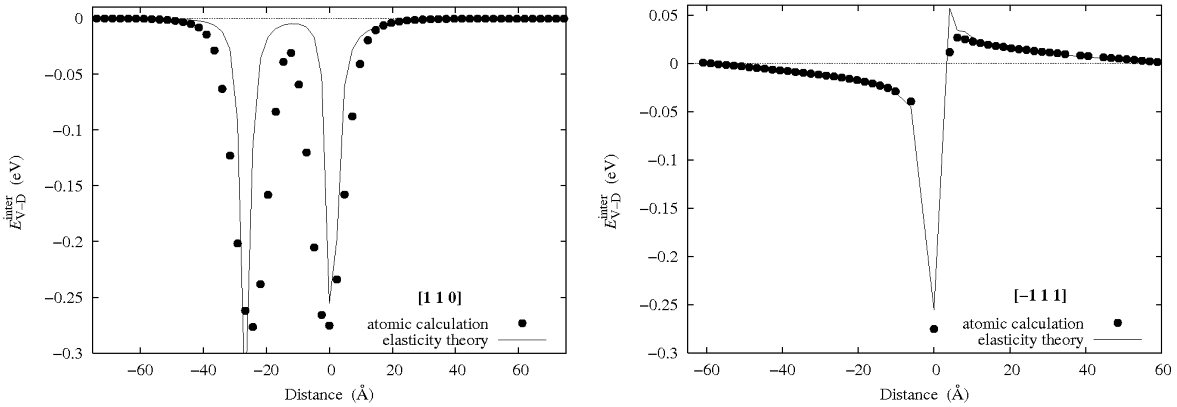

Figure 2. Variation with the separation distance of the vacancy - dislocation interaction energy $E^{\rm inter}_{\rm V-D}$ in [110] (left) and $[\bar{1}11]$ directions (right) in Ni. Symbols correspond to atomic simulation and lines to the isotropic elasticity theory (Eqn. 1) assuming dissociated dislocations.

As long as the vacancy is far enough from the dislocation, the interaction energy between both defects can be predicted using the elasticity theory [1]. Considering the size as well as the inhomogeneity interaction, this energy is given by

$$E^{\rm inter}_{\rm V-D} = P\,\delta\Omega_{\rm V} - \left(\alpha P^2 + \beta\bar{\sigma}^2\right), \qquad (1)$$

where P and $\bar{\sigma}$ are the pressure and the Von-Misès equivalent stress created by the dislocation at the lattice site where the vacancy lies. α and β are constants depending on the lattice parameter and on the elastic constants. $\delta\Omega_V$ is the vacancy relaxation volume. It is calculated directly from the atomic potentials.

For computing the pressure P and the stress $\overline{\sigma}$ appearing in Eqn. (1), we first use dislocation isotropy elasticity theory [6] taking full account of the periodic boundary conditions. When the separation distance between the vacancy and the dislocation is greater than a few interatomic distances, the elasticity theory manages to predict quantitatively the interaction energy (Fig. 2). One does not need to consider anisotropy elasticity as this does not lead to any significant change compared to isotropy elasticity. Taking into account the inhomogeneity interaction and not only the size effect improves predictions of the elastic calculations. The most significant change is that the interaction energy is not anymore symmetric with respect to the dislocation glide plane.

3. Edge dislocation with a jog

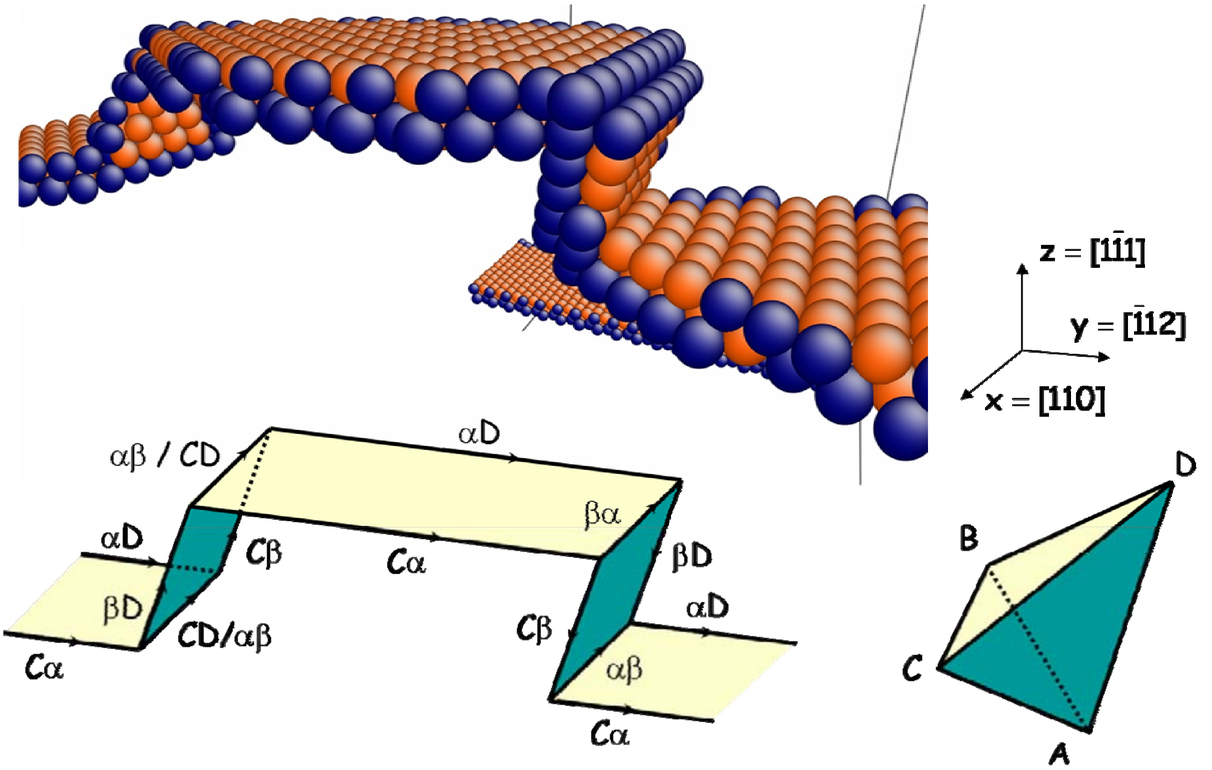

Figure 3. Atomic structure (top) of a jogged edge dislocation. The height of the jog is 5 (111) planes and its configuration is obtuse on the left and acute on the right. Only atoms which do not have fcc stacking are shown: dark atoms belong to the partial dislocation cores and light ones to the staking fault ribbon. The dissociation of the edge dislocation and of its jog in the α and β plane according to Hirsch [7] as well as the Thompson tetrahedron are shown in the bottom of the figure.

We study then the properties of an edge dislocation having a jog. Atomic simulations based on static relaxations give the stable structure of the jogged dislocation (Fig. 3). For all the considered heights of the jog (from 1 to 5 (111) planes), the most stable configuration is obtained when the jog takes a [112] direction making a ~125° angle with the dislocation line. Two different configurations therefore exist, an acute and an obtuse one. For both configurations, the jog dissociates in the (111) plane containing the dislocation Burgers vector and the jog direction, leading to a jogged dislocation that can glide without creating any point defect. These results obtained from atomic simulations correspond to the different configurations proposed by Hirsch [7] using line tension considerations.

Looking now at the interaction between a vacancy and a dislocation having a mono-layer high jog, we find that the most attractive positions of the vacancy correspond to the lattice sites forming the extended jogs, i.e. in the core of the stair rod dislocations defined by the acute or the obtuse jog. For these lattice sites, the vacancy can be fully absorbed and the jog advances from one atomic distance along the dislocation line. Although jogs on edge dislocations are dissociated, they are perfect sinks for vacancies. This is confirmed by the fact that this most attractive interaction energy equals the opposite of the vacancy formation energy, thus showing that a vacancy can be absorbed or emitted by a jog without any energy variation.

4. Conclusions

As long as the vacancy lies outside the dislocation core and the stacking fault ribbon, elasticity theory manages to predict quantitatively the interaction energy between a vacancy and an edge dislocation. When the separation distance is smaller than the dislocation core radius, an atomic calculation is needed. Such a calculation shows that jogs on dislocation are perfect sinks and sources for vacancies.

References

[1] E. Clouet, *The Vacancy-Edge Dislocation Interaction in FCC Metals: a Comparison between Atomic Simulations and Elasticity Theory*, Acta Mater. **54**, 3543 (2006).

[2] F. Ercolessi and J. B. Adams, *Interatomic Potentials from First-Principles Calculations: the Force-Matching Method*, Europhys. Lett. **26**, 583 (1994).

[3] J.E. Angelo, N.R. Moody, and M. I. Baskes, *Trapping of Hydrogen to Lattice Defects in Nickel*, Modelling Simul. Mater. Sci. Eng. **3**, 289 (1995).

[4] D.L. Medlin, S.M. Foiles, and D. Cohen, *A Dislocation-Based Description of Grain Boundary Dissociation: Application to a 90° <110> Tilt Boundary in Gold*, Acta Mater. **49**, 3689 (2001).

[5] Y. Mishin, M.J. Mehl, D.A. Papaconstantopoulos, A.F. Voter, and J.D. Kress, *Structural Stability and Lattice Defects in Copper: Ab Initio, Tight-Binding, and Embedded-Atom Calculations*, Phys. Rev. B **63**, 224106 (2001).

[6] J. P. Hirth and J. Lothe, *Theory of Dislocations* (Wiley, New York, 1982).

[7] P. B. Hirsch. *Extended Jogs in Dislocations in Face-Centred Cubic Metals*, Phil. Mag. **7**, 67 (1962).

Atomistic simulation of amorphization thermo-kinetics in lanthanum pyrozirconate

Jean-Paul Crocombette[1], *Alain Chartier*[2], *William J. Weber*[3]

[1]*CEA-Saclay, DEN/DMN/SRMP, 91191 Gif-Sur-Yvette, France*
[2]*CEA-Saclay, DEN/DPC/SCP, 91191 Gif-Sur-Yvette, France*
[3]*PNNL, P.O. Box 999, Richland, Washington 99352, USA*

Under irradiation, ceramics may experience amorphization. One experimentally observes that the irradiation dose needed to reach the amorphous state increases with temperature and then diverges at a so-called critical temperature, beyond which full amorphization becomes impossible. The rationalizations that exist for this behaviour rely either on the existence of some direct impact creating amorphous areas within the collision-cascade track, or on the accumulation of point defects. However, the thermo-kinetics of amorphization at the atomic scale are still unclear. Indeed to our knowledge, the temperature dependence of amorphization in ceramics has not been investigated using atomistic methods. We present here a molecular Dynamics (MD) study of lanthanum pyrozirconate ($La_2Zr_2O_7$) amorphization processes, simulated by continuous cation Frenkel Pair (FP) accumulation at various temperatures.

As a preliminary step [1] a rigid-core interatomic potential has been fitted on both experimental and ab initio data [2]. Using this potential we were able to show that displacement cascades produce point defects only [1] and that cation Frenkel pairs is the main driving parameter for the amorphization process [3], while the oxygen atoms simply rearrange around cations. In the last step [4], irradiation damage was simulated by continuous accumulation of cation Frenkel pairs at various temperatures. As observed experimentally, $La_2Zr_2O_7$ first transitions to the fluorite structure, independent of the temperature, and amorphization eventually occurs at low temperatures. A model fit of the simulated dosetemperature curve reproduces experimental results in the literature, with a low temperature amorphization dose D_0=1.1dpc (displacement per cation) and an activation energy E_{act}=0.036eV. Present simulations show that point defect recombinations [5] can control the temperature dependence of amorphization driven by point defect accumulation.

[1] A. Chartier, et al., Phys. Rev. B 67, 174102 (2003).
[2] A. Chartier, et al., Phys. Rev. B 65, 134116 (2002).
[3] A. Chartier, et al., Phys. Rev. Lett 94, 025505 (2005).
[4] J.P. Crocombette, et al., Appl. Phys. Lett. 88, 051912 (2006).
[5] J.P. Crocombette, et al., Nucl. Instrum. Meth. B, in press.

Interatomic potentials for materials with interacting electrons

S. L. Dudarev[1,2] and P. M. Derlet[3]

[1]*EURATOM/UKAEA Fusion Association, Culham Science Centre, Oxfordshire OX14 3DB, UK, e-mail: sergei.dudarev@ukaea.org.uk*
[2]*Department of Physics, Imperial College, Exhibition Road, London SW7 2AZ, UK, e-mail: s.dudarev@imperial.ac.uk*
[3]*ASQ/NUM - Materials Science & Simulation, Paul Scherrer Institute, CH-5232 Villigen PSI, Switzerland, e-mail: peter.derlet@psi.ch*

ABSTRACT

Evidence for the significant part played by magnetism in the picture of interatomic interactions in iron and iron-based alloys has recently emerged from density functional studies of the structure of radiation induced defects. In this paper we examine the range of validity of the currently available semi-empirical model interatomic potentials for iron, investigate the link between the Stoner and the LSDA+U models, and review atomistic simulations performed using the magnetic interatomic potential.

Introduction

Density functional calculations performed recently by the EdF, the Princeton, the CEA Saclay and by the UKAEA Culham groups [1]-[5] have revealed a pattern of systematic qualitative differences between the structure of vacancy and self-interstitial atom defects in iron and the non-magnetic bcc metals (see Table 1).

Table 1: Energies of formation and migration of vacancy and self-interstitial defects in body-centred cubic metals found using density functional theory in Refs. [3, 4, 5].

enhalpy (eV)	V	Nb	Ta	Cr	Mo	W	Fe
H^v	2.51	2.99	3.14	2.64	2.96	3.56	2.07
H^v_m	0.62	0.91	1.48	0.91	1.28	1.78	0.67
$H_{\langle 111\rangle\ \mathrm{DB}}$	3.367	5.253	5.832	5.685	7.417	9.548	4.45
$H_{\langle 111\rangle\ \mathrm{CR}}$	3.371	5.254	5.836	5.660	7.419	9.551	4.45
$H_{\langle 110\rangle}$	3.652	5.597	6.382	5.674	7.581	9.844	3.75
$H_{\mathrm{tetrahedral}}$	3.835	5.758	6.771	6.189	8.401	11.05	4.26
$H_{\langle 100\rangle}$	3.918	5.949	7.003	6.643	9.004	11.49	4.75
$H_{\mathrm{octahedral}}$	3.964	6.060	7.095	6.723	9.067	11.68	4.94

For example, while a highly mobile $\langle 111\rangle$ (the $\langle 111\rangle$ dumbbell or the $\langle 111\rangle$ crowdion) self-interstitial atom configuration has the lowest formation energy in all the non-magnetic body-centred cubic metals, in iron it is the significantly less mobile $\langle 110\rangle$ dumbbell that forms the ground state of the defect. This, as well as a significant amount of experimental information showing systematic differences between properties of magnetic iron and those of non-magnetic bcc transition metals, stimulated the development of a "magnetic" semi-empirical potential for molecular dynamics simulations [6, 7].

It is well known that electrons are responsible for the formation of chemical bonds, and hence it is natural to include electron correlation effects in the treatment of interatomic interactions, even at an empirical level of approximation. However, in practical large-scale molecular dynamics simulations performed so far electrons have almost invariably been treated as independent and non-interacting particles.

Electron correlations and the Stoner model

There are several conceptual points that need to be addressed in a computational scheme ('a semi-empirical potential') for fast evaluation of forces acting between atoms in a transition metal or in a transition metal alloy. Assuming that the problem of interatomic interactions is mapped onto a tight-binding Hamiltonian (see e.g. Ref. [8])

$$\begin{aligned}\hat{H} &= \sum_i \left[\frac{\overline{U}}{2}\sum_{m,m',\sigma}\hat{n}_{im,\sigma}\hat{n}_{im',-\sigma} + \frac{\overline{U}-\overline{J}}{2}\sum_{m,m',\sigma}\hat{n}_{im,\sigma}\hat{n}_{im',\sigma}(1-\delta_{mm'})\right] \\ &+ \sum_{i,j,\, i\neq j}\sum_{m,m',\sigma} t_{im,jm'}\hat{c}^{\dagger}_{im\sigma}\hat{c}_{jm'\sigma} + \sum_{i,m,\sigma}\epsilon_i \hat{c}^{\dagger}_{im\sigma}\hat{c}_{im\sigma} \qquad (1)\end{aligned}$$

where the term in square brackets describes interaction between electrons occupying the same site i, and the t-term is the kinetic energy of hopping between sites i and j, we see that a semi-empirical potential must be able to approximate three distinct effects contributing to the picture of interatomic interactions in a material.

The first is the formation of chemical bonds. Chemical bonds result from quantum hopping of electrons between lattice sites [9, 10], which is described by the kinetic energy t-term in equation (1). A hopping (or a hybridization) matrix element $t_{im,jm'}$ is the amplitude of a transition between an orbital m centered on site i, and an orbital m' centered on site j. In the absence of interaction between electrons, the $t_{im,jm'}$ terms in the Hamiltonian (1) result in the formation of bands of electronic states. In a real-space treatment the effects of inter-site hopping are approximated by means of a scalar (in the case of s-states) or a matrix (in the case of p, d, or f-states) recursion expansion truncated at a relatively low level of approximation. It is essential that in a real-space treatment of inter-site hopping the pathways extending over large distances in the crystal lattice are not retained. Calculating high-order terms corresponding to long trajectories of hopping that involve many lattice sites rapidly becomes computationally too expensive (e.g. even the simplest second-moment matrix recursion treatment of interaction between an atom and its environment involving subsets of d-states requires calculating 15 separate angular-dependent matrix elements [11]).

Hence an excessively accurate treatment of hopping eliminates the very advantage that a semi-empirical molecular dynamics simulation has over its density-functional based counterpart, namely its high computational speed derived from the simplicity of the method. In practical terms reaching the highest affordable accuracy of the recursion treatment of hopping involves retaining the fourth or the sixth moment of the density of states [10].

The second effect that an effective potential should be able to describe is the effective 'repulsion' between atoms at short distances. In molecular dynamics the short-range repulsion, as well as all the other terms that are not sufficiently accurately represented by the approximate treatment of the t-term, is described by a pairwise, in some cases by a complex many-body (for example if bond screening is included) term. The bonding and the repulsive parts of the potential are fitted simultaneously to a set of calculated and experimentally measured parameters characterizing a material in the hope that the mathematical consistency of the model would ensure that the range of validity of the resulting expression is broader than the range spanned by the data used in the fitting algorithm [12].

The third effect that until recently has not been investigated in connection with the semi-empirical treatment of interatomic interactions is the part played by the electron-electron interactions and magnetism. For example, the fact that electron-electron on-site repulsion suppresses hybridization and weakens chemical bonding between atoms in a material was noted in connection with the treatment of interatomic cohesion in uranium dioxide [13] and then investigated within the framework of the LSDA+U method [8]. On-site interaction between electrons is described by the many-body term of the Hamiltonian (1). In this term the parameter $\overline{U}$ represents the effective energy of interaction between two electrons with antiparallel spins occupying the same lattice site, and $\overline{J}$ is the matrix element of intra-atomic exchange between the electrons. The on-site part of the Hamiltonian has the form

$$\hat{H}_i = \overline{U} \sum_{m,m'} \hat{n}_{im\uparrow}\hat{n}_{im'\downarrow} + \frac{(\overline{U}-\overline{J})}{2} \sum_{m,m',\, m\neq m'} [\hat{n}_{im\uparrow}\hat{n}_{im'\uparrow} + \hat{n}_{im\downarrow}\hat{n}_{im'\downarrow}]. \tag{2}$$

Since this Hamiltonian refers to an isolated atom, it is instructive to start by investigating its eigenstates and eigenvalues. This leads to a somewhat unexpected conclusion that in the complex mathematical structure of this operator Hamiltonian only one small term is actually responsible for the occurrence of magnetic ordering.

An isolated atom of iron contains seven d-electrons, which can occupy the 10 available d-states. Let us assume that we have a configuration where five electrons have spin up and the two remaining electrons have spin down. In this case the energy of an atom is

$$E = \overline{U}\cdot 5\cdot 2 + \frac{(\overline{U}-\overline{J})}{2}(5\cdot 4 + 2\cdot 1) = 21\overline{U} - 11\overline{J},$$

and the magnetic moment is $(7-2)\mu_B = 3\mu_B$. We now compare this energy with the energy of a configuration where four electrons have spin up and three electrons have spin down. The energy of this configuration is

$$E = \overline{U}\cdot 4\cdot 3 + \frac{(\overline{U}-\overline{J})}{2}(4\cdot 3 + 3\cdot 2) = 21\overline{U} - 9\overline{J},$$

and the total magnetic moment is now $1\mu_b$. The energy of the high magnetic moment configuration is lower by the amount of $2\overline{J}$. In numerical terms, assuming that $\overline{U} = 10$ eV and $\overline{J} = 1$ eV, we find that the energy of the high-moment configuration is 199 eV while the energy of the low-moment configuration is 201 eV. The small 1% difference between the two energies is entirely due to the exchange interaction between electrons, and the much stronger direct Coulomb repulsion described by the $\overline{U}$ term plays no part in determining the magnetic state of an atom. The fact that the configuration with the highest magnetic moment has the lowest energy is a manifestation of the Hund rule.

Generalizing this treatment to the case of an arbitrary non-integer number of electrons occupying the atom, we write

$$E = \overline{U}N_\uparrow N_\downarrow + \frac{(\overline{U} - \overline{J})}{2}[N_\uparrow(N_\uparrow - 1) + N_\downarrow(N_\downarrow - 1)].$$

To simplify this equation we introduce two new variables, the total number N of electrons per atom $N = N_\uparrow + N_\downarrow$, and the magnetic moment M of an atom $M = N_\uparrow - N_\downarrow$. The energy of an atom now is

$$\begin{aligned} E &= \overline{U}\left(\frac{N+M}{2}\right)\left(\frac{N-M}{2}\right) + \frac{\overline{U}-\overline{J}}{2}\left[\frac{1}{4}(N+M)^2 + \frac{1}{4}(N-M)^2 - N\right] \\ &= \left(\frac{\overline{U}}{4} + \frac{\overline{U}-\overline{J}}{4}\right)N^2 - \frac{\overline{U}-\overline{J}}{2}N - \frac{\overline{J}}{4}M^2 \approx \frac{\overline{U}}{2}N(N-1) - \frac{\overline{J}}{4}M^2. \qquad (3) \end{aligned}$$

The main point illustrated by this equation is that the only term of the energy of interaction between electrons that explicitly depends on the magnetic moment M of an atom is

$$E_{\mathrm{magnetic}}(M) = -\frac{\overline{J}}{4}M^2. \qquad (4)$$

The magnitude of parameter $\overline{J}$ for a $3d$ transition metal atom is practically independent of the environment of the atom and is of the order of 1 eV [8]. Comparing this equation with the phenomenological Stoner model [10], where the energy of exchange interaction between electrons has the form,

$$E_{\mathrm{Stoner}}(M) = -\frac{I}{4}M^2, \qquad (5)$$

and where I is the Stoner parameter, we see that the exchange parameter $\overline{J}$ of the Hamiltonian (2) is *identical* to the parameter I of the Stoner model.

The energy of an atom (3) also contains a term $\overline{U}N(N-1)/2$ describing direct on-site Coulomb repulsion between electrons. It is the interplay between this term and the hopping t-term that suppresses chemical bonding in Mott insulators [13, 8]. In a metal the presence of self-screening [14] strongly reduces the strength of on-site Coulomb repulsion described by the parameter $\overline{U}$ of the Hamiltonian (1). Furthermore, the fact that in a metal the bandwidth $W \sim \sqrt{Z}|t|$, where Z is the effective number of neighbours of an atom in a lattice, is greater than $\overline{U}$, makes effects of on-site Coulomb repulsion considerably less significant than in the case of a Mott insulator.

Given that the seemingly strong effects of on-site Coulomb repulsion appear insignificant in the case of a metal, why do we need to include the rather small Stoner magnetic term in a semi-empirical treatment of interatomic interactions in iron and iron-based alloys? The simplest answer to this question is that we actually have evidence that the Stoner magnetic term influences interaction between atoms in a magnetic alloy and that the functional form of the contribution to the cohesive energy that this term makes is different from the functional form of the contribution describing conventional chemical bonding.

The semi-empirical magnetic potential.

Consider the one-particle terms of the Hamiltonian (1)

$$\hat{H}_{one-particle} = \sum_{i,j,\, i\neq j} \sum_{m,m',\sigma} t_{im,jm'} \hat{c}^{\dagger}_{im\sigma} \hat{c}_{jm'\sigma} + \sum_{i,m,\sigma} \epsilon_i \hat{c}^{\dagger}_{im\sigma} \hat{c}_{im\sigma}. \tag{6}$$

These matrix elements describe hopping between sites i and j, as well as the one-particle on-site energies of the electrons, and do not depend on the spin index. The operator (6) can be written in the form of a square matrix

$$H_{im,jm'} = \epsilon_i \delta_{im,jm'} + t_{im,jm'}.$$

The eigenvalues E_α of this matrix $H_{im,jm'}$ are found by a unitary transformation $U_{im,\alpha}$

$$E_\alpha \delta_{\alpha\alpha'} = \sum_{im,jm'} U^{\dagger}_{\alpha,im} [\epsilon_i \delta_{im,jm'} + t_{im,jm'}] U_{jm',\alpha'}.$$

Using these eigenvalues we define the projected on-site density of states $D_i(E)$

$$D_i(E) = \sum_{\alpha,m} |U_{im,\alpha}|^2 \delta(E - E_\alpha). \tag{7}$$

In a perfect crystal where all the sites are equivalent, the projected density of states is independent of site index i. Taking the on-site energy $\epsilon_i \equiv \epsilon$ as the origin of the energy axis, we write the total energy of the electrons as

$$E_{tot} = 2 \int_{-\infty}^{\epsilon_F} E D(E) dE.$$

By adding the Stoner term to this equation and noting that it *may* change the relative occupation numbers of the spin up and spin down states, we write the total energy of an atom as

$$E_{tot} = \int_{-\infty}^{\epsilon_{F\uparrow}} E D(E) dE + \int_{-\infty}^{\epsilon_{F\downarrow}} E D(E) - I M^2/4. \tag{8}$$

Here

$$M = \int_{-\infty}^{\epsilon_{F\uparrow}} D(E) dE - \int_{-\infty}^{\epsilon_{F\downarrow}} D(E) dE$$

is the magnetic moment of an atom. The total number of electrons occupying an atom, which in a metal remains constant due to the local charge neutrality condition, is given by

$$N = \int_{-\infty}^{\epsilon_{F\uparrow}} D(E)dE + \int_{-\infty}^{\epsilon_{F\downarrow}} D(E)dE = const. \tag{9}$$

In a conventional self-consistent electronic structure calculation the total energy (8) is minimized using the one-particle Kohn-Sham states. The energies of these states are

$$\begin{aligned} \epsilon_\uparrow &= \frac{\delta E_{tot}}{D(E)\delta n_\uparrow(E)} = E - \frac{I}{2}\left(\int\limits_{-\infty}^{\epsilon_{F\uparrow}} D(E)dE - \int\limits_{-\infty}^{\epsilon_{F\downarrow}} ED(E)dE\right) = E - \frac{I}{2}M \\ \epsilon_\downarrow &= \frac{\delta E_{tot}}{D(E)\delta n_\downarrow(E)} = E + \frac{I}{2}\left(\int\limits_{-\infty}^{\epsilon_{F\uparrow}} D(E)dE - \int\limits_{-\infty}^{\epsilon_{F\downarrow}} ED(E)dE\right) = E + \frac{I}{2}M. \end{aligned} \tag{10}$$

These equations give the impression that the presence of magnetism results in shifting the energy bands up or down by the amount $IM/2$, depending on the projection of spin of the electrons. However, the sum of these energies

$$\begin{aligned} E' &= \int\limits_{-\infty}^{\epsilon_{F\uparrow}} dE\left[E - \frac{I}{2}M\right] D(E) + \int\limits_{-\infty}^{\epsilon_{F\downarrow}} dE\left[E + \frac{I}{2}M\right] D(E) \\ &= \int\limits_{-\infty}^{\epsilon_{F\uparrow}} ED(E)dE + \int\limits_{-\infty}^{\epsilon_{F\downarrow}} ED(E)dE - \frac{I}{2}M^2, \end{aligned} \tag{11}$$

is *not* equal to the total energy of the system since it overestimates the magnetic term by a factor of two in comparison with the original expression (8). To compensate for the error we must add to (11) the so-called double counting correction

$$+\frac{I}{4}M^2. \tag{12}$$

This correction is not small, and the fact that it has to be introduced shows that in the problem of interacting electrons the meaning of the effective energies of single-particle states given by equation (10) is quite limited. Furthermore, our analysis shows that in equations (10) and (11) we cannot assume that the Fermi energies for the *shifted* spin-up and spin down states are the same. Fig. 1 shows the variation of the total energy as a function of magnetic moment $E(M)$ evaluated using equation (8)-(9), and equations (10)-(11). In the latter case the upper limits of integration are $\epsilon_{F\uparrow} = \epsilon_F + IM/2$ and $\epsilon_{F\downarrow} = \epsilon_F - IM/2$, implying that ϵ_F is a universal Fermi energy of the *shifted* spin-up and spin-down one-particle states. A comparison of the curve obtained using this single particle states with exact calculation based on equation (8) reveals only an agreement at the maximum and the minimum of the curve, clearly demonstrating the limited applicability of the single particle picture.

Owing to this fact, in our derivation of the functional form of the magnetic potential [6, 7] we did not use the concept of single-particle states. In the Born-Oppenheimer approximation

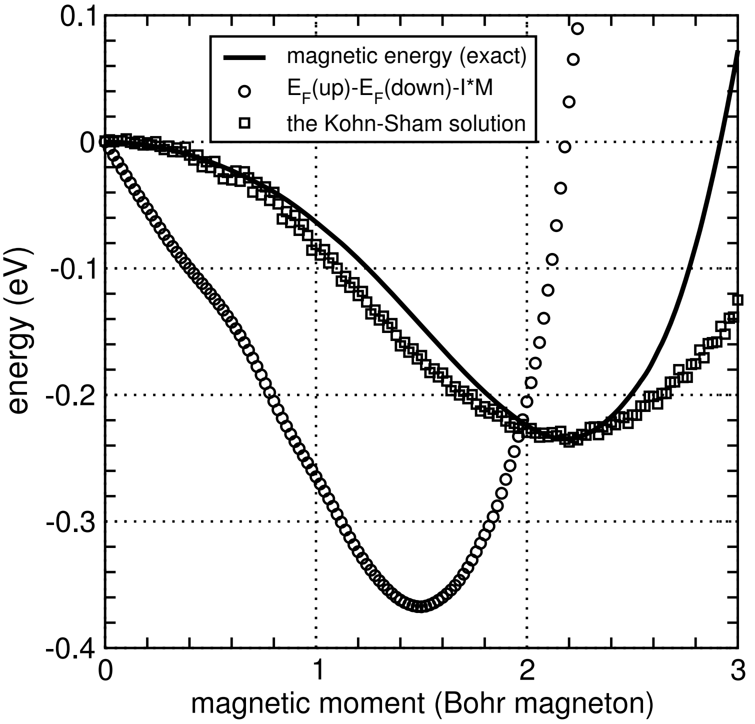

Figure 1: Solid black line: the magnetic part of the total energy calculated numerically using equations (8)-(9) in conjunction with an LMTO electronic density of states. Squares: the magnetic part of the total energy calculated numerically using equations (10)-(11) and the same LMTO-derived density of states. In both cases we assumed that $I = 0.78$ eV and $N = 6.57$. Circles show the difference $\epsilon_{F\uparrow}(M) - \epsilon_{F\downarrow}(M) - IM$ plotted as a function of magnetic moment M. This line crosses the horizontal axis at the point M where the total energy is minimum.

the electronic configuration is always at the minimum of energy corresponding to a given set of atomic coordinates. Hence the task of a semi-empirical potential is to follow and to reproduce, as accurately as possible, the value and the derivatives of the total energy *at its minimum* as a function of positions of atoms in the system. Instead of introducing the system of Kohn-Sham states we minimized the energy by differentiating the Fermi energies of the spin up and spin down states [6, 7]. We found that the condition for the minimum of energy has the form

$$IM = I\int_{\epsilon_{F\downarrow}}^{\epsilon_{F\uparrow}} D(E)dE = \epsilon_{F\uparrow}(N,M) - \epsilon_{F\downarrow}(N,M). \tag{13}$$

This condition is equivalent to the condition [10]

$$I\langle D(E)\rangle = 1, \tag{14}$$

where the angular brackets $\langle ... \rangle$ denote averaging over an interval of energies between $\epsilon_{F\downarrow}$ and $\epsilon_{F\uparrow}$. Figure 1 shows that equations (13) and (14) are indeed satisfied at the point where the total energy (8) is minimum.

Conclusions.

The analysis given above addressed the fundamental aspects of the concept of magnetic interatomic potential. A detailed description of the derivation of the functional form of the potential for molecular dynamics simulations of iron is given in Refs. [6, 7]. The potential tabulated in Refs. [6, 7] was fitted to a range of properties of magnetic bcc iron, as well as to the energies of vacancy and self-interstitial atom defects. It is just as easy to use and its numerical implementation is just as fast as that of any other semi-empirical potential. An additional benefit that a magnetic potential offers to a user is its ability to evaluate, *at no extra cost*, the magnitude of the local magnetic moment on every atom in a simulation cell.

So far the potential has been developed and fitted only for the case of pure iron, and the tests carried out so far show that it performs reasonably well in simulations of defect structures and dislocations. We are of the opinion that the work done so far has only scratched the surface of the fundamental problem of large-scale atomistic simulations of systems where electrons forming chemical bonds between atoms are treated as interacting particles. Further work is required to address the unusual behaviour exhibited by many materials, including magnetic alloys, where *d*- and *f*-electrons contribute to bonding between the atoms.

Bibliography

1. C. Domain and C. S. Becquart (2001) *Ab-initio calculations of defects in Fe and dilute Fe-Cu alloys*, Physical Review B**65**, 024103
2. S. Han, L. A. Zepeda-Ruiz, G. J. Ackland, R. Car and D. J. Srolovitz (2002) *Self-interstitials in V and Mo*, Physical Review B**66**, 220101
3. C.-C. Fu, F. Willaime, and P. Ordejón (2004) *Stability and mobility of mono- and di-interstitials in α-iron*, Physical Review Letters **92**, 175503
4. F. Willaime, C.-C. Fu, M. C. Marinica, and J. Dalla Torre (2005) *Stability and mobility of self-interstitials and small interstitial clusters in α-iron: ab-initio and empirical potentials calculations*, Nuclear Instruments and Methods B**228**, 92–99
5. D. Nguyen-Manh, A. P. Horsfield and S. L. Dudarev (2006) *Self-interstitial atom defects in bcc transition metals: group-specific trends*, Physical Review B**73**, 020101
6. S. L. Dudarev and P. M. Derlet (2005) *A 'magnetic' interatomic potential for molecular dynamics simulations*, Journal of Physics: Condensed Matter **17**, 7097–7118
7. P. M. Derlet and S. L. Dudarev (2006) *Million-atom molecular dynamics simulations of magnetic iron*, Progress in Materials Science, Festschrift Proceedings for David Pettifor's 60th birthday, in the press. The paper is available on the Culham laboratory website www.fusion.org.uk
8. S. L. Dudarev, G. A. Botton, S. Y. Savrasov, C. J. Humphreys and A. P. Sutton (1998) *Electron-energy-loss spectra and the structural stability of nickel oxide: an LSDA+U study*, Physical Review B**57**, 1505–1509
9. A. P. Sutton, M. W. Finnis, D. G. Pettifor and Y. Ohta (1988) *The tight-binding bond model*, Journal of Physics C: Solid State Physics **21**, 35–66
10. D. G. Pettifor (1996) *Bonding and Structure of Molecules and Solids* (Oxford University Press)
11. S. L. Dudarev (2006) *Angular-dependent matrix potentials for fast molecular-dynamics simulations of transition metals*, Journal of Physics: Condensed Matter **18**, S447-S461
12. M. W. Finnis (2003) *Interatomic Forces in Condensed Matter* (Oxford University Press, Oxford)
13. S. L. Dudarev, D. Nguyen-Manh and A. P. Sutton (1997) *Effect of Mott-Hubbard correlations on the electronic structure and structural stability of uranium dioxide*, Philosophical Magazine B**75**, 613–628
14. I. V. Solovyev and M. Imada (2005) *Screening of Coulomb interactions in transition metals*, Physical Review B**71**, 045103

Artificial Intelligence For Use In Atomistic Kinetic Monte Carlo Simulations

F.G. Djurabekova[1], R. Domingos[1], G. Cerchiara[2], N. Castin[3] and L. Malerba[1]

[1] SCK•CEN, Reactor Materials Research Unit, Boeretang 200, 2400 Mol, Belgium,
fdjurabe@sckcen.be, rdomingo@sckcen.be and lmalerba@sckcen.be; [2]University of Pisa, Italy,
cerchiara@ing.unipi.it; [3]Catholic University of Louvain-la-Neuve, Belgium, ncastin@skynet.be

ABSTRACT

A new approach to atomistic kinetic Monte Carlo (AKMC) simulations based on the determination of vacancy migration barriers as functions of the local atomic environment has been developed, with a view to provide a better description of the kinetic path followed by the system through diffusion of solute atoms in the alloy via vacancy mechanism. Tabulated values of barriers versus local atomic configurations (LAC) including atoms up to 2nd nearest neighbour shell, obtained by molecular dynamics (MD) techniques, have been used to train an artificial intelligence (AI) system to recognize the LACs and predict the barriers accordingly. Here some details on the method and preliminary results are presented and briefly discussed.

1. Introduction

The degradation of reactor pressure vessel ferritic steels in existing nuclear power plants (NPPs) as a consequence of neutron irradiation during operation is largely caused by radiation enhanced, or induced, Cu precipitation [1]. A correct prediction of the kinetics of the process of Cu precipitation is hence important for the safe exploitation of NPPs and atomistic simulations can potentially be extremely accurate for this purpose. Atomistic kinetic Monte Carlo (AKMC) approaches are especially suitable tools for the description of diffusion and precipitation processes involving vacancies [2,3]. The main input are the transition rates for the thermally activated mechanisms governing the evolution of the system which,. in this specific case, are exchanges of vacancies with neighbouring atoms (vacancy diffusion jumps, VDJ), whose activation energies are functions of the local atomic configuration (LAC). These energy barriers are generally estimated using heuristic approaches [2,3]. We propose a methodology, based on the application of artificial intelligence (AI) techniques, to improve the accuracy of the description of the complexity of the dependence of the VDJ activation energies on the LAC, extended, so far, to include the influence of atoms up to the 2nd nearest neighbour (2nn) shell. This methodology is expected to boost both the computational efficiency and the physical reliability of AKMC methods to describe the kinetic path followed by the system during Cu precipitation.

2. Problem statement

The frequency of a VDJ in an alloy according to standard transition state theory can be expressed as $\Gamma_j = \nu_0 \exp\left(-E_j / k_B T\right)$, where ν_0 is an attempt frequency that can be considered constant (on the order of the Debye frequency), k_B is Boltzmann's constant, T the absolute temperature and E_j the LAC dependent activation energy [2,3]. Given an interatomic potential the E_j can be exactly calculated for any LAC, including the effect of atomic relaxation, using e.g. a molecular dynamics (MD) code. In this case we used a recent FeCu potential fitted to the experimental phase diagram and to ab initio point-defect/solute-atom interaction energies [4]. Fig.1 shows as an example the mapping of MD calculated barriers (black dots) as functions of the energy variation after the jump for all LACs obtained changing the type of atoms (Fe or Cu) within the 1nn shell only. The linear relationship between the barriers and total energy variation before and after VDJ used e.g. in [2] clearly cannot reflect the complexity of the real relationship. The broken bonds method used in [3] strives to approach the real picture, but has also been seen to be approximated and largely insufficient.

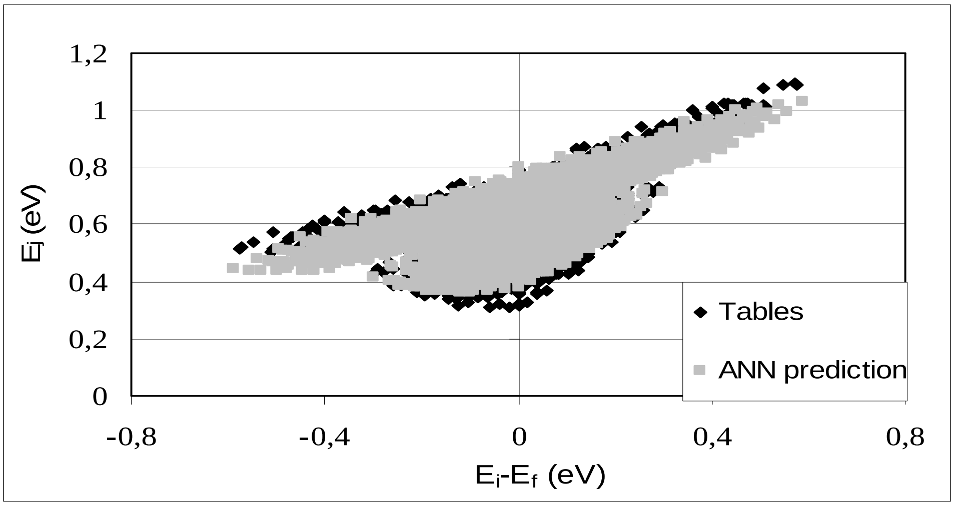

Fig.1 The energy barriers to VDJ versus total energy variation before and after jump.

3. Artificial Intelligence

An AI system has been developed and applied to reproduce the complexity of the relationship between E_j barriers and LACs. It consists of a specialized artificial neural network (ANN) [5], of a type extensively used for interpolation tasks (generalized regressed model). In order to predict the correct barrier given a LAC, the AI system must first learn how to classify the LACs into groups that provide energy barriers in a certain range. For the classification task the used architecture was a multilayer perceptron and the applied learning process was back propagation. After training on a limited (e.g. 15%) subset of randomly chosen cases, the ANN succeeds in correctly classifying a given configuration inside the corresponding energy range. Subsequently, additional layers allow the correct vaues to be interpolated within the correct range. For more details about the way LACs are defined and the AI see [6]. In Fig.1 the mapping of barriers predicted by AI (grey dots) in the 1nn approximation is shown as well. Although small differences exist, the prediction of AI conservs the original trend of the MD calculated and tabulated barriers and the error bar never exceeded 8% (about 0.05 eV). Including the atoms of the 2nn shell increases the input set of LACs enormously [6]. However, in this case the training subset can be reduced down to 2% of the total set to be predicted, thanks to the fact that the physics of the problem is better defined now and the AI system finds more easily the "logic" in it. Fig. 2 shows the comparison of AI-predicted with MD-calculated barriers in 2nn approximation after training the AI system on a subset of 2% randomly chosen cases. The AI system has been now implemented in the LAKIMOCA code AKMC code [2], so as to apply the latter to the simulation of long-term Cu-precipitation processes. Preliminary results show a clear improvement in the description of the formation of Cu precipitates, compared to using the 1nn approximation.

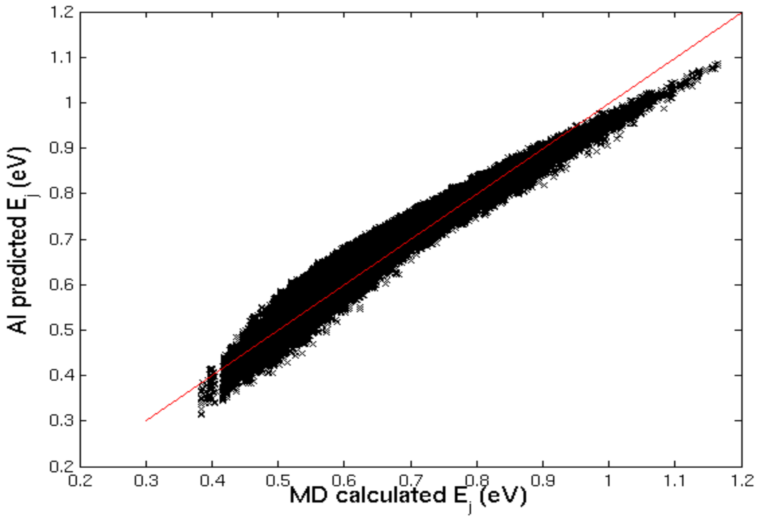

Fig. 2 Comparison of the AI predicted and MD calculated values of energy barriers to VDJ in 2nn approximation.

4. Summary

The implementation in an AKMC code of an AI system trained to predict the local-atomic-configuration dependent activation energies based on a subset of barrier values accurately calculated using an MD code with a valid interatomic potential boost the physical reliability of AKMC methods to describe the kinetic path followed by the system during e.g. Cu precipitation. Including the atoms of further shells for the definition of the LAC clearly improves the results of the method and is only feasible with the help of AI systems.

Acknowledgements

This work was performed in the framework of the PERFECT Integrated Project, WPII-2, partially funded by the European Commission.

References

[1] C.A. English, W.J. Phythian and R.J. McElroy, "Microstructure and modelling of RPV embrittlement", Mat. Res. Soc. Symp. Proc. Vol. **439**, 471 (1997).

[2] C. Domain, C.S. Becquart and J.-C. van Duysen, Mat. Res. Soc. Symp. Proc. Vol. **540** 643 (1999).

[3] Y.L.Bouar and Frederic Soisson, Phys. Rev. B **65**, 094103 (2002).

[4] L. Malerba and R.C. Pasianot, SCK•CEN Report ER-6, February 2006; R.C. Pasianot and L. Malerba, "*Potentials consistent with thermodynamics*", J. Nucl. Mater., submitted; R.C. Pasianot, G. Bonny and L. Malerba, " *Interatomic Potentials Consistent with Thermodynamics: The Cases of FeCu and FeCr*", these proceedings.

[5] S. Haykin, "*Neural Networks: A Comprehensive Foundation*", New York: MacMillian, 1994.

[6] F.G. Djurabekova, R. Domingos, G. Cerchiara, N. Castin and L. Malerba, "*Artificial intelligence applied to atomistic kinetic Monte Carlo simulations in Fe-Cu alloys*", Nucl. Instr. & Meth. B (2006), submitted.

Defect kinetics in electron irradiated steels: a multiscale modelling

Chu Chun Fu[1], *A. Barbu*[1] *J.L. Bocquet*[1], *L. Joly*[1], *F. Willaime*[1]

[1]*SRMP, CEA/SACLAY, 91191 Gif-sur-Yvette, France*

Evolution in microstructure of nuclear materials is mainly governed by the kinetics of defects produced by irradiation. The population of vacancies, self-interstitials, and their clusters can however be followed only indirectly, e.g. by macroscopic electrical resistivity measurements. The information on the mobility, recombination, clustering or dissociation of defects provided by such experiments is both extremely rich and difficult to interpret [1]. By combining ab initio and mesoscopic kinetic Monte Carlo methods, we have simulated the abrupt resistivity changes so called recovery stages observed upon annealing after electron irradiation in pure iron. New features in the mechanisms responsible for these stages have been revealed [2]. Carbon is one of the principal components of steels. Here we simulate, using the same multiscale approach, the resistivity recovery stages after electron irradiation in carbon doped iron. The results give important information on the defect population evolution under irradiation. In agreement with experimental evidences [1], C atoms are effective traps of isolated vacancies and a weaker attraction (Eb= 0.1 eV to 0.2 eV) is found between C and self-interstitial atoms. All the experimentally observed stages are successfully reproduced and interpreted. New stages related to carbon migration and clustering with self-defects are identified. At variance with the results in pure iron, the position in temperature of these peaks depends rather on the relative concentration of carbon and self-defects than on the irradiation dose. In addition, the resistivity of a carbon-vacancy complex should be diferent from the sum of the resistivity of the isolated defects in order to well reproduce the vacancy migration stage (Stage III).

1. S. Takaki et al., Radiat. Eff. 79, 87 (1983)

2. C.C. Fu et al., Nature Mat. 4, 68 (2005)

Atomic transport via interstitials in dilute Fe-P alloys

Chu Chun Fu [1], A. Barbu [1], E. Meslin [1], F. Willaime [1] F. Gao [2]

[1]SRMP, CEA/SACLAY, 91191 Gif-sur-Yvette, France

[2]Pacific Northwest National Laboratory, 99352 Richland, United States of America

Under irradiation conditions at T ≤ 300 °C, the phosphorus segregation at grain boundaries in low alloyed ferritic steels has been suggested to occur through flux coupling between P and self-interstitial atoms (SIAs).

By combining ab initio SIESTA method, an EAM Fe-P potential [1] and an analytical diffusion model [2], we investigate the P-SIA interaction and the diffusion of interstitial P and SIAs in dilute Fe-P alloys. Although P is a substitutional impurity in 1-iron, when a SIA approaches a substitutional P, the formation of an interstitial P occurs with an energy gain of about 1.0 eV. The octahedral and the <110> mixed dumbbell are the energetically most favourable configurations with similar stabilities. The P atoms are highly mobile in both configurations. The transition barriers between these configurations are also comparable to the migration energy barriers. The most likely mechanisms leading to long distance diffusion of an interstitial P are proposed by ab initio calculations and confirmed by the diffusion model. The resulting effective diffusion energy is 0.2 eV, which agrees with the result from the resistivity recovery experiments suggesting that the mixed Fe-P dumbbells are more mobile than the single SIAs.

The fast migrating interstitial P can be deeply trapped by a substitutional P. The resulting complexes are very stable with a binding energy up to 1.05 eV. Their mobility are investigated by means of the dimer method using an EAM Fe-P potential. The experimental evidences supporting the existence of such trapping configurations are also discussed.

[1] G. J. Ackland et al., J. Phys. Condens. Mater. 16, S2629 (2004)

[2] A. Barbu and A. B. Lidiard, Phil. Mag. A 74, 709 (1996)

Stability of open and collapsed vacancy type clusters in bcc iron

Mark R. Gilbert[1,4], **Sergei L. Dudarev**[1,2], **Peter M. Derlet**[3], **and David G. Pettifor**[4]

[1]EURATOM/UKAEA Fusion Association, Culham Science Centre, Oxfordshire, OX14 3DB, UK, e-mail: Mark.Gilbert@UKAEA.org.uk, [2]Department of Physics, Imperial College, Exhibition Road, London SW7 2AZ, UK , [3]Paul Scherrer Institute, 5232 Villigen PSI, Switzerland, [4]Department of Materials, University of Oxford, Parks Road, Oxford, OX1 3PH, UK.

ABSTRACT

In recent experiments by Yao, Jenkins, and Kirk [1], the appearance of vacancy loops during *in situ* irradiation of Fe has been seen to occur on timescales of about 0.1-0.2 seconds. Using the Dudarev-Derlet magnetic interatomic potential [2] and molecular dynamics (MD) simulations, we investigated the behaviour of various vacancy-type defects that form under the cascade irradiation used in experiments [1]. The atomic configurations and formation energies of spherical voids and planar vacancy loops were determined using lattice relaxations. In addition to these defects, where formation energies are dominated by the presence of open surfaces, we have also studied 'collapsed' vacancy loops that contain no free surfaces. The three defect types show a relationship between size and formation energy. For the void-type defects (open loops and nearly spherical voids) this relation is dominated by the increase of surface energy with surface area, while in the collapsed loop case the formation energy-defect size curve has a more complex shape as elastic energy plays a significant role.

1. Introduction

The results described in this paper represent a part of an investigation, the ultimate aim of which is to describe the mechanical processes associated with the phenomenon known as softening of dilute bcc alloys (see [3,4]). This requires carrying out MD simulations of dislocations in pure bcc metals, such as iron, and then bcc alloys, such as FeCr. As a starting point we have used the newly developed Dudarev-Derlet magnetic interatomic potential for bcc iron [2] and a combination of molecular statics and finite temperature molecular dynamics to study the nature of various vacancy-cluster defects. The stimulus for this investigation came from new experimental observations of the evolution of vacancy defects under cascade irradiation performed by Zhongwen Yao, Mike Jenkins and Mark Kirk [1].

2. Simulations of vacancy loops

The initial investigation focused on the behaviour of simple clusters of vacancies called 'vacancy loops'. These defects were created by removing discs of atoms from the perfect bcc lattice of iron. Experimentally these so-called 'open' vacancy loops (*i.e.* structures where the two circular faces of the disc have a distinct gap between them) are not observed, possibly because they do not produce the elastic strain fields visible in diffraction electron microscopy. Instead what is seen experimentally is a ring-like defect with a bulk lattice configuration in the centre of the loop. Such 'closed' vacancy loops are the structures we most wished to study, however as we shall see, the difficulties associated with their construction revealed that they do not constitute the minimum energy vacancy structures when modelled using the Dudarev-Derlet potential.

Initially, several ‘open’ vacancy loops of different size were relaxed using molecular statics, however ‘closure’ was not observed for any of them. This was due to the short range nature of the potential that prevented atoms on the opposing surfaces of the loop from interacting and thus collapsing. To overcome this problem it was thought that heating might provide the necessary impetus to collapse the loops. Simulations were performed on an $a/2\langle 111\rangle$ loop (*i.e.* one with its circular faces aligned along a (111) plane) created by removing 26 atoms from a perfect lattice of 15360 atoms (about 200nm^3 in volume), using periodic boundary conditions. After equilibrating this configuration in a constant energy MD simulation, a sequence of molecular dynamics simulations was performed for temperatures ranging from 200K to over 2000K. For each final finite temperature configuration, molecular statics was used to relax the structure to its zero temperature configuration from which the defect formation energy could be calculated. The graph shown in Fig. 1 shows the change in the formation energy of the defect as the temperature increases. Up to around 500K the loop remained unchanged. This corresponds to the constant formation energy region of the graph. Beyond this temperature the formation energy began to fall, and this was accompanied by a change in the shape of the defect. As the temperature increased further there was a definite change in the shape of the defect, so that by 1500K it had become a fully spherical void. The formation energy minimum in Fig. 1 corresponds to the temperature at which the defect was ‘most’ spherical. Beyond this minimum the defect begins to evaporate into single vacancies as the melting temperature of the material is approached.

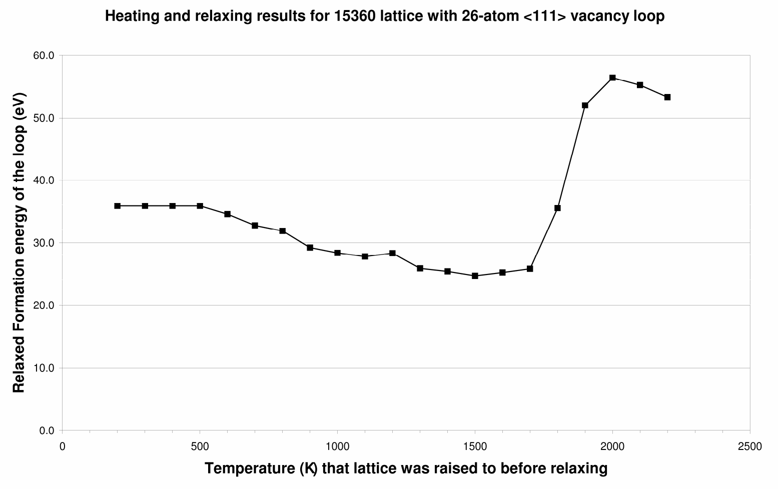

Figure 1: The change in the formation energy of an open vacancy loop due to heating.

The main implication of these results is that the spherical void configuration is the more energetically stable of the two, and heating overcomes the energy barrier between the two defect configurations allowing the system to relax into the low-energy structure.

2.1 An alternative approach for vacancy loops

The above analysis, whilst interesting, did not produce the collapsed vacancy loops that we intended to investigate in connection with experimental observations. An alternative way to create ‘closed’ loops, which overcame the difficulties caused by the short range of the interatomic potential, has been employed. This method involves making space for, and then inserting, *extra atoms* in the plane of the defect. This is done everywhere *except* for where the loop is to be located. The validity of this method has been checked for a range of loop sizes by relaxing the resulting configuration. It was confirmed that the regions where extra atoms had been inserted returned to a near perfect lattice configuration, leaving a closed vacancy loop in the middle of the plane. For large loop sizes the relaxed defect structure resembles a ring of vacancies with bulk lattice structure in the centre. However, for small radius loops the picture is less well defined. Some loops appear to default back to the open-loop structure mentioned earlier.

3. Formation energies of vacancy defects

To investigate the behaviour discussed in the previous section the formation energies of the two different loop-defect structures have been compared. Fig. 2 depicts a graph showing the formation energy of a loop against its size (*i.e.* the number of whole vacancies) for both the open and the closed vacancy loops, as well as for spherical voids. For reference note that in the case of vacancy loops the *x*-axis is equivalent to the radius squared, with a 50-atom loop having a radius of about 15 Å. For a void it is proportional to the radius cubed and the maximum internal radius considered was about 7 Å.

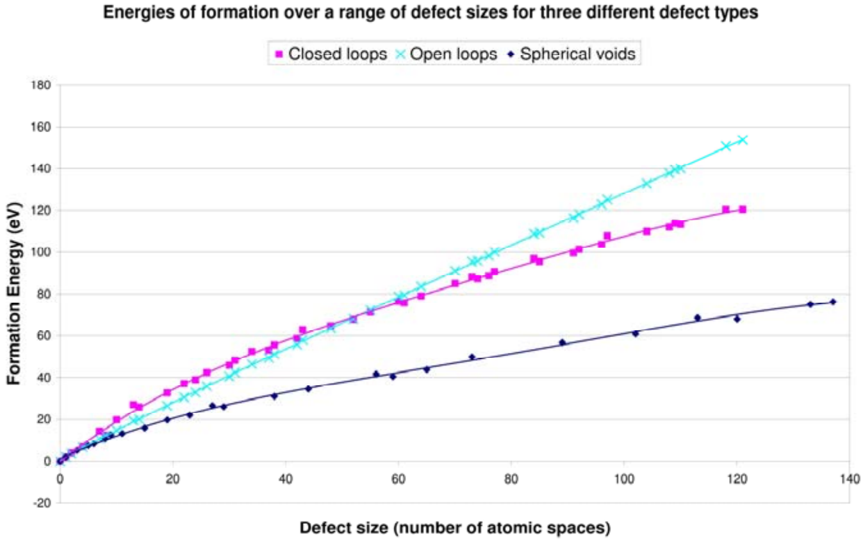

Figure 2: The variance of formation energy with size for the different defect types.

Fig. 2 shows that the spherical voids are the lowest energy configurations for all sizes, which implies that either of the other defect types would relax to these given enough time and provided the energy barriers could be overcome. This could offer an explanation for the sudden disappearance of closed vacancy loops in diffraction electron microscopy – they may transform into the stable spherical configuration, which is largely invisible due to the lack of elastic strain fields. For loop defects above 50 atomic spaces in size the closed-loop configuration is the most favourable, whilst below this level the reverse is true. This is borne out by studies of the relaxed structures of small closed loops, which show that they 'open-up' and revert to a configuration with well-defined internal surfaces.

This work was jointly funded by the Engineering and Physical Sciences Research Council and by EURATOM.

References

[1] Z. Yao, M. L. Jenkins, and M. A. Kirk (in preparation).
[2] S. L. Dudarev and P. M. Derlet, J. Phys.: Condens. Matter **17**, 7097 (2005); P. M. Derlet and S. L. Dudarev, Prog. Mat. Sci. (2006) in press.
[3] E. Pink and R. J. Arsenault, Prog. Mat. Sci. **24**, 1 (1979).
[4] D. Brunner and J. Diehl, Phys. Stat. Sol. **160**, 355 (1997).

Molecular dynamics modeling of cavity strengthening in irradiated iron

S. M. Hafez Haghighat, R. Schaeublin
Ecole Polytechnique Fédérale de Lausanne (EPFL), Centre de Recherches en Physique des Plasmas, Association Euratom-Confédération Suisse, CH 5232 Villigen PSI, Switzerland, masood.hafez@psi.ch

ABSTRACT

One of the most important problems in the field of nuclear industry is the relationship between irradiation-induced damage and the resulting induced mechanical response of the target metal and in particular ferritic base steels. In this work the molecular dynamics is used to simulate the nanoscale interaction between a moving dislocation and a defect, such as a cavity, as void or He bubble. The stress-strain curves are obtained under imposed strain rate condition using the atomic potentials based on the Fe potential of Ackland et al. 1997 for a void and He bubble as a function of He content and temperature. It appears that a 2 nm void is a stronger obstacle than a He bubble at low He contents, whereas at high He contents, the He bubble becomes a stronger obstacle. With increasing temperature the escape stress decreases and at the same time there is increasing degeneracy in the type of interaction.

1. Introduction

The structural components of the future fusion reactor will be submitted to high irradiation doses and heat loads due to the incident 14 MeV neutrons emitted by the fusion reaction. The materials for the plasma facing components are thus a key issue in the realization of fusion energy systems. Ferritic base steels are being extensively studied since these alloys are considered to be first candidate materials for the blanket and first wall of fusion reactors. Multiscale modeling appears nowadays as a major tool for the description of plasticity of materials. Modeling using molecular dynamics (MD) based on the embedded atom method approach allows investigations at the atomic level. It was extensively used to study the production and interaction of defects due to displacement cascades. Although various MD works have been done about strengthening of irradiation induced fcc and bcc materials by dislocation-obstacle interaction, e.g. by Osetsky [1] and Bacon [2] there is still lack of clear understanding about its temperature dependence, the effect of size and type of obstacle and the screw dislocation mobility, specially in bcc iron. The present work is focused on the MD simulation of the edge dislocation-cavity, as a void or a He bubble, interaction in pure α-iron, which is the basic material of the main candidate materials for future fusion reactors.

2. Simulation procedure

Molecular dynamics simulations mimic elementary atomistic path-dependent processes by solving the Newton equation of motion of all particles of a given system with empirical interatomic potentials [3]. The atomistic simulation of a dislocation interaction with a defect in an Fe crystal under an applied constant strain rate or stress includes mainly two steps. First step allows describing the atomic configuration of a dislocation using anisotropic elasticity of the continuum to create the sample for the simulation. And second step allows the dislocation to move using MD simulation with the embedded atom method. The first step is implemented in code ‘Disloc’ and the second one is implemented in the well-known code ‘Moldy’. The MD sample consists of a box including an edge dislocation in [112] direction and a defect (void or He bubble) on the dislocation slip plane, (110). The box is built up in several regions consisting in (1) the mobile region where atoms follow Newton equation, (2) an upper region whose atoms control the deformation of sample and are forming a free surface, (3) the bottom regions containing the thermal bath and (4) static atoms to anchor the specimen. In the thermal bath temperature is controlled by performing a velocity rescaling on every atom in this region every 100 steps according to the difference between the temperature measured in this region and the desired temperature. Periodic boundary condition is applied along other lateral sides of the box. In order to model deformation mode the shear stress resulting from an applied imposed stain rate is calculated at each time step from the internal force of atoms in the upper region of sample. The many-body empirical potentials derived by Ackland [4], Wilson-Jonson [5] and Beck [6] are used for Fe-Fe, Fe-He, and He-He interactions respectively, as suggested by Morishita and Wirth 2003 [7]. Simulations are mainly performed on the EPFL mainframe parallel computer MIZAR. Preliminary MD simulations conditions used in this work are presented in Tab. 1.

Table 1. Properties of MD simulation for edge dislocation and void/He bubble interaction.

Size of box	14×25×20 nm^3	Diameter of void or He bubble	2 nm
Num. of Fe atoms in the box	566586	Time step	1 fs
Real strain rate	3×18^7 s^{-1}	Annealing before straining	5 ps
Dislocation speed	60 m/s	Total simulation time	480 ps

3. Results and discussion

MD simulation of interaction between an edge dislocation and a 2 nm void in bcc iron at 10K is shown in Fig. 1. Fig. 1a shows the dislocation glide under imposed strain rate before dislocation-defect interaction and Fig. 1b indicates attraction of edge dislocation by void in the vicinity of void where the critical attraction distance is reached. The release of dislocation from defect is indicated in Fig. 1c where critical release stress and strain is reached. Shearing of void by dislocation is clear in this image as it is shown for He bubble in aluminum by Wirth [8]. The same phenomena of attraction and shearing have been observed in simulations of edge dislocation and He bubble interaction with different He contents.

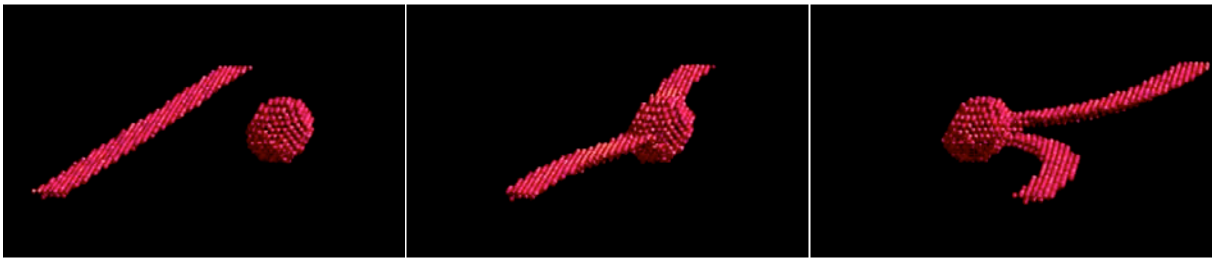

(a) (b) (c)

Fig. 1. Interaction of an edge dislocation and 2nm void in bcc iron simulated by MD method at 10K; a) dislocation glide under imposed strain rate, b) dislocation attraction in the vicinity of void, c) dislocation release by shearing of the void.

Results on the stress-strain response are presented in Fig. 2. In order to investigate the effect of He accumulation in the cavity on the dislocation-defect interaction, various He contents quoted as the ratio of He atoms per vacancy at various temperatures have been investigated. Figs. 2a and 2b show the stress-strain response in the presence of a cavity at 10K for different He contents and at different temperatures for 1He:1V bubble respectively. In these graphs the drop point at the beginning of the plots is due to the attraction phenomenon observed in Fig. 1b and the maximum point of each plot relates to the dislocation release. Fig. 2a indicates that with increasing of He content, the release stress and strain decrease up to 2 He and then start to increase from 3 He upward. Moreover, Fig. 2b shows a slight decrease in release stress and strain with temperature for 1He:1V cavity excluding the case at 100K, which shows an increase. For peer investigation the release stress and strain deduced from Fig. 2 are plotted in Fig. 3. This figure indicates that from void to a content of 1He:1V the release stress and strain slightly decrease at low temperatures but there is a small increase at high temperatures. A rise in the He content in the cavity causes a first large drop at 2He:1V and then second large drop at 4He:1V in the release stress and strain. This later drop becomes more pronounced at high temperatures. According to these results the 5He:1V cavity presents the largest obstacle strength to the impinging edge dislocation. These graphs show exceptions, to the above mentioned trends, especially at high temperatures and high He contents. It may relate to the intrinsic stochastic nature of the simulated phenomena. Indeed, the large amplitude of vibration of atoms at higher temperatures and the large distortion of the surrounding lattice at high He content result in largely varying results, depending on slight variations of the input, such as a varying anneal time.

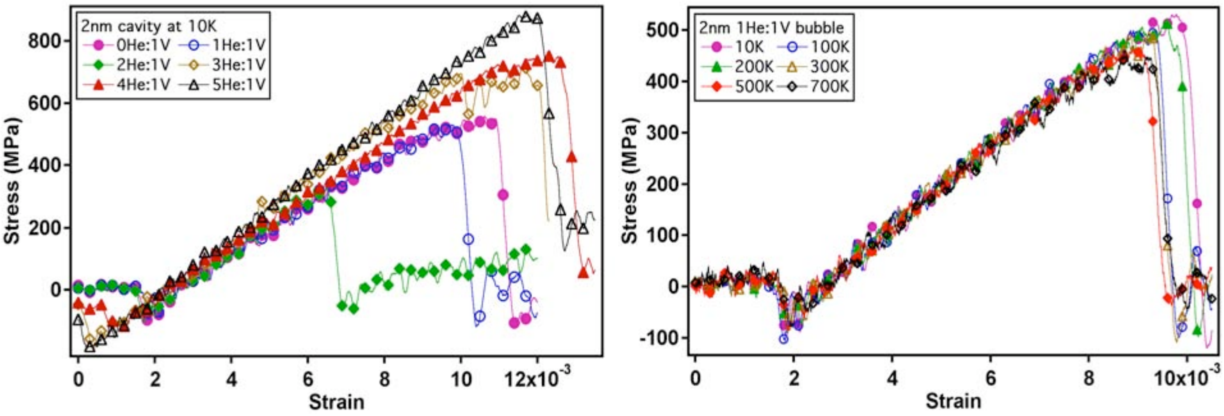

(a) (b)

Fig. 2. The stress-strain curve of edge dislocation interaction with 2nm cavity at, a) different He content for 10K, and b) different temperatures for 1He:1V cavity.

It appears that a 2 nm void is a stronger obstacle than a 2 nm He bubble at low He contents, whereas at the highest He content, especially at 5 He atoms per vacancy, the He bubble can become a stronger obstacle relative to void. On the basis of our studies, three criteria control dislocation-cavity interaction in the bcc iron. They are based on various microscopic mechanisms. One of them is a climb process, occurring when the dislocation escapes from the cavity after having sheared it, that was observed by Bacon and Osetsky [2] and presented as the main reason for passing of an edge dislocation by the void. Another mechanism is coherency of the He atoms with the bcc iron matrix lattice as shown by Morishita et al. [7], when the He content is low the configuration of He inside the cavity is bcc but at high He content the atomic arrangement has a close-packed configuration. The last mechanism implies that the passage of the dislocation through the cavity is governed by the internal pressure, which increases with increasing He content. Therefore on the basis of these mechanisms the behavior of dislocation-cavity can be rationalized as follows. For the case of void the main event to pass the defect is climb process where it becomes easier at high temperature and so decreases the release stress and strain with temperature. Furthermore mobility enhancement of screw part of dislocation at high temperatures could be another reason to ease the dislocation release. Adding 1He instead of 1vacancy acts as a bcc lattice inside the cavity and helps He bubble to be sheared by edge dislocation. In this situation temperature effects is less significant in comparison with 0He (void) due to decrease in the climb event probability. With further increase in He content the surrounding iron lattice starts to be distorted and prohibit dislocation movement but in the quantity of 2 and 4 He the coherent interface between He and iron seems to be main reason for release stress and strain drops. At 5 He the internal pressure initiates dislocation loop punching. Dislocation segments are emitted around the He bubble, which are strong obstacles to the mobile dislocation.

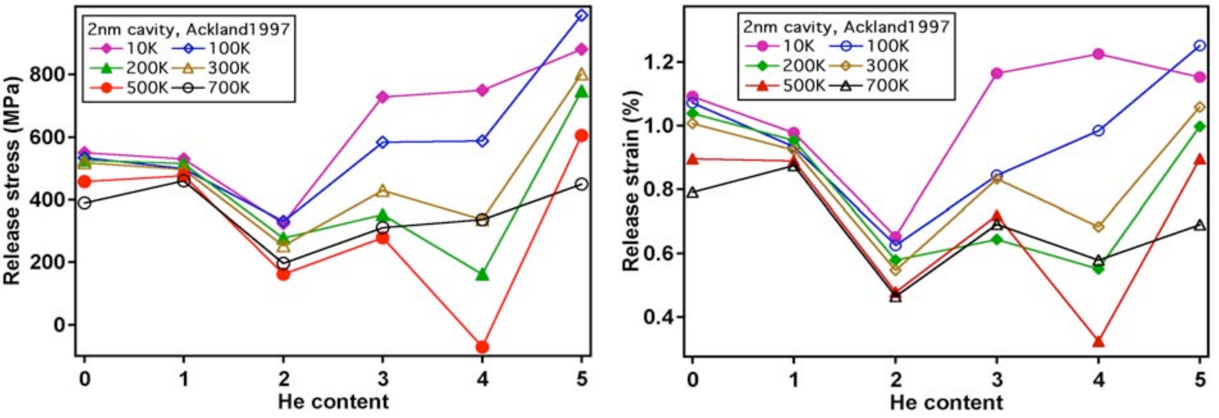

(a) (b)

Fig. 3. Resultant (a) release stress and (b) release strain of edge dislocation from 2nm cavity with different He contents and at different Temperatures.

4. Conclusion

In this work the interaction of an edge dislocation in Fe and cavity that may contain He was investigated using MD simulation. It appears that with increasing temperature the release stress and strain decrease. Furthermore it is proved that with increasing He content the cavity can either become softer or stronger as an obstacle. At the highest He content of 5 He atoms per vacancy loop punching occurs, which strongly increases the cavity resistance to the passage of the dislocation. But in general it could be state that low content He bubble is softer defect whereas high content He bubble is much stronger than empty 2nm cavity.

Acknowledgment

This research is funded by the European Fusion Development Agency (EFDA). PSI is acknowledged for the overall use of facilities.

References

[1] Yu.N. Osetsky, and D.J. Bacon, Modelling Simul. Mater. Sci. Eng. **11**, 427 (2003).
[2] D.J. Bacon, and Yu.N. Osetsky, Materials Science and Engineering A **365**, 46 (2004).
[3] D. Raabe, Computational materials science, WILEY-VCH, Germany, 1998, p. 87.
[4] G.J. Ackland, D.J. Bacon, A.F. Calder, and T. Harry, Philosophical Magazine A **75,** 713 (1997).
[5] W.D. Wilson, and R.D. Johnson, Rare gases in metals, in: P.C. Gehlen, J.R. Beeler Jr., R.I. Jaffee (Eds.), Interatomic Potentials and Simulation of Lattice Defects, Plenum, 1972, p. 375.
[6] D.E. Beck, Mol. Phsy. **14**, 311 (1968).
[7] K. Morishita, R. Sugano, B.D. Wirth, and T. Diaz de la Rubia, Nuclear Instruments and Methods in Physics Research B **202**, 76 (2003).
[8] B.D. Wirth, G.R. Odette, J. Marian, L. Ventelon, J.A. Young-Vandersall, and L.A. Zepeda-Ruiz, Journal of Nuclear Materials **329-333**, 103 (2004).

Impurity-induced decohesion in iron grain boundary
– A first-principles study –

Masatake Yamaguchi[1], **Yutaka Nishiyama**[2], **Motoyuki Shiga**[1],
Hideo Kaburaki[1], **H. Matsuzawa**[3]

[1]**Center for Computational Science and e-Systems (CCSE),** [2]**Nuclear Safety Research Center (NSRC), Japan Atomic Energy Agency (JAEA)**
[3]**Japan Nuclear Energy Safety Organization (JNES)**

ABSTRACT

First-principles calculations have been performed to simulate the grain boundary decohesion (embrittlement) in ferromagnetic bcc iron (Fe) $\Sigma3(111)$ symmetrical tilt grain boundary by adding various impurity or solute atoms (B, C, N, O, Si, P, S, Mn, Ni, Cu) to the boundary. We have successfully derived the segregation energy of the solute atom, tensile strength, and cohesive energy of the grain boundary, which are consistent with many empirical facts.

1. Introduction

It is well known that a small amount of impurity (solute) elements brings about a drastic change in the mechanical properties of metals. For example, sulfur segregates to grain boundaries (GBs) of metals and makes metals brittle. On the other hand, carbon segregation enhances the cohesion of the GBs. However, the microscopic mechanism of this cohesion/decohesion of the GBs is not well understood.

Recently, we have modeled the grain boundary decohesion by progressively adding sulfur atoms to a nickel $\Sigma5(012)$ grain boundary [1-3]. Our first-principles calculations have revealed that the aggregation of sulfur atoms to the grain boundary results in a drastic reduction of tensile strength by one order of magnitude.

In this paper, we briefly show the calculated results for the effects of various impurity or solute elements (B, C, N, O, Si, P, S, Mn, Ni, Cu) on the strength of the ferromagnetic bcc iron (Fe) $\Sigma3(111)$ symmetrical tilt grain boundary.

2. Calculations

The electronic structure calculations and crystal structure relaxations by force minimizations are performed using the Vienna Ab initio Simulation Package (VASP) with Projector Augmented Wave (PAW) potentials [4-7]. The cutoff energy for the plane wave basis set is about 280 eV. The Monkhorst Pack k-point mesh is 3x3x1. The Methfessel-Paxton smearing method with 0.1eV width is used. All calculations are done in the ferromagnetic state.

Figure 1 shows a unit cell modeling for bcc Fe$\Sigma3(111)[1\bar{1}0]$ symmetrical tilt grain boundary (STGB). The grain boundary (GB) plane lies horizontally at the center of the cell. The grain boundary plane is the crystallographic (111) plane and the tilt axis is $[1\bar{1}0]$ direction. The vacuum region is introduced in this cell to allow grain boundary sliding. This cell contains 76 Fe atoms. The Fe atom sites and vacancy site are labeled by numbers.

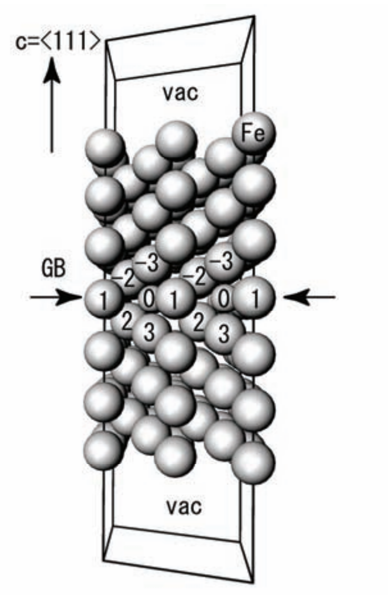

Figure 1. Unit cell model for bcc Fe Σ3 (111) [1$\bar{1}$0] symmetrical tilt grain boundary. Solid lines indicate the unit cell shape. This unit cell includes vacuum (vac) region. Numbers indicate atom sites. The site 0 indicates the grain boundary vacancy site. The other sites (spheres) indicate Fe atom sites. Site 0 and 1 are placed on the grain boundary (GB) plane. Four equivalent sites exist for each (number) site in this cell.

With this unit cell, we calculate the segregation energy. The segregation energy is an energy gain when segregant atoms move from the inner bulk region to the grain boundary region. We calculate the total energy difference between the above two states. Tensile strength and cohesive energy of the grain boundary are calculated by tensile test calculations. The details of the calculations will be described elsewhere [8].

3. Results and Discussion

Figure 2 shows the calculated segregation energy averaged over segregant atoms, tensile strength, and cohesive energy of the grain boundary with and without impurity (solute) segregation. We show the results for the two segregation concentration of 7.2 and 14.4 atom/nm^2, where 4 and 8 segregant atoms are segregated at the the GB in the unit cell as shown in Fig.1, respectively. Since the number of equivalent sites is four in the unit cell for each site, more than four segregant atoms cannot occupy one kind of site. The 0th-4th segregant atoms occupy site 0, site 1, or interstitial octahedral site (site 1o) depending on element without neighboring each other. The 5th-8th segregant atoms occupy site 2 or interstitial octahedral site (site 2o) close to site 2. Since the distance between site 0 (1, 1o) and site 2 (2o) is very close, segregant atoms neighbor each other.

Comparing the cohesive energy (2γ) and tensile strength (σ_{max}) results for each segregation case with those of clean FeΣ3 GB case in Fig. 1, we can interpret that each segregant atom is a cohesion enhancer or an embrittler. The important point of this study is that we derive the segregation energy simultaneously; a large segregation energy generally means that there is a possibility of realization for such a segregation. Roughly speaking, the average segregation energy above 1.0 eV/atom is very large. In this case, even several ten atomic parts per million (at.ppm) of the solute atoms can sufficiently segregate to the grain boundary under the ageing temperature of 800-1000 K according to the well-known McLean’s model for solute segregation.

Boron (B) and carbon (C) are well known to be cohesion enhancer of grain boundary. From Fig.2, we can see that B and C increase the cohesive energy of the GB (2γ) by keeping large segregation energy. High concentration (8N, 14.4atom/nm^2) of nitrogen(N) segregation reduces the 2γ by half. However, the segregation energy in this case is almost zero; this case is hard to realize.

The 2γ for sulfur (S) segregation case rapidly decreases with increasing sulfur concentration by keeping large segregation energy; this indicates that S is a strong embrittler. The 2γ for phosphorus (P) case slightly decreases up to 4 atom/unit cell (7.2atom/nm^2) by keeping large segregation energy, and then rapidly decreases up to 8atom/unit cell (14.4atom/nm^2) with rapidly decreasing segregation energy. This indicates that P works as an embrittler over 7.2 atom/nm^2, but this embrittling effect ceases with increasing segregation concentration. This is consistent with the experimental fact that P is a weak embrittler in contrast with S.

Copper (Cu) is known to precipitate to the grain boundary of iron by neutron irradiation. From Fig.1, we can see that the segregation energy of Cu increases with increasing segregation concentration up to 12 atom/unitcell (21.6 atom/nm^2). This indicates that Cu tends to precipitate to grain boundaries.

For other elements, there are some interesting findings. In particular, the embrittling effect of oxygen (O) is as large as sulfur (S). The details of discussion will be done elsewhere.

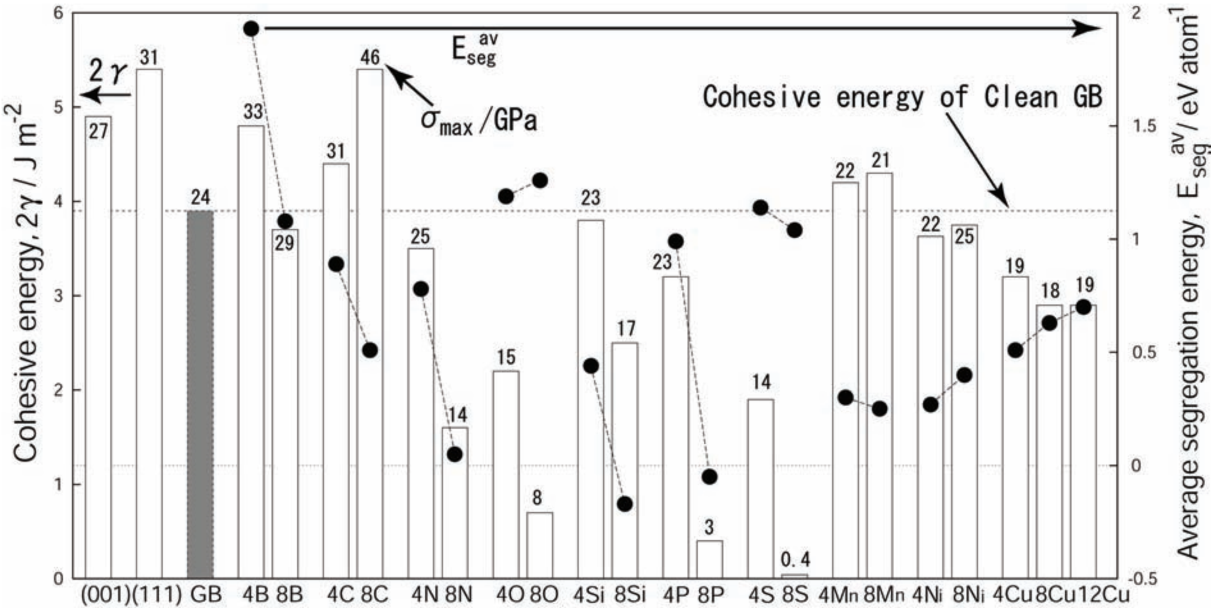

Figure 2. Calculated average segregation energy (E_{seg}^{av}, right), cohesive energy (2γ, left), and tensile strength (σ_{max}, shown numerically). The symbol (001) indicates the cleavage plane of bcc Fe, (111) the plane parallel to GB Σ3(111) plane, 'GB' the clean GB case (no segregation). '4B(8B)' indicates that 4(8) boron atoms are introduced in the GB region of the unit cell (Fig. 1) (4(8) atom/unit cell = 7.2(14.4) atom/nm^2).

Acknowledgements

We thank J. Kameda of University of Pennsylvania for helpful discussions.

References

[1] M. Yamaguchi, M. Shiga, and H. Kaburaki, Science 307, 393(2005).
[2] M. Yamaguchi, M. Shiga, and H. Kaburaki, Science 309, 1677d(2005).
[3] W.T. Geng, J.-S. Wang, and G.B. Olson, Science 309, 1677c(2005).
[4] G. Kresse and J. Hafner, Phys. Rev. B47, R558(1993).
[5] G. Kresse and J. Furthmueller, Phys. Rev. B54, 11169(1996).
[6] G. Kresse and D. Joubert, Phys. Rev. B59, 1758(1999).
[7] P. E. Bloechl, Phys. Rev. B50, 17953(1994).
[8] M. Yamaguchi, M. Shiga, H. Kaburaki, submitted to Mater. Trans.

Ageing of steels by nucleation and growth of Cu precipitates understood by a synopsis of various experimental methods, molecular dynamics and Monte-Carlo simulations of energy minimization

P. Kizler[1], **C. Kohler**[2], **P. Binkele**[1], **D. Willer**[1], **T. Al-Kassab**[3]

[1]**Materialprüfungsanstalt (MPA) Universität Stuttgart, Pfaffenwaldring 32, 70569 Stuttgart, peter.kizler@mpa.uni-stuttgart.de;** [2]**Inst. f. Materialprüfung, Werkstoffkunde und Festigkeitslehre (IMWF), Universität Stuttgart, Pfaffenwaldring 32, 70569 Stuttgart;** [3]**Inst. f. Materialphysik, Friedrich-Hund-Platz 1, 37077 Göttingen, Germany**

ABSTRACT

Atomic-scale simulation of the mechanical behaviour of solids is expected to provide insights into the mechanical behaviour of real materials such as steels. In the present contribution, precipitates in a thermally aged steel are characterized making use of Small Angle Neutron Scattering (SANS) and Atom Probe Field Ion Microscopy (APFIM). Information about their distribution in radii and distances and chemical composition results from Monte Carlo (MC) simulations of energy minimization. Molecular Dynamics (MD) simulations yield the critical resolved shear stress of selected configurations of precipitates. It is possible to merge this knowledge into a consistent understanding of the macroscopic experimental increase in yield strength due to thermal ageing of a Cu-alloyed steel.

1. Scope of the Study

The present study describes the linking of various structural information to a satisfying numerical understanding of precipitation strengthening. The involved methods are as follows: macroscale mechanical data (experimental), SANS (experimental), MC-simulations of energy minimization (theoretical), APFIM (experimental), and MD (theoretical).
.

1.1 Problem Definition and Macroscale Mechanical Data

The object of the present study is a steel with the denomination 15 NiCuMoNb 5 (WB36). After 10 years at 340°C, typical for power plant applications, the material's mechanical properties bear increases of yield strength by ~100 MPa and of Vickers hardness HV10 by ~35 [1]. The steel contains Cu, Ni and Mn with 0.63, 1.29 and 0.94 wt.-%, resp., together with smaller amounts of other elements. Precipitate formation of Cu, Ni and Mn is the reason for the change in mechanical properties, because they are obstacles to dislocation movement.

1.2 Small Angle Neutron Scattering (SANS)

Sizes and number densities of precipitates in the present steel samples were obtained previously by SANS [2]. After manufacturing, a fraction of Cu, Ni and Mn has already precipitated. After 10 years at 340°C, the number of precipitates has multiplied by ~10, with a mean radius of 1.29nm, a mean distance of ~18.0 nm and a number density of $1.6 * 10^{17} \mathrm{cm}^{-3}$ [2].

1.3 Monte-Carlo-(MC-) Simulations of energy minimization and precipitate growth

The nucleation and growth of precipitates in Fe can be simulated with a MC algorithm [3]. The algorithm of [3] was upgraded to include also Ni and Mn atoms. It turned out that Mn and, mainly, Ni atoms form a diffuse “shell” around a Cu-rich core of the precipitates.

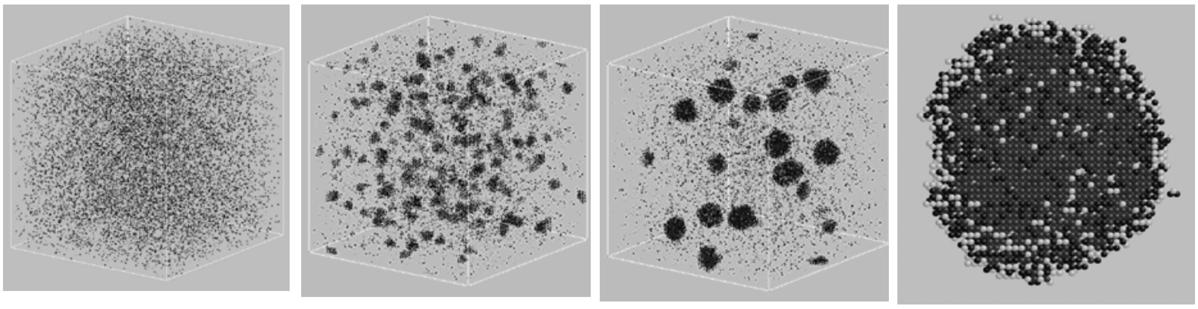

Start with random arrangement of atoms

T = 330°C, t = 40 months

T = 330°C, t = 360 years

cube length: 36.8 nm; 4194304 lattice sites. Fe atoms transparent

Section through a big precipitate. Cu = grey, Ni = light grey, Mn = dark grey; Fe = transp.

Fig. 1: Left three plots: several stages of simulated precipitate growth. **Right:** Enlarged section through one big precipitate, showing the Ni enrichment in its outer part.

The scatter of precipitate radii and mutual distances is a further result from the simulations:

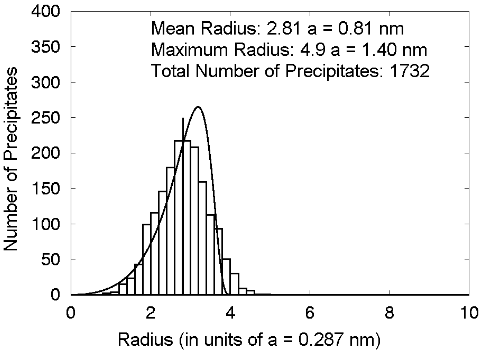

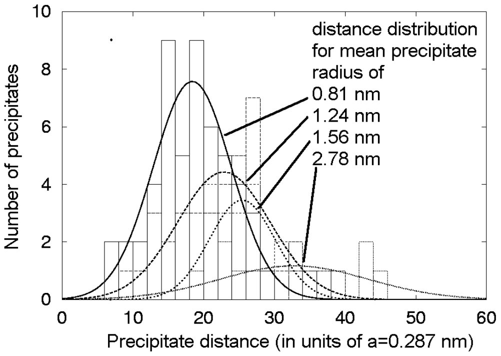

Fig. 2a (left): Distribution of precipitate **radii** for a distinct mean radius. Histogram bars = result from MC-simulations. Continuous line = continuum theory by Lifshitz-Slyozov-Wagner; see [3]. **Fig. 2b (right):** Distribution of precipitate **distances** for several mean radii.

1.4 Atom Probe Field Ion Microscopy, Tomographic Atom Probe (APFIM/TAP)

Atomwise detection of precipitates is possible by APFIM / TAP; for details: e.g. [4]. Again, a dense Cu core, a Ni/Mn “cloud” around it and a slight Si enrichment is detected. Equivalent results were obtained by other researchers for similar precipitates using APFIM.

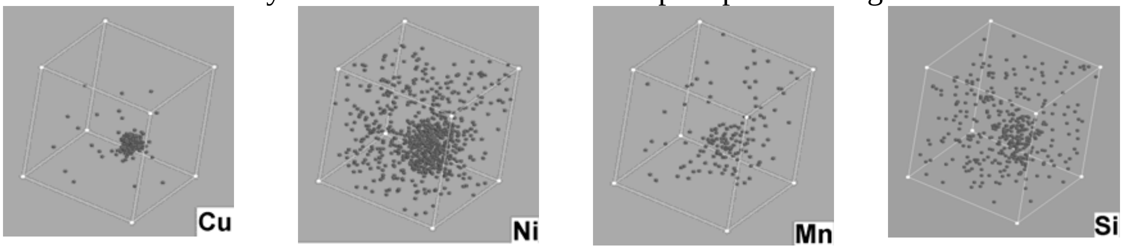

Fig. 3: Example of visualization of APFIM / TAP data obtained from one precipitate. Edge lengths of the cubes: 8nm. Fe atoms not shown. From left to right: Cu. Ni, Mn, Si.

1.5 Molecular Dynamics, MD

MD simulations are the essential method to study from atomic principles the interaction between dislocations and precipitates during plastic deformation. The increase $\Delta\tau_C$ of the critical resolved shear stress τ_C can be derived from them. Any MD simulation requires knowledge of the atomic structure of the solid under consideration, i.e. sizes, distances and chemical compositions. In the present study, these structural data are taken from the mentioned experiments and from the MC simulations. Fig. 4a shows series of $\Delta\tau_C$ for selected radii of pure Cu precipitates, aligned with defined distances L. For details and influences of further parameters (e.g. temperature, shape, admixture of Ni) see [5].

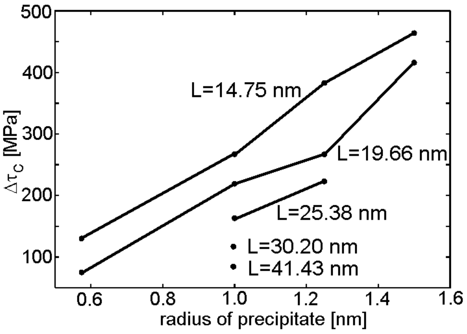

Fig. 4a: Dependence of $\Delta\tau_C$ on radius and distance of precipitates, aligned in linear order

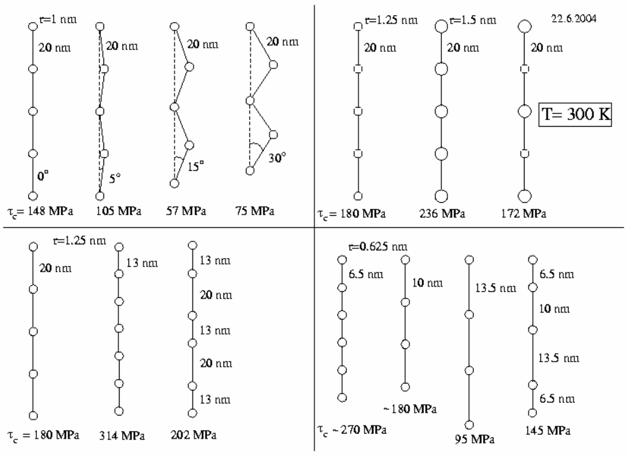

Fig. 4b: $\Delta\tau_C$ versus different kinds of disorders in size and arrangement of precipitates

1.6 Molecular dynamics (MD) and structural disorder

Contrary to the simplified case of Fig. 4a, the precipitates are neither of same size nor equidistant. A full MD treatment of a whole model like in Fig. 1 would exceed current computer resources. Instead, typical cases of scatter in radii, distances and arrangement of precipitates, see Fig. 4b, had to undergo a MD simulation. The amounts of disorder were derived from results like in Fig.2, joined with the SANS results. The decrease of the “strengthening power” of the precipitates was thus estimated from several extreme disordered arrangements.

1.7 Synopsis: Linking all information

In order to link the atomic scale data to the macroscopic experimental data, all effects shall be joined. The increase in critical resolved shear stress at –273°C for Cu precipitates with an average radius of 1.29 nm and the average distance of 18.0 nm amounts to $\Delta\tau_C$ = 300 MPa. This value shrinks for several reasons: Temperature of experiment with T = +90°C instead of T = -273°C reduces $\Delta\tau_C$ by ~33%; A nickel shell of 20% of total radius reduces by another 20%, the scatter of precipitate positions in direction of dislocation movement by 50%, and the scatter of precipitate radii and distances by 20%, respectively. All reduction factors multiplied with each other cause a reduction of $\Delta\tau_C$ by ~89%, leaving 33 MPa. To multiply this critical shear stress with the Schmid factor of 3 results in the critical tensile stress of 105 MPa, which agrees very well with the experimental value of 100 MPa.

2. Summary

The present study merges various experimental results (SANS, APFIM/TAP, tensile tests) and two atomistic simulation techniques (MD for dislocation movement and MC for precipitate growth) into a consistent numerical understanding of precipitate strengthening. The study has shown that it is possible to understand the change of a material's property from principles on the atomic scale. The study also extends previous knowledge about precipitate-hardened steel and emphasizes (i) the importance of precipitates with a size smaller than one can count by TEM, (ii) the chemical inhomogeneity and the geometrical scatter of the precipitate and (iii) withdrawal of the strengthening formula by Russell and Brown. The impact of structural disorder currently can be taken into account only by a consideration of "worst cases". A more precise approach would be to include also mesoscale dislocation movement calculations [6]. The change of the flow curve and the yield stress also changes the crack growth resistance of such a steel. As was shown in [7], knowledge of the change in flow curve data can be used to alter the input the data for finite element simulations of crack growth including damage models. Therefore, knowledge of the yield behaviour allows also to model more complex material properties such as the crack growth behaviour depending on the J-integral.

Acknowledgement

This work was supported by Bundesministerium für Wirtschaft und Arbeit, grant No 1501228

References

[1] M. Schick, J. Wiedemann, D. Willer, *Untersuchungen zur sicherheitstechnischen Bewertung von geschweissten Komponenten aus Werkstoff 15 NiCuMoNb 5 im Hinblick auf die Zähigkeitsabnahme unter Betriebsbeanspruchung.* BMU-Projekt SR2239, Materialprüfungsanstalt (MPA) University of Stuttgart (1997)

[2] J. Föhl, D. Willer, K.-H. Katerbau *Effect of Copper Precipitates on the Toughness of Low Alloy Steels for Pressure Boundary Components.* 30th MPA-Seminar, Proceedings, pp. 11.1 – 11.15 , Materialprüfungsanstalt (MPA) University of Stuttgart (2004). ISSN 0722-401X

[3] P. Binkele, S. Schmauder, *An Atomistic Monte Carlo Simulation of Precipitation in a Binary System,* Z. Metallkunde **94** (2003) 858-863, and: *Atomistic Computer Simulation of the Formation of Cu-Precipitates in Steel,* Computational Materials Science **24** (2002) 42-53.

[4] T. Al-Kassab, R. Kirchheim, *Investigation of phase decomposition in alloys with the tomographic atom probe,* Materials Science and Engineering **A 324** (2002) 168-173.

[5] C. Kohler, P. Kizler, S. Schmauder, *Atomistic Simulation of precipitation hardening in α-iron: influence of precipitate shape and chemical composition.* Modelling and Simulation in Materials Science and Engineering **12** (2005) 35-45.

[6] V. Mohles, B. Fruhstorfer, *Computer Simul. of Orowan Process Controlled Dislocation Glide in Particle Arrangements of Various Randomness,* Acta Mat. **50** (2002) 2503-2520.

[7] P. Kizler, D. Uhlmann, S. Schmauder, *Linking nanoscale and macroscale: calculation of the change in crack growth resistance in steels with different states of Cu precipitation using a modification of stress-strain curves owing to dislocation theory.* Nuclear Engineering and Design **196** (2000) 175-183.

Validation of an Improved Cluster Dynamics method with KMC Simulations

Joël Lépinoux

LTPCM (UMR 5614 CNRS), INPG
BP75, 38042 St Martin d'Hères, France
Joel.Lepinoux@ltpcm.inpg.fr

ABSTRACT

Before modelling the interaction of precipitates with other defects, one has to understand how they nucleate and grow. A simple situation (AlZr alloys) was considered to compare the prediction of a classical method (Cluster Dynamics) with a reference solution provided by Kinetic Monte Carlo simulations. This work aims at extending the domain of validity of CD towards high temperatures and high solute concentrations. The key data is the free energy of clusters, which has been accurately computed for the L12 structure in a wide range of temperature. Then it has been shown that at high temperature it is necessary to account for the entropy of the cluster gas. Another important effect, mostly at low temperature, is the passive coagulation, although its influence is finite in time.

1. Introduction

Like irradiation defects, precipitates can significantly influence mechanical properties (in particular) through their interaction with other defects (dislocations, grain boundaries, micro-cracks...). But contrary to irradiation, precipitation is a widely used process entering in the design of alloys. Indeed, the nature, the size and the distribution of precipitates can be used to control the grain size, through recrystallization and grain growth processes [1], as well as plastic deformation [2] at various stages.

In all these fields, numerical simulations have proved to be a privileged way to enhance our understanding of the involved mechanical, physical or chemical mechanisms. Compared with experimental tools which have experienced comparable improvements, the great advantage of numerical simulations is their ability to study model materials in which only the desired effect is present. The main task of multiscale modelling is to optimize the ratio between accuracy and computing time as required by industrial standards, for instance by expressing relevant information provided by simulations at microscopic scale in a convenient form for practical use.

As long as only chemical effects are involved, at the microscopic scale, Kinetic Monte Carlo (KMC) simulations on rigid lattice are the right choice (for a recent review, see [3]). On the other hand, the simplest method likely to provide a detailed picture of precipitation is Cluster Dynamics (CD) [4]. In the first case, atoms exchange with a vacancy according jump probabilities based on a carefully built interatomic potential, while in the second case, clusters capture or release solute atoms according two coefficients depending on the diffusion coefficient of solute atoms and the free energy of clusters. Thus, in practice, the question is: what can be learnt from KMC simulations which can be used to improve CD? CD is known to provide convenient results for very dilute alloys [4], at least from low to moderate temperatures. The aim of this work is to extend these limits toward high solute concentrations and high temperature, by comparing CD predictions with KMC simulations. For that purpose a simple situation, AlZr alloys, was chosen. KMC simulations were performed by E. Clouet [5] using a potential truncated at the second neighbours (*a* <110>) which is convenient to model precipitates of L_{12} structure in a FCC matrix. The diffusion coefficient of solute atoms was carefully measured and it was shown that only monomers can diffuse [5] which is the ideal situation for a comparison with CD. In classical CD, the evolution of a given class of cluster size *n* is given by the following master equation:

$$\dot{C}_n = \alpha_{n+1} C_{n+1} + \beta_{n-1} C_{n-1} - (\alpha_n + \beta)_n C_n \tag{1}$$

α_n and β_n are respectively the so-called evaporation and condensation factors which have to satisfy the detailed balance $\alpha_{n+1}\tilde{C}_{n+1} = \beta_{n-1}\tilde{C}_{n-1}$ where $\tilde{C}_n$ is the equilibrium concentration of the class *n*. given by $\tilde{C}_n = \left[\tilde{C}_1\right]^n \exp\left(-\Delta F_n / k_B T\right)$; ΔF_n is the difference of free energy between a *n*-mer and *n* 1-mers, *T* the temperature and k_B the Boltzmann constant. Precipitation being controlled by the long range diffusion it is assumed that any solute atom arriving on a cluster is immediately incorporated. Thus, all the information about the thermodynamical properties of clusters of size *n* is passed through the α_n coefficient. So finally, the only parameter one needs to calculate is the free energy of clusters.

2. Monte Carlo calculation of free energy

Instead of computing directly the free energy, an alternative approach was developed [6] to define consistently capture and release factors for a given size of cluster. These coefficients can provide interesting insights about the morphology of clusters; with other quantities like the real surface of clusters they can be computed very accurately by a Monte Carlo technique in a generic way for a given structure as a function of the reduced temperature T/T_w where T_w has been defined by $T_w = (W_{ab}/2k_B)$ and W_{ab} is the usual interaction energy parameter which for the L_{12} structure concerns the second neighbours ($W_{ab} = 2E_{ab} - (E_{aa} + E_{bb})$ E_{ij} being the interaction energy between atoms of nature *i* and *j*). With these notations, the capture and release factors can be computed using the following form, respectively:

$$w_{n,n+1} = \nu \left\langle \sum N_{bonds}^{shell} Exp + \left(N_{bonds}^{cluster} \left(\frac{T_w}{T} \right) \right) \right\rangle_{(n)} \tag{2}$$

$$w_{n+1,n} = \nu \left\langle \sum N_{bonds}^{shell} Exp - \left(N_{bonds}^{cluster} \left(\frac{T_w}{T} \right) \right) \right\rangle_{(n+1)} \tag{3}$$

N_{bonds}^{shell} and $N_{bonds}^{cluster}$ are the numbers of links between a candidate site (for emission or absorption) and the shell (the free solute layer surrounding a cluster) and the cluster, respectively; ν is a frequency related to the diffusion coefficient. It can be shown that the ratio of these two coefficients gives access to the free energy:

$$\frac{w_{n,n+1}}{w_{n+1,n}} = \exp\left(- \frac{\Delta F_{n+1} - \Delta F_n}{k_B T} \right) \tag{4}$$

Results obtained with this technique (Fig. 1) show that the classical capillary approximation is

convenient for clusters larger than 30, approximately, but an enhanced form is necessary to obtain accurate fits for smaller clusters (i.e. the free surface energy depends on cluster size). The L_{12} structure having a low number of coordination, at low temperature, the curve exhibits sharp changes due to the high weight of compact configurations. Comparisons with simpler method of calculatio
above 50

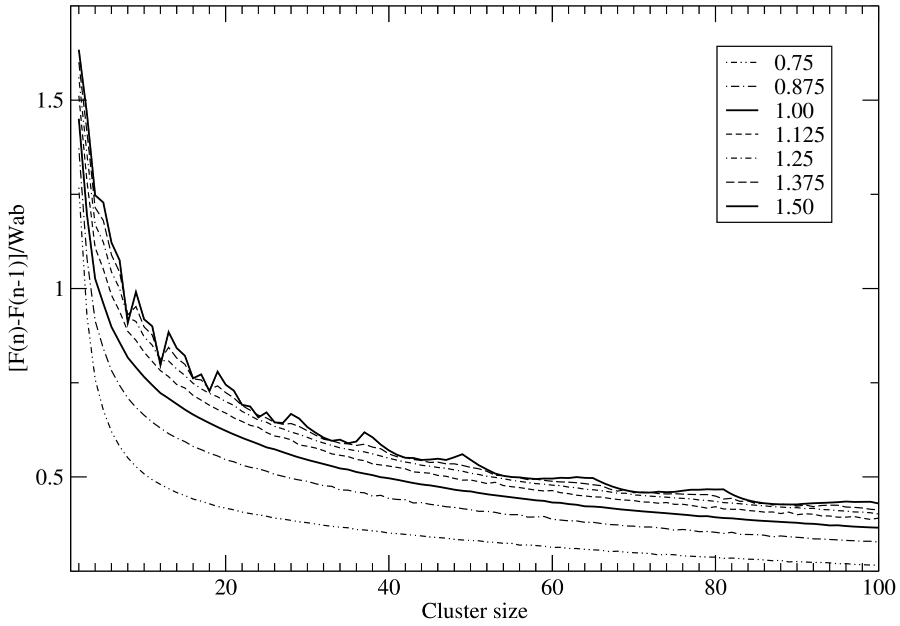

Figure 1: [*F(n)-F(n-1)*] normalized by *Wab* versus the cluster size (*n*) for different (*Tw/T*).

3. Comparing KMC and CD results

To compare with experimental results the most convenient quantities are clearly the average size of clusters and the number of clusters. But concerning the comparison of KMC and CD, due to its L shape, the curve of the average cluster size is a poor reference. Instead, the precipitated fraction, i.e. the product of the two above quantities is more convenient. For sake of simplicity, these quantities have been calculated for clusters larger than the initial critical size n^*. These average quantities are convenient to detect a divergence between KMC and CD results but cannot explain the origin of these differences. For that purpose one needs to compare the evolution of the cluster distribution, i.e. the state of the system as given by the two techniques, disregarding the physical time itself. Apparently this comparison is easy as both techniques provide easy access to this quantity. However there is a difficulty related to the finite size of the simulation box in KMC. Indeed, this implies a finite limit for the smallest possible concentration of a cluster size. For instance, for a system of 10^6 sites, a class represented by only one cluster has a concentration of 10^{-6}. This also means that many classes are empty. So finally the direct comparison of cluster concentrations is not self-sufficient. In addition, it is also recommended to compare the cumulated solute concentration defined by $\hat{C}_n = \sum_{k=1}^{n} kC_k$; it is equals to the concentration of monomers for n=1 and to the total solute concentration for n=n_{max}.. This curve is fairly invariant with the size of the KMC simulation box and empty classes are no more a problem. This quantity is certainly the best signature of KMC simulations. A particular component of this quantity is C_1 the concentration of monomers. Most results can be plotted versus C_1 instead of time to postpone the examination of the coupling with long range diffusion.

4. Matrix frustration and passive coagulation

In the classical theory of nucleation and CD, the equilibrium concentrations of clusters are calculated assuming that each cluster occupies only one atomic site, which is fully justified for very dilute systems. Accounting for the real volume of each cluster leads to an additional contribution to the total free energy of the system. Whatever the temperature, the main contribution arises from the arrangement of atoms within clusters, but at high temperature, the arrangement of clusters in the system is a contribution which has to be considered [8]. It leads to a modification of the ratio (4) through the modification of the equilibrium concentrations:

$$\tilde{C}_n = \tilde{C}_1^n \exp\left(-\frac{\Delta F_n}{k_B T}\right) \exp\left(-\sum_k \tilde{C}_k \, \Delta V_{k,n}\right) \tag{5}$$

with $\Delta V_{k,n} = \left(V_{k,n} - nV_{k,1}\right)$ the difference of volume forbidden to cluster k by a cluster n and n monomers; these quantities being calculated by the same method than the free energy.

At medium temperature the frustration of the matrix can be neglected, however an increasing deviation appears between both methods at the end of the nucleation stage and then decreases slowly during coarsening. This behaviour is the signature of a moderate coagulation process due to interaction of close growing clusters, without cluster diffusion, contrary to massive coagulation observed in aerosols, for instance. Passive coagulation is a purely statistical process whose probability is proportional to cluster concentration. It behaves like a perturbation of the master equation of CD. The clusters obtained in KMC have been analysed with Eqns. (2-3). A systematic deviation appear around n*, i.e. the structure of clusters is as expected for subcritical clusters but not for supercritical ones. From these measurements it is possible to deduct an effective free energy function to be used instead of the one computed previously for n>n*.

These corrections succeed to significantly extend the domain of validity of CD.

Acknowledgements

This work was initiated during the joint research program “CPR Precipitation” (Arcelor, Pechiney, CNRS and CEA). Dr. E. Clouet is gratefully acknowledged for stimulating discussions and for providing his KMC data.

References

[1] D. Weygand, Y. Bréchet and J. Lépinoux, “*Inhibition of Grain Growth by Particle Distributions*”, Mater. Scie. Eng. A, 292, 34 (2000)

[2] J. Lépinoux and Y. Estrin, “*Mechanical Behaviour of Alloys Containing Heterogeneously Distributed Particles*”, Acta mater., 48 , 4337 (2000)

[3] P. Bellon, “*Kinetic Monte Carlo simulations in crystalline alloys*” in Thermodynamics, Microstructures and Plasticity, Eds. A. Finel et al., Kluwer Academic Publishers (2003)

[4] E. Clouet, A. Barbu, L. Lae, and G. Martin, “*Precipitation Kinetics of Al3Zr and Al3Sc in Aluminium Alloys Modeled by Cluster Dynamics*”, Acta Materiala, 53, 2343 (2005)

[5] E. Clouet, M. Nastar and C. Sigli, “*Nucleation of Al3Zr and Al3Sc in Aluminium Alloys*”, Phys. Rev. B, 69, 064109 (2004)

[6] J. Lepinoux, “*Interfacial Reaction Rates and Free Energy*”, Phil. Mag., 30, 3585 (2005)

[7] J. Lépinoux, “*Contribution of Matrix Frustration to the Free Energy of Cluster Distributions in Binary Alloys*”, to appear in Phil. Mag. (2006)

Cluster Expansion-Based Monte Carlo Simulations of Fe-Cr Solid Solution

Mikhail Yu. Lavrentiev[1](*), Duc Nguyen-Manh[1], Ralf Drautz[2], Peter Klaver[3], Sergei L. Dudarev[1]

[1]EURATOM/UKAEA Association, Culham Science Centre, Abingdon, OX14 3DB, UK;
[2]Department of Materials, University of Oxford, Parks Road, Oxford OX1 3PH, UK;
[3]School of Mathematics and Physics, Queen's University Belfast, Belfast BT7 1NN, Northern Ireland, UK.
(*) Mikhail.Lavrentiev@ukaea.org.uk

ABSTRACT

Iron-chromium alloys are characterised by a complex phase diagram, the small negative heat of formation at low Cr concentrations in bcc α-structure of Fe and by the inversion of short-range order parameter. Here, we present Monte Carlo simulations of Fe-Cr alloy based on cluster expansion approximation for the enthalpy of the system. The set of cluster expansion coefficients is validated versus the DFT results on small clusters in bcc structure. The enthalpy of mixing is negative at small Cr concentrations up to high temperatures. Also, at small concentrations chromium atoms are well separated from each other. Clustering of Cr atoms begins at concentrations of about 10% at 800 K and 20% at 1400 K. Short-range order parameters were calculated and it was confirmed that negative values of the first and second parameters at low Cr concentrations change sign at about 10.5% Cr, in agreement with experiment. We demonstrate that complex ordering reactions in Fe-Cr and its properties may be described by a few concentration-independent expansion coefficients.

1. Introduction

The research and development of improved materials for future fusion power plant is widely recognized as the key element in the development of new energy sources [1]. One of the most serious challenges for the current work on prospective fusion reactors is the development of materials able to perform reliably for long time under specific conditions, which include high irradiation levels (total dose of 50 to 200 dpa) and high temperature (up to 1000°C). Two specific alloy systems that are currently investigated are the low-activation ferritic/martensitic steels typically containing 8 to 9% Cr and the so-called nanocomposite ferritic alloys with 13±2% Cr. Thus, thermodynamic and mechanical properties of iron-chromium alloys, especially with relatively low (up to 16-20%) Cr content, are of particular importance. The operational temperature of prospective fusion power plant corresponds to the low-temperature part of the phase diagram where the magnetic bcc α-phase is stable. This important region, which includes large miscibility gap separating Fe-rich α-phase and Cr-rich α'-phase, is the subject of this paper. It is much more difficult to access experimentally than the high-temperature region, because lowering temperatures results in the much longer times necessary to reach equilibrium, greatly exceeding the time available for the experiment. In these circumstances, modelling studies are of particular importance, since they allow us to avoid difficulties associated with conducting experimental investigations. This paper reports first results of Monte Carlo (MC) modelling of the properties of the α-phase, starting with cluster expansion Hamiltonian. The full version of the current study will be published elsewhere [2].

2. Methods

The cluster expansion (CE) method is used to describe the enthalpy of a crystal where the position of each atom can be assigned to a lattice site [3]. For binary systems, the occupation variable $\sigma = +1(-1)$, when a lattice site is occupied by the atomic species A(B), respectively, is introduced. The energy of the crystal is then calculated as a sum over all the clusters of the system. For the current study, an initial pool of 24 compact clusters on the bcc lattice was considered and reduced to only 12 CE coefficients.

In simulations of non-stoichiometric solid solutions using ‘standard’ MC, high potential barriers prevent sampling the whole of the configurational space since almost always only one arrangement of atoms, the initial configuration, is sampled. Exchange MC simulations, introduced recently [4], solve this problem for systems with configurational disorder by allowing explicit change of atomic configurations. In any step, an exchange between two randomly selected (different) atoms, resulting in a new configuration, is attempted. The decision whether to accept or reject the exchange is made according to the standard Metropolis scheme. Exchange MC allows us to calculate enthalpy of mixing, short-range order parameters and shape and size of precipitates of one phase in another (e.g. Cr clusters in α-phase). Most of the simulations reported in this paper were performed using a simulation box consisting of 40×40×40 bcc unit cells (128000 atoms). MC runs consisted of 10^8 exchange attempts in both equilibration and accumulation stages (3125 exchange attempts per atom).

3. Results

In Fig. 1, the lowest heats of formation, obtained by simulated annealing of small supercells as a function of concentration, are shown. We validated our results by comparing them with our own DFT data [5-6]. The DFT calculations consistently give negative heat of formation at low Cr concentrations, which changes sign at higher Cr concentrations, so that everywhere above ~10-12% Cr the mixing energy is positive. Despite consisting only of 12 CE coefficients, the cluster expansion gives good agreement with DFT, showing negative heat of formation only for Cr content <12%.

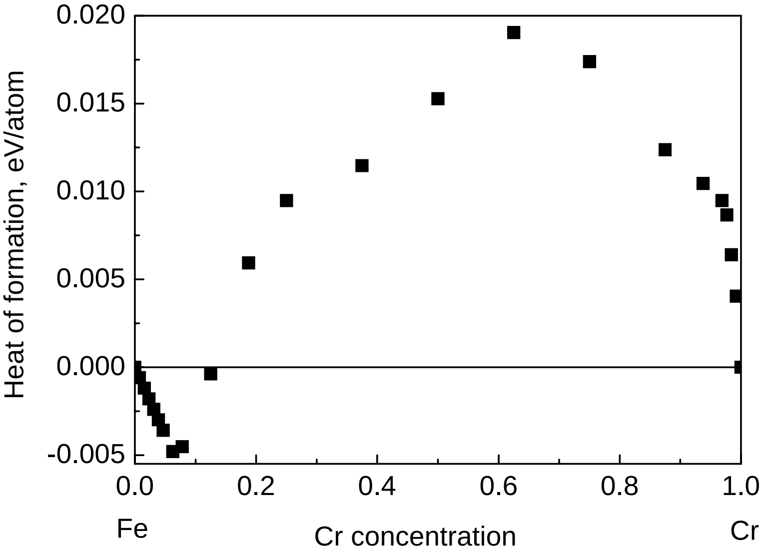

Figure 1. Heats of formation ($\Delta H = H_{\mathrm{alloy}} - x_{\mathrm{Fe}}H_{\mathrm{Fe}} - x_{\mathrm{Cr}}H_{\mathrm{Cr}}$) obtained by simulated annealing vs Cr concentration.

The presence of the minimum of the heat of formation results in the formation of a solid solution of Cr in Fe (α-phase) at small Cr concentrations for all temperatures. As the Cr concentration increases, the system separates into two phases.

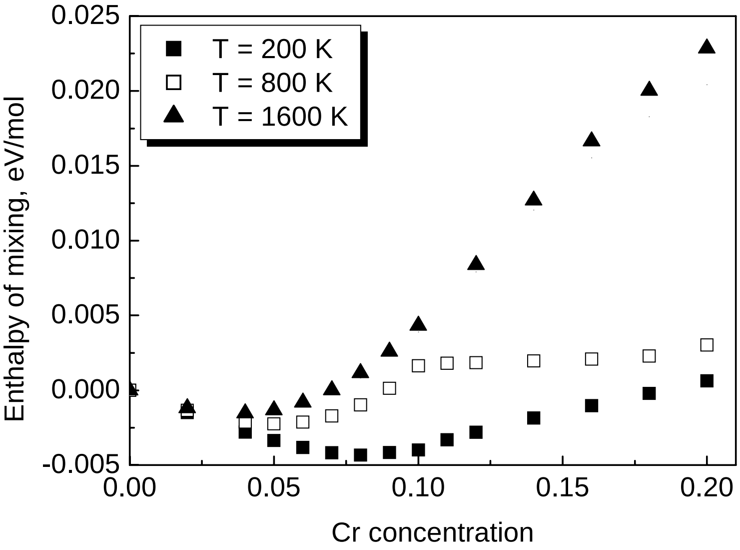

Figure 2. Enthalpy of mixing of the FeCr solid solution vs Cr concentration.

The transition from pure α-phase to phase separation is seen as a change of behaviour of the enthalpy of mixing as a function of Cr content. In Fig. 2, where the enthalpy of mixing is shown for a number of temperatures and Cr concentrations up to 20%, this change of behaviour is seen at about 10% Cr for T=800 K. At even lower temperature T=200 K, the enthalpy of mixing remains negative for the entire range of concentrations.

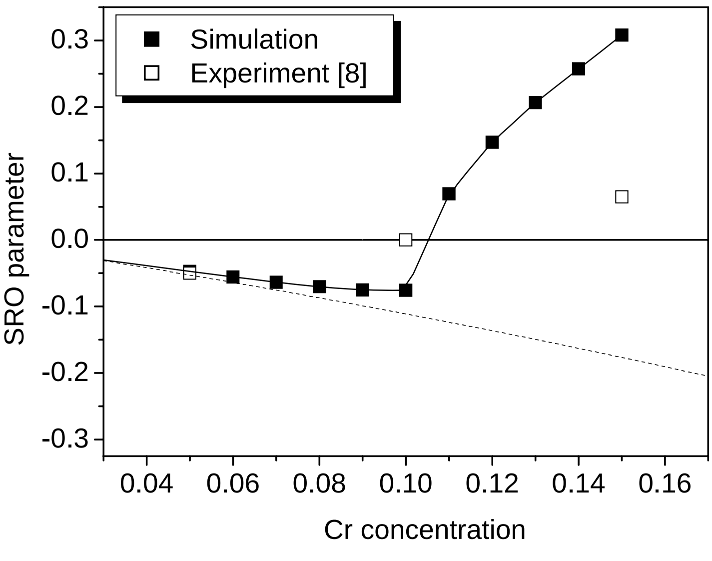

Figure 3. Calculated SRO parameter at T=750 K and the experimental data [8].

The first prediction of negative short-range order (SRO) parameters in FeCr at small Cr concentration with inversion of sign at the first nearest neighbour position to positive at about 25% Cr was made in 1983 [7], and later this effect was confirmed experimentally [8]. The actual concentration where the inversion takes place is approximately 10% Cr. We present results of our calculations of the SRO parameters at temperature T=750 K, close to the temperature of the original experiment (705 K), in Fig. 3. The dashed line shows the lowest possible theoretical value of the order parameter. For small concentrations of Cr, we found behaviour similar to the experimental: negative value of parameters, which is very close to theoretical minimum at 5% C, changes sign at 10.5% Cr. The discrepancy is larger at 15% Cr, where our results are substantially higher than the experimental values, indicating that the degree of clustering of Cr atoms at that concentration and T=750 K in our model is much larger than in the experiment. The reasons for that might be both the limitations of the used set of CE coefficients, and metastable structure of the experimental specimen.

Finally, we studied shapes of Cr clusters. At T=0 K and 10% Cr, the lowest-energy configuration consists of one large Cr cluster, with Cr-Fe interfaces parallel to the [110] planes. The same cluster shape remains at temperature T=200 K, but now the system consists of a number of smaller clusters. At T=800 K and 10% Cr, the clustering has not yet started, but after increasing Cr concentration by 1% only, large cluster already is created with many smaller clusters continuing to exist alongside the big cluster.

4. Conclusions

We performed a Monte Carlo study of properties of FeCr solid solution, based on the CE approximation, with special emphasis on low Cr concentration range (up to 20%). Our results proved usefulness and suitability of the combined cluster expansion and Monte Carlo approach to the study of iron-chromium alloys. The CE coefficients set, consisting of 12 clusters, was validated via comparison of energies with available experimental data and results of DFT calculations, and used in the large-scale MC simulations. The results obtained gave deeper insight into the clustering and short-range order in FeCr, and can be used in future studies of the phase diagram and non-equilibrium behaviour of this important system.

Acknowledgements

Fruitful discussions with Prof. A.P. Miodownik are gratefully acknowledged. This work was performed in the framework of the Materials for Fusion Power Plants consortium and funded by EFDA, EURATOM, UKAEA, UK-EPSRC and by EXTREMAT.

References

[1] I. Cook. Materials research for fusion technology. Nature Materials **5**, 77 (2006).
[2] M.Y. Lavrentiev, R. Drautz, D. Nguyen-Manh, P. Klaver, and S.L. Dudarev, to be published.
[3] J.M. Sanchez, F. Ducastelle, and D. Gratias. Generalized cluster description of multicomponent systems. Physica A **128**, 334 (1984).
[4] N.L. Allan, G.D. Barrera, M.Yu. Lavrentiev, I.T. Todorov, and J.A. Purton. Ab initio calculation of phase diagrams of ceramics and minerals. J. Mater. Chem. **11**, 63 (2001).
[5] T.P.C. Klaver, R. Drautz, and M.W. Finnis. Phys. Rev. B, submitted.
[6] D. Nguyen-Manh, M.Yu. Lavrentiev, and S.L. Dudarev, to be published.
[7] M. Hennion. Chemical SRO effects in ferromagnetic Fe alloys in relation to electronic band structure. J. Phys. F: Met. Phys. **13**, 2351 (1983).
[8] I. Mirebeau, M. Hennion, and G. Parette. First measurement of short-range-order inversion as a function of concentration in a transition alloy. Phys. Rev. Lett. **53**, 687 (1984).

Influence Of Cr Content On The Resistivity Recovery Of Electron Irradiated Fe-Cr Binary Alloys: A Model

Authors: Dmitry A. Terentyev[1], Lorenzo Malerba[1] and Pär Olsson[2]

Affiliations: [1]SCK•CEN, Reactor Materials Research Unit, Boeretang 200, B-2400 Mol, Belgium, dterenty@sckcen.be and lmalerba@sckcen.be; [2]EDF-R&D, MMC Dept., Les Renardières, 77750 Moret-sur-Loing, France, par.olsson@edf.fr

ABSTRACT

We used rate equations to model experimental resistivity recovery results for concentrated Fe-Cr alloys to obtain information about the concentration and strength of Cr configurational traps for self-interstitial atoms, that are expected to exist based on atomic level modelling.

1. Introduction

Fe-Cr binary alloys are model materials for low activation ferritic/martensitic steels considered for structural components in future nuclear power systems. The presence of Cr is known to determine, among other properties, good swelling resistance [1], which is one of the critical parameters for component design under irradiation. A number of reasons for this effect have been proposed [2], among them the existence of a point defect-solute attractive interaction, leading to enhanced recombination. Recent *ab initio* studies show indeed that single self-interstitial atoms (SIAs) can be strongly bound to Cr atoms; in particular, configurations involving two Cr atoms can provide a binding energy as high as 0.24 eV [3]. This Cr-SIA interaction has been claimed to exist also based on resistivity recovery experiments in diluted alloys, showing that SIAs in Fe-Cr diffuse with a slightly lower migration energy than in pure Fe (shift of stage I peak to lower temperature), but are trapped and then released at higher temperature (stage II) [4]. These traps have been proposed to be configurations including at least two Cr atoms [4,5]. In concentrated Fe-Cr alloys (4÷16%Cr) the effect of these traps becomes overwhelming and a progressive suppression of stage I with increasing Cr concentration has been found in [5,6] (see Fig. 1a).

Using interatomic potentials capable of reproducing this type of SIA-Cr interaction, it has been demonstrated that the mobility of small SIA loops that migrate in one-dimension is significantly reduced by the presence of Cr in Fe matrix and this has also been proposed to be a possible reason for swelling suppression in Fe-Cr versus Fe [7]. Similar studies are being now extended to small, three-dimensionally migrating defects such as single SIAs and show, consistently with experimental evidence, that the single SIA migration energy decreases with the addition of Cr. Nonetheless, in this case the timeframe of molecular dynamics simulations is not sufficient to provide complete information about all the possible trapping configurations encountered by a freely migrating defect. So, in order to obtain data for microstrucure evolution models parametrisation and benchmarking, other means must be found to obtain at least an indication about how the concentration of traps and their strength depend on Cr concentration. In this work we used rate equations to reproduce the experimental resistivity recovery curves from [6]. By parameterising the model based on assumptions coming from both experimental evidence and atomic-level modelling indications, it was possible to extract information on concentration and strength of SIA traps as a function of Cr content.

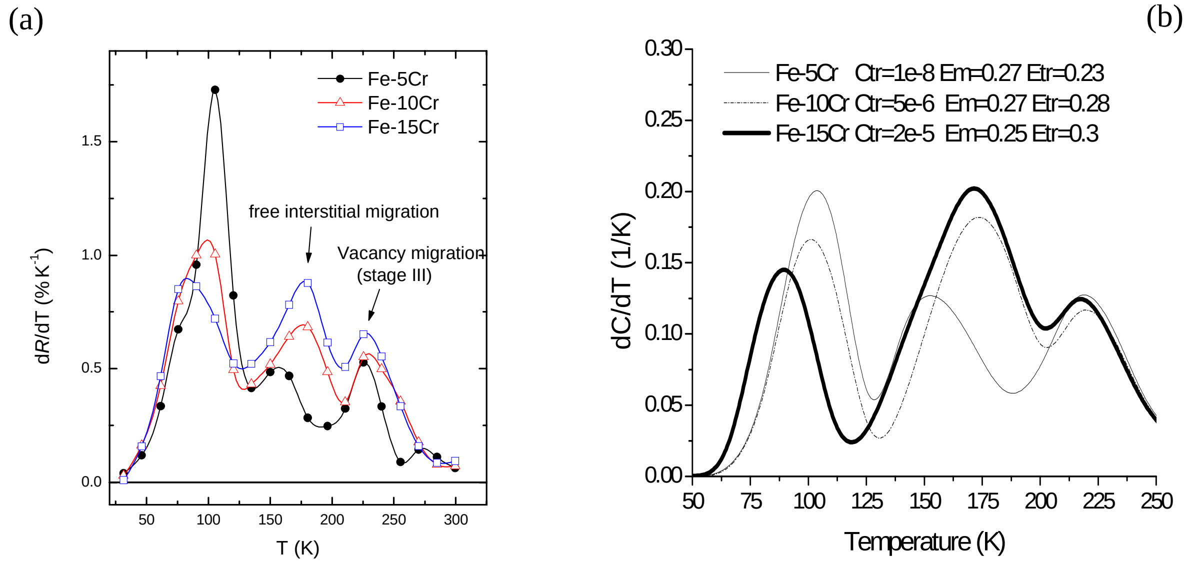

Figure 1. (a) Results of resisitivity recovery in Fe-5Cr, Fe-10Cr and Fe-15Cr alloys from [6]. Stage I is attributed to correlated recombination and long-range migration of SIAs; stage II is believed to be the release of SIAs from traps and stage III is due to free migration of vacancies. (b) Differential concentration of defects in Fe-Cr alloys as calculated in this work.

2. Model

The basic assumption of the model is that in Fe-Cr alloys configurational traps for SIA exist and their concentration (C_{tr}) and trapping energy (E_{tr}) depend on the Cr content. The concentration of traps for each alloy was chosen to provide good agreement with experimental data on the fractional recovery at stage II. The trapping energy was chosen to obtain good agreement with the experimental results on the position of the peak corresponding to stage II. The SIA migration energy has been varied to provide the correct position of stage I. The vacancy migration energy has been taken to be 0.55 eV as in pure Fe and largely independent of Cr concentration, based on *ab initio* indications [3]. Since single SIAs are the focus of the present work, the parameterization of the migration and interaction of SIA and vacancy clusters has been taken from [8]. The initial dose, annealing temperature and timesteps were the same as in the experiment [6]. However, we assumed that about 80% of the produced defects annihilated below stage I via close pair and correlated recombination, thus we took a Frenkel pair concentration of 80 appm at the beginning of stage I. Tab. 1 summarises the adjusted parameters.

3. Results

The derivative of the defect concentrations in Fe-Cr alloys versus temperature calculated using the parameters given in Tab. 1 are shown in Fig. 1b. The migration energy of the SIA in the Fe-Cr alloys must be lower than in Fe to obtain the correct position of stage I. Good agreement for the fractional recovery at stage I is obtained for Fe-10Cr and Fe-15Cr; less for Fe-5Cr, maybe due to an unaccounted for contribution from correlated recombination, which is strongly suppressed and does not contribute in the other two alloys. The position of the stage III peaks is reproduced in accordance with experimental data; their width, however, is not fully correct, as the "shoulder" at temperatures above 250 K is absent. This may be an effect of short-range order changes, which is unaccounted for in the present model. Another reason for the absence of the "shoulder" could be an incorrect parameterization of SIA cluster mobility, which in the absence of better information were assumed to be immobile above size 4 (following [8]). However, the detrapping of single SIAs as an explanation for stage II seems at least realistic. Although a priori the introduction of different traps for the single SIA could be considered, the experimental peaks at 150 K, 175 K and about 225 K can be explained by the presence of three kinds of traps, with different characteristic trapping energies depending on Cr content (Tab. 1). Note that a tiny concentration of these traps is enough to reproduce fairly well the results for Fe-5Cr, while it grows by 3 and 4 orders of magnitude, respectively, going to Fe-10Cr and Fe-15Cr. At the same time, the concentration of traps in these alloys is much lower than the approximate concentration of Cr-Cr pairs which were proposed to be possible traps for SIAs [5]. At the same time, the trapping energy in Fe-5Cr seems to be in reasonable agreement with the *ab initio* prediction for two-Cr configurations (0.24 eV) [3]. Traps in Fe-10Cr and Fe-15Cr may therefore consist of more than two Cr atoms. It should also be noted that in all cases the trapping energies were of the same order of magnitude as the migration energy of the SIA, or higher (e.g. in Fe-15Cr).

Table 1. Parameterization of SIA and vacancy migration properties in Fe-Cr.

	Fe-5Cr	Fe-10Cr	Fe-15Cr
E_{mig} (SIA), eV	0.27	0.27	0.25
E_{mig}(vacancy), eV	0.55	0.55	0.55
C_{tr}, appm	10^{-2}	5	20
E_{tr}, eV	0.23	0.28	0.30

4. Summary and conclusions

The defect recovery stages in Fe-Cr alloys containing 5, 10 and 15%Cr have been modelled using rate equations, under three main assumptions: (i) traps for single SIA exist and their concentration depends on Cr content, (ii) the migration energy of the single SIA (when not trapped) depends on the Cr content as well and decreases compared to pure Fe; (iii) the vacancy migration energy is largely unaffected by the presence of Cr. The first assumption is suggested by both resistivity recovery experiments in concentrated alloys [5] and ab initio calculations [3]; the second one is suggested by resistivity recovery experiments in diluted alloys [4] and confirmed by (yet unpublished) MD simulations; the third one is suggested by a number of experiments (here uncited) and ab initio calculations [3]. In the absence of precise data in FeCr, the properties of SIA and vacancy clusters were parameterized according to the scheme proposed in [8]. The objective of the calculation was to obtain data on the unknown trap concentration and strenght. The model provides reasonable agreement with experimental data from [6].

From the model it can be deduced that by increasing the Cr content in the limit of 5-15%Cr the concentration of traps for the SIA increases drastically (three order of magnitude); the trapping energy increases as well. Including a consistent treatment of migration properties for small interstitial clusters is the next step to be taken.

Acknowledgements

This work was partially funded by EFDA, task TTMS-007.

References

[1] E.A. Little and D.A. Stow, *Void-swelling in irons and ferritic steels : II. An experimental survey of materials irradiated in a fast reactor***,** J. Nucl. Mater. **87,** 25 ((1979).

[2] E.A. Little, *Void-swelling in irons and ferritic steels: I. Mechanism of swelling supression*, J. Nucl. Mater. **87,** 11 (1979); R. Bullough, M.H. Wood, and E.A. Little, *A microstructural explanation for the low swelling of ferritic steels*, ASTM STP 725, 1981, p. 593.

[3] P. Olsson, PhD thesis, *Modelling of Formation and Evolution of Defects and Precipitates in Fe-Cr Alloys of Reactor Relevance,* University of Uppsala, ISBN 91-554-6365-7, 2005.

[4] F. Maury, P. Lucasson, A. Lucasson, F. Faudot, and J. Bigot, *A study of irradiated FeCr alloys: deviation from Matthiessen's rule and interstitial migration*, J. Phys. F: Met. Phys. **17**, 1143 (1987); H. Abe and E. Kuramoto, *Interaction of solutes with irradiation-induced defects of electron-irradiated dilute iron alloys*, J. Nucl. Mater. **271&272**, 209 (1999).

[5] A.L. Nikolaev, *Stage I of recovery in 5 MeV electron-irradiated iron and iron-chromium alloys: the effect of small cascades, migration of di-interstitials and mixed dumbbells,* J. Phys.: Condens. Matter **11**, 8633 (1999).

[6] A. Benkaddour, C. Dimitrov, and O. Dimitrov, *Irradiation-induced defects in ferritic FeCr alloys*, Mater. Sci. Forum **15-18**, 1263 (1987); C. Dimitrov, A. Benkaddour, C. Corbell, P. Moser, Ann. Chim. Fr. **16**, 319 (1991).

[7] D. Terentyev, L. Malerba, and A.V. Barashev, *On the correlation between self-interstitial cluster diffusivity and irradiation-induced swelling in Fe-Cr alloys*, Phil. Mag. Lett. **85**, 587 (2005).

[8] C.C. Fu, J. Dalla Torre, F. Willaime, J.L. Bocquet, and A. Barbu, *Multiscale modelling of defect kinetics in irradiation iron*, Nature Mater., **4** 68 (2005).

Ordering And Clustering In Fe-Cr Binary Alloys: An Atomistic Simulation Study

Authors: Giovanni U. Bonny[1], Lorenzo Malerba[1], Dmitry A. Terentyev[1], Pär Olsson[2], Christophe Domain[2]

Affiliations: [1]SCK•CEN, Reactor Materials Research Unit, Boeretang 200, B-2400 Mol, Belgium, gbonny@sckcen.be, lmalerba@sckcen.be and dterenty@sckcen.be; [2]EDF-R&D, Dept. MMC, Les Renardieres, Route de Sens, 77750 Moret-sur-Loing, France, par.olsson@edf.fr and christophe.domain@edf.fr.

ABSTRACT

We performed atomistic kinetic Monte Carlo simulations using recently fitted two-band model potentials for FeCr. The results confirm the capability of these potentials to reproduce the peculiar thermodynamic behaviour of FeCr alloys, at least up to the region of 700 K.

1. Introduction

Fe-Cr binary alloys are model materials for low activation ferritic/martensitic steels considered for structural components in future nuclear power systems. Both early experiments [1] and recent ab initio calculations [2] reveal that the Fe-Cr system exhibits a change of sign of the mixing enthalpy, which is negative below a critical concentration of about 10%Cr (denoting full solubility and a tendency to partial ordering in this region) and positive above (where Cr clustering into a separate Cr-rich phase becomes favoured). This peculiar behaviour strongly influences the response of these alloys under irradiation. Above the critical concentration the appearance of the Cr-rich α' phase is well known to induce hardening and embrittlement after thermal ageing [3] and this effect becomes accelerated under irradiation [4]. Below, the formation of (partially) ordered solutions may also have an effect on the motion of dislocations and may even induce the formation of yet unknown fully ordered phases, thereby influencing the mechanical properties of the alloy. In addition, recent models suggest that the swelling behaviour of these alloys may be largely determined by the effect that the present phases have on the mobility of radiation-formed self-interstitial atom clusters [5]. These facts highlight the importance of having atomistic simulation tools capable of accounting for the correct thermodynamic behaviour of Fe-Cr systems, in view of studying radiation damage in these alloys. This objective has been partially reached with the recent development of two-band model (2BM) interatomic potentials capable of reproducing the change of sign of the mixing enthalpy versus concentration in this system [6]. These potentials have been qualitatively shown to be able to account for the formation of Cr-rich α' phase precipitates [6]. Here they are further validated using atomistic kinetic Monte Carlo (AKMC) methods [7] to show that they predict changes in the short-range order (SRO) parameter, in fair agreement with experiments. The same methodology is used to simulate the thermal ageing of Fe-Cr alloys above the critical concentration, using a specific technique to identify the formation of Cr-rich (but not Cr pure!) precipitates. In view of these results, strong and weak points of these potentials are briefly discussed.

2. Method

Two 2BM potentials for FeCr have been produced, each fitted to a different mixing enthalpy curve for ferromagnetic FeCr, calculated with a different ab initio technique [6]. From the used ab initio technique, they will be denoted as EMTO and PAW, respectively [6]. A set of AKMC simulations [7] has been performed using both potentials, for concentrations ranging from 2% to 30% Cr and temperatures from 500 to 1800 K (incremented by blocks of 50 K), using periodic boundary conditions. In these simulations the evolution of the system was driven by single vacancy diffusion jumps, with constant attempt frequency ($\nu_0=6.0\cdot10^{12}$ s^{-1}) and activation energy, E_a, linearly dependent on the total energy variation after the jump ($E_a=E_0+\Delta E/2$, with $E_0=0.65$ eV for Fe atoms and 0.56 eV for Cr atoms, following ab initio indications [8]). The associated jump frequency, $\Gamma=\nu_0\exp(E_a/k_BT)$, where k_B is Boltzmann's constant and T the temperature, was used to obtain the jump probability and select the event to occur according to the standard Monte Carlo algorithm. Boxes containing 54000 atoms (30×30×30 lattice units) were found to be large enough to build in them fully random initial distributions of atoms. Ten million MC steps were generally sufficient to reach convergence from the point of view of the SRO. The resulting atomic distributions were analysed by counting the 1st and 2nd nearest neighbour (1nn and 2nn) Fe-Fe, Fe-Cr and Cr-Cr pairs (denoted here as N_{ij}^{α}, with i,j=Fe,Cr and α=1,2 for the shell) and applying the definition:

$$SRO_\alpha = 1 - \frac{1}{c_{Fe}} \frac{N_{CrFe}^{\alpha}/2}{N_{CrCr}^{\alpha} + N_{CrFe}^{\alpha}/2} \qquad (1)$$

where the division by 2 is required because the SRO is calculated by sitting on Cr atoms only and c_{Fe} is the Fe concentration. It was checked that all initial atomic configurations provided $SRO_\alpha=0$ (as should be for random distributions) with an error bar of 10^{-3} maximum. To compare the results of the simulation with the experimental values provided by Mirebeau et al. [1], the average 1nn-2nn SRO was then obtained as $\overline{SRO}=(8SRO_1+6SRO_2)/14$.

Longer simulations for selected concentrations of Cr and temperatures have been run to obtain a qualitative picture of the microstructure predicted by the FeCr potentials after thermal ageing. To recognise and count precipitates we assigned to each lattice position a concentration, obtained as local concentration within a sphere extending to the 5nn shell. Based on the expected Cr concentration in the α' phase, each site with a concentration >80% was selected as part of the precipitate Then, all atoms within 5nn distance to each selected site were included in the same cluster. The average size was calculated assuming spherical shape.

3. Some results

Fig.1 shows the SRO parameter vs. Cr content at 700 K, which is the temperature for which experimental data, also shown, where produced in [1]. The potentials provide excellent agreement in the low Cr region, although they diverge above the critical concentration. This discrepancy is probably related to a Cr concentration in the α' phase somewhat higher than in the experiment and also to an overestimated extension to high temperature of the α-α' miscibility gap. The agreement is nonetheless satisfactory, in particular the change of sign is clearly very well reproduced.

Fig.2 displays the final configuration after 10^9 Monte Carlo steps of thermal ageing at 750 K of Fe-13%Cr: all Cr atoms (left) and the centres of the regions of high Cr content (right). These centres succeed in removing the noise due to the matrix Cr concentration and allow precipitate density and size to be unambiguously defined. The central inset shows for example the average diameter versus Monte Carlo timesteps. Although these results are for the moment only qualitative, they show the ability of the model to predict ordering and clustering in the correct Cr concentration regions. Possibly more importantly, the level of order is comparable with the experimental one and the concentration of Cr inside the precipitates is at least in the range that should be experimentally expected.

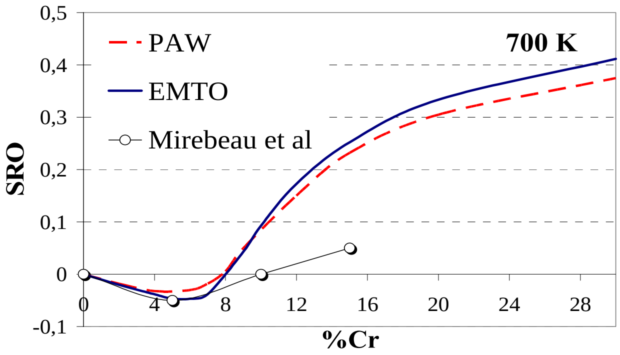

Figure 1. SRO vs. Cr concentration at 700 K for both 2BM potentials and in experiment.

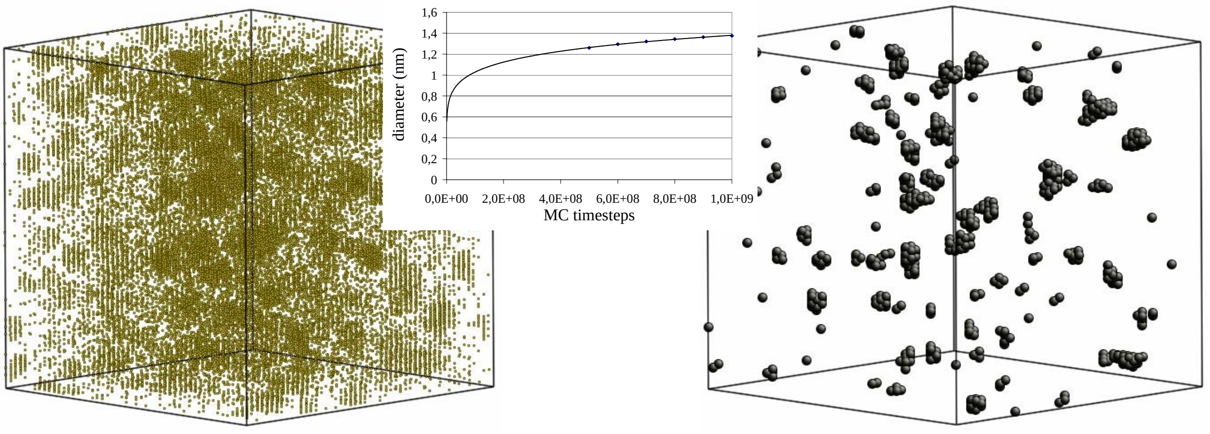

Figure 2. Final snapshot after 10^9 Monte Carlo steps of thermal ageing at 750 K of Fe-13%Cr. Left: all Cr atoms; Right: centres of regions with >80%Cr. Central inset: evolution in time of the precipitate average size

4. Conclusions

The 2BM potentials embody a reasonably correct description of the peculiar thermodynamic behaviour of FeCr and can therefore be safely used for radiation damage studies, at least up to the region around 700 K.

References

[1] I. Mirebeau, M. Hennion and G. Parette, Phys. Rev. Lett. **53(7)**, 687 (1984).
[2] P. Olsson, Ph.D. thesis, Uppsala University, 2005.
[3] P.J. Grobner, Metall. Trans. **4**, 251 (1973).
[4] P. Dubuisson, D. Gilbon and J.L. Séran, J. Nucl. Mater. **205**, 178 (1993).
[5] D.A. Terentyev, P. Olsson, L. Malerba and A.V. Barashev, J. Nucl. Mater., submitted.
[6] P. Olsson, J. Wallenius, C. Domain, K. Nordlund and L. Malerba, Phys. Rev. B **72**, 214119 (2005).
[7] C. Domain, C.S. Becquart and J.-C. van Duysen, Mater. Res. Soc. Symp. Proc. Vol. **540**, 643 (1999).

Object Kinetic Monte Carlo Study of Sink Strengths

Authors: Lorenzo Malerba[1], Charlotte Becquart[2], Christophe Domain[3]

Affiliations: [1]SCK•CEN, Reactor Materials Research Unit, Boeretang 200, B-2400 Mol, Belgium, lmalerba@sckcen.be; [2]LMPGM, UMR-CNRS 8517, U. Lille 1, 59655 Villeneuve d'Ascq, France, charlotte.becquart@univ-lille1.fr;[3]EDF-R&D, Dept. MMC, Les Renardieres, Route de Sens, 77750 Moret-sur-Loing, France, christophe.domain@edf.fr.

ABSTRACT

We have calculated the sink strength of spherical absorbers for defects migrating according to three- to one-dimensional paths using a kinetic Monte Carlo simulation technique, finding excellent agreement in the whole range of diffusion regimes with theoretical expressions used in rate equation models, including pure one-dimensional diffusion.

1. Introduction

The sink strength for three-dimensionally (3D) versus one-dimensionally (1D), or mixed 1D/3D migrating defects, in irradiated materials has attracted much attention because many experimental observations cannot be interpreted unless 1D or mixed 1D/3D migration patterns are assumed for self-interstitial atom clusters produced in cascades during irradiation [1]. Analytical expressions for the sink strenghts for defects migrating in 3D [2] and also in 1D [3] have been therefore developed and a "master curve" approach has been proposed to describe the transition from purely 1D to purely 3D defect migration [4]. Object kinetic Monte Carlo (OKMC) methods [5] have subsequently been used to corroborate the theoretical expressions [6] but, although good agreement was generally found, the ability of this technique to reach the 1D migration limit has been questioned, the limited size of the simulation box used in OKMC studies having been mainly blamed for the inadequacies of the model [3,6]. In the present work, we explore the capability of OKMC to reproduce the sink strengths of spherical absorbers in a wide range of volume fractions, for defects characterised by different migration dimensionality, from fully 3D to pure 1D. We show that this technique is capable of reproducing the theoretical expressions for the sink strengths in the whole range of conditions explored. We thereby demonstrate that, in spite of the limited size of the OKMC simulation box, the method is suitable to describe the microstructure evolution of irradiated materials for any defect migration pattern, including fully 1D migrating defects.

2. Simulation Model

The general features of the OKMC code used in the present work, LAKIMOCA, have been extensively described in a previous publication [5]. Here the model is used only for idealised situations, as was done by Heinisch and co-workers [6], where only one migrating defect at a time is present in the simulation box, in a microstructure defined by only one class of sinks at a time, of well defined geometry. In the present case these were unsaturable spherical absorbers randomly distributed in the simulation box, of radius varying from 0.75 to 10.2 nm and number density from 10^{16} to $1.5{\cdot}10^{17}$ cm^{-3} (corresponding to volume fractions from $1.8{\cdot}10^{-5}$ to $4.1{\cdot}10^{-1}$). Each simulation was done with all sinks characterised by the same radius and for a given density. The trajectory of each defect in the same simulation was followed until it was absorbed in a sink and at that point a new defect of the same type was introduced in the simulation box. The sink strength is thus obtained as:

$$k^2 = \frac{2n}{d_j^2 \langle n_j \rangle} \tag{1}$$

where $\langle n_j \rangle$ is the average number of jumps performed by the defects before being absorbed, d_j the jump distance and n the dimensionality of the motion. Since the defects are assumed to migrate in a bcc lattice, $d_j=\sqrt{3}/2a_0$, where a_0 is the lattice parameter (for α-Fe a_0=0.287 nm). The dimensionality of the motion of the simulated defects changed from case to case and was defined either by imposing that the defect must change direction after a fixed number of jumps n_j^0 (n_j^0=1 implies fully 3D motion), or by assigning an energy of re-orientation E_r (for consistency, n=3 in all cases). With the latter method, the change of direction is another possible stochastic event managed by the Monte Carlo algorithm. Between each re-orientation the defect moves along a $\langle 111 \rangle$ direction. The histories of at least 1000 defects were traced for each condition in order to obtain the average $\langle n_j \rangle$ and in most cases the number was as high as 10000. In addition, it was always verified that the value had actually converged. Non-cubic boxes with periodic boundary conditions (PBC) were used for all calculations. The use of non-cubic boxes was instrumental in order to simulate correctly the 1D migrating defects.

3. Theory

Given a defect that migrates following a path not coinciding with either the 3D or the 1D limit, the corresponding sink strength of spherical absorbers, $k_{1\text{-}3,s.a.}^2$, can be expressed as a function of the two limiting case sink strengths (3D and 1D) and of the typical length before change of direction, l_{ch}, using the master curve [4]:

$$y = 1/2\left[1+\sqrt{\left(1+4/x^2\right)}\right], \tag{2}$$

where $x^2 = l_{ch}^2 k_{1,s.a.}^2/12 + k_{1,s.a.}^4/k_{3,s.a.}^4$ and $y = k_{1-3,s.a.}^2/k_{1,s.a.}^2$ are two dimensionless variables and according to theory the sink strength of unsaturable spherical absorbers of radius R and density N for 3D migrating defects, $k_{3,s.a.}^2$, can be written as [2]:

$$k_{3,s.a.}^2 = 4\pi NR\left(1+R\sqrt{k_{3,s.a.}^2}\right), \tag{3}$$

customarily truncated at the first order, $k_{3,s.a.}^2=4\pi NR$, while for 1D migrating defects, $k_{1,s.a.}^2$, it is [3]:

$$k_{1,s.a.}^2 = 6\left(\pi RN\right)^2 \tag{4}$$

4. Simulation results

Fig. 1a shows the transition from 3D to 1D migration regime in terms of length before reorientation of the defect direction of motion (fixed amount of jumps). Fig. 1b provides the same information in terms of the master curve [4], including data for both fixed amount of jumps and rotation energies, showing that the choice of the method to impose the change of direction does not make any difference. Note that the simulation reproduces the complete 3D-to-1D transition and provides full agreement with the theoretical expressions, with relatively little scatter. More details and comparisons will be given in a forthcoming publication [7].

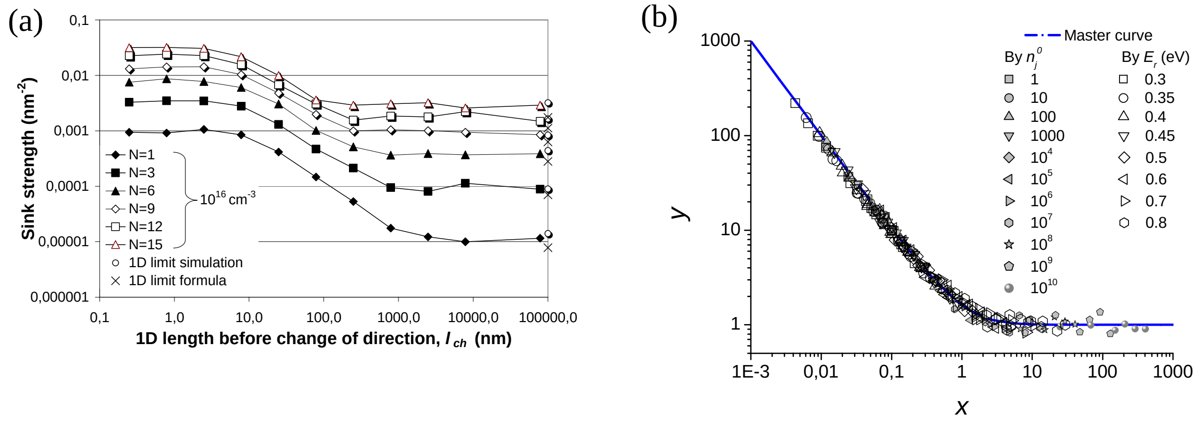

Figure 1. Transition from 3D to 1D sink strength for different spherical absorber densities and radii, (a) versus length of 1D segments before re-orientation (values for pure 1D limit according to theory and simulation are also given) and (b) in terms of master curve (eqn. 2).

5. Conclusions

These results show that the OKMC technique, in spite of its inherently stochastic and discrete nature, can trustfully describe the strength of sinks of given geometry, size and density in a large range of sink volume fractions, in full agreement with theoretical expressions obtained in the framework of a mean-field, continuum approach. In addition, in spite of the finiteness and relatively small size of the simulation box, this technique is capable of treating in a reasonably correct way also 1D migrating defects, whose migration path is orders of magnitude longer than the typical size of the box, provided that a non-cubic box is used for the simulation.

Acknowledgements

This work was performed as part of the PERFECT Integrated Project, partially funded by the European Commission (contract nr. FI6O-CT-2003-508840).

References

[1] H. Trinkaus, B.N. Singh, and A.J.E. Foreman, J. Nucl. Mater. **199**, 1 (1992); *ibid.* **206**, 200 (1993); ibid. **249**, 91 (1997); and *ibid.* **251**, 172 (1997).
[2] A.D. Brailsford and R. Bullough, Philos. Trans. R. Soc. London **302**, 87 (1981).
[3] A.V. Barashev, S.I. Golubov, and H. Trinkaus, Phil. Mag. **A81**(10), 2515 (2001).
[4] H. Trinkaus, H.L. Heinisch, A.V. Barashev, S.I. Golubov, and B.N. Singh, Phys. Rev. B **66**, 060105(R) (2002).
[5] C. Domain, C.S. Becquart, and L. Malerba, J. Nucl. Mater. **335**, 121 (2004).
[6] H. Heinisch, B.N. Singh, and S.I. Golubov, J. Nucl. Mater. **283-287**, 737 (2000); H.L. Heinisch and B.N. Singh, Philos. Mag. **83**(31-34), 3661 (2003).
[7] L. Malerba, C.S. Becquart, and C. Domain, J. Nucl. Mater., submitted.

A Dislocation Dynamics Approach for fcc Metals: Implementation of Partial Dislocations

Jaime Marian

Lawrence Livermore National Laboratory, 7000 East Avenue, L-367, 94551, Livermore, United States of America

The goal of this work is to study the interaction process between partial dislocations and stacking fault tetrahedra (SFT) using isotropic, non-singular, linear elasticity within the Dislocation Dynamics (DD) framework. To this end, a mechanism for node splitting governed by a local measure of the nodal energy has been implemented in our DD code. This allows us to explicitly resolve partial dislocations in fcc metals, including Shockley and Frank partials and stair-rod-type dislocations. In addition, due to the multifaceted (multiple glide planes) structure of SFTs, the Fleischer and Friedel-Escaig mechanisms for cross-slip have been implemented to enable a proper interaction between these two types of defects. Our DD formulation relies on a handful of parameters that need to be calibrated against experimental or modeling data. We have carried out Molecular Dynamics (MD) simulations to obtain the mobility functions for screw and edge dislocations in Cu. A numerical analysis correlating the Escaig stress, necessary for partial constriction, and the stress required to cross-slip at a given level of constriction has been performed. The dependence of these interactions with the other model parameters, such as core cutoff radius and non-singular stress shape function is assessed. In order to estimate the importance of core effects versus linear elastic effects, a connection with the atomistic scale is enabled by way of molecular statics calculations of cutoff radii and Shockley partial separation.

Combining *ab initio* and empirical potential calculations to study interstitial clusters in alpha-iron

Mihai-Cosmin Marinica [1], *Francois Willaime* [1]

[1] *Service de Recherches de Métallurgie Physique, CEA Saclay, Bat. 520, 91191 Gif sur Yvette Cedex, France*

Interstitial-type defects, which are formed by the clustering of self-interstitials produced under irradiation, have rather particular properties in α-iron: self-interstitials and – according to *ab initio* calculations – very small interstitial clusters are formed of <110> dumbbells, whereas larger interstitial clusters have either a <111> or a <100> orientation. This contrasts with other BCC metals where interstitial-type defects are predominantly <111>. The competition between these different orientations raises the question of their relative stabilities as function of size, and of the transformation mechanism from <111> to <100> orientation observed experimentally. Their mobilities is also a key issue in the interpretation of exper- iments. We have addressed these questions by combining *ab initio* and empirical potential approaches.

We have determined the stability and mobility of small self-interstitial defects by *ab initio* calculations performed on cells containing up to 250 atoms using the SIESTA code. We then used these results to fit and validate a new semi-empirical potential for iron, devel- oped starting from the EAM-type potential proposed by the Mendelev et al. This potential allowed us to complete the study of small clusters: (i) using the activation-relaxation technique (ART) we performed a systematic search of all possible cluster configurations and migration/rotation mechanisms; and (ii) using lattice-dynamics we studied their vibrational properties. Low frequency modes have been evidenced in <111>-type defects. The associ- ated large vibrational entropy is shown to have a significant effect on the relative stabilities at finite temperature. We then investigated the static and dynamic properties of dislocation loops containing up to 10^3 self-interstitials. We will discuss the sensibility to the potential of the results obtained for the stability and the mobility of large clusters and the effect of loop-loop interactions.

Defects produced in irradiated fused silica: influence of hydrogen concentration

F. Mota[1], M. J. Caturla[2], J. Mollá[3], J. M. Perlado[1], A. Ibarra[3]

[1] Instituto de Fusión Nuclear, Universidad Politécnica de Madrid, Madrid, Spain
[2] Dept. de Física Aplicada, Universidad de Alicante, Alicante E-03690, Spain
[3] Materiales para Fusion. Ciemat. Avda complutense 22, Madrid 28040, Spain

ABSTRACT

Molecular dynamics simulations are performed to obtain the damage produced during irradiation of fused silica for energies between the threshold displacement energy and 3.5 keV. The interatomic potential developed by Feuston and Garofalini specifically for amorphous SiO_2 is used in these calculations. The effect of Hydrogen in damage accumulation is also studied for an initial H concentration of 1%. Calculations show the formation of predominately four types of defects: Si3, Si5, O1 and O3 where the numbers denote their coordination . In the presence of H new defects appear while others are reduced. In particular, as expected, O-H complexes are formed, therefore reducing the number of oxygen atoms with coordination one.

1. Introduction

Fused silica has a wide range of applications. The interest on the effects of radiation in vitreous silica has increased recently due to its possible application as optical transmission component in fusion reactors. In this case, this material will be exposed to high neutron irradiation during operation. As a result point defects will be created that can lead to obscuration of the material; that is, degradation of the optical properties of silica. Among the defects observed under neutron irradiation are the Oxygen Deficient Centre (ODC), which is related to a silicon atom with coordination three instead of four, and the Non-Bridging Oxygen Hole Centre (NBOHC), which is related to an oxygen with coordination one.

Molecular dynamics simulations have proved to be useful in the description of defects produced by irradiation at keV energies in metals and semiconductors [1, 2], however the number of studies in oxides and in particular, in amorphous systems, is more reduced. We present molecular dynamics simulations of displacement cascades due to energetic recoils in amorphous silica. In particular, we have performed a statistical study of the different kinds of defects produced as a function of primary knock-on atom (PKA) energy. Our calculations show mainly four types of defects: Si3, Si5, O1 and O3 where the numbers denote their coordination . We present results for a PKA energy range between 0.4 eV and 3.5 keV. In addition, we compare these results with displacement cascades in the presence of a hydrogen concentrations of 1%, since hydrogen is always present in real conditions.

2. Simulation conditions

The interatomic potential developed by Feuston and Garofalini [3] specifically for fused silica has been used in these calculations. The same authors also developed a version of these potential for the H-Si-O system that has been used for the calculations of radiation effects in the presence of H [4]. This potential has been fitted for short range interactions to the Universal potential. The initial amorphous structure is generated by melting a beta-cristobalite lattice of SiO_2 and subsequently quenching down to 300K. For the calculations presented here a system with a total of 192000 atoms has been used, that is approximately 15x15x15 nm^3.

The evolution of an energetic particle is followed for times up to 5 picoseconds. The energetic particle in this case is always a silicon atom, and it is placed in the center of the simulation box. Periodic boundary conditions are used, with a bath control at the edges of the simulation box to maintain the temperature to 300K.

Defects are identified by its coordination. For the case of Si and O a cut-off distance between first and second nearest neighbors is used, obtained from the pair distribution function, and equal to 2.15 Å. For the case of H with Si or O a cut-off distance of 1.3 Å is used, also obtained from the pair distribution function. In the following we will use the notation *S#* where *S* will be the symbol corresponding to Si, H or O, and # is the coordination number of that atom in the lattice.

The initial concentration of defects is calculated, before the energetic recoil is placed. The four types of defects obtained are: Si5, Si3, O3 and O1. For the simulation box used in these calculations the concentration of these defects are 0.75%, 0.009%, 0.94% and 0.57% respectively. In order to understand the effect of H, this is included in the simulation in a concentration of 1%. The H is located at random positions in the lattice. Since the simulation is only followed for a few picoseconds before the energetic recoil is started, most of the H remains free, while 22% are forming O-H complexes. In this lattice containing H the number of defects present is (with respect to the 192000 atoms) 0.19% of Si5, 0.006% of Si3, 0.65% of O3, 0.31% of O1 and 0.22% of OH.

3. Defects produced by energetic particles

As mentioned above energetic particles are placed in the centre of the simulation box and their evolution is follow for a few picoseconds, until the number of defects does not change with time. Fig. 1 shows the average number of defects produced for the four different types found in the calculations Si5, Si3, O3 and O1, as a function of the recoil energy, and for the case where no H is included in the simulation. In order to observe only those defects produced by the energetic particles, the number of initial defects in the sample has been subtracted from the values on Fig.1. The number of defects of type Si3, O1 and O3 grow with recoil energy, and more oxygen type defects are formed than silicon type, as expected, due to their differences in mass. The number of Si5 defects does not show a clear trend with energy and in fact it is reduced. This could be related to healing of the defect due to the longer simulation time.

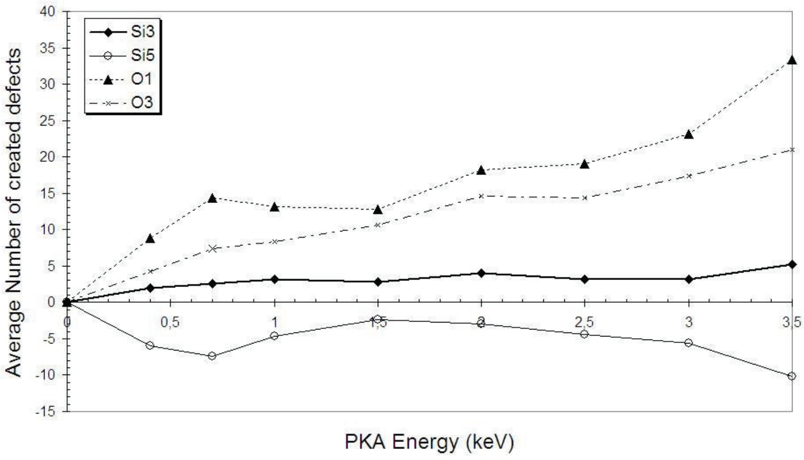

Figure 1: Average number of defects produced by the energetic atoms as a function of recoil energy.

Fig. 2 (a) shows the average number of defects for the case when 1% H is included in the initial lattice. The same four defects as in Fig. 1 are represented here, that is oxygen and silicon related defects. Notice that the number of O1 defects produced in this case is reduced with respect to the case above, while the number of O3 has increased. The number of Si3 has also decreased. In Fig. 2(b) those defects related to H are presented, in particular, the number of O-H type of defects. Two different types have been observed, a H connected to an O2 and a H connected to an O3. The O-H presented in the figure is the sum of these two types, while each of them are also presented. The H-free in the graph are the number of H atoms free in the lattice with respect to the ones that where free before the recoil. Clearly the number of free H is reduced with recoil energy and those H end up in O-H type configurations.

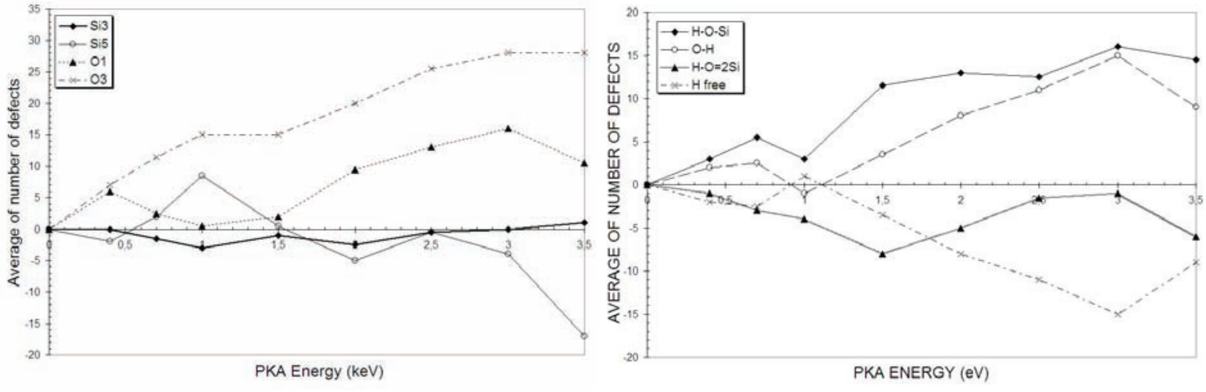

(a) **(b)**

Figure 2: Average number of defects produced by the energetic atoms as a function of recoil energy with 1% H in the sample. (a) Si5, Si3, O3 and O1 and (b) H related defects.

4. Conclusions

The main type of defects produced in fused silica under irradiation due to nuclear collisions has been obtained with molecular dynamics simulations. The main defects observed are oxygens with coordination one, which could be related to the NBOHC. Silicon atoms with coordination three are also observed, related to ODC.

When H is included in the lattice new defects appear, in particular O-H type of defects. The number of these defects increases with recoil energy, while the number of O1 defects is reduced with respect to those measured without H. This seems to indicate that as the recoil generates defects in the sample, free H migrates towards these newly generated defects creating O-H. Further calculations are being performed where most of the H is initially located at O-H sites.

Acknowledgments

This work has been supported by the Spanish MEC through the national Project FNT2001-3886-C02-01. One of the authors (MJC) thanks the Spanish MEC for support under the Ramón y Cajal program.

References

[1] M. J. Caturla, N. Soneda, E. Alonso, B. D. Wirth, T. Diaz de la Rubia, J. M. Perlado, "Comparative study of radiation damage accumulation inCu and Fe", J. of Nucl. Mater. **276** (2000) 13
[2] M. J. Caturla, T. Diaz de la Rubia, L. A. Marques, G. H. Gilmer, "Ion beam processing of Silicon at keV energies: a molecular dynamics study", Phys. Rev. B **54** (1996) 16683
[3] B.P.Feuston,S.H.Garofalini,"Empirical three-body potential for vitreous silica", J. Chem. Phy.,89 (1988)
[4] E. B. Webb and S. H. Garofalini " Molecular dynamics simulations of the approach and withdrawal of a model crystalline metal to a silica glass surface" J. Chem. Phys. 101 [11] 10101-10106 (1994)

Collective modes of mesodefects and “slow dynamics” of damage-failure transition in materials

Oleg Naimark [1], Sergey Permyakov [1], Vladimir Leont’ev [1], Yuri Bajandin [1], Vladimir Oborin [1]

[1] Institute of Continuous Media Mechanics of Russian Academy of Sciences, 1 Acad.Korolev str., 614013 Perm, Russia

Statistical thermodynamics of solid with mesodefects (dislocation structures) allowed the definition of order parameters and the form of potential (non-equilibrium free energy) as the generalized Ginzburg-Landau expansion in terms of the defect density tensor (defect induced strain) and structural scaling parameter. The kinetics of mentioned order parameters causes the relaxation ability of materials under the development of plastic shears and the transition from damage to failure. The nonlinearity of potential leads to the generation of collective modes of mesodefects with long relaxation times and, as the consequence, to the subjection of dynamics of observable variables (stress, strain, strain rate) to the dynamics of collective modes. The “slow dynamics” of these modes explained the specific features of plastic flow and damage-failure transition with the features similar to the aging (out-of-equilibrium) systems. The key point in the generalization of the Ginzburg-Landau phenomenology is the determination of thermalization conditions (effective temperature) of out-of-equilibrium mesoscopic system in the linkage with structural scaling parameter.

Structural susceptibility to the generation of mesodefects was investigated for Armco-iron, copper polycrystals and monocrystal of aluminum using the New View profilometry data (resolution from 1 nm) of the surface of deformed specimens and failure surface, correlation analysis and the original version of generalization of Fluctuation-Dissipation Theorem (FDT) for the definition of “effective temperature” of the current state of out-of-equilibrium system with mesodefects. The correlation analysis of the morphology of specimen surfaces induced by localized shears, damage localization areas and the usage of the FDT generalization for the estimation of structural susceptibility allowed us to establish the links between thermodynamic temperature, the scales of structural relaxation and to determine the scale thresholds corresponding to the transition to the “effective temperatures” of mesodefect ensemble.

Mentioned results showed the way of classification of mechanisms of structural relaxation and the morphology of structure of materials in various states (quasi-brittle, ductile, submicro- and nanocrystalline states) in the terms of generalized susceptibility, related to the dispersion properties of materials induced by mesodefects. The definition of effective temperatures, non-linearity of thermodynamic potential and the types of collective modes in mesodefect ensembles allowed us to propose the interpretation of characteristic features of plastic relaxation, damage-failure transition for mentioned material states.

The research was carried out in part in the frame work of RFBR projects (№ 04-01-96009-р2004урал_а, № 05-01-00863-а, №04-01-97514_офи).

Point defect diffusion in Zirconium under tensile strain

Kenichi Nakashima[1], A. Nomoto[1], N. Soneda[1], K. Kamimura[2], K. Ogata[2]

[1]Central Research Institute of Electric Power Industry, 2-11-1 Iwado-kita, 201-8511 Komae, Japan
[2]Japan Nuclear Energy Safety Organization, 105-0001 Tokyo, Japan

High burn-up fuel claddings of light water reactors are subjected to various stresses such as a hoop stress due to pellet-cladding interaction and internal stresses due to accumulation of hydrides and irradiation-induced dislocation loops. Therefore, the diffusion behavior of irradiation-induced point defects under such strain fields needs to be studied especially at high dose regime in order to understand the evolution of radiation damage in fuel claddings. In this paper, we study the effect of strain on the diffusion properties of a self-interstitial atom (SIA) and a vacancy in zirconium using molecular dynamics computer simulations with use of the inter-atomic potential developed by Ackland et al.

The migration energy of diffusion is calculated as an energy difference between the base-line and the saddle-point states along the migration path of potential valley. Pre-exponential factor of diffusion is also calculated using the second derivative of the potential curve around the base-line state following the procedure proposed by Vineyard. Stain field is given by changing the lattice constant of the crystal.

Diffusion coefficients of a SIA and a vacancy in zirconium under strain fields of 0~6% tensile strain in both a- and c-directions are calculated using the above method. Diffusion of a vacancy in zirconium, which is almost isotropic in spite of the anisotropic structure of the hcp zirconium crystal, becomes anisotropic with strain. The migration energy for the SIA diffusion drastically changes with strain, and the stable configuration of a SIA is also affected very much by strain.

Magnetic Properties of Point Defects and Nano-Clustering in Fe-Cr Alloys: An *Ab-initio* Study

Duc Nguyen-Manh (*), Mikhail Lavrentiev and Sergei Dudarev

EURATOM/UKAEA Association, Culham Science Centre,
Abingdon, OX14 3BD, United Kingdom.
(*) duc.nguyen@ukaea.org.uk

ABSTRACT

To understand the behaviour of point defects generated in irradiated FeCr ferritic/martensitic steels and to identify the kinetic pathways of microstructural evolution of binary model Fe-Cr alloys, we use a combination of density functional theory (DFT) with statistical approaches involving cluster expansion and Monte Carlo simulations. This makes it possible to generate in a systematic way the low-energy configurations required for the subsequent DFT study of intrinsic defects (vacancies, interstitials) and impurity-defect interactions over the entire range of Fe-Cr alloy compositions. In the limit of low Cr concentration, DFT calculations predict that an intermetallic compound Fe15Cr has the lowest negative heat of formation. At higher Cr concentrations, simulations performed using a 4x4x4 super-cell show that magnetism is responsible for the nano-segregation of the ferromagnetic Fe15Cr and anti-ferromagnetic (α'-Cr) phases giving rise to the formation of clusters characterised by a very low positive heat of formation. We perform a systematic investigation of formation energies of point defects and their energies of interaction with Cr atoms. Further investigation of interaction of interstitial and vacancy defects with impurities (V, Nb, Ta, Mo, W, Al, Si, P, S) also shows a complex picture of interplay between magnetism and short-range ordering that affects the interaction between defects and impurities in the presence of chromium in Fe-rich alloys.

1. Introduction

The binary body-centred cubic (bcc) Fe-Cr alloy is the base of many important industrial steels, especially in the nuclear industry. 9-12%Cr ferritic/martensitic steels are among the promising candidate materials for the first-wall and breeding-blanket structures in future fusion power plants. In Fe-Cr alloys, Cr plays a major part in determining the pathways of microstructural evolution under irradiation. In the concentration range between 2 and 9% Cr reduces void swelling in comparison with pure Fe, at the same time improving the ductility of steels at 9% concentration. The low activation ferritic-martensitic steels, contain, beside Cr, other transition metal solutes (Mo, W, Nb, Ta, V, Mn, Ni, Co, Cu) as well as sp-valence elements (C, B, N, Al, Si, P, S). Electrical resistivity recovery measurements show that some solute atoms in dilute iron-based alloys, such as Cr and Mn, interact with self-interstitial atoms (SIAs) and form mixed dumbbells mobile at temperatures below the onset of long-range SIAs migration. SIA trapping by configurations involving several Cr atoms (configuration trapping) has also been observed in concentrated Fe–Cr alloys [1]. Since such trapping can have a significant effect on the properties of SIAs, it may provide a mechanism responsible for the observed swelling resistance of Fe–Cr alloys.

2. Methodology

In contrast to fcc metals, bcc transition metals and alloys, including the binary Fe-Cr system, pose a particular challenge to multi-scale modeling of defects and mechanical behavior. This stems from the presence of partially filled d-band and effects of magnetism [2-4]. Spin-polarized DFT calculations performed using the generalized gradient approximations (GGA) were used to generate an ab-initio data base covering the entire range of Cr concentrations [5]. We use the Vienna Ab initio Simulation Package (VASP), where the pseudo-potentials were generated within the projected augmented wave approach (PAW) from the VASP library [6]. We find that for the Cr concentration of 6.25%, the heat of formation is negative (-6.4 meV/atom) with the local magnetic moment (1.25 μ_B per Cr atom) ordered antiferromagnetically with respect to the Fe atoms. The structure of this Fe15Cr intermetallic compound (space group Pm-3m) and its spin-polarized map calculated for the 4x4x4 super-cell are shown in Fig. 1. We see clearly that the maximum short-range order around Cr is up to the 5th nearest neighbor in this compound.

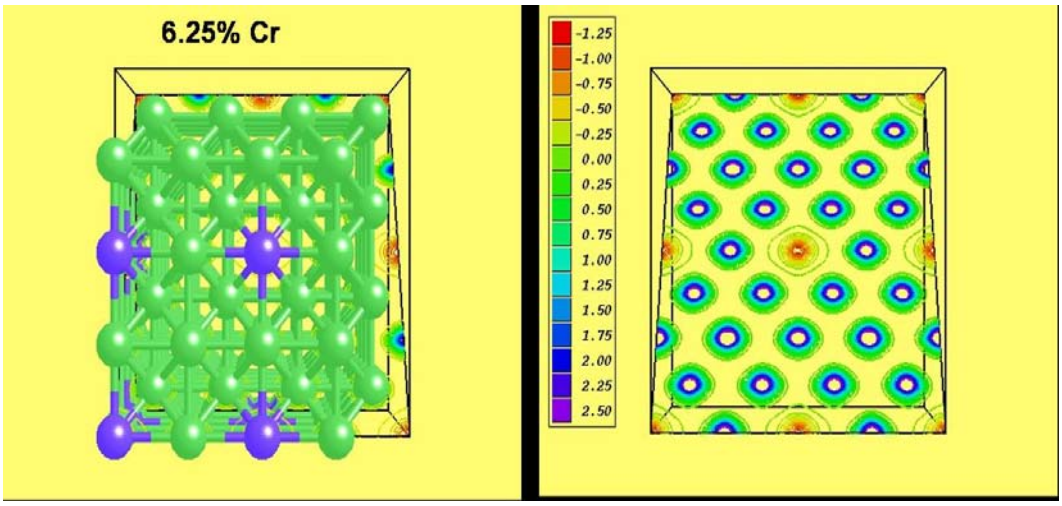

Figure 1. Atomic structure and spin-density map for ferromagnetic compound Fe15Cr.

3. Clustering of α' phase

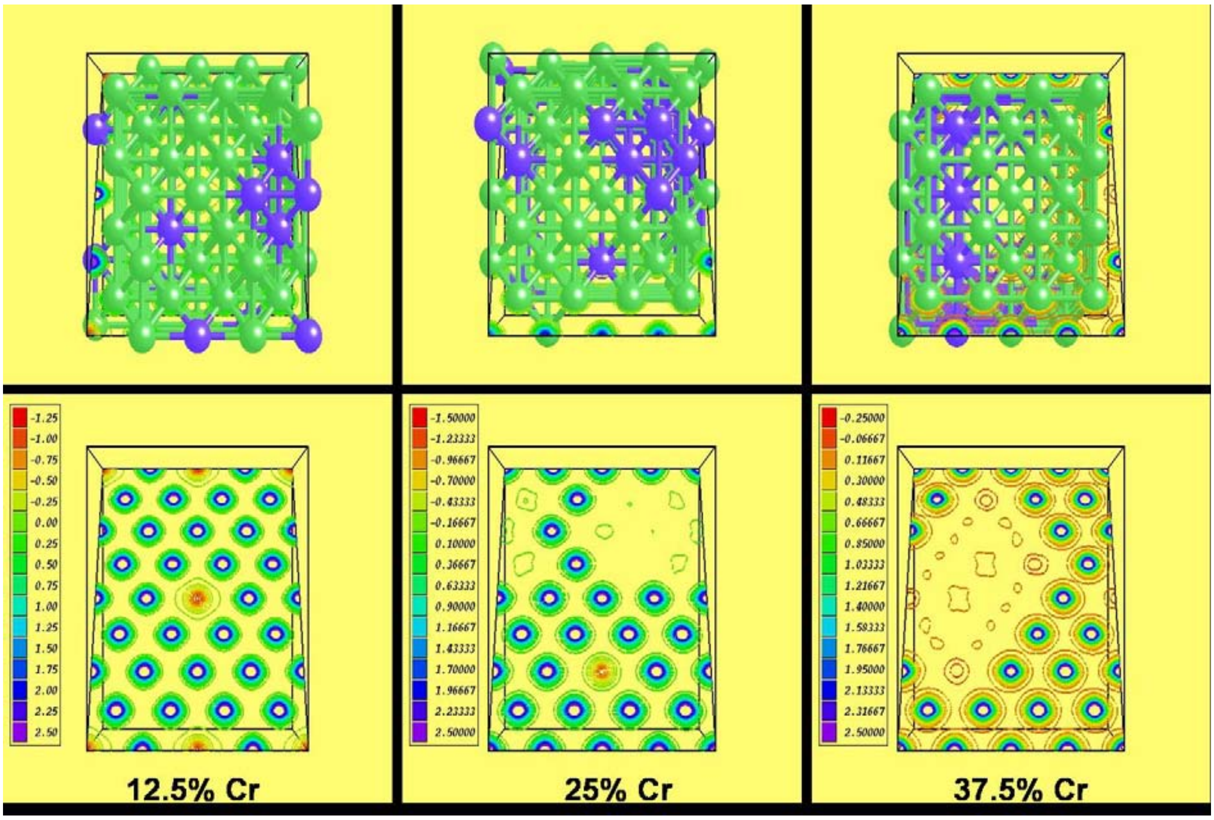

Figure 2. Nano-clustering in Fe-Cr alloys from spin density map at high Cr concentration

By combining DFT with Monte Carlo simulations [7], we are able to generate low-energy configurations for binary Fe-Cr alloys illustrated in Fig. 2 for 12.5, 25 and 37.5% Cr compositions. At 12.5%Cr, we see that there is a transition from an isolated Cr with high magnetic moment to the formation of small cluster of Cr (blue) atoms. Clustering is more clearly pronounced for the 25% Cr alloys, where the spin-density map shows a cluster with weak magnetic moments on the (110) plane. At 37.5% Cr, we observe formation of a Cr cluster bounded along the (110) planes, consistent with larger scale Monte Carlo simulations.

4. Impurity-point defect interaction

We also calculated the formation energies of point defects (vacancy, anti-site and self-atom interstitial) in Fe15Cr compound at its five different crystallographic sites, and compared the results with the data for the magnetic α-phase [5]. We found that the <110> dumbbell remains the most stable configuration among various SIA configurations for the Fe sites in the 6.25% Cr alloy. However, the formation energies of both Fe-Fe and mixed Fe-Cr dumbbells, as well as those of Fe vacancies, have decreased in comparison with the case of pure iron.

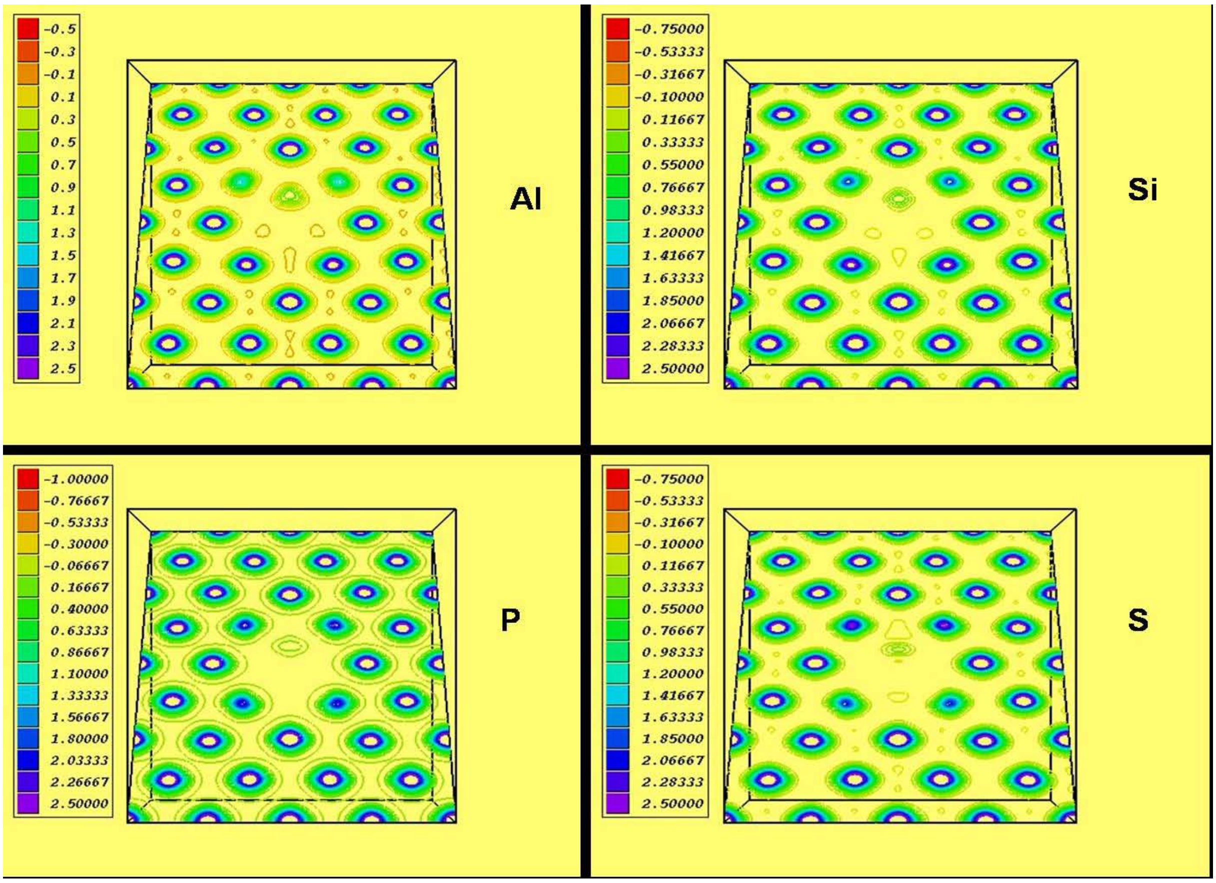

Figure 3. Spin-density map of a dumbbell interacting with sp-valent impurity atoms

Figs. 3 shows spin-density maps of mixed dumbbell configurations between Fe and different sp-valent impurity atoms, respectively. We find that the binding energies of mixed dumbbell are positive for Si, P and S in agreement with results based on the strain field of defects [8]. Due to weak magnetisation of atoms of sp-element, the sign of binding energies in the mixed dumbbell depends mainly on the size of a solute atom, as predicted by the elasticity. The situation with a bcc transition metal impurity (Fig. 4) is more complicated. We find that the binding energy of the mixed Fe-Cr dumbbell is also positive in variance with the strain field theories. For example, Fig. 4 shows that a Cr solute atom forming a part of a mixed SIA

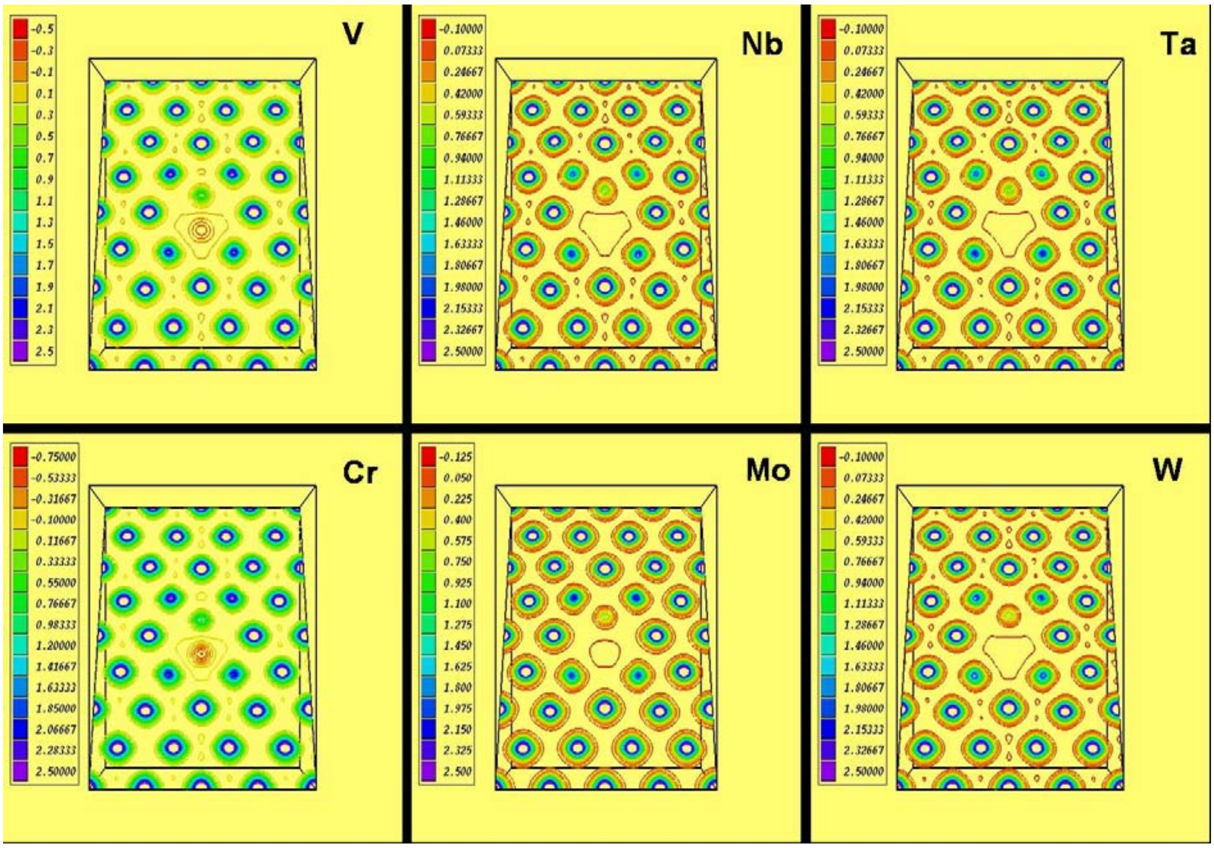

Figure 4. Spin-density map of a dumbbell interacting with a transition metal impurity atom

dumbbell configuration has a negative magnetic moment (-0.7 μ_B) in comparison with positive moment of a Fe atom. Note that this magnetic configuration differs from a dumbbell configuration occurring in pure Fe, where both Fe atoms have moments ordered antiferromagnetically with respect to the host. We conclude that magnetism is crucial for understanding the behaviour of defects not only in pure Fe but also in iron-chromium binary alloys.

Acknowledgements

This work was supported by the EXTREMAT project, UK EPSRC and by EURATOM. DNM would like to thank T. Martin and P. Knight for their help with using the supercomputer facilities at Culham Science Centre, and R. Faulkner and P. Miodownik for stimulating discussions.

References

[1] A.L. Nikolaev, J. Phys.: Condens. Matter, vol. 11 (1999) 8633.
[2] D. Nguyen-Manh, V. Vitek and A.P. Horsfield, Prog. Mater. Sci., (2006) in press.
[3] D. Nguyen-Manh, A.P. Horsfield and S.L. Dudarev, Phys. Rev. B, vol. 73 (2006) 020101.
[4] D. Nguyen-Manh and S.L. Dudarev, Mat. Sci. Eng. A, vol. 432 (2006) 74.
[5] D. Nguyen-Manh, M.Yu. Lavrentiev and S.L. Dudarev, to be published.
[6] G. Kresse, J. Hafner, Phys. Rev. B, 49 (1994), 14251; G. Kresse, J. Furthmuller, Phys. Rev. B, 54 (1996) 11169; G. Kresse, D. Joubert, Phys. Rev. B, 59 (1999) 1758.
[7] M.Yu. Lavrentiev, R. Drautz, D. Nguyen-Manh, P. Klaver and S.L.Dudarev, to be published.
[8] R.G. Faulkner, S.H. Song and P.E.J. Flewitt, Mater. Sci. Tech., 12 (1996) 904.

Vacancy effect on the precipitate nucleation in Fe-Cu alloy

Shigeto R. Nishitani[1], **Atsuto Seko**[2], **Koretaka Yuge**[2], **and Isao Tanaka**[2]

[1]**Dept. Informatics, Kwansei Gakuin University, Gakuen 2-1, Sanda, 669-1337, Japan.**
nishitani@ksc.kwansei.ac.jp.
[2]**Dept. Materials Science and Engineering, Kyoto University, kyoto 606-8501 , Japan.**

ABSTRACT

The activation barrier height of bcc-Cu precipitates in Fe-Cu alloy has been predicted using the first principles calculations. The predicted values of the critical number of 12 atoms and the critical free energy barrier of 0.6eV show good agreements with the experimentally estimated ones for the annealing temperature of 773K and the initial concentration of 1.4at%Cu. This approach also predicted that the vacancy prefers inside not at the interface of clusters.

1. Introduction

The nucleation phenomenon is one of the main targets of the multi-scale materials modeling. The recently proposed method [1-3] predicts the fundamental but hardly obtained values of activation barrier, critical size and free energy change of the precipitate nucleation precisely using the first principles calculations. Helmholtz free energy change is apparently defined and calculated by the purely enthalpic and entropic contributions between the initial state of the isolated solute atoms scattering around the matrix and the final state of a cluster of size *n* traveling around the matrix. The enthalpic term is calculated by the reliable first principles method, and the entropic term is estimated by the ideal solution model. This approach avoids the difficult calculations on the interface energy of small clusters. Firstly we will show the basic idea of the proposed method, and then the results of bcc Cu precipitation in a Fe-Cu alloy. Lastly the vacancy behavior in precipitates, which is crucial under the irradiated condition, will be discussed.

2. Calculating method

In classical nucleation theory, the free-energy change is described by the sum of negative driving force ΔF and positive interface energy $H\sigma$. The main ambiguity of the classical nucleation theory is the assumption that the interface energy is applied to a small cluster with a spherical interface area. By dividing into two components of enthalpy change ΔH and entropy change $-T\Delta S$, and treating enthalpy change ΔH and interface energy $H\sigma$ together, the free energy change is expressed as

$$\Delta F(n) = \{\Delta H(n) + H_\sigma(n)\} - T\Delta S(n) \tag{1}$$

where *n* is the number of atoms in a cluster.

Figure 1 shows schematic illustrations of precipitate nucleation. The initial state is described as the sum of the isolated solute atoms, and is the dilution limit of an alloy. The final state is

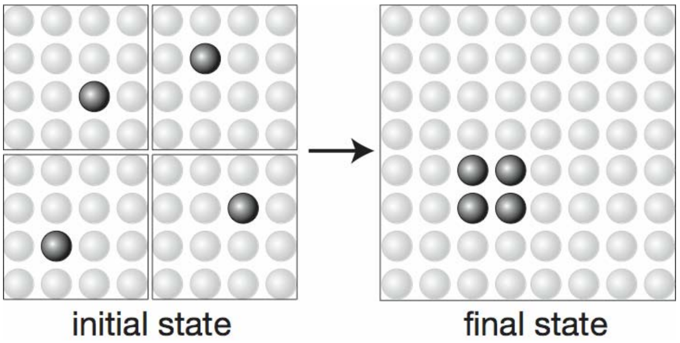

Figure 1. Schematic drawings of initial and final states of precipitation.

described as one cluster constructed by *n* solute atoms moving around on the matrix. The free-energy change is calculated from the enthalpy and entropy differences between these initial and final states.

The first term of Eqn.(1) is the cluster energy change, which includes all the environmental changes of solute and solvent atoms. The cluster energy change is assumed to be independent of temperature and can be calculated precisely by the density functional codes. The second term of Eqn.(1) is entropy change, and includes the interfacial entropy implicitly. The vibrational entropy contributions can be treated separately[3], and neglected here for the first approximation. The rest of the entropy contribution is the configurational change between the scattered atoms and the condensed cluster, which can be estimated by the simple ideal solution model as pointed out by Kamijo and Fukutomi[4],

$$\Delta S(n) = k_B (n-1) \ln x \tag{2}$$

where k_B is Boltzmann constant and *x* is an initial solute concentration.

3. Calculated results

The cluster energy, $\Delta H(n)+H\sigma$, is obtained by the usual density functional codes. The spin-polarized calculations have been performed using the *Vienna Ab Initio Simulation Package* (VASP)[5,6]. For the precipitates in Fe-rich Fe-Cu alloys, many experiments revealed that Cu clusters precipitate with the metastable bcc structure from the super satuated bcc-Fe alloys at the early stage of nucleation [7]. It was also shown that small Cu clusters with the bcc lattice possess spherical and coherent interfaces. The cluster energy has been calculated with 54 atoms (3 x 3 x 3 unit cells) for clusters smaller than or equal to 5, and 128 atoms (4 x 4 x 4 unit cells) for other larger clusters, under the non-relaxed condition of the equilibrium lattice constant of Fe. Cluster models were constructed by replacing some sites with Cu atoms.

The total free energy change is obtained by the sum of this cluster energy and entropy change, as shown in Fig. 2. The entropy change is estimated at the temperature of 773 K and the concentration of 0.014 at% Cu for the comparison with the result obtained by the classical treatment [7]. Estimated critical number *n** of 13 atoms and activation energy *F** of 0.67 eV, respectively are very close to the values of 13 atoms and 0.6 eV by the classical treatment.

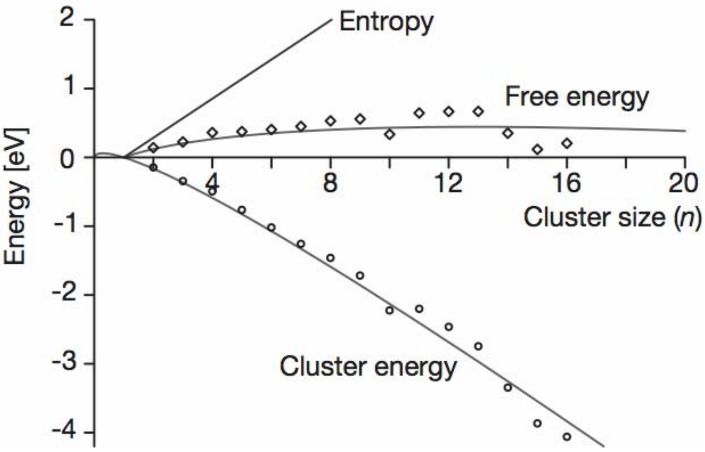

Figure 2. Activation barrier of the free energy due to the precipitate nucleation.

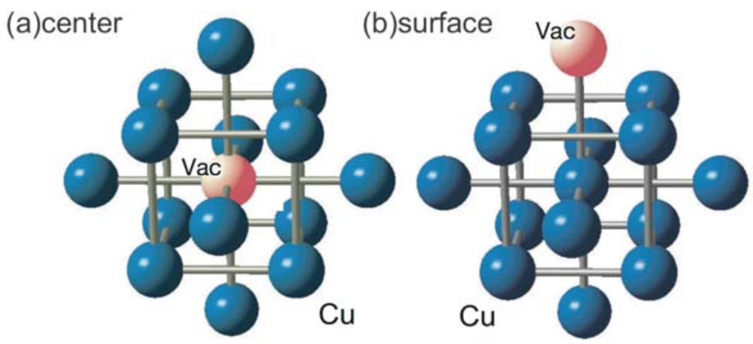

Figure 3. Atomic configurations for clusters including one vacancy and 14 Cu atoms.

Next we will see the vacancy contribution on the nucleation. The entropy change including the third element or vacancy is derived by

$$\Delta S(n)/k_{\mathrm{B}} = (n-1)\ln x_{\mathrm{M}} - n + \tfrac{3}{2}\ln n + \tfrac{1}{2}\ln(2\pi) + \ln x_{\mathrm{V}} \tag{2}$$

where x_{M} is the major solute element and x_{V} the third element or vacancy[2]. Thus the entropy contribution is assumed to be identical at the same concentration and the cluster size. The free energy is controlled only by the enthalpy difference.

The easiest comparison of the vacancy configuration is performed by n=15 cluster as shown in Fig. 3. We considered two extreme cases: one vacancy is located (a) at the center of the cluster, and (b) at the matrix/cluster interface. The enthalpy of (a), 0.8eV, is lower than that of (b), 1.25eV. This result suggests that vacancies shows the tendency to be surrounded by Cu atoms, which is consistent with the experimental observation by positron annihilation measurements [8]. This tendency is simply explained by the difference in vacancy formation energies for pure metals, 0.6 eV for bcc Cu and 2.3 eV for bcc Fe. By this enthalpic reduction, the activation barrier is reduced. At the same time, however, the diffusion constant is also reduced by the reduction of the vacancy density due to the highly trapping ability of clusters. Thus the acceleration of the precipitate reaction due to the vacancy formation is not concluded by our present calculation.

4. References

[1] S. R. Nishitani, A. Seko, I. Tanaka, H. Adachi, and E. F. Fujita, *Solid-Solid Phase Transformations in Inorganic Materials 2005,* Volume 2, Eds: J.M. Howe, D. E. Laughlin, J. K. Lee, U. Dahmen, and W. A. Soffa, TMS (The Minerals, Metals & Materials Society, 2005), pp.669-674.
[2] A. Seko, N. Odagaki, S. R.Nishitani, I. Tanaka and H. Adachi, Materials Trans., **45** (2004), 1978.
[3] K. Yuge, A. Seko, I. Tanaka and S. R. Nishitani, Phys. Rev. B, **72** (2005), 174201.
[4] T. Kamijo and H. Fukutomi, Phil. Mag. A, **48** (1983), 685.
[5] G. Kresse and J. Hafner, Phys. Rev. B, **47** (1993), 558.
[6] G. Kresse and J. Furthmüller: Phys. Rev. B, **54** (1996), 11169.
[7] S. R. Goodman, S. S. Brenner and J. R. Jow Jr., Metal. Trans., **4** (1973), 2363.
[8] Y. Nagai, Z. Tang, M. Hasegawa, T. Kanai and M. Saneyasu, Phys. Rev. B, **63** (2001), 134110.

Atomic-scale plasticity in presence of Frank loops

Authors: Thomas Nogaret[1,2], Christian Robertson[2], David Rodney[1]

[1]Génie Physique et Mécanique des Matériaux (UMR CNRS 5010),
INP Grenoble, 101 rue de la Physique, Saint Martin d'Hères, 38402, France
[2]Service de Recherche de Métallurgie Appliquée, CEA
DEN/DMN Saclay, Gif-sur-Yvette, 91191, France

ABSTRACT

The tensile behavior of irradiated metals is characterized by an increased yield stress and a localization of the deformation in shear bands free of irradiation defects after the deformation ("clear bands"). In this work, the formation of clear bands in austenitic steels is investigated. These materials are used as internal structural materials in nuclear reactors and their irradiation microstructure is dominated by interstitial Frank loops. The defect clearing process requires short-range interactions between the mobile dislocations and the irradiation defects, the latter being sheared, unfaulted or absorbed. Therefore, knowledge of dislocation dynamics in these conditions requires information from the atomic scale. In the present study we compare MD simulations of edge and screw dislocations interacting with Frank loops to post-mortem TEM observations of irradiated and deformed samples. We show in particular the different roles played by screw and edge dislocations in the process of clear band formation. For the MD simulations, in absence of realistic interatomic potentials for stainless steels, an EAM potential developed for Cu is used. This potential predicts low stacking fault energy, comparable to that of steels, with a resulting separation between Shockley partials that is larger than in most fcc metals. This specific feature is believed to play an important role in the interactions, since it controls the ability of the dislocations to cross-slip. We performed a systematic study of edge and screw dislocations interacting with Frank loops in all their possible respective configurations. The simulations are conducted at elevated temperature, 600K, the temperature of internal materials in nuclear reactors, with Frank loops of realistic diameters and densities. Transmission Electron Microscope observations of ion-irradiated samples deformed at 600K were undertaken, in order to validate the simulations results. We analyzed the dislocation microstructures in the clear bands by indexing the dislocation Burgers vectors. Our aim is to elucidate the respective role of edge and screw dislocations in the process of clear band formation. In this short text, only the MD simulations will be described.

1. Introduction

Irradiated materials present a significant hardening, a reduced ductility and, above a certain dose, an upper yield stress followed by softening [1]. Post-mortem Transmission Electron Microscopy (TEM) showed that hardening is due to the production of irradiation defects, and that the reduced ductility and the yield drop are due to the localization of the deformation in shear bands that are defect free ("Clear bands") [2]. In-situ TEM showed that these clear bands are formed by the passage of dislocations issued from heterogeneities (grain boundaries and cracks) that sweep the irradiation defects [3]. It was also used to study the interaction mechanism between individual dislocations and large SFTs [3]. However, the observations are limited by the TEM resolution and the speed of tape recording.

Molecular Dynamics (MD) has shown to be a powerful tool to investigate reactions involving dislocation cores with full atomistic resolution. The irradiation defects considered up-to-now in FCC materials are glissile and Frank [4] interstitial loops in nickel and SFTs in copper [5]. In the latter case, edge and screw dislocations in interaction with SFTs in all their possible respective geometries were simulated. Thereby, all the possible elementary reaction mechanisms were categorized. It was shown that SFT shearing is the most frequent reaction, but depending on the geometry, temperature and stress/strain rates, SFTs can also be partially absorbed by edge dislocations and can be transformed in two distinct and separated defect clusters by screw dislocations.

In the present study, austenitic 304 and 316 stainless steels (SS) are of prime interest. These materials constitute the internal structural components in Pressurized Water Reactors (PWR) and undergo neutron irradiation between 550 K and 600 K. The irradiation defects visible in TEM are interstitial Frank loops with edges in <121> directions. They increase the yield stress so that the twinning critical stress is reached at room temperature because of the low stacking fault energy (SFE) of the material. However at 600K, the yield stress is lower and the SFE higher, so that dislocation channelling occurs [6]. The present work focuses on the high temperature regime, i.e. the dislocation channelling regime.

A systematic study of the interaction mechanisms of edge and screw dislocations in presence of Frank loops in their different possible (111) habit planes was performed. Due to the crystal symmetries, the study can be limited to 3 screw configurations (SD/W-, SD/W+, SD/CS) and 3 edge configurations (ED/W-, SD/W+, ED/CS) (see Tab.1 for details). The studied loop size was mainly 6nm and the inter-loop distance was 50 nm, as observed in TEM by Pokor [7]. Since no potential was available to model complex alloys such as SS, we decided to keep only the main characteristic of these alloys, i.e. a SFE lower than that of usual FCC materials. Thus, a Cu Embedded Atom Method (EAM) potential developed by Mishin *et al* [8] with a SFE close to that of austenitic steels at 600 K was employed. Also, since in irradiated materials dislocations glide in pile-ups, the leading dislocation is helped by its followers in its glide through the defect environment. In order to investigate the influence of the pile-up, we performed simulations with one or two dislocations in the simulation cell, i.e., the smallest possible pile-up. The passage of several dislocations was also modelled by authorizing the dislocation(s) to return several times on the loop through periodic boundary conditions applied in the glide direction. The MD technique used here is similar to that presented in Ref [4]. The main difference is that the applied stress is increased non-monotonically during the simulations depending on the reaction rate between the dislocations and the Frank loops

2 Results

Depending on the configuration, three kinds of reactions were observed: shearing (R1/R2), loop unfaulting followed by absorption and drag (R3), and loop unfaulting followed by absorption with helical turn formation (R4). Table 1 gives the type of reaction (using the categories proposed in [5]) and the resistance for one and two edge and screw dislocations.

The 1st reaction is shearing (R1/R2). It is characteristic of edge dislocations. The associated unpinning forces are low (less than 100MPa for one dislocation) and it is an inefficient loop clearing mechanism since the damage created on the loop is limited (1b step). Moreover these steps are mobile in 1 out of 2 cases and annihilate on the loop border. The 2nd kind of reaction is loop unfaulting, absorption as mobile jogs and drag (R3). It is efficient for loop clearing.

The involved mechanisms are complex and require cross-slip. The associated unpinning forces are intermediate, around 150 MPa.

Table 1: Interaction matrix. Notation: B- = [-1-10] = dislocation Burgers vector, S- = the dislocation approaches the loop from the side of negative coordinates, P1=(11-1), P2=(111), P3=(-111) = loop habit plane. See Fig. 1 for crystal orientation

	W- = (B-/S-/P1)	**W+ = (B-/S-/P2)**	**CS = (B-/S-/P3)**
1 Screw Dislocation	**R4: 335 MPa**	**R1: 245 MPa**	**R3: 160 MPa**
2 Screw Dislocations	**R4: 180 MPa**	**R4: 180 MPa**	**R3: 125MPa**
1 Edge Dislocation	**R3: 130 MPa**	**R1: 95 MPa**	**R2: 65 MPa**
2 Edge Dislocations	**R3: 100 MPa**	**R1: 65 MPa**	**R1: 45 MPa**

The 3rd reaction is loop unfaulting and absorption with helical turn formation (R4). It is characteristic of screw dislocations. Figure 1 shows this reaction in the case of a two screw dislocations pile-up interacting with a loop in W- configuration (see Tab. 1). When the first dislocation comes into contact with the loop border, it spontaneously cross-slips due to the elastic field of the loop. A D-Shockley partial is created on the loop border that is mobile and progressively removes the double stacking fault of the loop (Fig. 1(a)). This mechanism was described in details in Ref. [4] and results in the absorption of the loop in the form of a helical turn on the screw dislocation (Fig. 1(b)). The helical turn expands along the entire length of the dislocation in order to minimize its length and the associated line tension energy. In this configuration, the dislocation does not belong to any specific (111) plane and is constricted along its entire length, since the helical turn has inherited the <121> contour of the initial loop.

The helical turn is an obstacle that pins the first dislocation because it can glide only in the Y-Burgers vector direction and not the X-glide direction. As the applied stress is increased, the second dislocation approaches. The two dislocations repel each other since they have the same Burgers vector. The portion of the helical turn near the second dislocation rotates and becomes perpendicular to the latter. This configuration (with perpendicular dislocation segments) minimizes the elastic repulsion between them. The same effect is observed with repulsive dislocation junctions. The rotation of the jogs implies a contraction of the helical turn and an extension of one arm of the first dislocation in an upper (1-11) glide plane, where it locally dissociates.

When the second dislocation comes into contact with the helical turn, the contact is punctual. The two dislocations spontaneously exchange arms, after which the helical turn is shared by the two dislocations, as seen in Fig. 1(c). Each jog now connects one segment of the first dislocation to another segment of the second dislocation. During this process, the upper dissociated arm continues to expand and bows out, being repelled by both the second dislocation and the applied stress. Then, this segment undergoes an Orowan process, unpins and leaves behind the second dislocation that now contains the helical turn (Fig. 1(d)). The net result is the absorption of the Frank loop into the core of a screw dislocation and the transfer of the other dislocation through the initial helical turn with re-emission in an upper (1-11) plane (*elevator effect).*

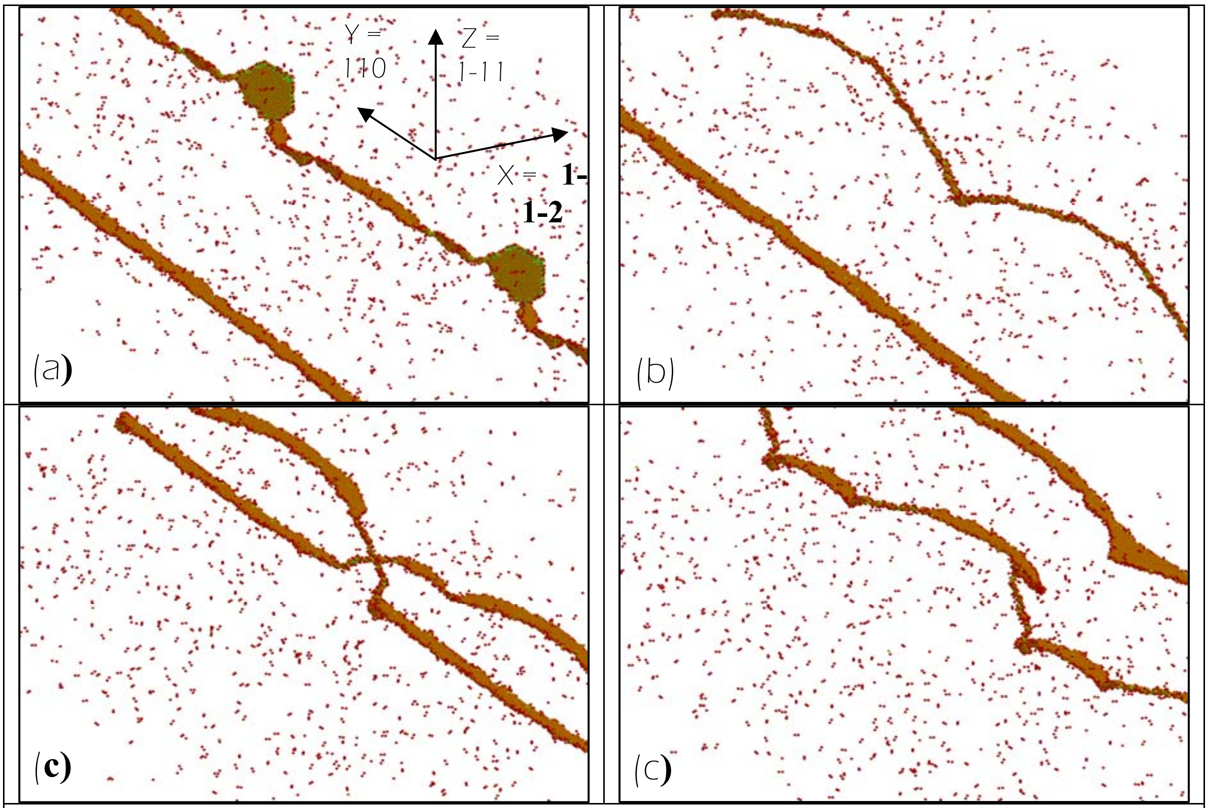

Fig 1.: Configuration SD/W- with two screw dislocations: snapshots shown at 5MPa, 15ps (a), 40MPa, 89ps (b), 180MPa, 153ps (c), 180MPa, 169ps (d)

3. Conclusion

It was seen that Frank loops can be unfaulted and absorbed by dislocations thanks to mechanisms that require cross-slip. Thus, loop absorption is controlled by parameters that control cross-slip (temperature, SFE, stress rate, non-glide stresses). The interaction matrix in Tab. 1 shows that screw and edge dislocations behave differently. Edge dislocations mainly shear the loops and are weakly pinned whereas screw dislocations are strongly pinned, systematically unfault the loops and broaden the channels thanks to the elevator effect.

References

[1] K. Farrell, Byun, T. S. and Hashimoto, N., J. Nucl. Mater. **335**, p471, (2004).
[2] J.V. Sharp, Phil. Mag. **16**, p77, (1967).
[3] J.S. Robac et al, Phil. Mag. **83**, p955, (2003).
[4] D. Rodney, Acta Mater. **52**, p607, (2004).
[5] Y.N. Osetsky, D. Rodney and D.J. Bacon, Phil. Mag. **86**, p2295, (2006).
[6] J. I. Cole and S. M. Bruemmer, J. Nucl. Mater. **225**, p53 (1995).
[7] C. Pokor et al, J. Nuc. Mat. **326**, p19 (2004)
[8] Y. Mishin et al, Phys. Rev. B **63**, p224106, (2001)

SIA-loop transformation and growth by cascade overlapping in bcc Fe

Akiyoshi Nomoto[1], *Naoki Soneda*[1], *Akiyuki Takahashi*[2]

[1]*Central Research Institute of Electric Power Industry, 2-11-1, Iwado Kita, Komae-shi, 201-8511 Tokyo, Japan*
[2]*Tokyo University of Science, Tokyo, Japan*

Displacement cascades occur on existing radiation damage in highly irradiated materials. This phenomenon, so-called cascade overlapping, potentially changes morphology of pre-existing point defect cluster such as dislocation loops. In this study, displacement cascades in bcc Fe matrix containing an SIA loop are studied using molecular dynamics simulations. Computation box of bcc Fe with size of 36x36x36nm containing 4M atoms is used for the simulations. A <111>a0 SIA loop of 1~4nm in diameter is located at the center of the box, and then 50keV kinetic energy is given to the primary knock-on atom near the SIA loop at 600K so that displacement cascade evolves over the SIA loop. Small SIA loops with the size around 1nm disappear after displacement cascade overlapping and no significant effect on displacement cascades is observed. SIA loops with size of 2nm and 4nm remain at their original position, but SIA loops sometimes become lager after displacement cascades. Furthermore, in some cases, the Burgers vector of the SIA loop changes after cascades, which has not been observed for such large size of SIA loops in molecular dynamics simulations as a thermally activated process.

Equilibrium structure and thermal activation of dislocation loops in BCC metals

Kazuhito Ohsawa and Eiichi Kuramoto

Research Institute for applied Mechanics, Kasuga-koen 6-1, Kasuga-shi, Fukuoka 8168580, Japan, ohsawa@riam.kyushu-u.ac.jp

ABSTRACT

We report thermally activated transport of prismatic dislocation loops in BCC metals by investigating their equilibrium structures, i.e., atomic configurations of grand state and saddle point, in a lattice model. According to an analysis in terms of a line tension model, two different types of saddle point configurations are considered to exist for dislocation loops, and the energetically lowest configuration is supposed to be realized in the thermally activated motion. The structural properties of the prismatic loops, in particular, in groups 5B and 6B transition metals, are well agreement with the analysis in terms of the line tension model.

1. Introduction

Computer simulations have shown that interstitial-type dislocation loops (I-loops) in BCC metals execute one-dimensional (1D) migration with high mobility. The 1D motion has profound significance on micro structural evolution in irradiated metals. In particular, it plays an important role in the production bias model. We have so far studied the 1D motion of the dislocation loops on the basis of a line tension model (LTM) where the dislocation loops are assumed to be a flexible elastic string [1]. According to our early work, it is possible to be two different types of saddle point configurations corresponding to the trivial and typical double-kink type solutions, and the lowest structure with respect to energy should be selected in the actual thermally activated transport. In the analysis on the basis of the LTM, we assume that the dislocation loops are located on a definite habit plane in the grand state. The purpose of the present paper is to calculate equilibrium structures of the I-loops in an actual lattice model using an empirical interatomic potential and investigate the validity of the analysis performed in the LTM. The saddle point configurations of the I-loops are determined by nudged elastic band method [2]. We here deal with regular hexagonal I-loops in BCC metals, Fe, Ta, and W, and compute their equilibrium structures of the grand state and saddle point. The analysis in the LTM is not appropriate to explain the atomic configurations of I-loops in Fe. On the other hand, the structural properties of I-loops in Ta and W are good agreement with the expectations derived from the LTM.

2. Numerical methods

We use here the embedded atom method (Finnis-Sinclair potential) [3] to represent the empirical potentials of the BCC metals. The single self-interstitial atom (SIA) is denoted as I and n-number SIA cluster is I_n. The number of SIAs, n, in the k-th hexagonal I-loop is represented as $n=3k(k+1)+1$. Therefore, prismatic loops dealt with in the present paper are denoted as I_7, I_{19}, I_{37}, I_{61}, etc. We use simulation box with about 104,000 atoms and the I-loop is embedded in the center of the simulation box, as shown in Fig. 1. The Burgers vector is denoted as b=1/2[111] in BCC. Then, the sense vector of a pure edge dislocation is denoted as a=1/3<11-2>. The periodic boundary conditions are imposed on the [111] direction.

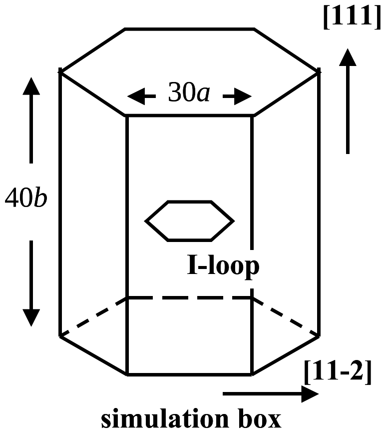

Fig.1: Simulation box used in the present work and embedded prismatic I-loop.

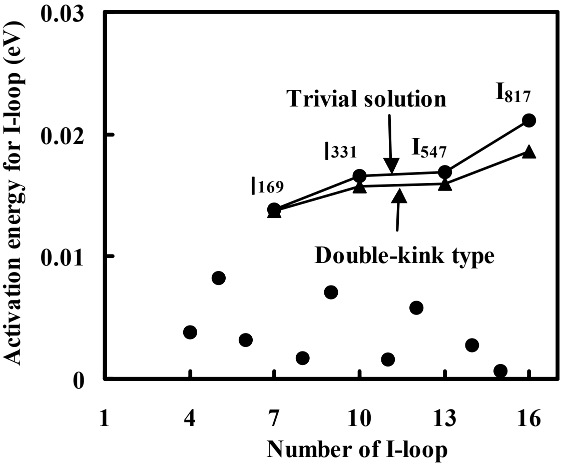

Fig. 2: Activation energy for a variety size of I-loops in W. Two different types of saddle points appear for the 7, 10, 13, 16-th I loops.

3. Results

The I-loops in Fe are not strictly located on the {111} plane in the grand state because of the formation of the intrinsic kinks, as pointed out by Wirth *et al* [4]. Therefore, it is not valid to apply the analysis on the basis of the LTM. On the other hand, sufficiently large I-loops in Ta and W are exactly located on the {111} plane. Therefore, we can easily observe the structural properties expected in analysis in terms of the LTM. From now on, we will mention the I-loops in W in detail. As shown in Fig. 2, every three I-loop, i.e., the 7, 10, 13, 16-th I-loops, has relatively large activation energy. Therefore, these I-loops are supposed to be very stable but we have not considered the reason yet. Anyway, we can clearly show the existence of the two different types of saddle point configurations for these I-loops. As an example, the atomic configurations of I_{817} in W will be mentioned. The two transition paths from one stable state to the next one are shown in Fig. 3. The paths A and B pass through saddle points corresponding to the trivial and double-kink type solutions, respectively. The activation energy for path B is smaller than that for path A. The profiles of the dislocation line are shown in Fig. 4. In this case, the position of the dislocation line is defined as the coordinate of the center of the dislocation core. The perimeter of the I_{817} is 96*a*, and the cause of the singularity appearing every 16*a* in the profiles is supposed to be corner effects of the prismatic loop. The lines (a) and (b) represent the profiles of the I-loops in the neighboring grand state (GS); (c) and (d) are saddle point configurations of the I-loops corresponding to the trivial and double-kink type solutions, respectively. In fact, the line (c) is relatively curved compared with the line (d).

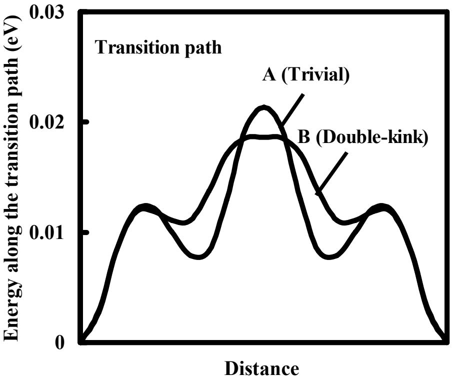

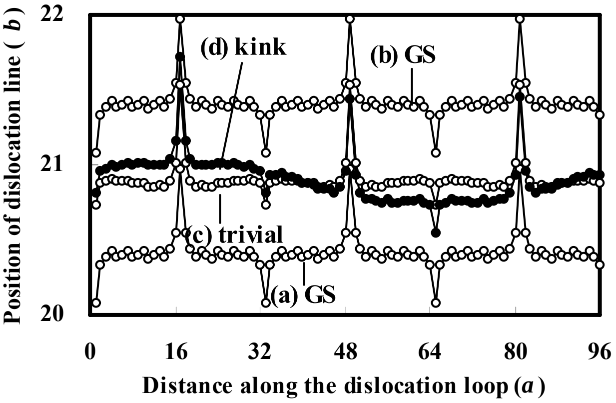

Fig. 3: Transition paths passing through trivial solution (A) and double-kink type solution (B) for I_{817} in W.

Fig. 4: Profiles of the I-loop, I_{817}, in W: (a) and (b) are grand states (GS), (c) and (d) are saddle point configurations corresponding to the trivial and double-kink type solutions, respectively.

4. Discussion

We calculate equilibrium structures of the prismatic I-loops in BCC metals, Fe, Ta, and W. Because the intrinsic kinks are nucleated on the dislocation line of the I-loops in Fe, the habit plane is not {111} plane. Therefore, the analysis on the basis of the LTM cannot be applied for I-loops in Fe. However, sufficiently large I-loops in Ta and W are exactly located on {111} plane. Let's consider Gb^2, i.e., energy density of dislocation line, to explain it. The values of Gb^2 are 4.69, 6,75, 12.06 (nJ/m) for Fe, Ta, W, respectively. Therefore, shorter I-loops are favorable for Ta and W, and the {111} habit plane is realized so as to reduce the elastic energy. In our early work [1], we have introduced the concept of the critical size for SIA clusters to classify point defect and dislocation. According to the criterion, small I-loop, I_{169}, in W is supposed to be classified into point defect.

References

[1] K. Ohsawa and E. Kuramoto, Phys. Rev. B **72**, 054105 (2005).
[2] G. Mills, H. Jonsson, and G. K. Schenter, Surf. Sci. **324**, 305 (1995).
[3] M. W. Finnis and J. E. Sinclair, Philos. Mag. A **50**, 45 (1984); **53**, 161 (1986).
[4] B. D. Wirth, G. R. Odette, D. Maroudas, and G. E. Lucas, J. Nucl. Mater. **276**, 33 (2000).

Atomic-scale mechanisms of cleared channels formation in neutron-irradiated fcc metals.

Yury Osetskiy[1], R.E. Stoller[2], S. Zinkle[2]

[1]Computer Science and Mathematics Division, Oak Ridge National Laboratory, Oak Ridge, TN 37831, USA
[2]Metals and Ceramics Division, Oak Ridge National Laboratory, Oak Ridge, TN 37831, USA

Clusters of self-interstitial atoms (SIAs) and vacancies are formed directly in high-energy displacement cascades in all metallic structural materials. In low stacking fault energy (SFE) metals they can be faulted and perfect interstitial loops (IL) which are sessile and glissile, respectively, and stacking fault tetra¬hedra (SFTs). These defects are obstacles for dislocation motion and sources for strengthening, hardening and loss of ductility of irradiated metals. These effects are often accompanied with a yield drop (strain softening) and plastic instability when significant plastic deformation occurs within a limited volume. These shear bands can also be cleared of radiation induced defects, leading to so called cleared channels. This phenomenon leads to unexpected material failure and is extensively studied by experimental and theoretical methods using a multiscale approach. A successful model for mechanical properties prediction must be able to describe creation and evolution of cleared channels which is impossible without knowledge of the atomic scale mechanisms of dislocation generation and motion through the high density of radiation defects (up to ~10^{24}m^3, i.e. about 10nm distance between defects). Due to small scale and fast, non-equilibrium conditions the atomic scale modelling is the only technique that permits the necessary information to be obtained. In this paper we present results of large-scale atomistic modelling of edge and screw dislocations interaction with IL and SFTs in model Cu crystals. We report a number of different mechanisms and suggest a possible scenario for how shear bands can be cleared of radiation defects. The results are discussed and compared with experimental observations.

Research sponsored by the Division of Materials Sciences and Engineering and the Office of Fusion Energy Sciences, U.S. Department of Energy, under contract DE-AC05-00OR22725 with UT-Battelle, LLC.

Interatomic Potentials Consistent with Thermodynamics: The Cases of FeCu and FeCr

R. C. Pasianot[1,2], **G. Bonny**[3], **and L. Malerba**[3]

[1]**Depto. de Materiales, CAC-CNEA, Avda. Gral. Paz 1499, 1650 San Martín, Argentina, pasianot@cnea.gov.ar;** [2] **CONICET;** [3] **Reactor Materials Research Unit, SCK-CEN, Boeretang 200, B-2400 Mol, Belgium.**

ABSTRACT

A most desirable property of interatomic potentials to be used in the atomistic simulation of microstructure evolution of irradiated metallic alloys is consistency with the experimental phase diagram, the solid solubilities in particular. A methodology to fit semi-empirical potentials aiming at the above, that was recently developed by the authors, is reviewed. It is based on the seamless coupling of the Cluster Variation Method technique, a known sophisticated mean field theory for solid phase diagrams computation, to other more standard requirements, such as compliance with the energetics of some crystal structures, point defects, etc. The method is applied to the construction of EAM many-body potentials for the FeCu system, a prototype alloy for the understanding of reactor pressure vessel steels embrittlement under irradiation. Coherence with *ab initio* computed formation energies of small point defect clusters as well as vacancy migration energies in the vicinity of Cu atoms, is incorporated. The potential is shown to match very reasonably the Cu solubility in the Fe matrix vs. temperature, and also obtains enhanced point defect kinetics behavior with respect to previous potentials. Current efforts to apply the methodology to the more challenging FeCr system are also described. Here, *ab initio* calculations predict slightly negative mixing enthalpies of magnetic origin for the random alloys of low Cr content. This entails extensions to the pure EAM interaction scheme to allow for ordering effects at those Cr concentrations.

1. Introduction

Interatomic potentials are the core of atomistic computer simulations and determine the degree of reliability of the results obtained from this type of models. In radiation damage studies, clearly the most important properties that the potential needs to describe are point defect configurations and energies. Also desirable are properties of more extended defects, such as clusters, dislocations, stacking faults and grain boundaries. In the case of alloys, however, the microstructural evolution under irradiation is decided by the interplay between defect formation and migration, and thermodynamic driving forces. It is therefore very desirable that an interatomic potential reproduces as closely as possible the stability of the phases that can appear in at least the concentration range of interest; this entails compliance with the experimental phase diagram.

Given a parameterized cohesive model, there are accurate but expensive methods to derive the corresponding phase diagram [1]; their inversion in order to extract those parameters appears therefore unfeasible. For a practical procedure to consider thermodynamic information, there is then no alternative to its early inclusion at the fitting stage. So, one must devise a formalism to express the thermodynamic functions of the considered alloy versus the fitting parameters of the potential. Restricting ourselves to solid phases, a reliable way to do this can be the so called Cluster Variation Method [2] (CVM), a generalized mean-field theory that provides analytic expressions for the configurational entropy in terms of clusters of lattice nodes of increasing size. CVM has been successfully applied for calculating the phase diagram of a wide variety of systems [3].

In this work a methodology based on the CVM theory, combined with the Embedded Atom Method (EAM) for interatomic potentials, is developed in order to optimize the potential fitting parameters aiming at reproducing as closely as possible the experimental phase diagram. The method is subsequently applied to the FeCu system, due to its relevance for the understanding of the RPV steels embrittlement during nuclear power plant operation. Some preliminary results for the FeCr system, a candidate relevant to future nuclear options, are also advanced.

2. Method

General statistical mechanics principles allow us to express free energies as variational problems in the configuration space (i.e. which species occupies what node), namely, the probability distribution function must be optimal. A very convenient set of variational parameters are the so called cluster correlation functions, ξ_α, in terms of which the Helmoltz free energy per lattice node is given as

$$f = \min_{\xi} \left\{ \sum_{\alpha \subseteq \alpha_M} m_\alpha E_\alpha \xi_\alpha + k_B T \sum_{\alpha \subseteq \alpha_M} m_\alpha a_\alpha \sum_{\sigma} p_\alpha(\sigma) \ln p_\alpha(\sigma) \right\} \qquad (1)$$

Here, clusters are indicated by α and belong to a (chosen) finite family of largest (but relatively small) clusters, α_M , $p_\alpha(\sigma)$ stands for the probability of finding cluster α in configuration σ , m_α is the cluster multiplicity , a_α are lattice symmetry coefficients defined within CVM, and E_α are energy expansion coefficients, carriers of the (fixed for now) potential parameters. The above minimization is subject to the constraints $p_{\alpha_M}(\sigma) \geq 0 \; \forall \sigma$, that define a convex domain due to the linear relationship between p's and ξ's .

Presently, E_α are obtained by expansion of the EAM form up to three-body interactions and recurring to triplet probabilities. Our method selects the pure species potentials as given and focuses on fitting the mixed (pair) interaction and the relative weight of the electron densities (in EAM parlance). From Eqn.(1) we write down the two equations of the common tangent construction that express the equilibrium between two phases at temperature T and solute concentrations c_1 and c_2 , taking these data from the experimental phase diagram. These equations are added to a whole set of more standard ones, such as compliance with alloy mixing enthalpies, formation energies of some defect structures, etc. (either from experiment or calculated by *ab initio* methods). The enlarged set is in turn matched in a minimum square sense by a further optimization on the potential parameters, eventually subject to bounds.

3. Applications

The outlined methodology is applied to fabricate a new FeCu potential, meant to be suitable for the study of Cu precipitation in Fe under irradiation, where the very low solubility of Cu in Fe is the main source of RPV steels embrittlement. Also, even though there are a couple of many-body potentials available from the literature [4,5], neither of them appears to be fully suitable for radiation damage studies. The most relevant result in the present context is shown in Fig.1, that gathers the Cu solubility limit in the Fe matrix for the two phases BCC-FCC in thermodynamic equilibrium. The prediction for the current FeCu potential, CO5.20, is there compared to the ones of previous potentials, AB[4] and LF[5], and to experimental measurements. Clearly, CO5.20 follows experiment very reasonably, the other two potentials giving too high solubilities.

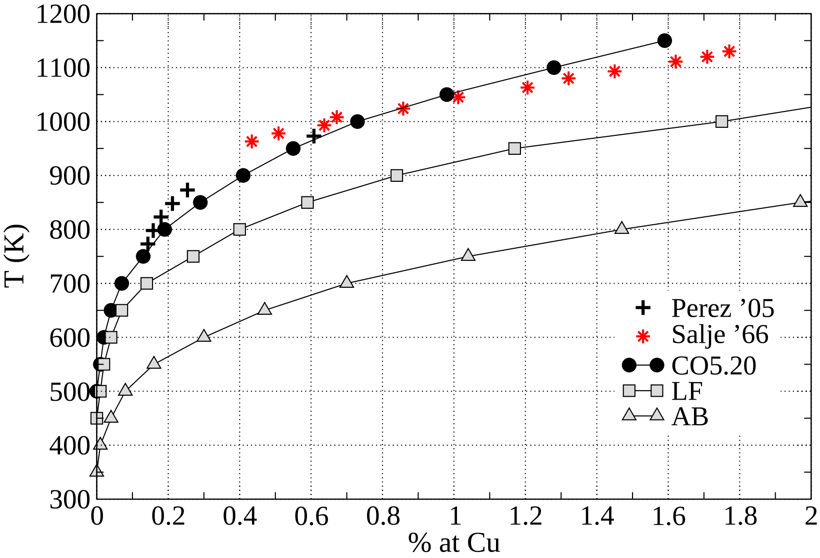

Figure 1. Cu solubility in the Fe matrix for the BCC/FCC equilibrium

Another unique feature of CO5.20 is its consistency with the dragging effect of Cu atoms by vacancies, supported by the formation of Cu hollow precipitates under irradiation as detected by positron annihilation. Such a feature was included in the fit with the help of Le Claire's five frequency model. Current efforts to apply the technique to the FeCr system have met only with partial success. The mixing enthalpy of the random alloy as predicted by *ab initio* calculations results slightly negative for low Cr content, implying a more involved energy expansion and also, possibly, a higher order CVM approach.

Acknowledgements

The authors acknowledge support from the PERFECT integrated project and the Belgian Scientific Policy Office. R.P. also acknowledges support from ANPCyT and CONICET.

References

[1] E.M. Lopasso, M. Caro, A. Caro, and P. Turchi, *Phase diagram of an empirical potential: The case of FeCu*, Phys. Rev. B **68**, 214205 (2003).
[2] R. Kikuchi, *A theory of cooperative phenomena*, Phys. Rev. B **51**, 988 (1951).
[3] G. Inden and W. Pitsch, Vol. 5 of *Materials Science and Technology*, (J. Wiley & Sons, 1991), pp. 497—552.
[4] G. Ackland, D.J. Bacon, A.F. Calder, and T. Harry, *Computer simulation of point defect properties in dilute FeCu alloy using a many-body interatomic potential*, Philos. Mag. A **75**, 713 (1997).
[5] M. Ludwig, D. Farkas, D. Pedraza, and M. Schmauder, *Embedded atom potential for FeCu interactions and simulations of precipitate-matrix interfaces*, Modelling Simul. Mater. Scie. Eng. **6**, 19 (1998).

Influence of inertia on dislocation dipoles strength

L. Pillon [1], *C. Denoual* [1], *R. Madec* [1], *Y.P. Pellegrini* [1]

[1] *CEA/DAM Ile de France, DPTA, BP n°12, 91680 Bruyères-le-Chatel, France*

The stability of an edge dislocation dipole is analyzed with two different simulation techniques. The first one utilizes the Peierls-Nabarro Galerkin method (PNG), where the time-dependent displacement field around dislocations is computed with a finite-element code. The method, used as a reference, naturally accounts for inertial effects and reproduces unsteady dislocation motion with accompanying stress waves emission when dislocations slow down. The second technique uses a two-dimensional dislocation dynamics code, which relies on expressions for relativistic effective dislocation masses and related analytic approximations of the interaction force. Comparison between the results obtained with the two dynamic techniques in the plane (viscosity, driving force) shows that inertial effects in this configuration are important at high dislocation velocity. These effects are also studied as a function of the distance between the two slip planes.

A First Principles Study of Palladium in Silicon Carbide

Guido ROMA

Service de Recherches de Métallurgie Physique, CEA Saclay, 91191 Gif sur Yvette, France

Silicon carbide has been used in nuclear industry and is still considered as a coating material for nuclear fuel. Its main role should be to retain fission products. It has been observed, however, that some fission products, like palladium and silver, attack the SiC layer and are supposed to be responsible for corrosion of the material, which could facilitate fission products release. We used first principles calculations based on Density Functional Theory (DFT) in order to investigate the energetic, structural, and kinetic properties of Pd impurities inside beta-SiC; we obtained solution and migration energies in pure SiC and use them to discuss some basic thermodynamical issues of the corrosion process. Moreover we consider some possible effects of the disorder which is known to be induced by irradiation in the form of amorphised regions.

Physical-chemical investigation and modeling of netlike polymerization of negative SU-8 resist during X-ray lithography processes

Elena Reznikova[1], *V. Nazmov*[1], *J. Mohr*[1], *A. Last*[1]

[1]*Institut fuer Mikrostrukturtechnik / Forschungszentrum Karlsruhe, 76021 Karlsruhe, Germany*

The physical-chemical properties of SU-8 polymer, the mechanisms of X-ray lithography processes and the criteria of their optimization are discussed.

Layers of multi-component SU-8 resist were investigated by the FT-IR spectroscopic method for a wave number range of 600 - 5000 cm^{-1} after each X-ray lithography process step (pre-exposure baking, exposure, post-exposure baking, development). The doses of absorbed X-ray radiation were varied from 0.1 J/cm^3 to 6000 J/cm^3 with uniform dose distribution in the layer depth. It was found that the monomers (a diglycidyl ether of bisphenol A novolac) are bonded to each other in initial pre-polymer by means of the end epoxy groups. A disruption of the epoxy groups of the pre-polymer molecules as well as a formation of polymer ester bonds occur during both the exposure process and post-exposure baking. The relative quantity of disrupted epoxy groups and the correspondent amount of a new formed polymer bonds in the resist layer are grown with an increase of the dose of the absorbed radiation up to saturation at about 1000 J/cm^3.

The dose dependence of a relative number of monomers in the insoluble phase of the polymer after the development process corresponds to the characteristic curve of a relative residual thickness of the resist layer. The dose of about 1 J/cm3 is a threshold for an appearance of the insoluble phase of the layer on a substrate surface. At approximately 30 J/cm^3 the shrinkage of the layer with the insoluble phase is close to zero. The experimental determination of the mass ratio of the insoluble and soluble phase in the resist layer in dependence on the dose of absorbed X-ray radiation are in quantitative agreement with results of the statistics modelling of netlike polymerization which includes the calculations of the quantity of absorbed photons and the track lengths of photo- and Auger-electrons.

Modeling of Irradiation of Titanium Powder With Nd: YAG Laser

DILIP SRINIVAS S

B-5/145 KAILASAPURAM TOWNSHIP, BHEL TRICHY, 620014 TRICHY, India

Rapid Prototyping using selective laser sintering is a popular method used to develop prototypes that can be used for functional applications. In this paper, a three-dimensional Computational Fluid Dynamics (CFD) model of selective laser sintering of titanium powder is presented. The model predicts the temperature distribution in a bed of titanium powder when an Nd: YAG laser beam in continuous wave mode of wavelength 1.06 µm, spot radius 0.025 mm and power 2 W is focused on the bed. The model incorporates temperature dependent convection and radiation boundary conditions. The thermal conductivity is modeled as a non-linear property. The kinetics of sintering is realized in the model through thermal conductivity. The model also incorporates temperature dependent radiation properties of the material. The results clearly demonstrate the pattern of energy flux dispersion in the bed that is under the laser scan. The results obtained are in good agreement with the previous experimental results reported in literature.

Atomistic simulations of irradiated magnetic nanocrystalline iron

Maria Samaras[1], *P.M. Derlet*[1], *H. Van Swygenhoven*[1], *M. Victoria*[1,2,3]

[1]*Paul Scherrer Institute, 5232 Villigen, Switzerland*
[2]*Lawrence Livermore National Laboratory, United States of America*
[3]*Polytechnical University of Madrid, Spain*

Atomistic simulations provide an understanding of microscopic properties which influence a material's lifetime. Such an understanding is important for understanding the formation of damage defect structures produced in irradiated materials. Grain boundaries have been seen to significantly influence the final damage state of irradiated materials both experimentally and computationally. Recently, ab initio calculations of iron have demonstrated the importance of magnetism in the energetic ordering of single interstitial dumbbell defects, where the most stable structure is the 110 dumbbell rather than the 111 dumbbell. This has important consequences for interstitial migration and therefore will influence the final defect structure of irradiated materials. In past work, irradiation of nanocrystalline fcc Ni has revealed that grain boundaries in the proximity of a cascade will act as interstitial sinks. In the present work we use molecular dynamics simulations of displacement cascades in nanocrystalline Fe using the recently developed magnetic potential in order to investigate the influence of magnetism during the primary damage state in the presence of grain boundaries and compare the results with previous explicitly non-magnetic empirical potentials for Fe.

The stability of vacancy clusters in fcc crystals

Mikhail Starostenkov

Altai State Technical University, Lenin st., 46, 656038, Barnaul, Russia

The present paper deals with the research of vacancy clusters stability in fcc metals Ni, Cu, Al by the method of molecular dynamics. The calculated block of an ideal crystal contained 27000 atoms in the model. Periodical boundaries were applied on its block. Interatomic interactions were described by pair central Morse potentials, which parameters were determined by experimental data of overall pressure module, sublimation energy and lattice parameter. Vacancy clusters were constructed by the removal of corresponding atoms from the calculated block. The following types of clusters were studied: pores, vacancy discs, stacking fault tetrahedrons, vacancy "tubes", which were constructed by the removal of the part of closely-packed atomic row, accidentally distributed single vacancies. The number of vacancies in every case varied from several units to several hundreds. The annealings of crystal block at the temperature from $0.5T_{melt}$ to T_{melt} during 100-500 ps with further cooling to the temperature of about 0 K were made to determine clusters stability. Diffusion coefficient and potential energy of the calculated block were calculated after cooling. It was studied the structure of crystal block by the visualizators of distribution of potential energy and atomic displacements.

According to molecular-dynamic experiments vacancy clusters having tetrahedron form were more stable and energetically profitable. The sides of the tetrahedron were oriented along the planes [111] and looked like stacking fault defects, sides – as partial dislocations oriented along the directions <111>. The sides of such tetrahedrons can be interpreted as vacancy disks. All the types of the considered vacancy clusters tended to take a tetrahedron form. Similar stacking fault tetrahedrons were stable until melting temperatures. Pores were less energetically profitable than flat clusters. Diffusion at the presence of pores in the crystal took place mainly along internal surface by so-called "rolling stone" mechanism. In a whole, it was found that the bigger the size of a cluster, the less mobility it had. In this connection, activation energy of diffusion with cluster migration was bigger.

Point Defects and Their Influence on Thermoactivated Disordering Process of Ni_3Al Intermetallide

Mikhail D. Starostenkov, **Gennady M. Poletaev, Natalia B. Cholodova**

Lenin st. 46, Altai State Technical University, Barnaul, 656038, Russia,
genphys@agtu.secna.ru

ABSTRACT

The role of different point defects (vacancies, interstitials and their complexes, Frenckel pairs) in diffusion processes leading to the disordering of Ni_3Al intermetallide was studied by the method of molecular dynamics. The temperature of the beginning of the disordering process and it's velocity for different types of point defects were determined. It was shown that interstitial atoms could form the complexes. The complexes were able to move collectively forming the disordering area. The effect of unification of point defects groups and their collective participation in a diffusion process of disordering can be characterized on the bases of self-organization conception of the system in a dynamics of a thermal activation process.

1. Introduction

Intermetallide Ni3Al have an important property for practical use – positive temperature dependence of the yield stress [1]. Similar property of the ordered alloys and intermetallides has been the subject of scientific researches for more than fifty years. However, the exact presentation on the mechanisms realized in the materials at the atomic level and leading to a similar dependence at the macroscopic level is absent. It is evident that the disordering process gives contribution in such property of the material. The peculiarities of diffusion mechanisms taking place at different temperatures are connected with this phenomenon. Point defects and their combinations should play an important role in such processes.

In the paper, the research of the influence of point defects (vacancies and their complexes, interstitial atoms) on the processes of Ni_3Al intermetallide thermoactivated disordering was made. A two-dimensional crystal of Ni_3Al intermetallide with the packing of atoms corresponding to the plane {111} of fcc lattice of $L1_2$ superstructure is chosen as the research object. The study of diffusion peculiarities in a two-dimensional crystal is of independent importance because similar processes in them have as general characteristics with volume crystals so the definite deviations. The study of similar problems is also important for the materials design on the basis of nanotechnologies. At the same time, it is possible to solve the problems of a computer simulation conformably to volume materials on the example of a two-dimensional crystal.

2. The Model

Computer simulation was made by the molecular dynamics method. The crystal block under study contained the cell consisting of 10000 atoms. The given structure repeated by periodical boundary conditions outside the cell. The interactions between different pairs of atoms were given by Morse potential functions. The interaction radius spread to 8 Å. The movements of atoms in a molecular dynamics model were described by Newton differential equations. The temperature of the calculated block was given through the initial velocities of the atoms movements. Every atom had an initial velocity which was equal to root-mean-square velocity corresponding to Maxwell distribution multiplied by $\sqrt{2}$. The directions of the initial velocities were given accidentally. However, the total impulse of all the atoms in the calculated block was to be equal to zero. Step interval of the movement equation was equal to 10^{-14} s. The equality of the total impulse to zero was controlled [2].

The definite types of point defects were introduced in the calculated crystal block. Then, it followed the system relaxation by an impulsive heating of about 0 K with the following cooling by the energy dissipation outside the calculated crystal block. Then the direct computer experiment consisting in an impulsive heating of the system to the definite temperature and the following material hardening took place. Structure-energetical reconstruction of the material was analyzed using different visualizators such as the change of closely-packed atomic rows, the visualizator of a radial distribution of atoms in the dependence on distance [3].

3. The Results and Discussion

The temperature of diffusion beginning in an ideal crystal approached to the melting temperature of Ni_3Al alloy. Crawdion and ring mechanisms of atoms displacements taking place only over the components sublattices were found at the first stages. They did not cause the system disordering. Ring displacements took place near the melting temperature and more higher temperatures over the sublattices Ni and Al, and led to the disordering. Dynamical Frenckel pairs began to form at those temperatures.

The temperature of diffusion beginning and the appearance of disordering areas considerably decreased at the presence of point defects. The value of temperature decrease was directly connected with the level of a local tension in a crystal energy. The tensions were caused by point defects and energy increase brought by the defect in a total crystal energy.

The picture of a local tension distribution near point defects is seen in Fig. 1, 2.

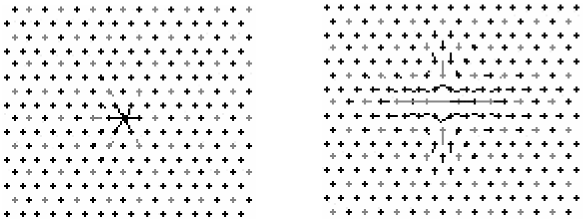

a) b)

Figure 1. The displacements of atoms near the vacancies of Al (a) and Ni (b). The scale of the displacements is increased in 10 times. Black atoms – Ni, grey – Al.

Two configurations – a vacancy in Ni site and a vacancy in Al site are possible at the presence of vacancies in the material. The configurations in $L1_2$ superstructure of the plane have different surroundings. That is why, the structure of local displacements near the vacancies is different; displacements near the vacancies in Al site are corresponded to the deformation of an overall pressure. More complex view of local atomic displacements is observed near the vacancies in Ni site. There are four variants of distribution of interstitial atoms Ni and Al in the mentioned superstructure type. Two of them have a local radial symmetry. It can be seen in the picture of local displacements distribution near interstitial atoms. In these cases, the inculcated atoms of Al or Ni are situated in the triangle center of the nearest neighbors of Ni atoms. When the triangle consists of two atoms Ni and one atom Al, the picture of local displacement appears to be slightly asymmetric. In a whole, the picture of atoms displacement corresponds to a local tension deformation. The total deformation value near interstitial atoms is considerably bigger in comparison with the deformation near vacant sites.

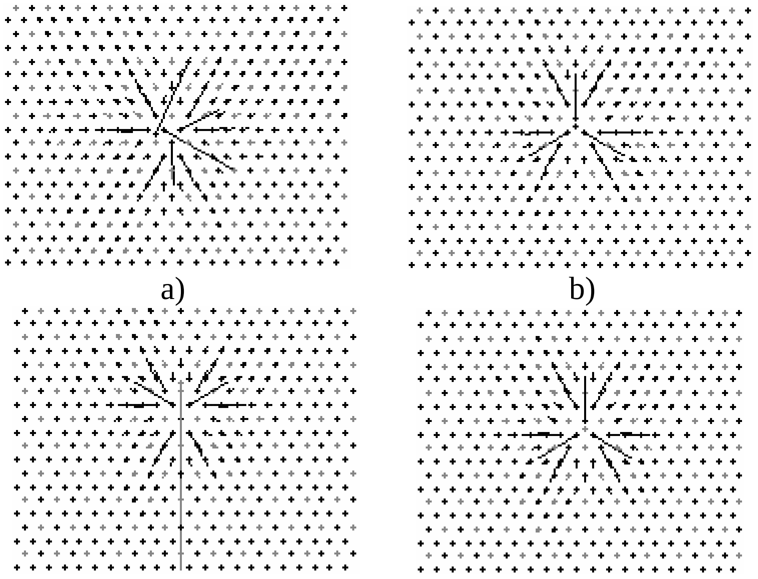
a) b)
c) d)

Figure 2. The displacements of atoms near interstitial Ni atoms in the configurations Ni-Ni-Al (a), Ni-Ni-Ni (b) and Al interstitial atoms in the configurations Ni-Ni-Al (c), Ni-Ni-Ni (d). The scale of the displacements is increased in 10 times.

It is evident that eight combinations of Frenckel pairs are possible in this superstructure type. Volume alloy crystal of $L1_2$ superstructure can have vacancies in two types of sites: Ni and Al as in a two-dimensional crystal. Radial symmetry of local displacements of neighboring atoms corresponds to the vacancy in Al site. The anisotropy of components atoms distribution is noticed near the vacancy in Ni site.

The definite sets of point defects were introduced in the calculated block of crystal. Then the crystal was impulsively heated to the definite temperature, it was being kept at those temperature during some time. Further, the hardening procedure was made by the dissipation of a kinetic energy component outside the calculated block of crystal. The analysis of a final state of the system was fulfilled using the definite visualizators. The first diffusion displacements of atoms by crawdion and ring mechanisms were found in an ideal crystal only at high temperatures. The displacements took place only over the sublattices of the components Ni or Al. But, the superstructure order was not broken.

Dynamical Frenckel pairs begin to appear at the temperatures close to the melting temperature in the places of the appliance of atoms crawdion displacements in two closely-packed directions. Their number is insignificant at the first stages. They are being observed for a short time and recombined rapidly. The atomic displacements take place as broken chains trajectories of the atoms displacements relatively to the interstitial atom. The vacancy can be stable. The displacement of atoms takes place over the sublattices Ni and Al and the disordering along the migration trajectories can be noticed. The number of Frenckel pairs increases with the growth of temperature and time of an impulsive heating. The unification process of interstitial atoms in aggregates, the formation of free vacancies, their unification in the divacancies and complexes are observed.

The temperature of the beginning of diffusion processes considerably decreases after the introduction of point defects. The value of the temperature decrease is directly connected with the level of local stresses, causing the presence of point defect in the crystal. It concerns the proper interstitial atoms and interstitial atoms of Frenckel pairs. The temperature of the beginning of the superstructure diffusion reconstruction corresponds to 50-100 K. Then it follows a big enough interval – to 600 K. Considerable diffusion transformations are not observed when the crystal structure have some vacancies, the diffusion is seen only at the order temperature 400 K. At higher temperatures, the vacancies begin to contribute in the disordering process.

All the mechanisms make some contribution in a diffusion process. The disordering process develops with a big velocity. The displacements of atoms in the crystal having two vacancies and one interstitial atom are shown in the Fig. 3 (a) as an example. The crystal is impulsively heated at the temperature 1100 K during 20 ps. One of the vacancies is located nearer to the interstitial atom. As it is seen from the figure, the biggest displacements of atoms along the complex crawdion trajectory are found relatively the interstitial atom. The neighboring vacancy displaces also over a long trajectory. But, it is worth to note that those defects remove from each other. The displacement trajectory of a free vacancy is directed to the side of an interstitial atom located in a new state. Here, crawdion displacements of atoms can be observed.

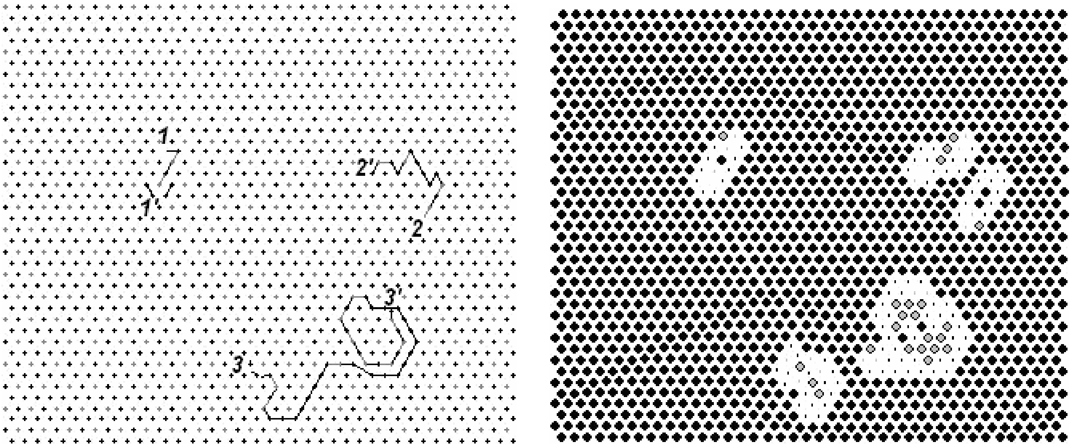

a) b)

Figure 3. a) The picture of the trajectories of atoms displacement. Black atoms – Ni, grey – Al. 1, 2 – the start position of vacancies; 1’, 2’ – the final position of vacancies; 3 and 3’ – the start and final positions of the interstitial atom. b) The picture of the change of the crystal phase composition. The black color corresponds to order phase Ni_3Al, grey – Ni_2Al, point – disorder phase.

The picture of the change of phase composition is presented in Fig. 3 (b). The elements of different phases determined by a short order are marked by the following symbols. It is seen from the figure that maximum order break is observed along the trajectories of atoms displacements relatively the interstitial atom. The germs and clusters of Ni_2Al phases appear inside the disordering area. The following point defect is a vacancy neighboring to the interstitial atom. The appearance of germs and clusters Ni_2Al is noticed in a disordering zone. The least order break is observed in a zone of the removed vacancy migration. The germs of Ni_2Al phase are found in this zone.

References

1. Noguchi O., Oya Y., Suzuki T. // Metall. Trans. A. **12**, (1981).
2. Poletaev G.M., Starostenkov M.D. // Technical Physics Letters. **29**, 6 (2003).
3. Poletaev G.M., Patzeva J.V., Gurova N.M., Starostenkov M.D. // Engineering Mechanics. **11**, 5 (2004).

Influence of Cr content on the microstructural evolution of electron irradiated Fe-Cr binary alloys: a multiscale modelling study

D. Terentyev, *L. Malerba*, *P. Olsson*

SCK-CEN, Boeretang 200, 2400, Mol, Belgium

Fe-Cr binary alloys are model materials for low activation ferritic/martensitic steels considered as structural materials in advanced nuclear power systems (ADS, fusion and GenIV reactors). The presence of Cr is known to determine good swelling resistance, which is critical parameter under irradiation. In a production bias model framework, proper understanding of the relative stability and mobility of point defect clusters is necessary to predict the process of formation and growth of the voids.

In this work we present results obtained by using a combination of atomistic modelling techniques, i.e. *ab initio*, molecular dynamics (MD) and damage accumulation models. One technique is used to parameterize the other one, so only few assumptions have been made, thereby providing a consistent example of multi-scale modelling. We first give a characterization of point defect properties in the Fe-Cr alloy as predicted by *ab initio* versus MD results, thereby showing the validity of the used interatomic potential, while comparing the results with available experimental data. Subsequently, the results of this study for the mobility of point defects and clusters have been used in a coarser-grained model to reproduce high-energy electron irradiation and its annealing in Fe-Cr for the stages of interstitial migration. The obtained results are discussed in the light of existing experimental observations.

Structure and Mobility of Radiation-Induced Defects in MgO

Blas Pedro Uberuaga

Los Alamos National Laboratory, MS G755, Los Alamos, NM 87545

ABSTRACT

Understanding how the defects formed during radiation damage evolve with time is a key component to predicting materials performance during irradiation. This problem is inherently multiscale, involving time scales from ps to years and length scales from nanometers to meters. Here, we give an overview of our work on radiation damage in MgO. Molecular dynamics is used to simulate the production of defects during collision cascades. We describe accelerated dynamics simulations, used to probe the long-time behavior of defects formed in collision cascades in MgO in which we find surprisingly high mobilities for larger interstitial clusters. We gauge the impact of these high mobilities with simple chemical rate theory models and find that these interstitial clusters and their high mobilities do impact predicted interstitial loop size.

1. Introduction

The phenomena associated with the production of radiation damage and its subsequent evolution are both complex and inherently multiscale. Damage is produced at the atomic scale via the collision of atoms. These collisions are both fast, lasting picoseconds, and confined to small dimensions (nanometers to fraction of a micrometer). However, as this damage evolves over longer time scales, it can take the form of voids or other complex microstructure, giving rise to macroscopic phenomena such as swelling and cracking which can take years to develop. This ultimately leads to, in for example a nuclear fuel application, failure of the fuel pin. No one simulation method can span all of these time and length scales. Any approach that focuses on just one method will be inadequate, missing key physics critical for accurate predictions of fuel performance. Thus, it is an absolute necessity to develop multiscale approaches that span both the time and length scales associated with radiation damage evolution in an irradiated material.

The term “multiscale modeling” has various meanings, depending on the context. Typically, multiscale modeling is subdivided into two categories: concurrent and sequential, or parameter passing. Concurrent multiscale modeling mixes different levels of modeling into the same simulation. For example, approaches that link an atomistic description of some key region of a problem (such as a crack tip) with a continuum level description of material far from the critical region are one type of concurrent multiscale modeling (see, e.g., [1]). Such approaches allow one to reach much larger length scales, but typically do not solve the time scale problem as the achievable times are limited by the most accurately described region. In the case of the crack tip, this would be the atomically resolved region, which, using a standard molecular dynamics (MD) description, would limit the times to nanoseconds.

The alternative is sequential multiscale modeling. In this approach, one level of modeling is used to characterize some properties of the material which are then used as input into a higher level of modeling. Typical examples of this approach include those that determine defect kinetic properties from an atomistic description (density functional theory or an empirical potential, for example) and feed those to something like kinetic Monte Carlo (KMC). These methods have the advantage of decoupling the different levels of simulation, overcoming the time-scale issue with concurrent multiscale modeling. However, this is also their disadvantage, in that there is no direct link or feedback between the different levels of simulation.

In this paper, we give an overview of our work on radiation damage in MgO [2-4]. We describe one approach to sequential multiscale modeling. We use MD to probe defect production during collision cascades in MgO. We then use temperature accelerated dynamics (TAD) [5] to probe kinetic behavior of the resultant defects out to long times. Finally, we use chemical rate theory (CRT) to qualitatively probe the impact of those kinetic properties on experimental observables, such as interstitial loop size.

2. Methodolgy

As mentioned we use a combination of MD, TAD and CRT to probe the production of defects, their long-time evolution, and their impact on macroscopic observables. These methods have been extensively described elsewhere. Here, we give just a brief overview of the methods.

MD is ideal for short-time, non-equilibrium situations such as the collision cascade stage of a radiation damage event. These events last on the order of ps and are highly non-equilibrium, making methods that rely upon the assumption of events governed by transition state theory (TST) unsuitable for this regime. In our MD simulations, we use a standard Buckingham potential with a Coulomb term for long-range electrostatics (potential parameters for MgO are described in Ref. [3]). Standard considerations when performing collision cascade simulations were applied (e.g., ZBL, thermostatic boundaries; see Ref. [3]). The MD simulations were used to simulate the production of defects during collision cascades and determine the number and nature of those defects.

In order to probe the long-time behavior of those defects, we used TAD [5]. TAD involves running MD at a temperature higher than that of interest, which accelerates the rate at which events happen. However, this MD is constrained so that, when events occur, they are characterized by finding their saddle point, and then the trajectory is placed back in the original state, so that events are not allowed to actually occur at the high temperature. With knowledge of the saddle point energy, the times of events at the high temperature can be extrapolated to the low temperature of interest. Once a stopping criterion is met, the event with the shortest time at the low temperature is accepted and the system moved to the corresponding state. This procedure gives exact state-to-state dynamics if harmonic TST holds for the system. See Ref. [6] for more details on the TAD procedure. All of the simulations described here are for a low temperature of 300 K. Using TAD, we are, in some cases, able to achieve simulation times of seconds for defects in MgO.

Finally, we also use CRT to obtain some insight into how defect properties impact larger-scale phenomenon. CRT is a well established modeling method; please see Ref. [4] for details on the particular implementation used here.

2. Defect Properties in MgO

1.1 Defect production

Using MD, we performed collision cascade simulations for several primary knock-on atom (PKA) energies and directions. Fig. 1 shows the results of a typical simulation for an Mg PKA with an energy of 0.4 keV. Only a few point defects remain after the cascade has settled. Two interstitials have combined to form an interstitial dimer. Such aggregation of point defects is typical of all of our simulations. We also observe, both from these cascade simulations as well as the TAD simulations, that interstitial mobilities are much larger than vacancy mobilities.

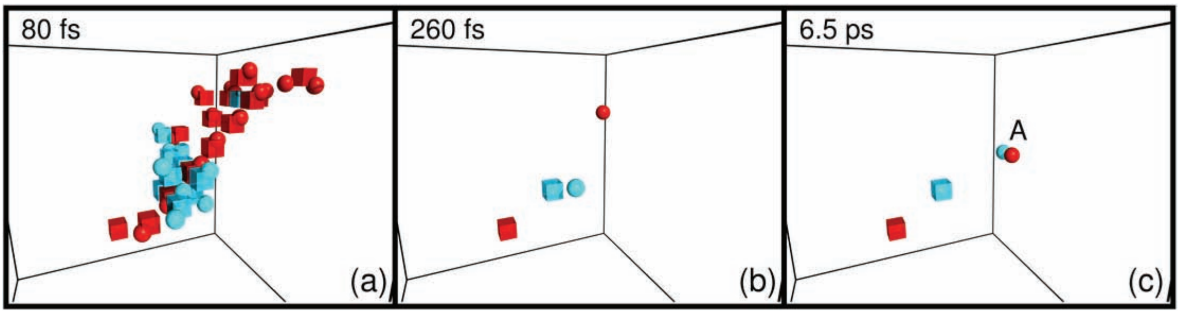

Figure 1. Evolution of a 0.4 keV cascade in MgO. Red objects represent O, blue Mg. Spheres are interstitials and cubes vacancies. After the cascade has settled, two vacancies, one of each type, and two interstitials, again one of each type, remain. After several ps, the two interstitials combine to form an interstitial dimer, labeled A in frame (c). This figure originally appeared in Ref. [4].

We also performed cascade simulations for PKA energies of 2 keV and 5 keV, over a number of directions on both sublattices. The results of all our simulations are given in Table 1. As expected, the number of defects increases with increasing PKA energy. The number of mono-interstitials and mono-vacancies is roughly equal for both sublattices (O and Mg). We also find that as the PKA energy is increased, more defect clustering occurs. For the larger energies, we observed some larger clusters than reported in Table 1, including 3- and 4-atom interstitial clusters. For the most part, however, the defects produced are dominated by mono-interstitials and mono-vacancies.

Table 1 Defects produced in collision cascades in MgO, measured as the number of Frenkel pairs remaining after 8 ps of MD. Also given are the distribution of various defect types.

PKA energy (keV)	*Number of trajectories*	*Number Frenkel pairs*	*Mono-int (O/Mg)*	*Mono-vac (O/Mg)*	*Di-int*	*Di-vac*	*Perfect lattice*
0.4	20	10	3/1	5/3	3	1	13
2	12	84	21/24	33/30	15	6	0
5	12	216	57/62	78/80	39	15	0

1.2 Defect kinetics

The long-time behavior of representative defects seen in the collision cascades were probed using TAD. We examined two types of behavior: defect aggregation and the kinetic properties of the resulting defect clusters While point defects are stable on the ps time scales associated with the MD simulations, we find that, given enough time, they often harmlessly recombine, completely healing the crystal. For example, in Fig. 2A, we show a TAD simulation of the recombination of an interstitial dimer with two vacancies. The initial configuration is very similar to that found at the end the collision cascade shown in Fig. 1. On the time scale of ps in the MD simulation, this was a stable configuration. However, the TAD shows that on the longer time scale of ms, the dimer is able to diffuse and recombine with first one of the vacancies and then the other, resulting in a perfect crystal after 10 ms. Depending on flux conditions, the time scale of ms might still be short compared to the time between damage events in such a region of material.

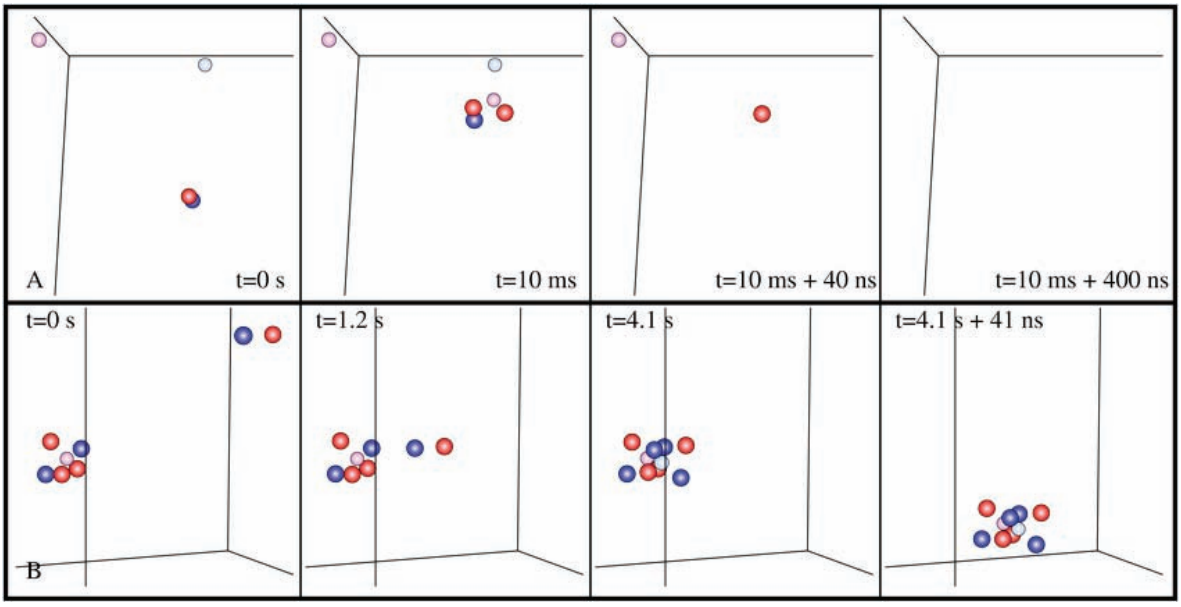

Figure 2. Results of TAD simulations at room temperature on point defect annihilation and aggregation. In all frames, blue represents Mg species, red represents O species, light-colored spheres are vacancies and dark-colored spheres are interstitials. In (A), an interstitial dimer recombines with O and Mg vacancies on the ms time scale. In (B), an interstitial dimer combines with an interstitial tetramer to form a 6-atom interstitial cluster which diffuses on the ns time scale at room temperature. The time scale associated with each frame is also given.

More interesting is the aggregation of defects, as illustrated in Fig. 2B. Here, we start with an interstitial dimer and an interstitial tetramer. We have found that the tetramer is a particularly immobile species, diffusing with a barrier of nearly 1.7 eV. The dimer, on the other hand, is significantly more mobile with a diffusion barrier of 0.75 eV. On the time scale of seconds, the dimer diffuses and is attracted to the tetramer (through higher-order moments of the Coulomb interaction) such that the two aggregate to form a six-interstitial cluster. This hexamer, after an annealing phase, exhibits extremely high mobility, diffusing on the ns time scale at room temperature. This structure of the hexamer is actually metastable and will decay on the order of years at room temperature to a more stable and less mobile structure.

We have seen similar behavior for other interstitial cluster defects in MgO. The five-interstitial cluster is particularly rich in this regard [7]. First, two types of pentamer cluster are possible:

Mg-rich $[Mg_3O_2]^{2+}$ and O-rich $[Mg_2O_3]^{2-}$. Both of these defect types can exist in one of at least three different structures, with correspondingly unique kinetic properties. The properties of these, and all interstitial clusters from size 1 to 6, are given in Fig. 3 in terms of their barrier for diffusion. Some preliminary data on cluster size 8 is also given, though we have yet to examine clusters larger than size 6 to any great extent.

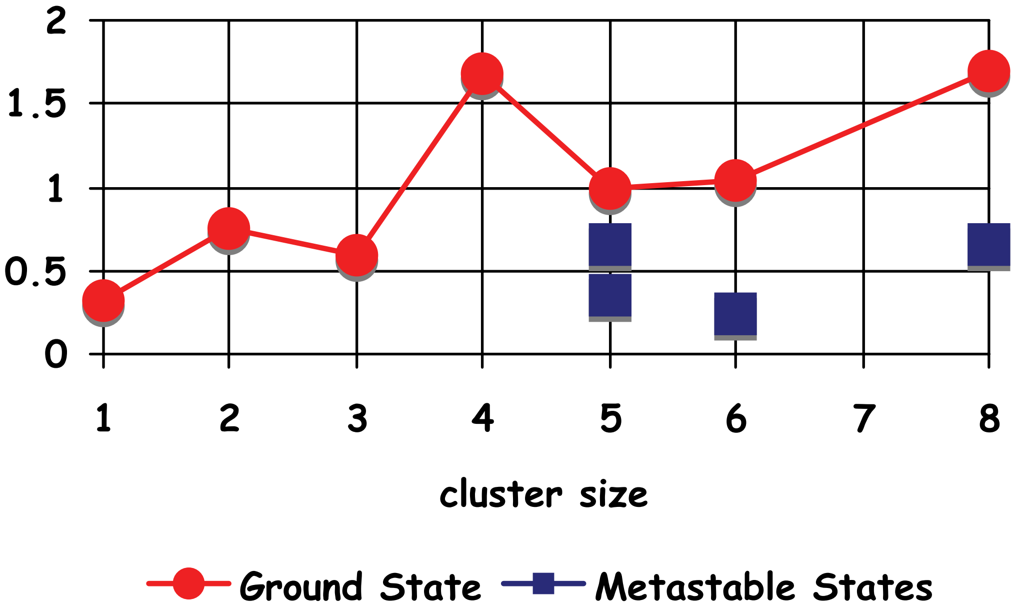

Figure 3. Diffusion barriers found via TAD simulations for interstitial clusters in MgO. For small clusters, there is one structure and thus one diffusion barrier. However, as the size of the clusters increases, multiple structures are found for each cluster size with unique diffusive characteristics. For both types of 5-atom interstitial clusters (Mg rich and O rich), three different structures were found. For both 6- and 8-atom interstitial clusters, we have found two different mobile structures.

1.3 Impact of point defect properties on large-scale phenomena

An obvious question that arises from the results on the kinetics of defect clusters in MgO is if these properties impact experimental observables such as interstitial loop growth. While the metastable forms of these clusters are likely to be unimportant under equilibrium conditions, especially at room temperature, they may be crucial to predicting correct behavior in non-equilibrium environments such as those present during irradiation. To probe this, we have performed CRT calculations using the defect properties determined with MD and TAD at the atomic scale.

Fig. 4 shows the results of our CRT simulations for MgO as a function of temperature once the system has reached steady-state. We performed simulations under two conditions: one in which we assumed only mono-interstitials were mobile and one in which all of the mobilities discovered via TAD were included. We see that including the mobility of larger clusters does change the predicted size of interstitial loops by a factor of 3 or so, depending on the temperature. The effects may be even greater for other conditions, such as when impurities are present, though we are just beginning to explore these effects.

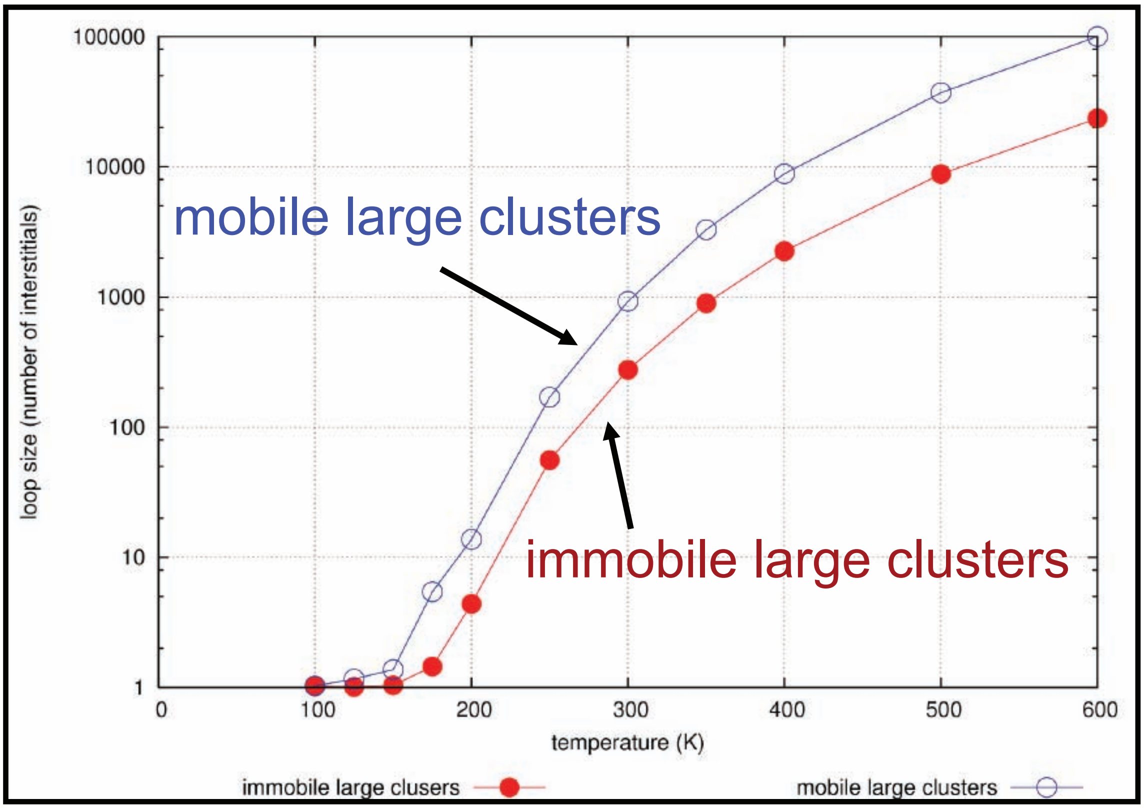

Figure 4: Results of chemical rate theory simulations on steady-state interstitial loop size as a function of temperature when only mono-interstitials are allowed to move (solid points) and when the diffusive properties of all clusters, as found in TAD simulations, are included (open points). The mobility of large interstitial clusters changes the loop size predicted at high temperature by a factor of 3.

4. Discussion and Conclusions

It is clear from the work presented here that exploring the long time behavior of defects produced in collision cascades is crucial for understanding their properties. While this has been known to be true in metals, where very large interstitial clusters can diffuse very quickly, it has only been recently demonstrated for ceramics. Not only do larger defect aggregates exhibit high mobilities, they also form in a variety of structures. Describing this “zoo” of defect types correctly in higher level models will be key for predicting materials response in non-equilibrium environments such as that present during irradiation. We are still in the beginning stages of understanding the ramifications of the existence of metastable structures for macroscopic phenomena and much work needs to be done. We are currently in the process of developing a KMC model that incorporates the defect properties found from MD and TAD. We will use this to both verify that the qualitative predictions of the CRT model are accurate as well as explore other aspects that are more difficult to capture in CRT, such as the one-dimensional nature of the diffusion of some of the interstitial clusters.

We are also beginning to study the impact that impurities, such as Al, have on radiation damage response in MgO [7,8]. Our preliminary work suggests that Al impurities affect both stages of radiation damage: the production and the evolution of defects. Al impurities have a homogenizing effect on damage production, reducing the anisotropy of damage production normally associated with pristine materials. On the other hand, the Al impurities act as strong traps for defect migration, reducing the overall diffusion length of the defects and rendering, to some degree, the high mobility of larger clusters less important.

Our ultimate goal is to be able to do a simulation of a material under conditions that match experiment. This means simulating the evolution of the defects from the full cascade, not just parts of it, until it is time for another cascade collision event in that region of material. At this time, even using accelerated molecular dynamics (AMD), we are not able to do this. Such a simulation may involve a coupling between MD, AMD and KMC methods in a hybrid concurrent-parameter passing mode. Such a simulation would allow us to understand the importance of defect diffusion and cascade overlap on properties such as swelling.

To conclude, we have applied molecular dynamics, temperature accelerated dynamics, and chemical rate theory to examine the response of MgO to radiation damage. We find that point defects and small defect clusters are formed in the collision cascade of a radiation damage event. Over times much longer than the collision cascade time scale, those defects can annihilate or aggregate. Defect aggregates tend to have high mobilities, leading to an enhancement in predicted interstitial loop size over what would be predicted if their mobilities were neglected. Thus, it is important to fully characterize point defect properties in order to accurately predict macroscopic response to irradiation.

Acknowledgements

This work would not have been possible without extensive collaborations with K.E. Sickafus and A.F. Voter at LANL, G. Henkelman at UT Austin, R.W. Grimes and his students A.R. Cleave and J.A. Ball at Imperial College and R. Smith at Loughborough University. This work was supported by the US Department of Energy, Office of Science, Office of Basic Energy Sciences.

References

[1] J. Rottler, S. Barsky and M. O. Robbins, “Cracks and crazes: on calculating the macroscopic fracture energy of glassy polymers form molecular simulations”, Phys. Rev. Lett. 89: 148304 (2002).
[2] B. P Uberuaga, R. Smith, A. R. Cleave, F. Montalenti, G. Henkelman, R. W. Grimes, A. F. Voter, and K. E. Sickafus, “Structure and mobility of defects formed from collision cascades in MgO”, Phys. Rev. Lett. 92: 115505 (2004).
[3] B. P Uberuaga, R. Smith, A. R. Cleave, G. Henkelman, R. W. Grimes, A. F. Voter, and K. E. Sickafus, “Dynamical simulations of radiation damage and defect mobility in MgO”, Phys. Rev. B 71: 104102 (2005).
[4] B. P. Uberuaga, R. Smith, A. R. Cleave, G. Henkelman, R. W. Grimes, A. F. Voter, and K. E. Sickafus, “Exploring long-time response to radiation damage in MgO”, Nucl. Instr. and Meth. B 228: 260 (2005).

[5] M. R. Sørensen and A. F. Voter, “Temperature-accelerated dynamics for simulation of infrequent events”, J. Chem. Phys. 112: 9599 (2000).
[6] A. F. Voter, F. Montalenti, and T. C. Germann, “Extending the time scale in atomistic simulation of materials”, Ann. Rev. Mat. Sci. 32: 321 (2002).
[7] B. P. Uberuaga, R. Smith, A. R. Cleave, R. W. Grimes, A. F. Voter, and K. E. Sickafus, “Accelerated molecular dynamics simulations of interstitial clusters in pure and Al-doped MgO”, Nucl. Instr. and Meth. B, in press.
[8] A. R. Cleave, R. W. Grimes, R. Smith, B. P. Uberuaga, and K. E. Sickafus, “Simulations of cascades in pure and alumina doped magnesia”, Nucl. Instr. and Meth. B, in press.

Core Structure and Mobility of Screw Dislocations in α-Fe from First Principles

L. Ventelon and **F. Willaime**

Service de Recherches de Métallurgie Physique, CEA/Saclay,
91191 Gif-sur-Yvette, France – lisa.ventelon@cea.fr

ABSTRACT

The structure and properties of the core of a/2 <111> screw dislocations in alpha iron are investigated by first principles electronic structure calculations carried out within the DFT framework using localized basis functions as implemented in the SIESTA code. The results obtained for the {211} and {110} generalized stacking fault energy (γ) surfaces suggest a non-degenerate core structure, symmetrically spread across the three {110} planes, in contrast with predictions from most empirical potentials. The core structure is investigated using two different cell arrangements: a periodic array of dislocation dipoles and a single dislocation within the cluster approach. The two sets of results are in very good agreement with each other. The degenerate easy core is confirmed to be the most stable structure, in particular with respect to the hard core, and the degenerate core decays to the non-degenerate core. The displacement field is very close to the elasticity theory. As a first step towards the mobility, the energy barrier of the Peierls potential has been calculated.

1. Introduction

The anisotropy of plasticity in bcc metals is directly related to the geometry of the core of screw dislocations, which was shown to be connected with the shape of the generalized stacking fault energy (γ) surface. Calculations in bcc transition metals using Finnis-Sinclair type interatomic potentials have predicted a core structure spreading into three {110} planes and falling into two classes: degenerate and non-degenerate core structures [1]. The comparison with the {110} and {211} γ-surfaces have lead Vitek and Duesbery to propose the following criterion for obtaining a core spreading asymmetrically along the <211> directions (i.e. degenerate core):

$$\gamma_{\{110\}}(b/3) < 2\gamma_{\{110\}}(b/6) \tag{1}$$

where $\gamma_{\{110\}}(b/3)$ and $\gamma_{\{110\}}(b/6)$ are the energy of the b/3 and b/6 faults respectively, for the <111> cross section of the {110} γ-surface. According to the γ surfaces obtained within density functional theory (DFT) calculations in V, Nb, Ta, Cr, Mo, W and Fe, this criterion suggests that all bcc transition metals have a non-degenerate core [2]. Direct calculations of the cores have been performed within DFT in Mo, Ta and Fe [2-4]]. In the three cases, the core is indeed found to be non-degenerate. The hard core can be either unstable (Mo) or metastable (Ta) [3]. Two types of cell geometries have been used: the so-called cluster approach, with an isolated dislocation in a "cylinder", and the dipole approach with periodic boundary conditions in the three directions of the supercell making an array of interacting dislocations [5]. Flexible boundary conditions have been developed in the cluster approach to study the effect of an external stress; they have been applied to determine the Peierls stress in

Mo and Ta [4]. The mobility of dislocations in Fe has not been addressed yet, mainly because these calculations based on plane wave basis sets are particularly time consuming in Fe. The aim of the present work is to achieve it by using localized basis sets and to compare the cluster and the dipole approaches (Fig. 1).

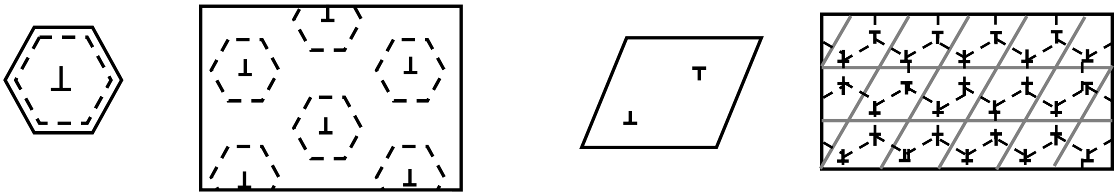

(a) (b)

Fig. 1. Schematic representation of the unit cells and boundary conditions used for the present dislocation calculations within the cluster (a) and the dipole (b) approaches.

2. Methodology

The present first principles electronic structure calculations have been performed within the DFT framework using localized basis sets as implemented in the SIESTA code. The pseudopotential and basis set for Fe – made of only 10 localized functions – have been validated by defect calculations [6]. The charge density is represented on a regular real space grid with a grid spacing of 0.06 Å instead of 0.08 Å as in previous studies, because of the higher accuracy required in the present calculations. This approach has been validated here on γ surfaces by performing a comparison with reference plane-wave results obtained using the PWSCF code. We have also investigated the effect of the exchange-correlation functional (LDA versus GGA). For the core structure, only the results obtained within GGA – which is known to perform better for the bulk properties in Fe – are presented. The γ surface calculations have been carried out using ten-layer slabs. For the calculations within the cluster approach the positions of the outer atoms are fixed to the elasticity theory solution. The unit cells for the dipole calculations are similar to the ones proposed in Ref. [2], but with additional components of the cell vectors along the dislocation line adapted in order to allow for the simulation of both easy and hard cores for every cell size. The effect of the size of the supercell has been investigated using cells containing up to 300 atoms.

3. Results and discussion

The results obtained for the {110} and {211} γ-lines along the <111> direction are summarized in Fig. 2. The effect of the exchange correlation functional is rather large, with a 25% increase from GGA to LDA. The discrepancy between SIESTA and plane-wave results is rather small in comparison; this validates the use of SIESTA for this type of calculations. These three sets of results are in very good agreement with Ref. [2]. These {110} γ-lines suggest a non-degenerate core structure according to the Duesbery-Vitek criterion. For comparison, we have also plotted the result obtained using one of the recently published improved empirical potential for iron [7]. A good agreement is obtained with the lower bound of DFT results. The complete DFT-GGA γ-surfaces obtained with the SIESTA code are represented in Fig. 3.

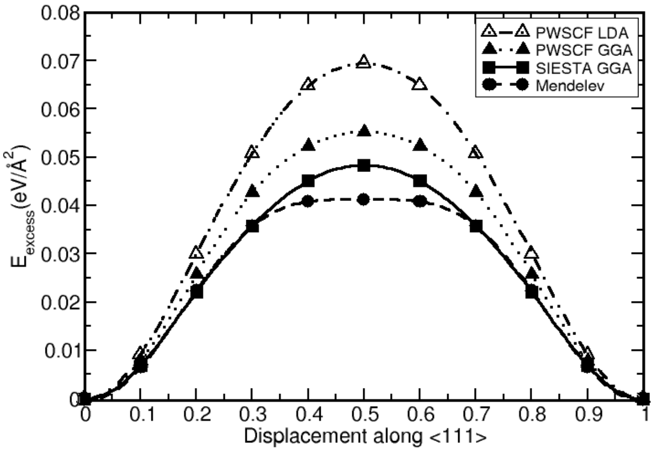

Fig. 2: Relaxed {110} γ-surface along the <111> direction. The x axis is given in units of the Burgers vector ½ <111>.

The core structures of the a/2 <111> screw dislocation in bcc Fe obtained within the cluster and the dipole approaches are in excellent agreement with each other. In both cases the degenerate core is found to decay to the non-degenerate structure. The differential displacement (DD) maps for the relaxed easy core show no sign of broken symmetry or splitting along the <211> directions (Fig. 4.(a)). The relaxed core structures are very close to elasticity theory (Fig. 4.(b)) with very small displacements within the (111) plane (Fig. 4.(c)). These results are also in very good agreement with Ref. [2]. The magnetic moment on the three central atoms is found to be reduced by 0.2 μ_B compared to the bulk value (2.3 μ_B) both for the easy and the hard cores.

We have also gained some insight into the mobility of the dislocation by calculating the Peierls barrier using the drag method. Further investigations are required to evaluate the effect of boundary conditions, but preliminary results suggest significant discrepancies between DFT and empirical potential results.

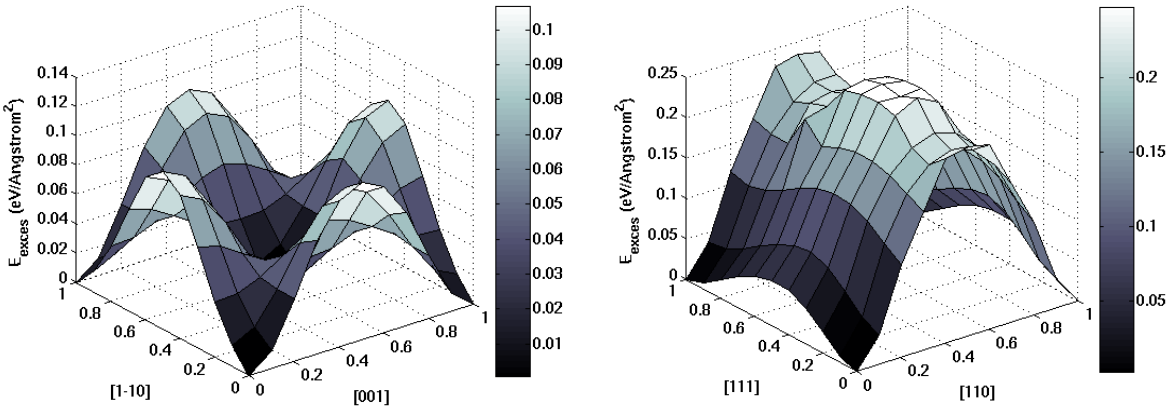

{110} {211}

Fig. 3: {110} and {211} γ-surfaces in Fe obtained after relaxation within the DFT-GGA approximation. The x and y axes are given in units of the Burgers vector ½ <111>.

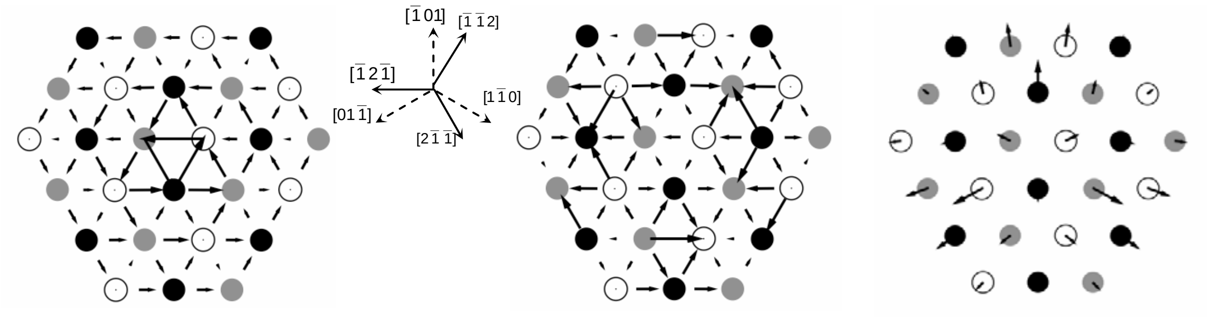

(a) **(b)** **(c)**

Fig. 4. (a): Differential displacement map of the relaxed structure of the easy core obtained in Fe within DFT-GGA using the cluster approach. (b): Displacement field after subtraction of the elastic field and magnification by a factor of 10. (c): Displacement field in the (111) plane magnified by a factor of 50.

Acknowledgements

C.-C. Fu (CEA/Saclay, France) is acknowledged for her help with the SIESTA code. This work is funded by the European fusion materials modelling programme.

References

[1] M.S. Duesbery and V. Vitek. *Plastic anisotropy in bcc transition metals.* Acta. Mater. **46**, 1481 (1998).

[2] S.L. Frederiksen and K.W. Jacobsen. *Density functional theory studies of screw dislocation core structures in bcc metals.* Philos. Mag. **83**, 365 (2003).

[3] D. E. Segall et al. *Ab initio and finite-temperature molecular dynamics studies of lattice resistance in tantalum*. Phys. Rev. B **68**, 014104 (2003).

[4] C. Woodward and S.I. Rao. *Flexible boundary conditions: simulating isolated dislocations in bcc Mo and Ta*, Phys. Rev. Lett. **88** 216402 (2002).

[5] W. Cai, V.V. Bulatov, J. Chang, J. Li and S. Yip. *Periodic image effects in dislocation modeling.* Philos. Mag. **83**, 539 (2003).

[6] C.C. Fu, F. Willaime and P. Ordejón. *Stability and mobility of mono- and di-interstitials in α-Fe.* Phys. Rev. Lett. **92**, 175503 (2004).

[7] M.I. Mendelev, S. Han, D.J. Srolovitz, G. Ackland, D.Y. Sun and M. Asta. *Development of new interatomic potentials appropriate for crystalline and liquid iron.* Philos. Mag. **83**, 3977 (2003).

Modeling the effects of irradiation and the need for experimental validation

Max Victoria [1,2]

[1]Instituto de Fusion Nuclear, Universidad Politecnica Madrid, E.T.S. Ingenieros Industriales, José Gutiérrez Abascal 2, 28006 Madrid, Spain

[2]Lawrence Livermore National Laboratory, United States of America

The evolution of radiation damage in metals and alloys is an intrinsically "multiscale" program, but such modeling without experimental validation is ineffectual. The need for a modeling program focused on being able to predict properties and stability (particularly under irradiation) of ferritic/martensitic steels will be discussed, using mainly examples from the EU Fusion Materials Modeling Task activities. The strategy is based in obtaining the physics information at each of the scales and validates it with preexisting experimental data or by designing "model experiments", in which the conditions of the experiment itself are modeled. A proposal will be discussed for future areas to be covered by modeling and in particular, new experimental methods that should be used to verify it.

Interdependent nucleation of self-interstitial and vacancy clusters in displacement cascades in Cu.

Roman Voskoboynikov

University of Oxford, Mathematical Institute, 24-29 St Giles', OX1 3LB, Oxford, United Kingdom

Molecular dynamics modeling was carried out for simulation of primary damage creation and point defect cluster formation in displacement cascades in copper that is the archetypal fcc metal with low stacking fault energy. Over 450 displacement cascades for four temperatures (T=100K, 300K, 600K and 900K) and five primary knock-on atom (PKA) energies (Epka=5, 10, 15, 20, 25 keV) in series of at least 20 cascades per (Epka, T) pair were simulated. Comprehensive statistical treatment of the obtained data was performed. In order to reveal peculiarities of point defect/ cluster formation we applied three different identification techniques. Correlated formation of self-interstitial (SIA) loops and SFT-like vacancy clusters was detected. We suggested two quantitative measures describing spatial and size correlation of SIA-loops and SFT-like clusters.

Interdependent nucleation of point defect clusters is essential in the context of radiation resistance of structural materials exposed to high dose irradiation (e.g. in modern breeder reactors) when overlapping of displacement cascades takes place. We conducted investigation of the stability of isolated regular SFT and a pair irregular SFT- SIA loop inside an overlapping region. It was found that an SFT-like vacancy cluster being destroyed in the collision stage is always recreated. Being completely enveloped by the displaced atoms domain the pair SFT-SIA loop is dissolved with corresponding recombination of Frenkel pairs and decrease of the number of residual point defects, whereas partial overlapping nearly doubles the number of point defects and leads to increase in size of both SFT and SIA loop.

Stability and mobility of self-interstitials in hcp-Zr from first principles

Francois Willaime[1], G. Verite[1], C. C. Fu[1]

[1]CEA, SRMP, CEA/Saclay, 91191 Gif-sur-Yvette, France

Zirconium alloys are widely used in the nuclear industry but the mechanisms at the atomic scale which govern their microstructural evolution under irradiation remain poorly understood. It is the case of the properties of points defects in particular the self-interstitial atoms (SIAs). This study aims at determining their structure and their mobility from first principles calculations performed with the Density Functional Theory SIESTA code. The relative stabilities of the various configurations of SIAs in hcp zirconium were determined using simulation cells containing up to 385 atoms. These results were then compared with interatomic potential calculations based on the second-moment approximation.

The SIA formation energies in the hcp structure turned out to be particularly sensitive to the size and symmetry of the supercell. The calculations revealed four new low energy metastable configurations in addition to the eight configurations commonly accepted in hcp materials. The predicted formation energies of the four most stable configurations lie within ~0.2 eV. We discuss the analogies and differences between first principles and empirical potential results. Finally we present the calculated migration barriers of the most stable configurations and confront them with experimental evidences such as resistivity recovery measurements.

Kinetic Monte Carlo modeling of cascade aging and damage accumulation in Fe-Cu alloys

Brian Wirth [1], *G. Robert Odette*[1], *Paul R. Monasterio* [1]

[1]*University of California, Berkeley, Nuclear Engineering Department, 94720-1730 Berkeley, USA*

Irradiation embrittlement in nuclear reactor pressure vessel steels results from the hardening associated with the production of a high number density of nanometer scale features. In steels with more than about 0.10% Cu, the dominant hardening features are generally Cu-rich precipitates, which are alloyed with Mn, Ni and Si. At low Cu and low-to-intermediate Ni levels, secondary hardening features are known as so-called matrix features, and are believed to be vacancy-solute cluster complexes or their remnants. This paper describes a kinetic lattice Monte Carlo model to simulate the long-term evolution of neutron irradiated Fe-Cu alloys and the recent progress in modeling damage accumulation at conditions relevant to reactor pressure vessel embrittlement. Algorithms have been developed to introduce additional displacement damage, to treat self-interstitial atom – vacancy recombination and to introduce a flux of diffusing vacancies due to the highly supersaturated vacancy concentrations under irradiation. These algorithms provide the ability to effectively model the wide range of timescales inherent to irradiation induced nanostructural evolution at low dose rates. The Monte Carlo simulations reveal the continuous formation and dissolution of three-dimensional vacancy-Cu clusters from the remnants of the vacancy-rich displacement cascade core, in addition to the formation of a high number density of copper clusters which grow with increasing irradiation dose. Initial simulations to investigate the effect of irradiation temperature and dose rate are also reported and are consistent with experimental observations.

MD simulations of dislocation interactions with stacking fault tetrahedron and Frank loops in Cu

Brian Wirth[1], *Hyon-Jee Lee*[1], *Lucie Saintoyant*[1]

[1]*University of California, Berkeley, Nuclear Engineering Department, 94720-1730 Berkeley, USA*

Molecular dynamics simulations of the interaction between gliding dislocations and faulted frank loops or stacking fault tetrahedron are presented. An examination of various factors, including dislocation type (edge, screw and mixed), temperature, SFT size, stacking fault energy, dislocation velocity and the interaction geometry lead to the conclusion that SFT are very strong obstacles to dislocation motion. Regardless of dislocation character, the trailing Shockley partial detaches by an Orowan-type mechanism, suggesting that shearing of the SFT, and not annihilation or absorption, is the most common result of dislocation interaction. Complete SFT annihilation and absorption into the dislocation core, which is believed to govern the onset of plastic flow localization, may be possible, but only for specific interactions. Dislocation interactions with Frank loops have been observed to produce shear of the loop, or the transformation into a perfect, prismatic loop.

Modeling radiation damage evolution in Fe-Cr alloys

Brian Wirth[1], *Babak Sadigh*[1], *Jae-Hyeok Shim*[1], *Hyon-Jee Lee*[1], *Kevin Wong*[1]

[1] *University of California, Berkeley, Nuclear Engineering Department, 94720-1730 Berkeley, USA*

Ferritic/martensitic Fe-(10-12%)Cr alloys are candidate structural materials for advanced fission and fusion reactor applications. Modeling radiation damage evolution in these alloys presents many challenges associated with the ferromagnetic and anit-ferromagnetic interactions between Fe and Cr. In this presentation, results from a multiscale modeling approach to predicting the interaction between Cr and vacancy/self-interstitial atom defects is presented. The results, obtained from ab-initio calculations plus atomistic molecular dynamics and kinetic Monte Carlo simulations based on semi-empirical potentials, describe the complex interactions that appear to result in binding between Cr atoms with both vacancies and self-interstitial atoms in bcc Fe. The implications of the complex Cr-point defect interactions are discussed in terms of the radiation-induced segregation behavior, and are compared to the available experimental data.

Modeling point defect interactions in pure Fe and Fe-Cr alloys

Kwan Wong[1], *J.H. Shim*[1], *B.D. Wirth*[1]

[1]*Nuclear Engineering Department, 4151 Etcheverry Hall, MC-1730, UC Berkeley, 94720-1730 Berkeley, USA*

Fe-Cr alloys are candidate structural materials for Generation IV and Fusion reactor applications at temperatures up to 550°C. Predicting the performance of Fe-Cr alloys under irradiation requires a thorough understanding of point defect interactions with Cr solute atoms, transmutant impurities, and microstructural features. In this work, atomistic molecular dynamics (MD) simulations were used to investigate the behavior of single interstitials and di- and tri- interstitial clusters in pure Fe and Fe-Cr alloys. For pure Fe, both the Ackland [1] potential and the new magnetic Dudarev-Derlet [2] potential were used. Two different Finnis-Sinclair type potentials [3] have been used for Fe-Cr alloys, predicting Cr as over- and under- sized solutes relative to Fe. The results of the MD simulations predict contrasting interactions between Cr atoms and self-interstitial defects and are used in a Kinetic Monte Carlo (KMC) model to simulate isochronal annealing recovery following electron irradiation in Fe-Cr alloys. The KMC results will be compared to experiments performed by Maury and co-workers [4] to validate the modeling results and determine the effect of Cr on point defect behavior in Fe-Cr alloys.

[1] G.J. Ackland, D.J. Bacon, A.F. Calder, T. Harry, Philos. Mag. A 75 (1997) 713.

[2] S.L. Dudarev, P.M. Derlet, J.Phys.:Condens. Matter 17 (2005) 7097.

[3] J.-H. Shim, H.-J. Lee, B.D. Wirth, J. Nucl. Mat., in press.

[4] F. Maury, P. Lucasson, A. Lucasson, F. Faudot, J. Bigot, J. Phys. F: Met. Phys. 17 (1987) 1143.

Atomistic Measures of Strength, Deformation and Reactivity: Toward Multiscale Modeling of Chemo-Mechanical Phenomena

Sidney Yip [1], *Ju Li* [2], *Ting Zhu* [3]

[1] *Massachusetts Institute of Technology, Room 24-208, MIT, 77 Mass Ave., 02139-4307 Cambridge, USA*
[2] *Department of Materials Science and Engineering, Ohio State University, 43210 Columbus, USA*
[3] *Department of Mechanical Engineering, Georgia Institute of Technology, 30332 Atlanta, USA*

In multiscale modeling of large-strain deformations, atomistic simulations of stress- induced structural instability in solids can lead to insights into certain defect nucleation processes, which also bear analogy to localization phenomena. In nano-indentation, discrete displacement bursts are shown to be homogeneous dislocation generation events which can be rationalized by a site-specific stiffness criterion. In affine shear, electronic- structure calculations show that redistribution of charge densities during deformation is essential to understanding the different ideal shear strengths of two fcc metals. Additionally, molecular dynamics results reveal a 4-stage wave distortion scenario in the localization of a deformation twin in a crystal under shear. In the advancement of sharp crack front under critical loading in a metal and a semiconductor, materials-specific behavior are revealed by determining the saddle-point configuration using reaction pathway sampling. On the basis of this kind of experience we have begun to model a unit process of water-silica reaction in which a single water molecule hydrolyzes the siloxane bond, where the dependence of the activation barrier on bond strain is explicitly treated. This is a first step toward probing chemo-mechanical processes by exploiting multiscale materials modeling capabilities to address long-standing problems at the interface of chemistry and mechanics. Potential applications to stress corrosion cracking and nuclear waste transport to gain fundamental understanding will be discussed.